THE UNIVERSITY
of EDINBURGH

Cuts, discontinuities and the coproduct of Feynman diagrams

Samuel François Souto Gonçalves de Abreu

Doctor of Philosophy

The University of Edinburgh

2015

Lay Summary

Comparing physical theories to experimental results is fundamental to test the validity of said theories. To make this comparison, a widely used method relies on the evaluation of so-called Feynman diagrams. These are a graphical representation of complicated mathematical expressions. Evaluating them requires the computation of specific integrals, called Feynman integrals. In this thesis, we develop new methods to study these diagrams and the functions they evaluate to.

Computing Feynman integrals is a very complicated task and the focus of a lot of ongoing research. We make use of some recently developed mathematical formalism to shed new light on the analytic structure of the functions these integrals evaluate to. We show how purely graphical operations on Feynman diagrams capture the analytic structure of Feynman integrals, and how this allows to find new and more efficient ways of computing these integrals.

Abstract

We study the relations among unitarity cuts of a Feynman integral computed via diagrammatic cutting rules, the discontinuity across the corresponding branch cut, and the coproduct of the integral. For single unitarity cuts, these relations are familiar, and we show that they can be generalized to cuts in internal masses and sequences of cuts in different channels and/or internal masses. We develop techniques for computing the cuts of Feynman integrals in real kinematics. Using concrete one- and two-loop scalar integral examples we demonstrate that it is possible to reconstruct a Feynman integral from either single or double unitarity cuts.

We then formulate a new set of complex kinematics cutting rules generalising the ones defined in real kinematics, which allows us to define and compute cuts of general one-loop graphs, with any number of cut propagators. With these rules, which are consistent with the complex kinematic cuts used in the framework of generalised unitarity, we can describe more of the analytic structure of Feynman diagrams. We use them to compute new results for maximal cuts of box diagrams with different mass configurations as well as the maximal cut of the massless pentagon.

Finally, we construct a purely graphical coproduct of one-loop scalar Feynman diagrams. In this construction, the only ingredients are the diagram under consideration, the diagrams obtained by contracting some of its propagators, and the diagram itself with some of its propagators cut. Using our new definition of cut, we map the graphical coproduct to the coproduct acting on the functions Feynman diagrams and their cuts evaluate to. We finish by examining the consequences of the graphical coproduct in the study of discontinuities and differential equations of Feynman integrals.

Declaration

Except where otherwise stated, the research undertaken in this thesis was the unaided work of the author. Where the work was done in collaboration with others, a significant contribution was made by the author.

Samuel François Souto Gonçalves de Abreu
September 2015

Acknowledgements

I am very grateful to my supervisor Einan Gardi for his support and guidance throughout my PhD, for always being available for many useful discussions, for setting ambitious research goals for my PhD, and for incentivising me to collaborate with other researchers. I learnt a lot from Einan, in particular to persevere when faced with problems that first seemed insurmountable.

I would like to thank Claude Duhr for introducing me to the subject of polylogarithms, suggesting the idea for the work presented in chapter 6 and for many useful discussions. Special thanks for sharing his `MATHEMATICA` package `PolyLogTools` which was crucial for most of the work presented in this thesis.

Finally, I am very grateful to Ruth Britto for the close collaboration throughout my PhD, and effectively having been my second supervisor. I am specially grateful for the invitation to spend one year at the IPhT, where a lot of the work presented in this thesis was done.

During my PhD, I also benefited from useful discussions with Øyvind Almelid, Hanna Grönqvist, Mark Harley, David Kosower, Tony Kennedy, Kasper Larsen, Alexander Ochirov, Erik Panzer and Jenni Smillie.

I am very grateful to Jenni Smillie and Thomas Gehrmann for accepting to be the examiners in my PhD defence.

Many thanks to all the people I have met in Edinburgh which have made the time I have spent here very enjoyable. I am particularly thankful to James, Hari, Ben, Enrico, Susanne and Seb for being such nice flatmates, Chiara and Sean for reminding me there are such things as experiments, Ashley, Karthee, Nathan

and Tom who started their PhDs at the same time as me, and my various office mates Eliana, Gavin, Jamie, Mark, Øyvind and Sam B.

I would also like to thank the academic and non-academic staff of the Physics department of the University of Edinburgh, in particular those of the PPT group, for making my PhD easier. I am specially grateful to Jane Patterson for all the help with administrative issues, and to the professors who gave me the opportunity to be a teaching assistant on their courses, an experience I found very enjoyable: Richard Ball, Luigi Del Debbio, Martin Evans, Einan Gardi and Jenni Smillie.

A special thanks to the regular members of the Friday night whisky club over the years: Arjun, Brian, Chris, Dom, Donal, Jamie, Oliver, Sam Y., Simon, Vlad, etc.

A big thank you to Pippa for putting up with me during my PhD, in particular while it was being written. It can't have been easy!

Finally, I am very grateful to my parents for the education they have given me and their support throughout the years, and to my sister for giving me a kick up the backside when I was being lazy.

My PhD was supported by Fundação para a Ciência e a Tecnologia, Portugal, through a doctoral degree fellowship (SFRH/BD/69342/2010), and by the Research Executive Agency (REA) of the European Union under the Grant Agreement number PITN-GA- 2010-264564 (LHCPhenoNet). I also acknowledge the hospitality of the Centre National de la Recherche Scientifique (CNRS) and the Institute for Theoretical Physics (IPhT) of the Commissariat à l'énergie atomique et aux énergies alternatives (CEA) during one year of my PhD.

Contents

List of Figures

List of Tables

Chapter 1

Introduction

The Standard Model of particle physics has been extremely successful in describing data collected in a wide range of collider experiments to an unprecedented level of accuracy. This makes it one of the best tested theories in physics. The ever increasing precision of the experimental measurements must be matched by an increase in the accuracy of theoretical predictions.

Scattering amplitudes are fundamental tools in making the connection between quantum field theories, like the Standard Model, and experimental observations. Roughly speaking, squared amplitudes describe the (differential) probability of a given process to happen. They allow to determine the cross-sections of scattering processes, which can be measured in collider experiments, from the underlying theory that governs them.

In the framework of perturbative quantum field theory, amplitudes are written as an expansion over so-called Feynman diagrams. Feynman diagrams are a graphical representation of the terms appearing in the Taylor expansion of the generating functional of the theory, defined in terms of its Lagrangian density. The Taylor expansion is an expansion in powers of some small coupling constant of the theory. Feynman graphs with a certain number of loops first appear at a specific order in this expansion. It is thus common to refer to the accuracy of theoretical predictions by either counting the power of the coupling at which we truncate the expansion, or by counting the maximal number of loops of the Feynman diagrams we consider.

For most processes, the state of the art is next-to-leading order (NLO) accuracy (although for some inclusive processes we can reach much higher

accuracy, a notable example being the recent determination of the Higgs production by gluon fusion at three-loops (N^3LO) [1]). This was possible to achieve thanks to the development of powerful methods to efficiently evaluate one-loop amplitudes. These methods build on the observation that one-loop amplitudes can be written in terms of a small number of *scalar Feynman diagrams*, i.e., Feynman diagrams with unit numerators.

The fact that diagrams with complicated numerators can be rewritten in terms of scalar diagrams was first noticed by Passarino and Veltman [2]. The calculation of one-loop amplitudes was then done by expanding it in terms of Feynman diagrams, reducing all diagrams to scalar integrals, and then computing all contributing integrals. However, even at one-loop, the number of diagrams soon becomes unmanageable as one increases the number of particles taking part in the interaction.

In more recent methods [3–17], using modern unitarity techniques, one-loop amplitudes are themselves projected onto a small basis of scalar integrals, the only integrals that must be evaluated, thus bypassing the expansion in terms of complicated Feynamn diagrams and their reduction to scalar ones. In four dimensions, only diagrams with one, two, three or four propagators are necessary (diagrams with five propagators can also be necessary to obtain the so-called rational parts of the amplitudes). These methods are called unitarity methods because they use discontinuities to project the amplitude onto the basis of scalar integrals.

The work in this thesis builds on two main lessons learnt in the development of these techniques. The first lesson is that scalar Feynman integrals constitute the fundamental building blocks of amplitudes at one loop. This is not true beyond one loop as some of the numerator structures that appear cannot be reduced in the sense of [2], but it is still true that scalar diagrams play a fundamental role. Throughout this thesis, we will thus focus on scalar Feynman diagrams. Although we will not always be explicit about it, every time we mention Feynman diagrams we will be referring to scalar Feynman diagrams.

The second lesson is that understanding the discontinuity structure of Feynman diagrams (and more generally amplitudes) is important to find efficient ways of computing them. Indeed, discontinuities of amplitudes are interesting to study as physical objects. It was realised a long time ago [18–20] that

they can be given a physical interpretation in terms of so-called *unitarity cuts*, corresponding to the original diagrams with some of the propagators put on-shell. Some years later, it was shown that the same can be said for individual Feynman diagrams [21–23]. In a nutshell, discontinuities appear at the threshold for production of on-shell physical states. From these observations, important tools were developed, such as the S-matrix theory [20], the optical theorem which relates the discontinuity of forward-scattering amplitudes to the total cross-section, or the largest time equation [21, 23].

More recently, the calculation of Feynman integrals was revolutionised by new developments in the study of a specific class of transcendental functions, the so-called multiple polylogarithms (MPLs). Indeed, a large class of Feynman diagrams can be expressed in terms of these functions, in particular all one-loop diagrams. Multiple polylogarithms are defined as iterated integrals, and carry a lot of unexpected algebraic structure. They form a Hopf algebra [24, 25], which turns out to be a natural tool to capture their discontinuities. In this thesis, we will thus study the discontinuities of scalar Feynman diagrams using tools drawn from the Hopf algebra of multiple polylogarithms, in particular its *coproduct*.

To be clear about the scope of this thesis, we will mostly be concerned with scalar and planar Feynman integrals, with generic configurations of internal and external masses, computed in dimensional regularisation. Some of our discussion can be generalised to non-planar diagram, but we did not investigate this type of diagrams in detail. Beyond one loop, we will restrict our discussion to diagrams that evaluate to MPLs, although it is known that generic Feynman integrals can involve other types of transcendental functions [26–35]. In the latter parts of this thesis, chapters 5 and 6, we will further specialise our discussion to one-loop diagrams.

In chapter 2, we will start by explaining in detail how discontinuities are captured by the coproduct of the Hopf algebra of MPLs. For that, we will be concrete about what we mean by discontinuity, by defining an operator Disc. This operator acts on MPLs, and can be iterated to compute *sequential discontinuities*. We will then show that this operator can be related to specific *entries of the coproduct* of MPLs, computed through the action of an operator δ. We will establish precise relations between these two operations, thus making it apparent

that the coproduct is a natural tool to study the discontinuities of Feynman integrals that evaluate to MPLs.

Following [18–23], in chapter 3 we will then show that the discontinuities of Feynman integrals can be computed through a specific set of so-called cutting rules, that define the unitarity cuts of Feynman diagrams. These rules have already been established for single discontinuities, and in this thesis we build on this to propose a consistent set of generalised rules reproducing multiple discontinuities. We will thus define an operator Cut, acting on Feynman diagrams, which computes *multiple unitarity cuts*. These can be cuts on external massive channels, or on internal massive propagators. We will then relate this operator to the other two operators which compute discontinuities, Disc and δ. We will thus conjecture a relation between unitarity cuts, discontinuities and specific coproduct entries.

To check our relations, we had to develop techniques to compute cut diagrams. We did so for a variety of triangle diagrams, with or without internal masses, as well as for a two-loop example, the three-point ladder integral with three-external massive legs. We verified that our conjectured relations between Cut, Disc and δ were satisfied in all the examples we investigated.

In chapter 4, we explore the question of whether Feynman diagrams can be computed from the knowledge of their cuts. The idea for this was based on [21–23], where it was shown that individual Feynman diagrams have a dispersive representation (it had been known for a while that amplitudes have a dispersive representation [20]). We were able to verify that unitarity cuts greatly constrain the analytic structure of Feynman diagrams.

As we will make clear in our discussion, while the operator Cut is enough to reproduce the discontinuities across physical branch cuts of Feynman diagrams, it is not enough to capture the full structure of the coproduct of Feynman integrals. In chapter 5 we will thus develop a new set of cutting rules, which is consistent with Cut when both are applicable, but captures as much as possible of the analytic structure of Feynman diagrams. These rules will be developed in the context of one-loop Feynman diagrams. Unlike Cut, which was defined strictly in real kinematics, these new rules are defined in complex kinematics which allows us to compute new types of cuts. For instance, with the new set of rules we will be able to compute the four-propagator cut of the fully massless box diagrams to

all orders in ϵ, which is beyond what can be achieved with Cut.

Finally, we will address what was our main motivation for the study of cut diagrams, discontinuities and the coproduct of Feynman diagrams. It started from the realisation that some coproduct entries, the ones corresponding to discontinuities, have a diagrammatic representation. It was then natural to ask ourselves whether it would be possible to have a completely diagrammatic representation of the full coproduct of Feynman diagrams. In this thesis, we show that this is possible for one-loop Feynman diagrams. We explain how a purely graphical coproduct acting on one-loop Feynman graphs can be constructed, and how its action on Feynman graphs matches the action of the coproduct of MPLs on Feynman integrals. This representation of the coproduct has practical applications given the way the coproduct interacts with discontinuity and differential operators. In particular, we will show that differential equations of one-loop Feynman integrals are determined by their cuts, and can be easily obtained from their graphical coproduct.

Chapters 2, 3 and 4 of this thesis form a coherent whole by themselves. They correspond to work that was published in two papers, [36] and [37]. Chapter 5 contains work that has not yet been published. Although it should be contrasted with the work presented in chapter 3, it can be read on its own. Chapter 6 is also unpublished work. It is largely self contained, although it uses many results established in chapter 5. In chapter 7 we summarise the conclusions of our work and discuss directions for further study.

In the appendices, we summarise our notations and conventions, appendix A, and include most of the explicit results of our calculations of uncut and cut Feynman diagrams, appendices B and C. These include some calculations and proofs that do not belong in the main body but we thought should be present, such as section B.3 where we compute triangles with three external massive legs and one or two massive propagators, and section B.4.8 where we compute the box with four massive external legs. Finally, in appendix D we briefly comment on how some of our results generalise in the case where some masses are equal but non-zero, which we always assume not to be the case in the main body of this thesis.

We finish this introduction by noting that some of the results necessary to perform the checks of the diagrammatic coproduct are not explicitly included in this thesis, as some diagrams evaluate to rather large expressions. However, all of them are available in a separate `MATHEMATICA` package [38], which we believe is a more suitable format to present such large expressions. This package can be downloaded from:
`http://www2.ph.ed.ac.uk/~s1039321/resultsOfDiagramsDiagCoprod.zip`.

Chapter 2

Multiple polylogarithms and discontinuities of Feynman diagrams

2.1 Introduction

In this first chapter we will introduce concepts and tools which will be important throughout this thesis. The content covered here is also presented in refs. [36] and [37].

We will start by introducing a specific class of transcendental functions, the so-called multiple polylogarithms (MPLs). We will define MPLs and review some of their properties. This will not be a complete review of the subject as it is a very broad field of study. Instead, we will focus on what will be used in the remaining of this thesis, in particular the Hopf algebraic structure of MPLs and the associated coproduct.

The reason we are interested in this particular class of functions is that many Feynman integrals evaluate to MPLs. In particular, it is conjectured, and observed in a wide variety of examples, that all one-loop diagrams can be written in terms of these functions. Beyond one-loop, elliptic functions can appear but MPLs still play an important role, specially for diagrams depending on few scales. We will introduce and review several topics which have allowed to make progress in the understanding of the analytic structure of Feynman integrals over recent years, such as the concept of symbol and symbol alphabet or the so-called first-

entry condition.

It is well known that the branch cuts of Feynman integrals are related to discontinuities which have a physical meaning, as they are associated to thresholds for the production of on-shell physical states [18, 20]. The position of the branch points of Feynman integrals can be found through the so-called *Landau conditions* [18] (see e.g. [39] for a modern discussion of the Landau conditions in the context of one-loop diagrams. We also give a very short review of the Landau conditions in the introduction of chapter 6, section 6.1). Understanding the analytic structure of Feynman integrals thus benefits from having a physical perspective on these functions, and not only a purely mathematical approach.

In this chapter, we will give a precise definition of Disc, an operator computing discontinuities across physical branch cuts of Feynman integrals which evaluate to MPLs, and will argue that the coproduct of the Hopf algebra of MPLs is a natural tool to study these discontinuities. For this purpose, we will define an operator δ which corresponds to a truncation of the coproduct tensor.

We will explain how to identify the kinematic region where the Feynman integral is away from any branch cut, the so-called *euclidean region*, and how by moving away from that region in a controlled way we can select the discontinuities associated with specific kinematic invariants. We will then establish precise relations between discontinuities and coproduct entries, i.e., relations between Disc and δ, and explain in detail how these can be obtained. We will finish by giving an example to make our discussion more concrete: we will get the relations between discontinuities and coproduct entries for three-point functions with massive external legs and massless propagators.

This chapter is a mixture of well established results—section 2.2—and work developed during the course of my PhD, in collaboration with Ruth Britto, Claude Duhr, my supervisor Einan Gardi, and Hanna Grönqvist for the study of diagrams with internal masses—section 2.3.

2.2 The Hopf algebra of multiple polylogarithms

Feynman integrals in dimensional regularisation usually evaluate to transcendental functions whose branch cuts are related to the physical discontinuities of S-matrix elements. Although it is known that generic Feynman integrals

can involve elliptic functions [26–35], large classes of Feynman integrals can be expressed through the classical logarithm and polylogarithm functions,

$$\log z = \int_1^z \frac{dt}{t} \quad \text{and} \quad \mathrm{Li}_n(z) = \int_0^z \frac{dt}{t}\,\mathrm{Li}_{n-1}(t) \quad \text{with} \quad \mathrm{Li}_1(z) = -\log(1-z)\,, \tag{2.1}$$

and generalisations thereof (see, e.g., refs. [40–46], and references therein). In this work we will concentrate exclusively on integrals that can be expressed entirely through the so-called *multiple polylogarithms* (MPLs), and in the rest of this section we will review some of their mathematical properties.

2.2.1 Multiple polylogarithms

Multiple polylogarithms (MPLs) are defined by the iterated integral [25, 47]

$$G(a_1, \ldots, a_n; z) = \int_0^z \frac{dt}{t - a_1}\, G(a_2, \ldots, a_n; t)\,, \tag{2.2}$$

with $a_i, z \in \mathbb{C}$. In the special case where all the a_i's are zero, we define, using the obvious vector notation $\underline{a}_n = (\underbrace{a, \ldots, a}_{n})$,

$$G(\underline{0}_n; z) = \frac{1}{n!}\,\log^n z\,. \tag{2.3}$$

The number n of integrations in eq. (2.2), or equivalently the number of a_i's, is called the *weight* of the multiple polylogarithm, denoted w. As simple cases, we have

$$\begin{aligned} &G(0; z) = \log z, \qquad G(a; z) = \log\left(1 - \frac{z}{a}\right), \qquad G(0, a; z) = -\mathrm{Li}_2\left(\frac{z}{a}\right), \\ &G(a, b; z) = \mathrm{Li}_2\left(\frac{b-z}{b-a}\right) - \mathrm{Li}_2\left(\frac{b}{b-a}\right) + \log\left(1 - \frac{z}{b}\right)\log\left(\frac{z-a}{z-b}\right), \end{aligned} \tag{2.4}$$

where the last equality holds for a and b different and nonzero [48]. Note that some constants, corresponding to specific values of MPLs, inherit the weight from the functions that define them. For instance,

$$\log(-1) = \pm i\pi \Rightarrow w(\pi) = 1\,, \qquad \mathrm{Li}_n(1) = \zeta_n \Rightarrow w(\zeta_n) = n. \tag{2.5}$$

In the following we denote by $\overline{\mathcal{H}}$ the $\mathbb{Q}$-vector space spanned by all multiple polylogarithms. In addition, $\overline{\mathcal{H}}$ can be turned into an algebra. Indeed, iterated integrals form a *shuffle algebra*,

$$G(\vec{a}_1; z)\, G(\vec{a}_2; z) = \sum_{\vec{a} \in \vec{a}_1 \text{ ш } \vec{a}_2} G(\vec{a}; z)\,, \tag{2.6}$$

where $\vec{a}_1 \text{ ш } \vec{a}_2$ denotes the set of all shuffles of $\vec{a}_1$ and $\vec{a}_2$, where $\vec{a}_1 = (a_{1,1}, \ldots, a_{1,n})$ and $\vec{a}_2 = (a_{2,1}, \ldots, a_{2,m})$, i.e., the set of all permutations of their union that preserve the relative orderings inside $\vec{a}_1$ and $\vec{a}_2$. It is obvious that the shuffle product preserves the weight, and hence the product of two multiple polylogarithms of weight n_1 and n_2 is a linear combination of multiple polylogarithms of weight $n_1 + n_2$. We can formalise this statement by saying that the algebra of multiple polylogarithms is *graded* by the weight,

$$\overline{\mathcal{H}} = \bigoplus_{n=0}^{\infty} \overline{\mathcal{H}}_n \quad \text{with} \quad \overline{\mathcal{H}}_{n_1} \cdot \overline{\mathcal{H}}_{n_2} \subset \overline{\mathcal{H}}_{n_1+n_2}\,, \tag{2.7}$$

where $\overline{\mathcal{H}}_n$ is the $\mathbb{Q}$-vector space spanned by all multiple polylogarithms of weight n, and we define $\overline{\mathcal{H}}_0 = \mathbb{Q}$.

The coproduct of the Hopf algebra of MPLs: Multiple polylogarithms can be endowed with more algebraic structures. If we look at the quotient space $\mathcal{H} = \overline{\mathcal{H}}/(\pi\,\overline{\mathcal{H}})$ (the algebra $\overline{\mathcal{H}}$ modulo π), then $\mathcal{H}$ is a Hopf algebra [24, 25]. In particular, $\mathcal{H}$ can be equipped with a *coproduct* $\Delta : \mathcal{H} \to \mathcal{H} \otimes \mathcal{H}$, which is coassociative,

$$(\mathrm{id} \otimes \Delta)\, \Delta = (\Delta \otimes \mathrm{id})\, \Delta\,, \tag{2.8}$$

respects the multiplication,

$$\Delta(a \cdot b) = \Delta(a) \cdot \Delta(b)\,, \tag{2.9}$$

and respects the weight,

$$\mathcal{H}_n \xrightarrow{\Delta} \bigoplus_{k=0}^{n} \mathcal{H}_k \otimes \mathcal{H}_{n-k}\,. \tag{2.10}$$

The coproduct of the ordinary logarithm and the classical polylogarithms are

$$\Delta(\log z) = 1 \otimes \log z + \log z \otimes 1, \tag{2.11}$$

or, more generally,

$$\Delta(\log^n z) = \sum_{k=0}^{n} \binom{n}{k} \log^k(z) \otimes \log^{n-k}(z), \tag{2.12}$$

and

$$\Delta(\mathrm{Li}_n(z)) = 1 \otimes \mathrm{Li}_n(z) + \sum_{k=0}^{n-1} \mathrm{Li}_{n-k}(z) \otimes \frac{\log^k z}{k!}\,. \tag{2.13}$$

For the definition of the coproduct of general multiple polylogarithms we refer to refs. [24, 25].

The coassociativity of the coproduct implies that it can be iterated in a unique way. If $(n_1, \ldots, n_k)$ is a partition of n, we define

$$\Delta_{n_1,\ldots,n_k} : \mathcal{H}_n \to \mathcal{H}_{n_1} \otimes \ldots \otimes \mathcal{H}_{n_k}\,. \tag{2.14}$$

Note that the maximal iteration of the coproduct, corresponding to the partition $(1, \ldots, 1)$, agrees with the symbol of a transcendental function F [49–53]

$$\mathcal{S}(F) \equiv \Delta_{1,\ldots,1}(F) \in \mathcal{H}_1 \otimes \ldots \otimes \mathcal{H}_1\,. \tag{2.15}$$

Since every element of $\mathcal{H}_1$ is a logarithm, the 'log' sign is usually dropped when talking about the symbol of a function. Note that not every element in $\mathcal{H}_1 \otimes \ldots \otimes \mathcal{H}_1$ corresponds to the symbol of a function in $\mathcal{H}$. Instead, one can show that if we take an element

$$s = \sum_{i_1,\ldots,i_n} c_{i_1,\ldots,i_n}\, \log x_{i_1} \otimes \ldots \otimes \log x_{i_n} \in \mathcal{H}_1 \otimes \ldots \otimes \mathcal{H}_1\,, \tag{2.16}$$

where the coefficients $c_{i_1,\ldots,i_n} \in \mathbb{Q}$ are rational numbers, then there is a function $F \in \mathcal{H}_n$ such that $\mathcal{S}(F) = s$ if and only if s satisfies the *integrability condition*

$$\sum_{i_1,\ldots,i_n} c_{i_1,\ldots,i_n}\, d\log x_{i_k} \wedge d\log x_{i_{k+1}}\, \log x_{i_1} \otimes \ldots \otimes \log x_{k-1} \otimes \log x_{k+2} \otimes \ldots \otimes \log x_{i_n} = 0\,, \tag{2.17}$$

where $\wedge$ denotes the usual wedge product on differential forms.

While $\mathcal{H}$ is a Hopf algebra, we are practically interested in the full algebra $\overline{\mathcal{H}}$ where we have kept all factors of π. Based on similar ideas in the context of motivic multiple zeta values [54], it was argued in ref. [48] that we can reintroduce π into the construction by considering the trivial comodule $\overline{\mathcal{H}} = \mathbb{Q}[i\pi] \otimes \mathcal{H}$. The coproduct is then lifted to a comodule map $\Delta : \overline{\mathcal{H}} \to \overline{\mathcal{H}} \otimes \mathcal{H}$ which acts on $i\pi$ according to

$$\Delta(i\pi) = i\pi \otimes 1. \tag{2.18}$$

For n even, ζ_n is proportional to π^n, and we thus also have

$$\Delta(\zeta_n) = \zeta_n \otimes 1 \qquad \text{for } n \text{ even}, \tag{2.19}$$

while

$$\Delta(\zeta_n) = \zeta_n \otimes 1 + 1 \otimes \zeta_n \qquad \text{for } n \text{ odd}, \tag{2.20}$$

as follows naturally from eq. (2.13). In the following we will, by slight abuse of language, refer to the comodule as the Hopf algebra $\overline{\mathcal{H}}$ of multiple polylogarithms.

Note that for $\overline{\mathcal{H}}$ (more precisely $\mathcal{H}$) to be a Hopf algebra, it has to be equipped with more structures such as a *counit* and an *antipode*, see e.g. [48,55]. These will not play a role in the remaining of this thesis, so we will not study them further.

Let us conclude this review of multiple polylogarithms and their Hopf algebra structure by discussing how differentiation and taking discontinuities interact with the coproduct (see section 2.3.1 for a precise definition of discontinuity in this work). In ref. [48] it was argued that the following identities hold:

$$\Delta \frac{\partial}{\partial z} = \left(\mathrm{id} \otimes \frac{\partial}{\partial z}\right) \Delta \tag{2.21a}$$

$$\Delta \,\mathrm{Disc} = (\mathrm{Disc} \otimes \mathrm{id})\,\Delta\,. \tag{2.21b}$$

In other words, differentiation only acts in the last entry of the coproduct, while taking discontinuities only acts in the first entry.

Let f_n be an element of weight n in $\overline{\mathcal{H}}$. The derivative of f_n is thus a product of a rational function and a function which is an element of weight $n-1$ in $\overline{\mathcal{H}}$,

given by

$$\frac{\partial f_n}{\partial z} = \mu \left[\left(\mathrm{id} \otimes \frac{\partial}{\partial z} \right) \Delta_{n-1,1} f_n \right], \tag{2.22}$$

where $\mu : \overline{\mathcal{H}} \otimes \overline{\mathcal{H}} \to \overline{\mathcal{H}}$ denotes the multiplication in $\overline{\mathcal{H}}$.

Since discontinuities are proportional to $i\pi$, which appears only in the first entry of the coproduct, it follows from eq. (2.21b) that for an element f_n of weight n in $\overline{\mathcal{H}}$,

$$\mathrm{Disc}\, f_n \cong \mu \left[(\mathrm{Disc} \otimes \mathrm{id})\, \Delta_{1,n-1} f_n \right], \tag{2.23}$$

i.e. we simply multiply the two factors in the coproduct, and $\cong$ denotes equivalence modulo π^2, because the weight $(n-1)$ part of the coproduct in the right-hand side is only defined modulo π.

The two relations in eq. (2.21) will play a central role in the remaining of this work. The relation between discontinuities and the coproduct will be important throughout, and the relation between differential operators and the coproduct will allow us to relate cuts and differential equations in chapter 6.

2.2.2 Pure Feynman integrals

Throughout this thesis, we will be concerned with connected planar Feynman integrals in dimensional regularisation. In $D = d - 2\epsilon$ dimensions, for d even, an L-loop Feynman integral $F^{(L)}$ defines a Laurent series,

$$F^{(L)}(\epsilon) = \sum_{k=-2L}^{\infty} F_k^{(L)}\, \epsilon^k . \tag{2.24}$$

In the following we will concentrate on situations where the coefficients of the Laurent series can be written exclusively in terms of multiple polylogarithms and rational functions, and a well-known conjecture states that the weight of the transcendental functions (and numbers) that enter the coefficient $F_k^{(L)}$ of a L-loop integral is such that

$$w\left(F_k^{(L)}\right) \leq \frac{d\,L}{2} + k. \tag{2.25}$$

If all the polylogarithms in $F_k^{(L)}$ have the same weight, the integral is said to have *uniform (transcendental) weight*. In addition, we say that an integral is *pure* if the coefficients $F_k^{(L)}$ do not contain rational or algebraic functions of the external kinematical variables.

It is clear that pure integrals are the natural objects to study when trying to link Hopf algebraic ideas for multiple polylogarithms to Feynman integrals. For this reason we will only be concerned with pure integrals in the rest of this thesis. However, the question naturally arises of how restrictive this assumption is. In ref. [56] it was noted that if a Feynman integral has unit leading singularity [57], i.e., if all the residues of the integrand, obtained by integrating over compact complex contours around the poles of the integrand, are equal to one, then the corresponding integral is pure. Furthermore, it is well known that Feynman integrals satisfy integration-by-parts identities [58], which, loosely speaking, allow one to express a loop integral with a given propagator structure in terms of a minimal set of so-called master integrals. In ref. [59] it was conjectured that it is always possible to choose the master integrals to be pure integrals, and the conjecture was shown to hold in several nontrivial cases [60–63]. Hence, if this conjecture is true, it should always be possible to restrict the computation of the master integrals to pure integrals, which justifies the restriction to this particular class of integrals.

In practice, in this thesis we will always work with Feynman integrals evaluating to functions of uniform weight, with a single rational factor. This will require to choose the value of d according to the number of propagators. For one-loop diagrams with n propagators, we will choose d to be the even number such that $d-2 < n \leq d$. For instance, tadpoles and bubbles are computed in $D = 2 - 2\epsilon$, triangles and boxes in $D = 4 - 2\epsilon$, pentagons and hexagons in $D = 6 - 2\epsilon$, etc. The coefficient $F_0^{(1)}$ of one-loop integrals will then evaluate to functions of weight $d/2$. It is not yet clear to us how to generalise this procedure to general diagrams at higher loop order, but for the two-loop diagram we will analyse in this work choosing $D = 4 - 2\epsilon$ gives a uniform weight function, of weight 4, which saturates the upper bound in eq. (2.25).

We finish with two comments. First, we only require to have integrals evaluating to functions of uniform weight because it makes our discussion simpler. Indeed, most of our conclusions are still valid for functions of non-uniform weight, but we would need to treat separately the components of different weights. Second, it will be convenient to think of the dimensional regularisation parameter ϵ as having weight -1. We can then assign a weight to a diagram in dimensional regularisation (instead of only to the coefficients in its Laurent expansion): given

our choice of varying the dimensions with the number of propagators for one-loop diagrams, they have weight $d/2$. This will mean that in its Laurent expansion, the coefficient of the order ϵ^k is a function of weight $d/2 + k$.

2.2.3 The symbol alphabet

The most natural kinematic variables for a given integral might be complicated functions of the momentum invariants. Indeed, it is known that the Laurent expansion coefficients in eq. (2.24) are *periods* (defined, loosely speaking, as integrals of rational functions), which implies that the arguments of the polylogarithmic functions are expected to be algebraic functions of the external scales [64]. In practice it is more convenient to find a parametrisation of the kinematics such that the arguments of all polylogarithmic functions are rational. More precisely, if we have a Feynman integral depending on n independent scales s_i (e.g. Mandelstam invariants), we want to find $n-1$ independent variables z_i such that

$$s_i/s_n = f_i(z_1, \ldots, z_{n-1}) \,, \tag{2.26}$$

where the f_i are rational functions such that all the arguments of the polylogarithms are rational functions of the z_i variables. While no general algorithm is known that allows one to find the parametrisation eq. (2.26), such a parametrisation exists for a wide variety of diagrams. The inverse relations to eq. (2.26), expressing z_i in terms of the Mandelstam invariants $\{s_j\}$, are algebraic functions, often involving square roots of polynomials of the invariants $\{s_j\}$.

In this thesis, we will focus on diagrams for which we have found a rational parametrisation and simply comment on some borderline cases in sections B.3.5 and B.4.8. Let us give some concrete examples of rational parametrisations. For three-point diagrams with massless propagators and three massive external channels, let's say p_1^2, p_2^2 and p_3^2, a very useful parametrisation was introduced in [65]. We start by defining two dimensionless ratios

$$u_i = \frac{p_i^2}{p_1^2}, \quad \text{for} \quad i = 1, 2, \tag{2.27}$$

and then define the variables z and $\bar{z}$ as

$$u_2 = z\bar{z}, \qquad u_3 = (1-z)(1-\bar{z}). \tag{2.28}$$

As mentioned above, the inverse relations involve algebraic functions:

$$z = \frac{1 + u_2 - u_3 + \sqrt{\lambda(1, u_2, u_3)}}{2}, \qquad \bar{z} = \frac{1 + u_2 - u_3 - \sqrt{\lambda(1, u_2, u_3)}}{2}, \quad (2.29)$$

where $\lambda(a, b, c)$ is the usual Källén function,

$$\lambda(a, b, c) = a^2 + b^2 + c^2 - 2ab - 2ac - 2bc. \quad (2.30)$$

In the following, we will sometimes write $\lambda \equiv \lambda(1, u_2, u_3)$, when there is no ambiguity about the arguments.

In [37], the same idea was applied to integrals with massive internal propagators. If an external massive leg of mass p_1^2 is attached to two internal massive propagators of masses m_{12}^2 and m_{13}^2, then simply by working out the kinematics of such a vertex one can see that it is convenient to introduce the analogue of eq. (2.29) in the following way. We define the two dimensionless ratios

$$\mu_{ij} = \frac{m_{ij}^2}{p_1^2}, \quad \text{for} \quad i = 1, \ j = 2, 3, \quad (2.31)$$

and then define the variables w_1 and $\bar{w}_1$ as

$$\mu_{12} = w_1 \bar{w}_1, \qquad \mu_{13} = (1 - w)(1 - \bar{w}_1). \quad (2.32)$$

The inverse relation is then

$$w_1 = \frac{1 + \mu_{12} - \mu_{13} + \sqrt{\lambda(1, \mu_{12}, \mu_{13})}}{2}, \qquad \bar{w}_1 = \frac{1 + \mu_{12} - \mu_{13} - \sqrt{\lambda(1, \mu_{12}, \mu_{13})}}{2}. \quad (2.33)$$

Throughout this work, most of our examples will be three-point functions, and so these sets of variables will appear very often. Other examples of rational parametrisations can be found in the literature. These can be obtained either by intuition (e.g. [66]), a connection with twistor theory (e.g. [67,68]), or a connection with scattering equations [69].

If a parametrisation of the type (2.26) has been determined for a given Feynman integral, it is easy to see that the entries of the symbol of this integral will be rational functions of the z_i. Moreover, due to the additivity of the symbol, we can assume that the entries of the symbol are polynomials

with integer coefficients[1] in the variables z_i, which without loss of generality we may assume to be irreducible over $\mathbb{Z}$. In other words, once a rational parametrisation (2.26) has been determined, we can assign to every Feynman integral a set $\mathcal{A} \subset \mathbb{Z}[z_1, \ldots, z_{n-1}]$ of irreducible polynomials. In the following we call the set $\mathcal{A}$ the *symbol alphabet* of the integral, and its elements, which we generically denote by x_i, will be called the *letters* of the alphabet. Some comments are in order: First, we note that the symbol alphabet $\mathcal{A}$ is not unique, but it is tightly connected to the choice of the rational parametrisation (2.26). A different choice for the rational functions f_i may result in a different symbol alphabet $\mathcal{A}$. Second, we emphasise that although the parametrisation (2.26) only involves the external scales, its form is in general dependent on the loop order and/or the order in the expansion in the dimensional regulator ϵ and the topology of the integral under consideration. Third, it is easy to see that once a symbol alphabet $\mathcal{A}$ is fixed, the symbol of a polylogarithmic function of weight k takes values in $\mathbb{Q} \otimes_{\mathbb{Z}} \mathbb{Z}[\mathcal{A}]^{\otimes k}$, the k-fold tensor product (with rational coefficients) of the free abelian group of rational functions whose generators are the polynomials in the set $\mathcal{A}$. Finally, we note that it is expected that the arguments of the polylogarithms take values in a subset of the free abelian group $\mathbb{Z}[\mathcal{A}]$, and an explicit (conjectural) construction of this subset was presented in ref. [53].

In practical applications it is often advantageous to know the symbol alphabet underlying a specific problem a priori. For example, if the alphabet is determined, it is possible to write ansätze for the symbols and/or the function spaces for Feynman integrals or amplitudes, which can then be fixed using additional physical information (e.g., behaviour in certain limits) [65, 70–76]. Unfortunately, as already mentioned, no general algorithm to determine a rational parametrisation (2.26), and thus the letters $x_i \in \mathcal{A}$ is known. One possible way to determine the alphabet is to analyze the differential equations satisfied by Feynman integrals [59, 77–80], where the letters x_i appear as the singularities of the differential equations.[2] In the rest of this paper we argue that another way of determining the letters x_i consists in analyzing (iterated) unitarity cuts of Feynman integrals. Indeed, as we will argue in the next section, cut integrals are tightly connected to the entries in the coproduct (and hence the symbol) and the

[1] We allow the polynomials to be constants.

[2] We note, however, that also in that case a rational parametrisation has to be determined by independent means.

discontinuities of a Feynman integral, but they are sometimes easier to compute because the transcendental weight is reduced.

This review of the properties of multiple polylogarithms is a very short summary of an interesting and broad subject, that we tailored to the needs of this thesis. To learn this subject, we mainly benefited from studying references [48] and [53], as they present the subject in a manner more suited to non-mathematicians. Furthermore, the lectures in [81] are a very good review of the subject as well as a good source of references. More recently, we found [55] useful as a short summary of the properties of Hopf algebras. Finally, for a reference which deals exactly with the subject of polylogarithms and Feynman integrals from the mathematics community, but which we found to be accessible nevertheless, we refer to [82].

2.3 Iterated discontinuities and coproduct entries

Having given a succinct introduction to the analytic structure of multiple polylogarithms in the previous section, we now focus on discontinuities of MPLs and how they are related to coproduct entries. We will start by giving our definition of discontinuity, and then define an operator δ that truncates the coproduct tensor of MPLs. Finally, we show how iterated discontinuities and the action of δ are related. These two operations are defined for general polylogarithms, and our next step is to make the discussion more specific to Feynman integrals by commenting on their analytic structure. In particular, we will introduce the concept of *first entry condition*. This will allow us to determine the natural kinematic region in which discontinuities should be evaluated.

2.3.1 Discontinuities and coproduct entries

Disc: Discontinuity across branch cuts

We define an operator $\text{Disc}_s F$ giving the direct value of the discontinuity of F as the variable s crosses the real axis. By convention we choose the branch cut of the logarithm function to be the negative real axis. If there is no branch cut

in the region of s for which $F(s)$ is defined, or if F does not depend on s, then the value is zero. Concretely,

$$\mathrm{Disc}_s\left[F(s \pm i0)\right] = \lim_{\varepsilon \to 0}\left[F(s \pm i\varepsilon) - F(s \mp i\varepsilon)\right], \tag{2.34}$$

where the $i\varepsilon$ prescription must be inserted correctly in order to obtain the appropriate sign of the discontinuity, and we assume s to be real valued. For example, $\mathrm{Disc}_s \log(s+i0) = 2\pi i\,\theta(-s)$. Understanding the correct sign of the $\pm i0$ associated to a given variable in detail is important, but we leave that discussion for when we relate Disc to diagrammatic cuts in the next chapter.

The sequential discontinuity operator $\mathrm{Disc}_{r_1,\ldots,r_k}$ is defined recursively:

$$\mathrm{Disc}_{r_1,\ldots,r_k} F \;\equiv\; \mathrm{Disc}_{r_k}\left(\mathrm{Disc}_{r_1,\ldots,r_{k-1}} F\right). \tag{2.35}$$

In the context of Feynman diagrams, we should think of the r_i as associated to kinematic invariants, either Mandelstam invariants or (squared) internal masses.

Note that Disc may be computed in any region after careful analytic continuation. In particular, sequential Disc will be computed in different regions at each step. We will sometimes write

$$\mathrm{Disc}_{r_1,\ldots,r_k;R}\, F \tag{2.36}$$

to make explicit the region R in which $\mathrm{Disc}_{r_1,\ldots,r_k}$ is to be computed, after having analytically continued F to this same region.

δ: Entries of the coproduct

If F is of transcendental weight n and has all its symbol entries drawn from the alphabet $\mathcal{A}$, then we can write without loss of generality

$$\Delta_{\underbrace{1,1,\ldots,1}_{k\text{ times}},n-k} F \;=\; \sum_{(x_{i_1},\ldots,x_{i_k})\in\mathcal{A}^k} \log x_{i_1} \otimes \cdots \otimes \log x_{i_k} \otimes g_{x_{i_1},\ldots,x_{i_k}}\,, \tag{2.37}$$

and we define

$$\delta_{x_{j_1},\ldots,x_{j_k}} F \;\cong\; \sum_{(x_{i_1},\ldots,x_{i_k})\in\mathcal{A}^k} \delta_{i_1 j_1}\,\ldots\,\delta_{i_k j_k}\, g_{x_{i_1},\ldots,x_{i_k}}, \tag{2.38}$$

where the congruence symbol indicates that $\delta_{x_{j_1},\ldots,x_{j_k}} F$ can be defined only modulo π. If the integral contains overall numerical factors of π, they should be factored out before performing this operation.

The definition of $\delta_{x_{j_1},\ldots,x_{j_k}} F$ is motivated by the relation in eq. (2.23) between discontinuities and coproducts. In particular, if $\delta_x F \cong g_x$, then $\mathrm{Disc}_x F = \pm 2\pi i\, g_x$. The sign is determined by the $i0$ prescription of x in F. The precise form of the relation between the Disc and δ operations will be discussed in more detail in the following subsection.

Relation between iterated discontinuities and coproduct entries

Recall from eq. (2.23) that for an element F of weight n of the Hopf algebra,

$$\mathrm{Disc}\, F \cong \mu\left[(\mathrm{Disc}\otimes\mathrm{id})(\Delta_{1,n-1}F)\right] , \tag{2.39}$$

To be precise, F should not include overall factors of π. If it does, these are stripped out before performing the operation on the right-hand side, and then reinstated. It follows from this relation that the discontinuity of any element of the Hopf algebra is captured by the operation δ as defined in eq. (2.38). To apply the relation, we must take great care with the sequential analytic continuation of the discontinuities and the locations of the branch cuts. Finally, since the first entries of $\Delta_{1,n-1}F$ are of weight 1, the Disc operation on the right-hand side is computing discontinuities of ordinary logarithms.

Let us specialise to the discontinuity computed in a given variable r. We can expand the coproduct in terms of the full symbol alphabet by writing

$$(\mathrm{Disc}_r\otimes\mathrm{id})(\Delta_{1,n-1}F) \cong (\mathrm{Disc}_r\otimes\mathrm{id}) \sum_{x\in\mathcal{A}} (\log(\pm x)\otimes\delta_x F) . \tag{2.40}$$

Note that this relation applies generally, so it also applies to the case where F is the sequential discontinuity of some other function $\tilde{F}$. We stress for a last time that, as noted below eq. (2.39), overall factors of π in F are handled separately: this is particularly noteworthy if F is a sequential discontinuity where powers of π will have been generated from previous discontinuities.

For Feynman diagrams, we require Disc to be computed in a specific kinematic region. We then require that the sign in the argument of the logarithm in

eq. (2.40) be chosen so that the argument is positive and the expression is thus real-valued in the kinematic region for which F is away from its branch cut in r. In taking Disc_r, the coproduct will be analytically continued to the region in which there is a branch cut in r. In this new region, the arguments of the logarithms may become negative, and if the letter x depends on the invariant r, then there will be a nonzero contribution to Disc.

Sequential discontinuities of F are computed by the sequential use of eq. (2.40). We thus claim they are captured by δ in the relation

$$\mathrm{Disc}_{r_1,\ldots,r_k} F \cong \Theta \sum_{(x_1,\ldots,x_k)\in\mathcal{A}^k} \left(\prod_{i=1}^{k} a_i(r_i,x_i)\right) \delta_{x_1,\ldots,x_k} F, \tag{2.41}$$

where the sum runs over all ordered sequences $(x_1,\ldots,x_k)$ of k letters. We recall that the congruence symbol in eq. (2.41) indicates that despite the fact that the discontinuity function $\mathrm{Disc}_{r_1,\ldots,r_k} F$ is unique, the right-hand side only captures terms whose coproduct is nonvanishing, and it therefore holds modulo $(2\pi i)^{k+1}$. Furthermore, since the coproduct is the same in all kinematic regions (because it is defined modulo π, it is invariant under analytic continuation), we have inserted the schematic factor Θ to express the restriction to the region where the left-hand side is computed. Finally, the factors $a_i(r_i,x_i)$ are related to the discontinuity of a real-valued logarithm after analytic continuation from one kinematic region (R_{i-1}) to another (R_i). Specifically,

$$a_i(r_i,x_i) = \mathrm{Disc}_{r_i;R_i} \left[\!\!\left[\log(\pm x_i) \right]\!\!\right]_{R_{i-1}}, \tag{2.42}$$

where the double-bracket means that the sign of the argument of the logarithm should be chosen so that the argument is positive in the region R_{i-1}, or equivalently,

$$\left[\!\!\left[\log(\pm x_i) \right]\!\!\right]_{R_{i-1}} = \log(x_i)|_{R_{i-1}\cap\{x_i>0\}} + \log(-x_i)|_{R_{i-1}\cap\{x_i<0\}} \tag{2.43}$$

In the simplest cases, each $a_i(r_i,x_i)$ will simply take one of the values $\pm 2\pi i$ or 0. In more complicated cases, one might find a further division into nonempty subregions of phase space.

We note that although we focus on Feynman integrals in the remaining of this

work, the mathematical relation between Disc and δ applies in a more general context. The essential requirement is that the function has no branch cut in r_i in region R_{i-1}, but does in region R_i.

In section 2.3.3 we make eq. (2.41) more concrete by looking at an example. We will compute the coefficients $a_i(r_i, x_i)$ of eq. (2.42) in detail for single and double discontinuities of three-point functions with massless propagators.

2.3.2 Euclidean region and the first-entry condition

The operations Disc and δ are defined for any multiple polylogarithm. However, as we will now see, the branch cut structure of Feynman integrals is constrained by physical considerations which allow to state some general results for the relation between discontinuities and the coproduct of Feynman integrals.

We start by discussing the case where all propagators are massless. In this case, it is known that the branch points of the integral, seen as a function of the invariants $s_{ij} = (p_i + p_j)^2$, where p_i are the external momenta (which can be massive or massless), are the points where one of the invariants is zero or infinite [18]. It follows then from the second relation in eq. (2.21b) (or equivalently (2.23)) that the first entry of the coproduct of a Feynman integral can only have discontinuities in these precise locations. In particular, this implies the so-called first entry condition, i.e., the statement that the first entries of the symbol of a Feynman integral with massless propagators can only be (logarithms of) Mandelstam invariants [36, 83]. This observation, combined with the fact that Feynman integrals can be given a dispersive representation, provided the motivation for a lot of the work presented here, namely the study of the discontinuities of Feynman integrals through the lens of the Hopf algebraic language reviewed in the previous section.

In [37], we extended the first-entry condition to cases with internal masses. We argued that the coproduct can always be written in such a form where: *(i)* the first entries of the coproduct component $\Delta_{1,n-1}$ are either consistent with the thresholds of Mandelstam invariants or are internal masses ; *(ii)* the second entry is the discontinuity across the branch cut associated with the corresponding first entry, as is the case for diagrams with no internal masses.[3]

[3]We remark that property *(ii)* does not follow from property *(i)*, as we shall see in an example at the end of this section.

Feynman integrals with massive propagators have a much more intricate analytic structure than in the massless case. Let us then be a bit more specific about them. Planar Feynman integrals are most easily computed in the kinematic region of the invariants where the integral is well-defined independently of the $\pm i0$-prescription of the propagators [18]. This region is characterised by having the Mandelstam invariants below their threshold for production of on-shell physical states, and the (squared) masses of internal propagators being positive. In this region, the *euclidean region*, we are away from any branch cut.

As an example, the euclidean region for a triangle diagram with massive propagators is (see appendix A for the notation):

$$p_1^2 < \left(\sqrt{m_{12}^2} + \sqrt{m_{13}^2}\right)^2, \quad p_2^2 < \left(\sqrt{m_{12}^2} + \sqrt{m_{23}^2}\right)^2, \quad p_3^2 < \left(\sqrt{m_{13}^2} + \sqrt{m_{23}^2}\right)^2,$$
$$m_{12}^2 > 0\,, \qquad m_{23}^2 > 0\,, \qquad m_{13}^2 > 0\,. \tag{2.44}$$

For triangles where some of the masses vanish, the euclidean region can be obtained from the above by taking the appropriate limit. For instance, as already mentioned above, in the absence of internal masses the euclidean region is the region where all external invariants are negative.

As we depart from the euclidean region, we are sensitive to branch cuts of the integral, and the $\pm i0$-prescription indicates which side of the branch cut we are on. The discontinuity, as defined in eq. (2.34), corresponds to the difference of the results computed with different prescriptions.

Eq. (2.21b) implies that the first entries of the coproduct tensor of a Feynman diagram must have the same branch cut structure as the Feynman diagram itself. In particular, this means that when looking at the $\Delta_{1,n-1}$ component, the weight one cofactors appearing in the first entries must be simple logarithms with branch points at the boundaries of the euclidean region.

From this observation, and by looking at eq. (2.44), we see two ways in which the first entry condition of [83] must be generalised in the presence of internal masses. The first is that we no longer have logarithms of Mandelstam invariants themselves, but instead logarithms with branch cuts at the mass threshold for the corresponding invariant. The second is that the squared masses of the propagators themselves appear as first entries.

As predicted by eq. (2.21b), the second entries of the $\Delta_{1,n-1}$ component of the

coproduct of a Feynman diagram then correspond to the discontinuities associated to the branch cut identified in the corresponding first entry. These discontinuities can be associated either to Mandelstam invariants going above their thresholds, or to internal masses becoming negative.

In this thesis, we will give ample evidence illustrating this observation. However, we should make a comment related to how apparent the first entry is depending on the variables used. As we discussed above, we prefer to have symbol alphabets with rational letters. If that is the case when using the Mandelstam invariants themselves as variables (or ratios of them, if we want to work with dimensionless quantities), the above properties are very easy to check. In more complicated cases where we need to change variables to have a rational symbol alphabet, let's say by using variables as defined in eqs. (2.29) or (2.33), the situation is not as clear. We claim that even though the first entry condition might not be apparent in the most compact expressions for the symbol (or, equivalently, the coproduct), we can always rearrange the different terms of the symbol tensor so that they are in the form described above by using logarithmic identities. We now give two examples, one for each type of behaviour.

Example 1: Consider the triangle $T(p_1^2, 0, 0; m_{12}^2, 0, 0)$, whose symbol is given in eq. (B.11) up to order ϵ^0. The first term of the finite contribution has $\log(m_{12}^2)$ as its first entry, and the second term has $\log(m_{12}^2 - p_1^2)$ as its first entry. The latter is written in a form in which the argument of the logarithm is positive in the euclidean region where the integral is originally evaluated.

Example 2: As another example, consider the triangle $T(p_1^2, 0, 0; m_{12}^2, 0, m_{13}^2)$, whose symbol is given in eq. (B.21). We have changed variables according to eq. (2.33) to have a rational symbol alphabet. Because the new variables have a more complicated relation to the Mandelstam invariants, the first entry condition is not as apparent as in the previous example. However, as mentioned above, the symbol of $\mathcal{T}(p_1^2, 0, 0; m_{12}^2, 0, m_{13}^2)$ can be rewritten as

$$\begin{aligned}\mathcal{S}\left[\mathcal{T}(p_1^2, 0, 0; m_{12}^2, 0, m_{13}^2)\right] = &(w_1\bar{w}_1) \otimes \frac{w_1}{1-w_1} + ((1-w_1)(1-\bar{w}_1)) \otimes \frac{1-\bar{w}_1}{\bar{w}_1} \\ &+ (w_1(1-\bar{w}_1)) \otimes \frac{\bar{w}_1(1-w_1)}{w_1(1-\bar{w}_1)}\,. \end{aligned} \tag{2.45}$$

The first entry of the first term is $\log(m_{12}^2/p_1^2)$, and its second entry is associated with the discontinuity in the variable m_{12}^2. The first entry of the second term is $\log(m_{13}^2/p_1^2)$, and its second entry is associated with the discontinuity in the variable m_{13}^2. The first entry of the third term corresponds to the threshold at $p_1^2 = (\sqrt{m_{12}^2} + \sqrt{m_{13}^2})^2$, and its second entry is associated with the discontinuity in the variable p_1^2. The argument of the logarithm in the first entry of this term is not a direct change of variables of $p_1^2 - (\sqrt{m_{12}^2} + \sqrt{m_{13}^2})^2$, which would not be a rational function. Nevertheless, one can verify that the condition $w_1(1-\bar{w}_1) > 0$ is exactly equivalent to the condition $p_1^2 > (\sqrt{m_{12}^2} + \sqrt{m_{13}^2})^2$, whenever $p_1^2 > 0$.

In this analysis, we have neglected the denominators p_1^2 in each of the first entries of eq. (2.45). We did this because the denominators are simply used to normalise the variables to be dimensionless: as we know, the physically meaningful first entry is the one including the mass threshold, which is nonzero for the p_1^2 channel. Indeed, since the three corresponding second entries sum to zero, we see that the term whose first entry would be p_1^2 has zero as its second entry.

We finish with a word of caution. Our claim is that one can generally write symbols of Feynman integrals in a form such as eq. (2.45), where *(i)* the first entries are directly identified with kinematic invariants and thresholds, and *(ii)* the second entries are the corresponding discontinuities, but that these two properties do not follow from one another. To see that property *(ii)* does not follow from property *(i)*, consider Example 2 above. The symbol of this triangle can also be written in the form

$$(w_1\bar{w}_1) \otimes \frac{\bar{w}_1}{1-\bar{w}_1} + ((1-w_1)(1-\bar{w}_1)) \otimes \frac{1-w_1}{w_1} + ((1-w_1)\bar{w}_1) \otimes \frac{w_1(1-\bar{w}_1)}{\bar{w}_1(1-w_1)}\,.$$

Here, the first entries have the same properties as in eq. (2.45), but the second entries do not correspond to the expected discontinuities. (In this case, the discrepancy is due to the choice of branch of the square root in the definitions of the variables w_1 and $\bar{w}_1$; the kinematics of the cut require a consistent choice of the positive branch.)

It is now clearer in which kinematic region it is natural to evaluate the discontinuity associated to a given kinematic invariant (this is also the region where discontinuities will be related to cuts of Feynman diagrams): it is the region

in which that particular invariant, be it a Mandelstam invariant or a squared internal mass, is outside of the euclidean region, while all other invariants remain in the euclidean region. Of course Disc is defined for any region: if we were to compute it in the region where all invariants remain in the euclidean region we would get zero. Conversely, the choice of taking only one of the invariants out of the euclidean region is made for simplicity, as we are thus sure that all branch cuts we probe are related to that particular invariant.

For iterated discontinuities, eq. (2.35), we simply iterate our procedure: we evaluate the iterated discontinuity in the region where all the invariants we are taking the discontinuity on are outside the euclidean region. In the relation between iterated discontinuities and the coproduct, eq. (2.41), the coefficients a_i are evaluated in the region R_i which is the region where the invariants $r_1, \ldots, r_i$ have been moved away from the euclidean region.

To make the calculation of discontinuities and their relation with the coproduct completely precise, we still have to say how the $\pm i0$ of the invariants is determined. This will be done in the next chapter when the connection with cuts of Feynman diagrams is established.

2.3.3 Example

We close this section with a simple example of the proposed relation in eq. (2.41) to make it more concrete.

Consider a three-point planar Feynman integral in $D = 4$ dimension with no massive propagators. After normalisation to unit leading singularity, it will be a dimensionless function of two ratios of Mandelstam invariants,

$$F\left(\frac{p_2^2}{p_1^2}, \frac{p_3^2}{p_1^2}\right). \tag{2.46}$$

We define variables $z, \bar{z}$ as in eq. (2.29),

$$\frac{p_2^2}{p_1^2} = z\bar{z}, \qquad \frac{p_3^2}{p_1^2} = (1-z)(1-\bar{z}), \qquad z > \bar{z}. \tag{2.47}$$

Suppose that we know that the symbol alphabet can be taken to be

$$\mathcal{A}_{\triangle} = \{z, \bar{z}, 1-z, 1-\bar{z}\}. \tag{2.48}$$

This is, in fact, the alphabet of the three-point ladder in $D = 4$ dimensions with massless propagators and any number of rungs [72, 84], and thus illustrates the parametrisation of eq. (2.26) for this class of diagrams.

The integral F is originally defined in the euclidean region where all $p_i^2 < 0$, i.e., in the massless limit of eq. (2.44). In terms of real-valued z, $\bar{z}$, there are three separate components of the euclidean region [65],

$$\bar{z} < z < 0\,, \qquad 0 < \bar{z} < z < 1, \qquad \text{and} \qquad 1 < \bar{z} < z.$$

For concreteness, we choose the component $R_{0,<} = \{\bar{z} < z < 0\}$, but the relations work equally well starting from either of the other components.

Let us take the first discontinuity in the channel $s_1 = p_2^2$. We analytically continue F to the region R_1 of the first cut, where $p_2^2 > 0$ and $p_1^2, p_3^2 < 0$. In terms of z and $\bar{z}$, $R_1 = R_{\triangle}^2 = \{\bar{z} < 0 < z < 1\}$, see table 2.1. For each letter $x_1 \in \mathcal{A}_{\triangle}$, the logarithms $\log x_1$ in the definition of $a_1(p_2^2, x_1)$ are written with positive arguments in the region $R_{0,<}$. For example, in $a_1(p_2^2, z)$ we compute the discontinuity of the analytic continuation of $\log(-z)$ rather than $\log(z)$. According to the usual Feynman rules the invariants have a positive imaginary part, $p_2^2 + i0$. We can thus deduce the corresponding imaginary parts in $z + i0$ and $\bar{z} - i0$ for the symbol alphabet, and we get:

$$\begin{aligned} a_1(p_2^2, z) &= \mathrm{Disc}_{p_2^2;R_1} \log(-z - i0) = -2\pi i\,, \\ a_1(p_2^2, \bar{z}) &= \mathrm{Disc}_{p_2^2;R_1} \log(-\bar{z} + i0) = 0\,, \\ a_1(p_2^2, 1-z) &= \mathrm{Disc}_{p_2^2;R_1} \log(1 - z - i0) = 0\,, \\ a_1(p_2^2, 1-\bar{z}) &= \mathrm{Disc}_{p_2^2;R_1} \log(1 - \bar{z} + i0) = 0\,. \end{aligned} \tag{2.49}$$

The discontinuities $\mathrm{Disc}_{p_2^2;R_1}$ have been computed directly using the definition in eq. (2.34). According to eq. (2.41), our relations among Disc and the coproduct is then

$$\mathrm{Disc}_{p_2^2} F \cong -(2\pi i)\, \Theta\, \delta_z F\,. \tag{2.50}$$

Let us take the second discontinuity in the channel $s_2 = p_3^2$. We analytically continue F to the region R_2 where $p_2^2, p_3^2 > 0$ and $p_1^2 < 0$. In terms of z and $\bar{z}$, $R_2 = R_{\triangle}^{2,3} = \{\bar{z} < 0, z > 1\}$, see table 2.1. The a_1's are the same as above. To compute the $a_2(p_3^2, x_2)$'s, we write the logarithms of the alphabet, $x_2 \in \mathcal{A}_{\triangle}$,

Name	Region of the p_i^2	Region of $z, \bar{z}$
$R_\triangle^1$	$p_1^2 > 0,\ \ p_2^2, p_3^2 < 0$	$\bar{z} < 0, \quad 1 < z$
$R_\triangle^{2,3}$	$p_1^2 < 0,\ \ p_2^2, p_3^2 > 0$	
$R_\triangle^2$	$p_2^2 > 0,\ \ p_1^2, p_3^2 < 0$	$\bar{z} < 0 < z < 1$
$R_\triangle^{1,3}$	$p_2^2 < 0,\ \ p_1^2, p_3^2 > 0$	
$R_\triangle^3$	$p_3^2 > 0,\ \ p_1^2, p_2^2 < 0$	$0 < \bar{z} < 1 < z$
$R_\triangle^{1,2}$	$p_3^2 < 0,\ \ p_1^2, p_2^2 > 0$	
$R_\triangle^*$	$p_1^2, p_2^2, p_3^2 > 0,$ and $\lambda < 0$	$z^* = \bar{z}$

Table 2.1: Some kinematic regions of 3-point integrals, classified according to the sign of the Mandelstam invariants. In the first six rows, $\lambda > 0$, so that z and $\bar{z}$ are real-valued, and we take $z > \bar{z}$ without loss of generality. z and $\bar{z}$ are defined in eq. (2.29)

with positive arguments in the region $R_1 = R_\triangle^2$. We will now decide that the imaginary part of p_3^2 should be conjugated when taking the second discontinuity (the reason for this will become clear when the connection with cut diagrams is established), so we deduce the signs of the imaginary parts in $z - i0$ and $\bar{z} - i0$ from $p_3^2 - i0$[4].

$$\begin{aligned} a_2(p_3^2, z) &= \mathrm{Disc}_{p_3^2;R_2} \log(z - i0) = 0\,, \\ a_2(p_3^2, \bar{z}) &= \mathrm{Disc}_{p_3^2;R_2} \log(-\bar{z} + i0) = 0\,, \\ a_2(p_3^2, 1-z) &= \mathrm{Disc}_{p_3^2;R_2} \log(1 - z + i0) = 2\pi i\,, \\ a_2(p_3^2, 1-\bar{z}) &= \mathrm{Disc}_{p_3^2;R_2} \log(1 - \bar{z} + i0) = 0\,. \end{aligned} \tag{2.51}$$

The only surviving term is $a_1(p_2^2, z)\, a_2(p_3^2, 1-z) = -(2\pi i)^2$, and the iterated discontinuity is then related to the coproduct according to:

$$\mathrm{Disc}_{p_2^2,p_3^2} F \cong -(2\pi i)^2\, \Theta\, \delta_{z,1-z} F\,. \tag{2.52}$$

Finally, we could consider taking discontinuities in all three channels with the operation $\mathrm{Cut}_{p_2^2,p_3^2,p_1^2}$. The region in which we would hope to detect this triple discontinuity has all $p_i^2 > 0$. Because F is a function of ratios of the Mandelstam invariants, eq. (2.46), this region is indistinguishable from the branch

[4]Determining the $\pm i0$ of symbol letters is not always as simple as we seem to suggest here. We comment on this issue in section 3.4.2.

cut-free euclidean region in $D = 4$. Therefore the function does not have any discontinuities in this region.

For completeness and for future reference, we close with the full list of relations for single and double discontinuities of this class of integrals.

$$\mathrm{Disc}_{p_1^2} F \cong (2\pi i)\,\Theta\,[\delta_z + \delta_{1-z}]F\,, \tag{2.53a}$$
$$\mathrm{Disc}_{p_2^2} F \cong -(2\pi i)\,\Theta\,\delta_z F\,, \tag{2.53b}$$
$$\mathrm{Disc}_{p_3^2} F \cong -(2\pi i)\,\Theta\,\delta_{1-z} F\,, \tag{2.53c}$$

$$\mathrm{Disc}_{p_1^2,p_2^2} F \cong (2\pi i)^2\,\Theta\,[\delta_{z,\bar{z}} + \delta_{1-z,\bar{z}}]F\,, \tag{2.54a}$$
$$\mathrm{Disc}_{p_2^2,p_1^2} F \cong (2\pi i)^2\,\Theta\,[\delta_{z,\bar{z}} + \delta_{z,1-z}]F\,, \tag{2.54b}$$
$$\mathrm{Disc}_{p_1^2,p_3^2} F \cong (2\pi i)^2\,\Theta\,[\delta_{z,1-z} + \delta_{1-z,1-z}]F\,, \tag{2.54c}$$
$$\mathrm{Disc}_{p_3^2,p_1^2} F \cong (2\pi i)^2\,\Theta\,[\delta_{1-z,\bar{z}} + \delta_{1-z,1-z}]F\,, \tag{2.54d}$$
$$\mathrm{Disc}_{p_2^2,p_3^2} F \cong -(2\pi i)^2\,\Theta\,\delta_{z,1-z} F\,, \tag{2.54e}$$
$$\mathrm{Disc}_{p_3^2,p_2^2} F \cong -(2\pi i)^2\,\Theta\,\delta_{1-z,\bar{z}} F\,. \tag{2.54f}$$

In the next chapter, we will show how these discontinuities are related to cuts of Feynman diagrams. There, we will also give further support for the relation between Disc and the coproduct by considering Feynman integrals with internal masses.

2.4 Summary and discussion

In this chapter we reviewed some important properties of MPLs that will be useful throughout this thesis. In particular, we discussed in some detail the coproduct of their Hopf algebra, which we saw was a natural tool to study the discontinuities of these functions. We introduced concepts such as the symbol and the symbol alphabet, which will play an important role in several of the following chapters.

We defined an operator Disc which computes discontinuities across physical branch cuts of Feynman integrals. We explained how one could define a kinematic region where we are away from any discontinuities, the euclidean region, which

is thus the natural region to evaluate Feynman integrals. We then saw that by moving away from the euclidean region we started to be sensitive to branch cuts associated with specific kinematic invariants. This allowed us to define a natural kinematic region where each discontinuity should be computed, depending on which branch cuts they were probing.

Finally, we established precise relations between the discontinuity operator Disc, and an operator δ, acting on the coproduct tensor, which selects specific truncations of this tensor. These relations contain the so-called first-entry condition (which we generalised to cases with massive propagators), corresponding to the evaluation of a single discontinuity, but were generalised to allow for iterated discontinuities. In section 2.3.3, we finished with explicit examples of these relations for three-point Feynman diagrams with massless propagators.

Some questions raised in this chapter were left unanswered, as for instance how to keep track of the imaginary part associated with each kinematic invariant when taking multiple discontinuities. Another question we did not address was whether all coproduct entries could be given an interpretation as multiple discontinuities on kinematic invariants. In the next chapter we will answer the first question, and make progress in answering the second. This will be achieved by giving a diagrammatic representation to the discontinuities of Feynman integrals, the so-called *cut Feynman diagrams*, and defining a set of rules to interpret and evaluate these diagrams.

Chapter 3

Cuts as iterated discontinuities

3.1 Introduction

In chapter 2, we studied the discontinuities of Feynman integrals evaluating to multiple polylogarithms across physical branch cuts, and related them to the coproduct of these functions. We established precise relations between multiple discontinuities and specific truncations of the coproduct tensor. In this chapter, we will give a diagrammatic representation to these discontinuities. The work presented here is covered in refs. [36, 37].

This subject has a long history. Indeed, soon after the formulation of the Landau conditions that identify the positions of branch points of Feynman integrals, a diagrammatic solution of these conditions was proposed in ref. [19]. This led to the development of so-called unitarity methods [20], which aimed at computing amplitudes and cross-sections by the study of their analytic properties, in particular their discontinuities, even in non-perturbative quantum field theories. Because of the successes of perturbation theory in the study of phenomenologically relevant quantum field theories in the late 70's, the 80's and the 90's, the interest of the community in unitarity based methods decreased.

However, it was then realised that these methods allowed to find very efficient ways of studying the properties of amplitudes at the loop level or even of computing them, both numerically and analytically. This led to the development of so called generalised unitarity methods [4, 5, 85, 86]. These are now widely used to make predictions for LHC phenomenological studies (see e.g. the reviews [87–90]).

In this chapter, we will look at unitarity in a form closer to the original formulation of [18, 19], with a similar approach to that of [21, 23]. In these references, the authors showed that a lot of the unitarity-based results obtained in the study of cross-sections and amplitudes were valid for individual Feynman diagrams. In particular, we will be interested in the observation that the discontinuity of Feynman integrals can be given a diagrammatic representation, through the so called *largest time equation*. The diagrams that evaluate to discontinuities of Feynman diagrams are called *cut diagrams*.

In this chapter, we review the work of [21, 23] about single unitarity cuts of Feynman diagrams. We then extend their results by defining multiple unitarity cuts. In [21,23] and [36], only cuts in external invariants were considered. In [37], rules were developed for cuts in internal masses. In sections 3.2 and 3.3 we present explicit rules for interpreting and evaluating the cut Feynman integrals in both cases. These rules will make clear how to determine the $i0$-prescription of invariants, a question we had left open in chapter 2.

We will then relate multiple unitarity cuts to discontinuities of Feynman integrals across physical channels. Using the results of the previous chapter, this implies a relation between unitarity cuts and coproduct entries. In section 3.4 we thus obtain a relation between Cut, the operator computing unitarity cuts of Feynman diagrams, Disc, the operator computing discontinuities across physical branch cuts of Feynman integrals, and δ, a well defined truncation of the coproduct tensor. These relations were first presented in [36] for diagrams with massless propagators and in [37] for diagrams with massive propagators.

To test our relations we had to develop efficient ways to compute cut diagrams. In section 3.5 we explain our methods in the context of a variety of one-loop examples. Then, in section 3.6 we study a two-loop example, the two-loop three-point ladder with three external massive legs. We checked the conjectured relations hold for all these examples. In appendices B and C we collected the explicit expressions we obtained for the cuts of the examples we investigated.

This chapter starts by reviewing the work of [21,23], but most of it corresponds to work done during my PhD, in collaboration with Ruth Britto, Claude Duhr, my supervisor Einan Gardi, and Hanna Grönqvist for the study of diagrams with internal masses.

3.2 Cuts in kinematic channels

We start by defining a cut in a kinematic channels: the operator Cut_s gives the sum of *cut* Feynman integrals, in which some propagators in the integrand of F are replaced by Dirac delta functions. These propagators themselves are called *cut propagators*. The sum is taken over all combinations of cut propagators that separate the diagram into two parts, in which the momentum flowing through the cut propagators from one part to the other corresponds to the Mandelstam invariant s. Furthermore, each cut is associated with a consistent direction of energy flow between the two parts of the diagram, in each of the cut propagators. In this work, we follow the conventions for cutting rules established in refs. [21,23], and extend them for sequential cuts.

First cut. Let us first review the cutting rules of refs. [21, 23]. We start by enumerating all possible partitions of the vertices of a Feynman diagram into two sets, coloured black (b) and white (w). Each such coloured diagram is then evaluated according to the following rules:

- Black vertices, and propagators joining two black vertices, are computed according to the usual Feynman rules.

- White vertices, and propagators joining two white vertices, are complex-conjugated with respect to the usual Feynman rules.

- Propagators joining a black and a white vertex are *cut* with an on-shell delta function, a factor of 2π to capture the complex residue correctly, *and* a theta function restricting energy to flow in the direction $b \to w$.

For a massless scalar theory, the rules for the first cut may be depicted as:

(3.1)

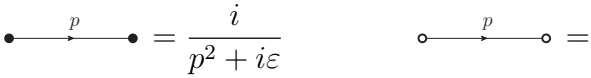

(3.2)

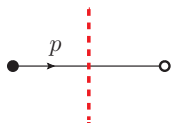

$$= 2\pi\,\delta\left(p^2\right)\theta\left(p_0\right) \tag{3.3}$$

The dashed line indicating a cut propagator is given for reference and does not add any further information. We write Cut_s to denote the sum of all diagrams belonging to the same momentum channel, i.e., in each of these diagrams, if p is the sum of all momenta through cut propagators flowing in the direction from black to white, then $p^2 = s$. Note that cut diagrams in a given momentum channel will appear in pairs that are black/white colour reversals — but of each pair, only one of the two can be consistent with the energies of the fixed external momenta, giving a potentially nonzero result.

We note that $\mathrm{Cut}_s\, F(z_1, \ldots, z_k)$ is a function of the variables z_i mentioned in eq. (2.26), which we recall can be complicated algebraic functions of the Mandelstam invariants. Finding the correct z_i in which to express a given Feynman integral is a nontrivial problem. Since cut Feynman integrals depend on the same variables as uncut diagrams but are simpler functions, the z_i can be more easily identified by computing cuts.

Sequential cuts. The diagrammatic cutting rules of refs. [21, 23] reviewed so far allow us to consistently define cut integrals corresponding to a single unitarity cut. These rules are insufficient for sequences of cuts, as they only allow us to partition a diagram in two parts, corresponding to connected areas of black and white vertices. In [36], the rules were then generalised to allow multiple unitarity cuts in different channels, and we now review the rules presented there. At this stage, we only state the rules, whose consistency is then backed up by the results we find in the remainder of this work.

In a sequence of diagrammatic cuts, energy-flow conditions are overlaid, and complex conjugation of vertices and propagators is applied sequentially. We continue to use black and white vertex colouring to show complex conjugation. We illustrate an example in fig. 3.1, which will be discussed below.

Consider a multiple-channel cut, $\mathrm{Cut}_{s_1,\ldots,s_k} I$. It is represented by the sum of all diagrams with a colour-partition of vertices for each of the cut invariants $s_i = p_i^2$. Assign a sequence of colours $(c_1(v), \ldots, c_k(v))$ to each vertex v of the diagram, where each c_i takes the value 0 or 1. For a given i, the colours c_i

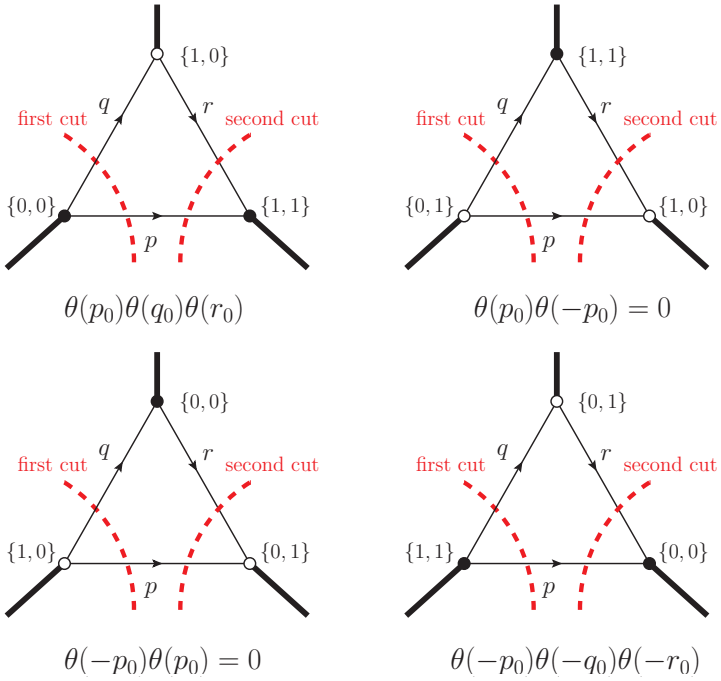

Figure 3.1: Sequential cuts of a triangle diagram, whose vertices v are labelled by all possible colour sequences $(c_1(v), c_2(v))$ encoding the cuts. Energy flows from 0 to 1 for each cut, giving the restrictions listed below each diagram.

partition the vertices into two sets, such that the total momentum flowing from vertices labeled 0 to vertices labeled 1 is equal to p_i. A vertex v is finally coloured according to $c(v) \equiv \sum_{i=1}^{k} c_i(v)$ modulo 2, with black for $c(v) = 0$ and white for $c(v) = 1$. The rules for evaluating a diagram are as follows.

- Black vertices are computed according to the usual Feynman rules; white vertices are computed according to complex-conjugated Feynman rules.

- A propagator joining vertices u and v is uncut if $c_i(u) = c_i(v)$ for all i. Then, if the vertices are black, i.e. $c(u) = c(v) = 0$, then the propagator is computed according to the usual Feynman rules, and if the vertices are white, i.e. $c(u) = c(v) = 1$, then the propagator is computed according to complex-conjugated Feynman rules.

- A propagator joining vertices u and v is cut if $c_i(u) \neq c_i(v)$ for any i. There is a theta function restricting the direction of energy flow from 0 to 1 for each i for which $c_i(u) \neq c_i(v)$. If different cuts impose conflicting energy flows, then the product of the theta functions is zero and the diagram gives no contribution.

- We exclude crossed cuts, as they do not correspond to the types of discontinuities captured by Disc and δ.[1] In other words, each new cut must be located within a region of identically-coloured vertices with respect to the previous cuts. In terms of the colour labels, this is equivalent to requiring that for any two values of i, j, exactly three of the four possible distinct colour sequences $(c_i(v), c_j(v))$ are present in the diagram. We give an example of a crossed cut we exclude in figure 3.2.

- Likewise, we exclude sequential cuts in which the channels are not all distinct. This restriction is made only because we have not found a general relation between such cuts and Disc or δ. In principle, there is no obstacle to computing these cut diagrams.

- We restrict ourselves to the use of real kinematics, both for internal and external momenta[2]. This implies, in particular, that diagrams with on-shell

[1] A similar restriction was proposed in refs. [91–93]. In chapter 5, we will see how crossed cuts can be computed as residues.

[2] This restriction will also be lifted in the generalised definition of cut given in 5.

massless three-point vertices must vanish in dimensional regularisation. The consistency of this choice will be verified in the examples considered in subsequent sections.

For massless scalar theory, the rules for sequential cut diagrams may then be depicted as follows:

(3.4)

(3.5)

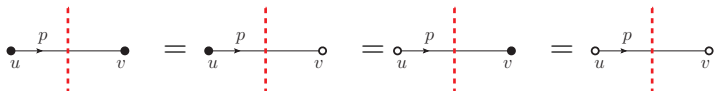

(3.6)

Let us make some comments about the diagrammatic cutting rules for multiple cuts we just introduced. First, we note that these rules are consistent with the corresponding rules for single unitarity cuts presented at the beginning of this section. Second, using these rules, it is clear that sequential cuts are independent of the order of cuts. Indeed, none of our rules depends on the order in which the cuts are listed. Finally, the dashed line is an incomplete shorthand merely indicating the location of the delta functions, but not specifying the direction of energy flow, for which one needs to refer to the colour indices. Our diagrams might also include multiple cut lines on individual propagators, such as

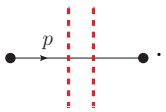

(3.7)

We also introduce notation allowing us to consider individual diagrams contributing to a particular cut, and possibly restricted to a particular kinematic region. When no region is specified for the planar examples given in this thesis, it is assumed that the cut invariants are taken to be above their threshold, i.e., outside of the euclidean region, while all other consecutive Mandelstam invariants

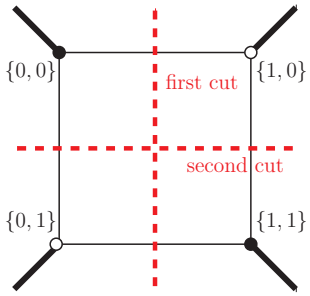

Figure 3.2: An example of crossed cuts, which we do not allow.

are below threshold, i.e., in the euclidean region, see the discussion in section 2.3.2. We write

$$\mathrm{Cut}_{s,[e_1\cdots e_w],R} D \tag{3.8}$$

to denote a diagram D cut in the channel s, in which exactly the propagators $e_1 \cdots e_w$ are cut, and computed in the kinematic region R. Rules of complex conjugation and energy flow will be apparent in the context of such a diagram.

Examples of sequential cuts. We briefly illustrate the diagrammatics of sequential cuts. Consider taking two cuts of a triangle integral. At one-loop order, a cut in a given channel is associated to a unique pair of propagators. We list the four possible colour partitions $\{c_1(v), \ldots, c_k(v)\}$ in fig. 3.1. The first graph is evaluated according to the rules above, giving

$$e^{\gamma_E \epsilon} \int \frac{d^D k}{\pi^{D/2}} i^2 (-i) (2\pi)^3 \, \delta(p^2)\delta(q^2)\delta(r^2) \, \theta(p_0)\theta(q_0)\theta(r_0). \tag{3.9}$$

The second and third graphs evaluate to zero, since the colour partitions give conflicting restrictions for the energy flow on the propagator labeled p. The fourth graph is similar to the first, but with energy flow located on the support of $\theta(-p_0)\theta(-q_0)\theta(-r_0)$. Just as for a single unitarity cut, in which only one of the two colourings is compatible with a given assigment of external momenta, there can be at most one nonzero diagram for a given topology of sequential cuts subject to fixed external momenta. In the examples calculated in the following sections of this paper, we will thus omit writing the sequences of colours $(c_1(v), \ldots, c_k(v))$. We may also omit writing the theta functions for energy flow in the cut integrals.

We include an example of crossed cuts, which we do not allow, in fig. 3.2.

Notice that there are four distinct colour sequences in the diagram, while we only allow three for any given pair of cuts.

Vanishing of cuts with on-shell massless three-point vertices. We now show more explicitly why a cut isolating a massless three-point vertex should vanish in dimensional regularisation. Let's look at an example, the box with two adjacent massive external legs (legs 1 and 2) and two massless ones (legs 3 and 4), the so-called two-mass-hard box. We consider the cut in the $t = (p_2 + p_3)^2$ channel and in the p_2^2 channel, see figure 3.3. This cut isolates a massless three-point vertex at the top right corner.

It is well known that this vertex, considered in real Minkowski space, requires collinear momenta. Let us see how this property manifests itself in the computation of the cut integral. Parametrise the loop momentum by $\ell = xp_3 + yp_4 + w\vec{q}$, where q is integrated over all values satisfying $q^2 = -1$ and $q \cdot p_i = 0$ for $i = 3, 4$. Then

$$\begin{aligned}\int d^D\ell\ \delta(\ell^2)\ \delta((\ell - p_4)^2)\ f(\ell) = &\int \frac{s}{2}\ dx\ dy\ w^{D-3} dw\ d\Omega^{D-3}\ \delta(xys - w^2) \\ &\delta((x(y-1)s - w^2)\ f(\ell) \\ =&\frac{1}{4}\int dy\ d\Omega^{D-3}\ dw\ \delta(w)\ w^{D-4}\ f(\ell).\end{aligned}$$

The delta functions set $x = w = 0$, so that $\ell = yp_4$, which is the familiar collinearity condition. We see that this cut vanishes for $D > 4$, which is what is required to regularise the infrared divergences appearing in massless diagrams. We will come back to this example in more detail in section 3.5.7, and will see how one can make sense of some cuts isolating massless three-point vertices in chapter 5.

3.3 Cuts in internal masses

In [37] we introduced a new kind of cut, a single-propagator cut, corresponding to discontinuities across branch cuts related to internal masses. Our discussion will be in the context of one-loop diagrams, but this is solely for the simplicity of the expressions, and all the results can be straightforwardly generalised to the planar multi-loop case.

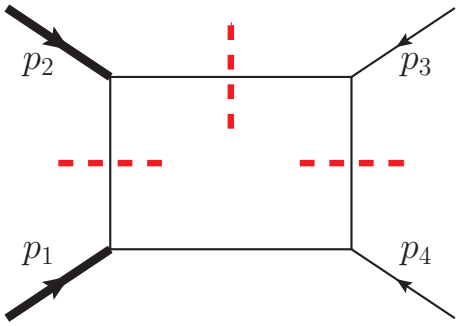

Figure 3.3: Cut isolating on-shell massless three-point vertices.

Let F be a one-loop diagram with n external legs of momentum p_i, with $i = 1, \ldots, n$, all incoming, massive or not, and with internal masses $m^2_{i,i+1}$ between legs i and $i+1$, which we assume are all distinct (we comment on the degenerate case in appendix D). Furthermore, we define $q_j = \sum_{i=1}^{j} p_i$, for $j = 1, \ldots, n$, so that $q_n = 0$. Then, according to our Feynman rules,

$$F(q_i \cdot q_j; m^2_{1,2}, \ldots, m^2_{1,n}) = (-1)^n e^{\gamma_E \epsilon} \int \frac{d^{D/2}k}{\pi^{D/2}} \prod_{i=1}^{n} \frac{1}{(k+q_i)^2 - m^2_{i,i+1} + i0} \,. \quad (3.10)$$

The integral F is evaluated away from any branch cut in the euclidean region of all kinematic invariants. The $+i0$ of the propagator can be reabsorbed into the squared mass, which means we can associate a $-i0$ prescription to the masses:

$$m^2_{i,i+1} \to m^2_{i,i+1} - i0 \,.$$

Although it does not correspond to a physical region, we can analytically continue F to a region where the square of one of the masses is negative (without loss of generality, say $m^2_{1,n} < 0$), while keeping all the other kinematic invariants in the euclidean region. In this region, following the definition of eq. (2.34), we

isolate the discontinuity associated with $m_{1,n}^2$:

$$\begin{aligned}
&\mathrm{Disc}_{m_{1,n}^2} F = F(q_i \cdot q_j; m_{1,2}^2, \ldots, m_{1,n}^2 - i0) - F(q_i \cdot q_j; m_{1,2}^2, \ldots, m_{1,n}^2 + i0) \\
&= (-1)^n e^{\gamma_E \epsilon} \int \frac{d^{D/2}k}{\pi^{D/2}} \left(\frac{1}{k^2 - m_{1,n}^2 + i0} - \frac{1}{k^2 - m_{1,n}^2 - i0} \right) \prod_{i=1}^{n-1} \frac{1}{(k+q_i)^2 - m_{i,i+1}^2} \\
&= (-1)^{n+1} e^{\gamma_E \epsilon} \int \frac{d^{D/2}k}{\pi^{D/2}} (2\pi i) \delta(k^2 - m_{1,n}^2) \prod_{i=1}^{n-1} \frac{1}{(k+q_i)^2 - m_{i,i+1}^2} \\
&\equiv \mathrm{Cut}_{m_{1,n}^2} F \,,
\end{aligned} \tag{3.11}$$

which shows that mass discontinuities do indeed correspond to single-particle cuts. We again stress that although we are discussing one-loop integrals, this is just for simplicity of the expressions. The same result holds for a multi-loop diagram.

Furthermore, we notice that F can also be a cut Feynman diagram as long as the propagator with mass $m_{1,n}^2$ has not been cut previously. Cuts in internal masses can then be combined with cuts in external channels to compute sequential discontinuities in internal masses and external channels.

We can thus deduce the rules for single-propagator cuts, corresponding to mass discontinuities: we simply replace the cut propagator by a delta function, according to

$$\frac{\pm i}{p^2 - m^2 \pm i0} \to 2\pi \delta(p^2 - m^2) \,, \tag{3.12}$$

without any condition on the energy flow or any further conjugation of other parts of the diagram. Unlike cuts in kinematic channels, the black and white colourings are unaffected by these cuts, as there is no notion of separation into two regions where one is complex-conjugated.

Diagrammatically, we will denote cuts in internal masses with a thick (thicker than for channel cuts) dashed line,

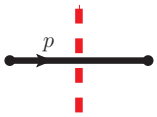

$$= 2\pi \, \delta \left(p^2 - m^2 \right) . \tag{3.13}$$

3.4 Cuts, discontinuities and coproduct entries

In the previous chapter, we introduced two operators giving consistent results for discontinuities, Disc, which computes discontinuities explicitly, and δ, which computes discontinuities by truncating specific components of the coproduct tensor. In the previous section, we introduced another type of discontinuity, corresponding to cut diagrams. We now show how these three types of discontinuities are related.

3.4.1 Cut diagrams and discontinuities

The rules for evaluating cut diagrams are designed to compute their discontinuities. For single cuts in internal masses, the relation is straightforward as can be seen from eq. (3.11). For cuts in external channels, there are some subtleties which we now review.

The original relation for the first cut in an external channel follows from the largest time equation [21–23], and the derivation may be found in refs. [21, 23]. The original relation is

$$F + F^* = -\sum_s \mathrm{Cut}_s\, F, \tag{3.14}$$

where the sum runs over all momentum channels. In terms of diagrams with coloured vertices, the left-hand side is the all-black diagram plus the all-white diagram. The right-hand side is -1 times the sum of all diagrams with mixed colours. We can isolate a single momentum channel s by analytic continuation into a kinematic region where among all the invariants, only s is away from the euclidean region. There, the left-hand side of eq. (3.14) can be recast[3] as $\mathrm{Disc}_s\, F$, while the right-hand side collapses to a single term:

$$\mathrm{Disc}_s\, F = -\,\mathrm{Cut}_s\, F. \tag{3.15}$$

In this relation, the discontinuity is evaluated with $s = s + i0$. Indeed, for an uncut diagram, the $+i0$-prescription of the propagators translates into a $+i0$-prescription for Mandelstam invariants.

[3]The apparent difference in relative sign between eq. (2.34) and eq. (3.14) is due to an explicit overall factor of i in every diagram, due to the Fourier transform from position to momentum space. Note therefore that eq. (2.34) should *not* be interpreted as the imaginary part of the function, and is in fact typically real-valued.

For sequential cuts in external channels, we argued in ref. [36] that the relation could be generalised so that $\mathrm{Cut}_{s_1,\ldots,s_k} F$ captures discontinuities through the relation

$$\mathrm{Cut}_{s_1,\ldots,s_k} F = (-1)^k \,\mathrm{Disc}_{s_1,\ldots,s_k} F, \tag{3.16}$$

where $\mathrm{Cut}_{s_1,\ldots,s_k} F$ is to be computed according to the rules given above for multiple cuts.

Eq. (3.16), like eq. (3.15), is valid in a specific kinematic region. As mentioned in the previous section, $\mathrm{Cut}_{s_1,\ldots,s_k} F$ is evaluated in the region where $s_1, \ldots, s_k$ are above their respective thresholds, the remaining external channels are below their thresholds, and all internal masses are positive. On the right-hand side, we proceed step by step according to the definition in eq. (2.35): each $\mathrm{Disc}_{s_1,\ldots,s_i}$ is evaluated after analytic continuation to the same region in which $\mathrm{Cut}_{s_1,\ldots,s_i} F$ is evaluated[4]. The $\pm i0$-prescription associated to each s_i is read from the cut diagram in which the cuts correspoding to $\mathrm{Cut}_{s_1,\ldots,s_{i-1}} F$ have been taken.

The relation between cuts in internal masses and discontinuities is trivial. For a single cut, the relation is given in eq. (3.11). It can be straightforwardly generalised as

$$\mathrm{Cut}_{m_1^2,\ldots,m_k^2} F = \mathrm{Disc}_{m_1^2,\ldots,m_k^2} F. \tag{3.17}$$

We can now combine cuts in internal masses and external channels through

$$\mathrm{Cut}_{s_1,\ldots,s_l,m_1^2,\ldots,m_k^2} F = (-1)^l \,\mathrm{Disc}_{s_1,\ldots,s_l,m_1^2,\ldots,m_k^2} F\,. \tag{3.18}$$

In order for eq. (3.18) to produce the correct signs, the $\pm i0$ associated to the internal masses on the right hand side are determined from the cut diagram in which all l of the channel cuts have been taken. (We recall that according to our rules, channel cuts imply complex conjugation of certain regions of the diagram, which affects the $i0$-prescription of the internal propagators. Hence we make it a rule to take channel discontinuities before mass discontinuities.) Furthermore, on the right hand side, we take a specific order of the listed invariants. Indeed, while sequential cuts are independent of the order in which the invariants are listed, the correspondences to Disc are derived in sequence so that the right-hand

[4]As mentioned in the discussion below eq. (2.41), we now see how the region where Disc should be evaluated follows from the region where Cut is evaluated.

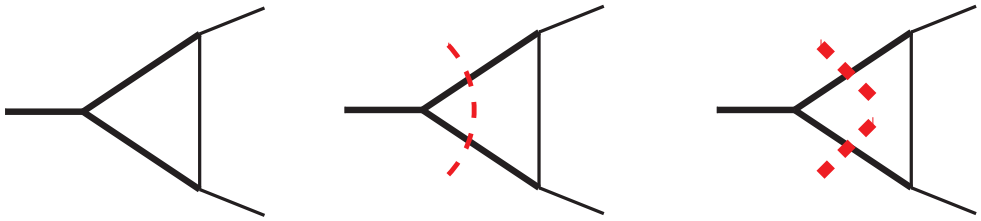

(a) $T(p_1^2; m_{12}^2, m_{13}^2)$ (b) $\text{Cut}_{p_1^2} T(p_1^2; m_{12}^2, m_{13}^2)$ (c) $\text{Cut}_{m_{12}^2, m_{13}^2} T(p_1^2; m_{12}^2, m_{13}^2)$

Figure 3.4: The uncut and two-propagator cuts of the triangle $T(p_1^2; m_{12}^2, m_{13}^2)$

side of eq. (3.18) takes a different form when channels and masses on the left-hand side are permuted. Thus, eq. (3.18) implies relations among the different $\text{Disc}_{s_1,\ldots,s_l,m_1^2,\ldots,m_k^2} F$.

We note one restriction: the cut integrals reproduce sequential discontinuities through the above relations only if each additional invariant in the subscript—whether a momentum channel or a mass—introduces at least one new cut propagator in the Feynman diagrams. For example, we would not consider $\text{Cut}_{p_1^2, m_{12}^2}$ of a one-loop triangle, since the propagator of mass m_{12}^2 was already cut in the first step, $\text{Cut}_{p_1^2}$.

A limit on multiple mass cuts

Cuts in multiple massive propagators vanish if the diagram is equivalent to the complete cut in a momentum channel. Consider for instance two massive propagators attached to the same external massive leg of a one-loop integral, as for example in fig. 3.4. Then the double discontinuity in those two internal masses will vanish. Let us now see why this is the case. Without loss of generality, we consider the cut in $m_{1,2}^2$ of $\text{Cut}_{m_{1,n}^2} F$ as given in eq. (3.11). The integral with cuts of the two propagators of masses $m_{1,n}^2$ and $m_{1,2}^2$, which is given by

$$(-1)^n \int \frac{d^{D/2}k}{\pi^{D/2}} (2\pi i)^2 \delta(k^2 - m_{1,n}^2) \delta((k+p_1)^2 - m_{1,2}^2) \prod_{i=2}^{n-1} \frac{1}{(k+q_i)^2 - m_{i,i+1}^2}\,, \tag{3.19}$$

can be used for either of the cut integrals $\text{Cut}_{m^2_{1,n},m^2_{1,2}}F$ as in fig. 3.4c, or $\text{Cut}_{p_1^2}F$ as in fig. 3.4b, depending on the kinematic region where it is evaluated.[5] If $p_1^2 \neq 0$, then the uncut integral F has a branch cut in p_1^2. As a consequence of the largest time equation, the integral $\text{Cut}_{p_1^2}F$ is proportional to the discontinuity of F across this branch cut [21, 23]. In particular, the discontinuity is zero when we are below the threshold of p_1^2, which can be realised either for $m^2_{1,2}, m^2_{1,n} > 0$ or $m^2_{1,2}, m^2_{1,n} < 0$, and in this case the integral eq. (3.19) vanishes as well.

Now, the double-cut integral $\text{Cut}_{m^2_{1,n},m^2_{1,2}}F$ must be evaluated in the region where $m^2_{1,2}, m^2_{1,n} < 0$ and all other invariants are below their thresholds. In particular, since p_1^2 is below its threshold, i.e. $p_1^2 < m^2_{1,2}+m^2_{1,n}+2\sqrt{m^2_{1,2}m^2_{1,n}}$ where we note that the right-hand-side is still real despite the masses being imaginary, the integral vanishes by the argument given above. We will see an example of this type of vanishing double cut in $T(p_1^2, 0, 0; m^2_{12}, 0, m^2_{13})$ in Section 3.5.4.

However, if $p_1^2 = 0$, then F has no branch cut associated with this external channel, and the largest time equation does not give any constraint on the result of eq. (3.19). In this case, the double discontinuity in the masses $m^2_{1,2}$ and $m^2_{1,n}$ can indeed be nonzero. We will see an example of this type of nonvanishing double cut in $T(p_1^2, 0, 0; m^2_{12}, m^2_{23}, 0)$ in Section 3.5.2.

This argument will hold for any pair of massive propagators in a one-loop diagram, not necessarily adjacent, provided that the corresponding momentum channel p satisfies $p^2 \neq 0$. At higher loops, one needs to be more careful: indeed, one might have more than one cut diagram contributing to the cut in a given channel, so it is no longer true that a cut diagram by itself must vanish if not evaluated in the region where the corresponding channel is below threshold.

3.4.2 Cuts and the coproduct

Having related cuts to discontinuities in the previous section and discontinuities to coproduct entries in section 2.3.1, it is now straightforward to relate cuts to coproduct entries. Combining the relations eq. (2.41) and eq. (3.18), we arrive at:

[5] For the first cut in a given timelike momentum channel, the consistent direction of energy flow in the cut propagators is an automatic consequence of the on-shell conditions.

$$\mathrm{Cut}_{s_1,\ldots,s_l,m_1^2,\ldots,m_k^2} F \cong$$
$$\Theta \sum_{(x_1,\ldots,x_l,y_1,\ldots,y_k)\in\mathcal{A}^{k+l}} (-1)^l \left(\prod_{i=1}^{l} a_i(s_i,x_i) \prod_{j=1}^{k} a_j(m_j^2,y_j)\right) \delta_{x_1,\ldots,x_l,y_1,\ldots,y_k} F\,. \quad (3.20)$$

We recall that on the left-hand side the s_i and the m_j^2 may be written in any order, and correspondingly permuted on the right-hand side, but we require that we act first with all the s_i and then with the m_j^2. It is not obvious that permutations of the sets $\{s_i\}$ and $\{m_j^2\}$ give equivalent results on the right-hand side, but this property follows from the commutativity of cuts. This implies nontrivial relations among coproduct entries.

$\pm i0$-prescription of symbol letters

In most examples considered in this thesis, it is simple to determine the sign of the $i0$-prescription of a given symbol letter once we know the prescription of the invariant to which it is associated and the kinematic region in which we are working (we recall the $i0$-prescription is read from the Feynman rules of cut diagrams). Indeed, whenever the symbol letters are linear combinations of invariants, this is a trivial problem. However, we observe that in more complicated cases there can be an ambiguity in the sign of the imaginary part of some symbol letters (more precisely, we encounter this problem for diagrams which require the use of eq. (2.29) to get a rational alphabet and have internal massive propagator). We need to resolve this ambiguity, because this sign is needed to obtain the correct sign in eq. (2.41).

The simplest case where we observe this problem is the triangle with three external masses and one internal mass, $T(p_1^2,p_2^2,p_3^2;m_{12}^2,0,0)$, whose symbol is given in eq. (B.64). For instance, when considering the double cut first in p_2^2 and then in p_1^2, we need to determine the sign of the imaginary part of $\bar{z}-\mu_{12}$, as inherited from the prescription of the second cut invariant, p_1^2-i0. One can easily check that this sign is the same as the sign of the quantity

$$\frac{\bar{z}(1-\bar{z})-\mu_{12}(z-\bar{z})}{z-\bar{z}}\,.$$

which can be either positive or negative in the region where the double cut is

computed,

$$z > 1\,, \quad 0 < \bar{z} < 1\,, \quad 0 < \mu_{12} < 1\,, \quad \bar{z} - \mu_{12} > 0\,.$$

If the imaginary part of $\bar{z} - \mu_{12}$ is negative, then we are in the subregion

$$z > 1\,, \qquad 0 < \bar{z} < 1\,, \qquad \frac{\bar{z}(1-\bar{z})}{z-\bar{z}} < \mu_{12} < \bar{z}\,,$$

and if it is positive, in the subregion

$$z > 1\,, \qquad 0 < \bar{z} < 1\,, \qquad 0 < \mu_{12} < \frac{\bar{z}(1-\bar{z})}{z-\bar{z}}\,.$$

We note that if we are in the first situation we cannot smoothly take the internal mass (μ_{12}) to zero. However, if we are in the second situation, corresponding to a positive imaginary part of $\bar{z} - \mu_{12}$, we can take μ_{12} to zero without any problem, which is naturally a desirable property. We thus associate a positive imaginary part to the symbol letter $\bar{z} - \mu_{12}$. We can confirm this is indeed the correct result by considering the same double cut in the opposite order, where there are no sign ambiguities. We treat this example in detail in section 3.5.

All other cases where we have found sign ambiguities can be solved in the same way: *we always require being in a kinematic region where massless limits can be taken smoothly*. Furthermore, we have found in all of our examples of multiple cuts that there is always an ordering of the cuts where there is no ambiguity. We have then verified that any possible ambiguities were correctly lifted through the method just described.

3.5 Examples — One-loop

We now give a range of examples of one-loop diagrams for which we have verified that the relations between cuts, discontinuities and the coproduct, eqs. (2.41), (3.18) and (3.20), give consistent results. Most of our examples will be three-point functions, with two exceptions: we will explore the two-mass-hard box as it shows we must be careful with choosing the right kinematic region when comparing cuts with discontinuities, and we will also look at the box with four external masses which in four dimensions turns out to be related to the triangle with three external masses. We will start by outlining the method used

to compute cuts, both in external channels and external masses, and then apply our methods to concrete examples.

3.5.1 Calculation of cut diagrams

We now outline our strategy for the calculation of cuts of the three-point functions studied in this section. For cuts in external channels, we use the method presented in ref. [36]. For the single-propagator cuts, we use the method presented in ref. [37]. All cuts given in appendices B.1, B.2 and B.3 were obtained through the methods described here.

Cuts in external channels. When computing a single cut in the channel p_i^2, we work in the region where p_i^2 is above its threshold, all other external channels are below threshold, and all masses are positive. We parametrise the external momenta as

$$p_i = \sqrt{p_i^2}(1, 0, \mathbf{0}_{D-2}), \qquad p_j = \sqrt{p_j^2}\left(\alpha, \sqrt{\alpha^2 - 1}, \mathbf{0}_{D-2}\right), \tag{3.21}$$

where α is trivial to determine in terms of the kinematic variables. If $p_j^2 = 0$, then an equivalent parametrisation is trivial to find.

We route the loop momentum so that the propagators of momentum k and $(p_i - k)$ are cut, and if possible the propagator of momentum k is massless. We parametrise k as

$$k = k_0(1, \beta\cos\theta, \beta\sin\theta\ \mathbf{1}_{D-2}), \tag{3.22}$$

where $\theta \in [0, \pi]$, and $k_0, \beta > 0$, and $\mathbf{1}_{D-2}$ ranges over unit vectors in the dimensions transverse to p_i and p_j. If the propagator of momentum k is massless, then $\beta = 1$.

In the most general case we need to consider for this thesis, using the delta function that puts the propagator of momentum k on-shell, the integration measure becomes

$$\begin{aligned}&\int d^{4-2\epsilon}k\,\delta(k^2 - m^2)\theta(k_0) = \\ =&\frac{2^{1-2\epsilon}\pi^{1-\epsilon}}{\Gamma(1-\epsilon)}\int_0^\infty dk_0\left(\sqrt{k_0^2 - m^2}\right)^{1-2\epsilon}\int_0^1 dx(1-x)^{-\epsilon}x^{-\epsilon},\end{aligned} \tag{3.23}$$

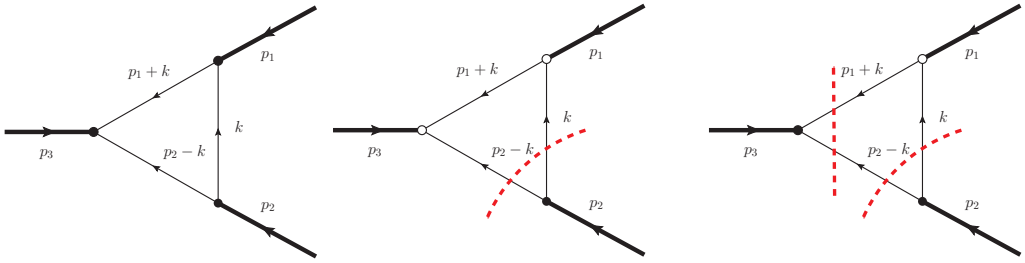

(a) $T(p_1^2, p_2^2, p_3^2)$ (b) $\text{Cut}_{p_2^2} T(p_1^2, p_2^2, p_3^2)$ (c) $\text{Cut}_{p_2^2, p_3^2} T(p_1^2, p_2^2, p_3^2)$

Figure 3.5: The triangle integral, with loop momentum defined as in the text; and with cuts in the p_2^2 and p_3^2 channels.

where we made a change of variables from $\cos\theta$ to

$$x = \frac{1 + \cos\theta}{2}. \tag{3.24}$$

The k_0 integral can be trivially performed using the delta function putting the propagator of momentum $(p_i - k)$ on-shell.

The remaining uncut propagator, of momentum $(p_j + k)$, is linear in the x variable, and so the most complicated result we will get for the single cut of a one-loop three-point function can be written to all orders in ϵ as a Gauss hypergeometric function, eq. (A.13), as can be seen in the several examples collected in appendices B.1, B.2 and B.3.

If the triangle has two or three external masses (say $p_i^2 \neq 0$ and $p_j^2 \neq 0$), we can compute its sequential cuts in the external channels p_i^2 and p_j^2, in the region where they are both above threshold, while the remaining external channel is below threshold and all internal masses are positive. The extra delta function makes the x integration in eq. (3.23) trivial (note, however, that it might restrict the kinematic region in which the cut is nonzero). The most complicated functions we get as a result are invariants raised to powers that are linear in ϵ, producing powers of logarithms upon expansion in ϵ. Again, our examples are collected in appendices B.1, B.2 and B.3.

Let's apply the procedure we just discussed to the triangle with three external masses and no internal massive propagators, $T(p_1^2, p_2^2, p_3^2; 0, 0, 0)$. We will compute the cut in the p_2^2 channel and then the double cut in the p_2^2 and p_3^2 channels, see figure 3.5. We will use the variables in eq. (2.29).

For the cut in p_2^2, the integral we have to compute is

$$\mathrm{Cut}_{p_2^2} T(p_1^2, p_2^2, p_3^2) = -(2\pi)^2 \frac{e^{\gamma_E \epsilon}}{\pi^{2-\epsilon}} \int d^{4-2\epsilon}k \frac{\delta^+(k^2)\,\delta^+((p_2-k)^2)}{(p_1+k)^2} \tag{3.25}$$

We parametrise the momenta as

$$p_2 = \sqrt{p_2^2}\,(1, \mathbf{0}_{D-1})\ , p_1 = \sqrt{p_1^2}\left(\alpha, \sqrt{\alpha^2-1}, \mathbf{0}_{D-2}\right). \tag{3.26}$$

Working out the kinematics,

$$\sqrt{p_1^2}\sqrt{p_2^2}\alpha = p_1^2 \frac{u_3 - 1 - u_2}{2}\,, \qquad \sqrt{p_1^2}\sqrt{p_2^2}\sqrt{\alpha^2-1} = -p_1^2 \frac{\sqrt{\lambda(1,u_2,u_3)}}{2}. \tag{3.27}$$

The loop momentum is parametrised as discussed above. Because one of the Dirac δ-functions sets $k^2 = 0$, $\beta = 1$. The other δ-functions fixes $k_0 = \sqrt{p_2^2}/2$. After changing variables as in eq. (3.24), we then have

$$(p_1+k)^2 = p_1^2\left(\frac{1+u_3-u_2-\sqrt{\lambda}}{2} + x\sqrt{\lambda}\right) = p_1^2(1-z)\left(1 - \frac{x(z-\bar{z})}{z-1}\right), \tag{3.28}$$

with z and $\bar{z}$ as defined in eq. (2.29). We note that these variables appear naturally in the calculation of the cut, simply as the variables that rationalise the parametrisation of the kinematics. The integral that remains to be computed is

$$\mathrm{Cut}_{p_2^2} T(p_1^2, p_2^2, p_3^2) = -2\pi \frac{e^{\gamma_E \epsilon}}{\Gamma(1-\epsilon)} \frac{(p_2^2)^{-\epsilon}}{p_1^2(1-z)} \int_0^1 dx \frac{(x(1-x))^{-\epsilon}}{\left(1 - \frac{x(z-\bar{z})}{z-1}\right)}. \tag{3.29}$$

It is easy to see that in the region where $p_2^2 > 0$ and $p_1^2, p_3^2 < 0$ this integral is well defined—see table 2.1 for the translation to a region for z and $\bar{z}$—and that it reproduces the result given in eq. (B.56).

For the double cut in the p_2^2 and p_3^2 channels, we now work in the region where $p_2^2, p_3^2 > 0$ and $p_1^2 < 0$, and we again refer to table 2.1 for the equivalent in terms of z and $\bar{z}$. We are now evaluating the integral

$$\begin{aligned}\mathrm{Cut}_{p_2^2,p_3^2} T(p_1^2, p_2^2, p_3^2) = \\ = i(2\pi)^3 \frac{e^{\gamma_E \epsilon}}{\pi^{2-\epsilon}} \int d^{4-2\epsilon}k\, \delta^+\left(k^2\right) \delta^+\left((p_2-k)^2\right) \delta^+\left((p_1+k)^2\right).\end{aligned} \tag{3.30}$$

We proceed exactly as for the cut in p_2^2, but the last equation is now trivial because of the new δ-function:

$$\delta\left((p_1+k)^2\right) = -\frac{1}{p_1^2(z-\bar{z})}\delta\left(x+\frac{1-z}{z-\bar{z}}\right). \tag{3.31}$$

Performing the integrations over k_0 and β as for the single cut, the remaining integral is

$$\begin{aligned}\mathrm{Cut}_{p_2^2,p_3^2}T(p_1^2,p_2^2,p_3^2) &= \\ &= -4\pi^2 i\frac{e^{\gamma_E\epsilon}}{\Gamma(1-\epsilon)}\frac{(p_3^2)^{-\epsilon}}{p_1^2(z-\bar{z})}\int_0^1 dx\delta\left(x+\frac{1-z}{z-\bar{z}}\right)(x(1-x))^{-\epsilon}\end{aligned} \tag{3.32}$$

which reproduces the result in eq. (B.58).

We should note that for one-loop integrals, a three-propagator cut has previously been interpreted as a discontinuity of a diagrammatic unitarity cut. In ref. [94], it was used in a double dispersion relation to verify the region of integration in phase space for semileptonic D decay. More recently, in ref. [8], a similar interpretation was given, in the spirit of the Feynman Tree Theorem [95–97], capitalizing on progress in unitarity methods for one-loop amplitudes.

Cuts in internal masses. Cuts in internal masses are harder to compute than cuts in external channels. We present two ways of computing them. In either case, we compute discontinuities, which are trivially related to cuts through eq. (3.11). The first way is a brute-force method that works in all cases considered here. The second way is more elegant, but only suitable for special configurations of the external and internal masses. Because we do not have a proof that it should work, we present it as an observation. In all cases where both can be applied we find they agree, giving evidence for the validity of the second way. We will illustrate both in the context of the triangle $T(0,p_2^2,p_3^2;m_{12}^2,0,0)$, see section B.2.3.

The first method relies on getting a Feynman parameter representation for the diagram, and then computing the discontinuity of the integrand across the branch cut associated with the internal mass. It is of course valid for any configuration

of the internal and external masses. As an example, we have:

$$T(p_2^2, p_3^2; m_{12}^2) = i\frac{e^{\gamma_E\epsilon}\Gamma(1+\epsilon)}{\epsilon}\int_0^1 dx(1-x)^{-\epsilon}\frac{((-p_3^2x)^{-\epsilon} - (m_{12}^2 - p_2^2x)^{-\epsilon})}{m_{12}^2 + x(p_3^2 - p_2^2)}\,, \tag{3.33}$$

which we obtain by computing the trivial and the first non-trivial Feynman parameter integrals. We then use

$$\text{Disc}_{m_{12}^2}\left[(m_{12}^2 - p_2^2x)^{-\epsilon}\right] = \frac{2\pi i\epsilon}{\Gamma(1-\epsilon)\Gamma(1+\epsilon)}(p_2^2x - m_{12}^2)^{-\epsilon}\theta\left(\frac{m_{12}^2}{p_2^2} - x\right)\,,$$

where we recall $m_{12}^2 = m_{12}^2 - i0$ and we are in the region $p_2^2 < m_{12}^2 < 0$, to get

$$\begin{aligned}\text{Cut}_{m_{12}^2}T(p_2^2, p_3^2; m_{12}^2) =& \,\text{Disc}_{m_{12}^2}\,T(p_2^2, p_3^2; m_{12}^2)\\ =& \frac{2\pi e^{\gamma_E\epsilon}}{\Gamma(1-\epsilon)}\int_0^{m_{12}^2/p_2^2} dx(1-x)^{-\epsilon}\frac{(p_2^2x - m_{12}^2)^{-\epsilon}}{m_{12}^2 + x(p_3^2 - p_2^2)}\,.\end{aligned} \tag{3.34}$$

which is trivial to evaluate to any desired accuracy in ϵ, see eq. (B.47).

The second way only works if there is a massive external leg non-adjacent to the massive internal leg being cut. More precisely, in our notation, if we look at the cut in the internal propagator of mass m_{ij}^2, we need $p_k^2 \neq 0$. We can then compute a three-propagator cut corresponding to $\text{Cut}_{p_k^2, m_{ij}^2}$ in the region where $m_{ij}^2 < 0$ and p_k^2 is above threshold. This is trivial to evaluate because all propagators are cut. The single-propagator cut is finally obtained through a dispersive integration in the p_k^2-channel of the three-propagator cut. This is not guaranteed to work a priori, because we have no proof that the m_{ij}^2-discontinuity function has a dispersive representation. However, it does give the correct answer in all the cases we have considered. The reason why this method is not valid for any configuration of internal and external masses is because there is no sequential cut associated to an external mass and an internal mass if they are adjacent.

For our example, we have $(i, j, k) = (1, 2, 3)$. The three-propagator cut is computed in the region where $p_3^2 > 0$ and $m_{12}^2 < 0$ and is given by

$$\begin{aligned}&\text{Cut}_{m_{12}^2, p_3^2}T(p_2^2, p_3^2; m_{12}^2) =\\ &\quad= -\frac{4\pi^2 i e^{\gamma_E\epsilon}}{\Gamma(1-\epsilon)}\frac{(p_3^2)^{-\epsilon}(-m_{12}^2)^{-\epsilon}}{(p_3^2 - p_2^2)^{1-\epsilon}}(p_3^2 + m_{12}^2 - p_2^2)^{-\epsilon}\theta(p_3^2 + m_{12}^2 - p_2^2)\,,\end{aligned} \tag{3.35}$$

Through a standard dispersive integral, see e.g. the brief discussion in section 4.2, we obtain

$$\begin{aligned}\mathrm{Cut}_{m_{12}^2} T(p_2^2, p_3^2; m_{12}^2) &= \mathrm{Disc}_{m_{12}^2} T(p_2^2, p_3^2; m_{12}^2) \\ &= -2\pi \frac{e^{\gamma_E \epsilon}}{\Gamma(1-\epsilon)} (-m_{12}^2)^{-\epsilon} \int_0^\infty \frac{ds}{s - p_3^2} \frac{s^{-\epsilon}}{(s-p_2^2)^{1-2\epsilon}} (s + m_{12}^2 - p_2^2)^{-\epsilon} \,. \end{aligned} \tag{3.36}$$

The integral is trivial to compute at any order in ϵ, and matches the result obtained in eq. (3.34).

In appendices B.1, B.2 and B.3, we collect several examples of cuts in massive internal legs. Whenever possible, the cuts were computed in both ways described above, and the results agreed.

Now that we have presented our methods for evaluating cuts of one-loop three point functions, we verify their predicted relations with discontinuities and the coproduct in a variety of examples, chosen to illustrate specific features we found relevant. All expressions will be written only up to finite terms of order ϵ^0, but we have checked their agreement to higher orders in ϵ.

3.5.2 $T\left(p_1^2, 0, 0; m_{12}^2, m_{23}^2, 0\right)$

In this example, we illustrate iterated cuts in internal masses and iterated cuts in one external channel and one internal mass. Expressions for the integral, its symbol and cuts can be found in appendix B.1.4. The euclidean region, which we denote by R_0, is

$$R_0 \,: \qquad m_{12}^2 > 0 \,, \qquad m_{23}^2 > 0 \,, \qquad p_1^2 < m_{12}^2. \tag{3.37}$$

Single cuts: For the single cut in the invariant r, where $r \in \{p_1^2, m_{12}^2, m_{23}^2\}$, we will move away from the euclidean region and into region R_1^r. These regions are, respectively,

$$\begin{aligned} R_1^{p_1^2} \,: &\qquad m_{12}^2 > 0 \,, \qquad m_{23}^2 > 0 \,, \qquad p_1^2 > m_{12}^2 \,, \\ R_1^{m_{12}^2} \,: &\qquad m_{12}^2 < 0 \,, \qquad m_{23}^2 > 0 \,, \qquad p_1^2 < m_{12}^2 \,, \\ R_1^{m_{23}^2} \,: &\qquad m_{12}^2 > 0 \,, \qquad m_{23}^2 < 0 \,, \qquad p_1^2 < m_{12}^2 \,. \end{aligned} \tag{3.38}$$

Recalling the prescriptions $p_1^2 + i0$ and $m_{ij}^2 - i0$, we can compute the coefficients $a_1(r, x_1)$ as defined in eq. (2.42). They are computed respectively in $R_1^{p_1^2}$, $R_1^{m_{12}^2}$ and $R_1^{m_{23}^2}$, and turn out to be equal. We find:

$$a_1(p_1^2, m_{12}^2 - p_1^2) = a_1(m_{12}^2, m_{12}^2) = a_1(m_{23}^2, m_{23}^2) = -2\pi i\,.$$

We then get:

$$\begin{aligned}
\mathrm{Cut}_{p_1^2} T &= -\,\mathrm{Disc}_{p_1^2}\, T \cong -\frac{2\pi}{p_1^2}\Theta\delta_{m_{12}^2-p_1^2}\mathcal{T} = \frac{2\pi}{p_1^2}\log\left(1 - \frac{m_{12}^2 - p_1^2}{m_{23}^2}\right), \\
\mathrm{Cut}_{m_{12}^2} T &= \mathrm{Disc}_{m_{12}^2}\, T \cong \frac{2\pi}{p_1^2}\Theta\delta_{m_{12}^2}\mathcal{T} = -\frac{2\pi}{p_1^2}\log\left(\frac{m_{23}^2}{m_{23}^2 - m_{12}^2}\right), \\
\mathrm{Cut}_{m_{23}^2} T &= \mathrm{Disc}_{m_{23}^2}\, T \cong \frac{2\pi}{p_1^2}\Theta\delta_{m_{23}^2}\mathcal{T} = \frac{2\pi}{p_1^2}\log\left(1 - \frac{p_1^2}{m_{12}^2 - m_{23}^2}\right),
\end{aligned} \tag{3.39}$$

which are consistent with the results in appendix B.1.4.

All relations for single cuts follow the same pattern, so we will simply list them without further details in the remaining examples, unless we wish to illustrate some particularity in a given case.

Double cuts: According to our rules, there are two different cuts to consider: $\mathrm{Cut}_{p_1^2,m_{23}^2}$ and $\mathrm{Cut}_{m_{12}^2,m_{23}^2} = \mathrm{Cut}_{m_{23}^2,m_{12}^2}$. We start with $\mathrm{Cut}_{p_1^2,m_{23}^2}$, for which we go from the region $R_1^{p_1^2}$ to the region

$$R_2^{p_1^2,m_{23}^2}\ :\qquad m_{12}^2 > 0\,,\qquad m_{23}^2 < 0\,,\qquad p_1^2 > m_{12}^2\,. \tag{3.40}$$

Given our conventions for multiple cuts, we now have the prescription $m_{23}^2 + i0$. Then,

$$a_2\left(m_{23}^2, m_{23}^2\right) = 2\pi i\,,\qquad a_2\left(m_{23}^2, p_1^2 + m_{23}^2 - m_{12}^2\right) = 2\pi i\theta\left(m_{12}^2 - p_1^2 - m_{23}^2\right)\,,$$

where we have only listed the coefficients leading to nonzero contributions. We finally find

$$\begin{aligned}
\mathrm{Cut}_{p_1^2,m_{23}^2} T &= -\,\mathrm{Disc}_{p_1^2,m_{23}^2}\, T \\
&\cong -\frac{4\pi^2 i}{p_1^2}\Theta\left[\delta_{m_{12}^2-p_1^2,m_{23}^2} + \theta\left(m_{12}^2 - p_1^2 - m_{23}^2\right)\delta_{m_{12}^2-p_1^2,m_{12}^2-p_1^2-m_{23}^2}\right]\mathcal{T}
\end{aligned}$$

$$= -\frac{4\pi^2 i}{p_1^2}\theta(m_{23}^2 + p_1^2 - m_{12}^2)\,, \tag{3.41}$$

which matches the result of the direct calculation in B.1.4. Interestingly, even the theta functions are correctly reproduced, which is a feature observed in all our examples. We recall that when computing multiple cuts in external channels and internal masses, we insist on taking the discontinuity first in the external invariants, and then in the masses. It can easily be checked that if we had taken the opposite order, we would have had the opposite sign in the above equation.

We now consider the double cut in the internal masses. This is an example of the behaviour described in section 3.4.1, where a double cut in internal masses attached to the same external massless leg is nonzero. We only give details for one order of the invariants, first m_{12}^2 and then m_{23}^2. The opposite order can be done in exactly the same way.

To compute $\mathrm{Cut}_{m_{12}^2,m_{23}^2}$, we must go from $R_1^{m_{12}^2}$ to

$$R_2^{m_{12}^2,m_{23}^2}\ : \qquad m_{12}^2 < 0\,, \qquad m_{23}^2 < 0\,, \qquad p_1^2 < m_{12}^2\,.$$

Because mass cuts do not require complex conjugation of any region of the diagram, we still have the prescription $m_{23}^2 - i0$. The coefficients $a_2(m_{23}^2, x_2)$ giving nonzero contributions are

$$a_2(m_{23}^2, m_{23}^2) = -2\pi i\,, \qquad a_2(m_{23}^2, m_{23}^2 - m_{12}^2) = -2\pi i\theta(m_{12}^2 - m_{23}^2).$$

We then find

$$\begin{aligned}\mathrm{Cut}_{m_{12}^2,m_{23}^2} T &= \mathrm{Disc}_{m_{12}^2,m_{23}^2} T \\ &= -\frac{4\pi^2 i}{p_1^2}\Theta\left[\delta_{m_{12}^2,m_{23}^2} + \theta(m_{12}^2 - m_{23}^2)\delta_{m_{12}^2,m_{23}^2-m_{12}^2}\right]\mathcal{T} \\ &= \frac{4\pi^2 i}{p_1^2}\theta(m_{12}^2 - p_1^2 - p_{23}^2)\theta(m_{23}^2 - m_{12}^2)\,,\end{aligned} \tag{3.42}$$

which matches the result of the direct calculation in B.1.4. Taking the discontinuities in the opposite order, we would have found

$$\begin{aligned}
&\mathrm{Cut}_{m_{23}^2,m_{12}^2} T = \mathrm{Disc}_{m_{23}^2,m_{12}^2} T \\
&= -\frac{4\pi^2 i}{p_1^2}\Theta\left[\theta(p_1^2+m_{23}^2-m_{12}^2)\delta_{m_{23}^2,m_{12}^2-p_1^2-m_{23}^2}+\theta(m_{23}^2-m_{12}^2)\delta_{m_{23}^2,m_{23}^2-m_{12}^2}\right]\mathcal{T} \\
&= \frac{4\pi^2 i}{p_1^2}\theta(m_{12}^2-p_1^2-p_{23}^2)\theta(m_{23}^2-m_{12}^2)\,, \qquad (3.43)
\end{aligned}$$

which also matches the direct calculation.

While it is obvious that $\mathrm{Cut}_{m_{12}^2,m_{23}^2} T = \mathrm{Cut}_{m_{23}^2,m_{12}^2} T$, we see that they are related to different coproduct entries. This is an example of how the underlying relation between coproduct entries and cut diagrams constrains the symbol/coproduct of Feynman diagrams.

We finish this example with a comment. As mentioned previously, for triangle integrals we cannot set up a double cut in an external momentum and an internal mass attached to it, like p_1^2 and m_{12}^2 in this example, because there is no additional propagator to cut at the second stage. Correspondingly, if we were to attempt to relate Disc and the coproduct for this double cut as in the above exercise, we would be stuck when taking the second discontinuity, as the $\pm i0$ prescription of the second invariant is not well-defined. Thus, even in this case, there is no conflict among Cut, Disc and the coproduct.

3.5.3 $T\left(0, p_2^2, p_3^2; m_{12}^2, 0, 0\right)$

In this example, we illustrate iterated cuts in external channels, and we give another example of iterated cuts in one external channel and one internal mass. Expressions for the integral, its symbol and cuts can be found in appendix B.2.3. The euclidean region, which we denote R_0 (we reuse the same notation as above for all examples, since there is no ambiguity and to avoid having too many indices), is

$$R_0: \qquad m_{12}^2 > 0\,, \qquad p_2^2 < m_{12}^2\,, \qquad p_3^2 < 0. \qquad (3.44)$$

The single discontinuities are treated as above and obey the expected relations, so we will not go through the derivation. The result for the cuts can be found in eqs. (B.45), (B.46) and (B.47). For double discontinuities, we consider two different double cuts: $\mathrm{Cut}_{p_3^2,m_{12}^2}$ and $\mathrm{Cut}_{p_2^2,p_3^2} = \mathrm{Cut}_{p_3^2,p_2^2}$. The first one is very similar to what we did before so we will not address it in detail here, the result

for this double cut is found in eq. (B.49). The second one is a new kind. In particular, we will show that both orders of taking the discontinuities give the same result.

(p_2^2, p_3^2) : We must analytically continue the function from

$$R_1^{p_2^2} : \qquad m_{12}^2 > 0\,, \qquad p_2^2 > m_{12}^2\,, \qquad p_3^2 < 0\,, \tag{3.45}$$

to

$$R_2^{p_2^2,p_3^2} : \qquad m_{12}^2 > 0\,, \qquad p_2^2 > m_{12}^2\,, \qquad p_3^2 > 0. \tag{3.46}$$

In this region, the nonvanishing coefficients $a_2(p_3^2, x_2)$ are

$$a_2(p_3^2, p_3^2) = 2\pi i\,, \qquad a_2(p_3^2, p_2^2 - m_{12}^2 - p_3^2) = 2\pi i\theta(m_{12}^2 - p_2^2 + p_3^2).$$

We then find

$$\begin{aligned}\mathrm{Cut}_{p_2^2,p_3^2} T &= \mathrm{Disc}_{p_2^2,p_3^2} T \\ &\cong \frac{4\pi^2 i}{p_2^2 - p_3^2}\Theta\left[\delta_{p_2^2 - m_{12}^2, p_3^2} + \theta(m_{12}^2 - p_2^2 + p_3^2)\delta_{p_2^2 - m_{12}^2, p_2^2 - m_{12}^2 - p_3^2}\right]\mathcal{T} \\ &= \frac{4\pi^2 i}{p_2^2 - p_3^2}\theta(p_2^2 - m_{12}^2 - p_3^2)\,.\end{aligned} \tag{3.47}$$

(p_3^2, p_2^2) : We now start in the region

$$R_1^{p_3^2} : \qquad m_{12}^2 > 0\,, \qquad p_2^2 < m_{12}^2\,, \qquad p_3^2 < 0 \tag{3.48}$$

and go to the same region $R_2^{p_3^2,p_2^2}$ as above. The coefficients $a_2(p_2^2, x_2)$ are

$$a_2(p_2^2, m_{12}^2 - p_2^2 + p_3^2) = 2\pi i\theta(p_2^2 - m_{12}^2 - p_3^2)$$

and thus

$$\begin{aligned}\mathrm{Cut}_{p_3^2,p_2^2} T &= \mathrm{Disc}_{p_3^2,p_2^2} T \\ &\cong \frac{4\pi^2 i}{p_2^2 - p_3^2}\Theta\left[\theta(p_2^2 - m_{12}^2 - p_3^2)\delta_{p_3^2, m_{12}^2 - p_2^2 + p_3^2}\right]\mathcal{T} \\ &= \frac{4\pi^2 i}{p_2^2 - p_3^2}\theta(p_2^2 - m_{12}^2 - p_3^2)\,,\end{aligned} \tag{3.49}$$

as above.

As expected, the two orderings of taking discontinuities match the direct calculation of the double cut, and we again find non-trivial relations between coproduct entries.

3.5.4 $T\left(p_1^2, 0, 0; m_{12}^2, 0, m_{13}^2\right)$

In this example, we show how the relations between discontinuities and the coproduct generalise when we must use variables such as the ones defined in eq. (2.33) to get a symbol with rational letters. In particular, we hope to make clearer the discussion below eq. (2.45). Finally, we also illustrate the discussion in section 3.4.1: as predicted, we show that the double cut in the two internal masses vanishes.

Expressions for the integral, its symbol, and its cuts can be found in appendix B.1.5. The euclidean region is

$$R_0 : \qquad m_{12}^2 > 0\,, \qquad m_{13}^2 > 0\,, \qquad p_1^2 < \left(\sqrt{m_{12}^2} + \sqrt{m_{13}^2}\right)^2 . \tag{3.50}$$

To simplify our discussion, we will restrict the euclidean region to the subregion R_{0*}, defined by

$$R_{0*} : \qquad m_{12}^2 > 0\,, \qquad m_{13}^2 > 0\,, \qquad p_1^2 < 0 \quad \Rightarrow \quad \bar{w}_1 < 0\,, \qquad w_1 > 1. \tag{3.51}$$

Our discussion would be similar if we had started from the other subregion of the euclidean region (i.e., the region where p_1^2 is positive but below threshold).

Single cuts: For the single cut in the invariant r, with $r \in \{p_1^2, m_{12}^2, m_{23}^2\}$, we will move away from the euclidean region and into region R_1^r. These three regions are

$$\begin{aligned}
R_1^{p_1^2} &: \quad m_{12}^2 > 0\,, \quad m_{13}^2 > 0\,, \quad p_1^2 > \left(\sqrt{m_{12}^2} + \sqrt{m_{13}^2}\right)^2 \Rightarrow \quad 0 < \bar{w}_1 < w_1 < 1, \\
R_1^{m_{12}^2} &: \quad m_{12}^2 < 0\,, \quad m_{13}^2 > 0\,, \quad p_1^2 < 0 \quad \Rightarrow \quad 0 < \bar{w}_1 < 1 < w_1, \\
R_1^{m_{13}^2} &: \quad m_{12}^2 > 0\,, \quad m_{13}^2 < 0\,, \quad p_1^2 < 0 \quad \Rightarrow \quad \bar{w}_1 < 0 < w_1 < 1\,.
\end{aligned} \tag{3.52}$$

For the discontinuity in the p_1^2 channel, we first note that, in region $R_1^{p_1^2}$, p_1^2+i0 implies w_1+i0 and $\bar{w}_1-i0$. Then, the nonzero coefficients $a_1(p_1^2,x_1)$ are

$$a_1(p_1^2,\bar{w}_1)=2\pi i\,,\qquad a_1(p_1^2,1-w_1)=2\pi i\,. \tag{3.53}$$

The relation between Cut, Disc and the coproduct is

$$\begin{aligned}\mathrm{Cut}_{p_1^2}T=&-\mathrm{Disc}_{p_1^2}T\\ \cong&\frac{2\pi}{p_1^2}\Theta\left[\delta_{\bar{w}_1}+\delta_{1-w_1}\right]\mathcal{T}\\ =&\frac{2\pi}{p_1^2}\left(\log\left(\frac{w_1}{1-w_1}\right)-\log\left(\frac{\bar{w}_1}{1-\bar{w}_1}\right)\right).\end{aligned} \tag{3.54}$$

Similarly, for the discontinuity in the mass m_{12}^2, we note that, in region $R_1^{m_{12}^2}$, m_{12}^2-i0 implies w_1+i0 and $\bar{w}_1+i0$. The nonzero coefficients $a_1(m_{12}^2,x_1)$ are

$$a_1(m_{12}^2,\bar{w}_1)=-2\pi i\,, \tag{3.55}$$

and we then find

$$\mathrm{Cut}_{m_{12}^2}T=\mathrm{Disc}_{m_{12}^2}T\cong\frac{2\pi}{p_1^2}\Theta\delta_{\bar{w}_1}\mathcal{T}=\frac{2\pi}{p_1^2}\log\left(\frac{w_1}{w_1-1}\right). \tag{3.56}$$

Finally, for the discontinuity in the mass m_{13}^2, we note that, in region $R_1^{m_{13}^2}$, m_{13}^2-i0 implies w_1-i0 and $\bar{w}_1-i0$. The nonzero coefficients $a_1(m_{13}^2,x_1)$ are

$$a_1(m_{13}^2,1-w_1)=-2\pi i\,, \tag{3.57}$$

and we find

$$\mathrm{Cut}_{m_{13}^2}T=\mathrm{Disc}_{m_{13}^2}T\cong\frac{2\pi}{p_1^2}\Theta\delta_{1-w_1}\mathcal{T}=-\frac{2\pi}{p_1^2}\log\left(\frac{-\bar{w}_1}{1-\bar{w}_1}\right). \tag{3.58}$$

We finish the discussion of these single cuts with three comments. First, we note that eqs. (3.54), (3.56) and (3.58) reproduce the direct calculation of the cuts in eqs. (B.22), (B.23) and (B.24) as expected. Second, we have confirmed eq. (2.45) as, in that form, we can indeed read the correct (symbol of the) discontinuity across the branch cut of each of the invariants appearing in the

first entry. Finally, we have shown that writing the symbol in the special form of eq. (2.45) is not necessary or even natural from the point of view of the relations between Disc and δ, as the relations are formulated in terms of individual symbol letters and not some particular combination of them. In other cases where similar variables are needed, we prefer to present the most compact expression of the symbol.

Double cuts: The only double cut we can consider is the double cut in the internal masses. Since the two masses are connected to an external massive leg, we claimed in section 3.4.1 that these double cuts should vanish. We now show this observation agrees with what one gets from the coproduct.

The double cut $\mathrm{Cut}_{m_{12}^2,m_{13}^2}T = \mathrm{Cut}_{m_{13}^2,m_{12}^2}T$ is computed in the region

$$R_2^{m_{12}^2,m_{13}^2}: \qquad m_{12}^2<0\,, \qquad m_{13}^2<0\,, \qquad p_1^2<\left(\sqrt{m_{12}^2}+\sqrt{m_{13}^2}\right)^2. \tag{3.59}$$

In terms of the variables w_1 and $\bar{w}_1$, this region is split into two disconnected subregions $R_{2a}^{m_{12}^2,m_{13}^2}$ and $R_{2b}^{m_{12}^2,m_{13}^2}$,

$$R_{2a}^{m_{12}^2,m_{13}^2}: \quad \bar{w}_1<w_1<0\,; \qquad\qquad R_{2b}^{m_{12}^2,m_{13}^2}: \quad 1<\bar{w}_1<w_1. \tag{3.60}$$

For $\mathrm{Cut}_{m_{12}^2,m_{13}^2}T$, we start in region $R_1^{m_{12}^2}$. In $R_{2a}^{m_{12}^2,m_{13}^2}$, m_{13}^2-i0 implies w_1+i0, and the nonvanishing coefficients $a_2(m_{13}^2,x_2)$ are

$$a_2(m_{13}^2,w_1)=2\pi i\,, \qquad a_2(m_{13}^2,1-w_1)=2\pi i\,.$$

We then get

$$\mathrm{Cut}_{m_{12}^2,m_{13}^2}T=\mathrm{Disc}_{m_{12}^2,m_{13}^2}T\cong-\frac{4\pi^2 i}{p_1^2}\Theta\left[\delta_{\bar{w}_1,w_1}+\delta_{\bar{w}_1,1-w_1}\right]\mathcal{T}=0\,. \tag{3.61}$$

In $R_{2b}^{m_{12}^2,m_{13}^2}$, all the coefficients $a_2(m_{13}^2,x_2)$ vanish so that we again find

$$\mathrm{Cut}_{m_{12}^2,m_{13}^2}T=\mathrm{Disc}_{m_{12}^2,m_{13}^2}T=0\,. \tag{3.62}$$

For $\mathrm{Cut}_{m_{13}^2,m_{23}^2}T$, we start in region $R_1^{m_{13}^2}$. In $R_{2a}^{m_{12}^2,m_{13}^2}$, all the coefficients

$a_2(m_{13}^2, x_2)$ vanish and we get

$$\mathrm{Cut}_{m_{13}^2,m_{12}^2} T = \mathrm{Disc}_{m_{12}^2,m_{13}^2} T = 0\,. \tag{3.63}$$

In $R_{2b}^{m_{12}^2,m_{13}^2}$, $m_{12}^2 - i0$ implies $\bar{w}_1 + i0$. The nonvanishing coefficients $a_2(m_{13}^2, x_2)$ are

$$a_2(m_{12}^2, \bar{w}_1) = 2\pi i\,, \qquad a_2(m_{12}^2, 1-\bar{w}_1) = 2\pi i$$

and we get

$$\mathrm{Cut}_{m_{13}^2,m_{12}^2} T = \mathrm{Disc}_{m_{12}^2,m_{13}^2} T \cong \frac{4\pi^2 i}{p_1^2} \Theta\left[\delta_{1-w_1,\bar{w}_1} + \delta_{1-w_1,1-\bar{w}_1}\right] \mathcal{T} = 0\,. \tag{3.64}$$

We thus find consistent results in all subregions and for either order of the discontinuities: in all cases, the result of the double discontinuity is zero. As already mentioned, this result illustrates the discussion in 3.4.1.

3.5.5 $T(p_1^2, p_2^2, p_3^2; 0, 0, 0)$

Single cuts: We already discussed the relations between discontinuities and the coproduct of the three-mass triangle in some detail in section 2.3.3. What was missing there was the relation with cuts, but we can now complete these relations (we keep F as a function describing a general three-point function with massless propagators and three-massive external legs):

$$\mathrm{Cut}_{p_1^2} F = -\,\mathrm{Disc}_{p_1^2} F \cong -(2\pi i)\,\Theta\left[\delta_z + \delta_{1-z}\right] F\,, \tag{3.65a}$$

$$\mathrm{Cut}_{p_2^2} F = -\,\mathrm{Disc}_{p_2^2} F \cong (2\pi i)\,\Theta\,\delta_z F\,, \tag{3.65b}$$

$$\mathrm{Cut}_{p_3^2} F = -\,\mathrm{Disc}_{p_3^2} F \cong (2\pi i)\,\Theta\,\delta_{1-z} F\,, \tag{3.65c}$$

These relations can be checked with the results in eq. (B.3.1), and by taking $F = \mathcal{T}(z, \bar{z})$ as defined in eq. (B.53).

Double cuts: As for single cuts, the relation between coproduct and discon-situies for double discontinuities as already been described in section 2.3.3. We

now complete them by relating them to cuts.

$$\mathrm{Cut}_{p_1^2,p_2^2} F = \mathrm{Disc}_{p_1^2,p_2^2} F \cong (2\pi i)^2 \,\Theta\,[\delta_{z,\bar{z}} + \delta_{1-z,\bar{z}}]F\,, \tag{3.66a}$$

$$\mathrm{Cut}_{p_2^2,p_1^2} F = \mathrm{Disc}_{p_2^2,p_1^2} F \cong (2\pi i)^2 \,\Theta\,[\delta_{z,\bar{z}} + \delta_{z,1-z}]F\,, \tag{3.66b}$$

$$\mathrm{Cut}_{p_1^2,p_3^2} F = \mathrm{Disc}_{p_1^2,p_3^2} F \cong (2\pi i)^2 \,\Theta\,[\delta_{z,1-z} + \delta_{1-z,1-z}]F\,, \tag{3.66c}$$

$$\mathrm{Cut}_{p_3^2,p_1^2} F = \mathrm{Disc}_{p_3^2,p_1^2} F \cong (2\pi i)^2 \,\Theta\,[\delta_{1-z,\bar{z}} + \delta_{1-z,1-z}]F\,, \tag{3.66d}$$

$$\mathrm{Cut}_{p_2^2,p_3^2} F = \mathrm{Disc}_{p_2^2,p_3^2} F \cong -(2\pi i)^2 \,\Theta\,\delta_{z,1-z} F\,, \tag{3.66e}$$

$$\mathrm{Cut}_{p_3^2,p_2^2} F = \mathrm{Disc}_{p_3^2,p_2^2} F \cong -(2\pi i)^2 \,\Theta\,\delta_{1-z,\bar{z}} F\,. \tag{3.66f}$$

These relations can be checked with the results in eq. (B.3.1), and by taking $F = \mathcal{T}(z,\bar{z})$ as defined in eq. (B.53).

We see once more that because cuts act simultaneously in the various channels, there are nontrivial relations among entries of the coproduct. For example, $\mathrm{Cut}_{p_2^2,p_3^2} F = \mathrm{Cut}_{p_3^2,p_2^2} F$ implies that $\delta_{z,1-z}F \cong \delta_{1-z,\bar{z}}F$.

The relations between cuts, discontinuities and the coproduct given in this section will also be relevant for the two-loop example we will study below—see section 3.6.

3.5.6 $T\left(p_1^2, p_2^2, p_3^2; m_{12}^2, 0, 0\right)$

With our last example of three-point functions at one-loop, we come back to the case already mentioned in section 3.4.2 to show that we have lifted the ambiguity of the imaginary part in some symbol letters correctly.

The relations among cuts, discontinuities and the coproduct in this example are straightforward to obtain. Indeed, the nonzero internal mass is a simple generalisation of the previous example. We give the full set of relations for cuts in external channels, to verify that the procedure described in section 3.4.2 to fix this ambiguity does indeed give the correct result. We will not present cuts in the internal mass here, because we have already given several examples of this type of discontinuity, and they would not teach us anything new.

To get rational symbol letters, we use the variables defined in eq. (2.29), and also define as usual $\mu_{12} = m_{12}^2/p_1^2$. Expressions for the integral, its symbol, and its cuts can be found in appendix B.3.3. The regions where single cuts are computed

are

$$\begin{aligned}
R_1^{p_1^2} &: \quad p_1^2 > m_{12}^2\,, \quad p_2^2 < 0\,, \quad p_3^2 < 0\,, \quad m_{12}^2 > 0\,, \\
R_1^{p_2^2} &: \quad p_1^2 < 0\,, \quad p_2^2 > m_{12}^2\,, \quad p_3^2 < 0\,, \quad m_{12}^2 > 0\,, \\
R_1^{p_3^2} &: \quad p_1^2 < 0\,, \quad p_2^2 < 0\,, \quad p_3^2 > 0\,, \quad m_{12}^2 > 0\,.
\end{aligned} \tag{3.67}$$

We note that these regions are not the complete regions in which single cuts are nonzero. For instance, in $R_1^{p_1^2}$ we could have allowed $0 < p_2^2 < m_{12}^2$. This complicates the discussion in terms of the z and $\bar{z}$ variables, so in this discussion we restrict the cut regions to the subregions defined above, although we have performed some checks that the relations are consistent for the full euclidean region and other parts of the cut regions. In terms of z, $\bar{z}$ and μ_{12}, the chosen euclidean subregion and the subregions for single cuts listed above are

$$\begin{aligned}
R_{0*} &: \; 0 < \bar{z} < z < 1\,, \;\; \mu_{12} < 0\,, \;\; z\bar{z} - \mu_{12} > 0 \\
R_1^{p_1^2} &: \; z > 1\,, \;\; \bar{z} < 0\,, \;\; 0 < \mu_{12} < 1\,, \;\; z - \mu_{12} > 0\,, \;\; \bar{z} - \mu_{12} < 0\,, \;\; z\bar{z} - \mu_{12} < 0 \\
R_1^{p_2^2} &: \; 0 < z < 1\,, \;\; \bar{z} < 0\,, \;\; \mu_{12} < 0\,, \;\; z - \mu_{12} > 0\,, \;\; \bar{z} - \mu_{12} < 0\,, \;\; z\bar{z} - \mu_{12} < 0 \\
R_1^{p_3^2} &: \; z > 1\,, \;\; 0 < \bar{z} < 1\,, \;\; \mu_{12} < 0\,, \;\; z - \mu_{12} > 0\,, \;\; \bar{z} - \mu_{12} > 0\,, \;\; z\bar{z} - \mu_{12} > 0\,.
\end{aligned} \tag{3.68}$$

For single cuts, knowing that $p_i^2 = p_i^2 + i0$, there is no ambiguity in determining the sign of the imaginary part of the relevant symbol letters in the relevant kinematic region. We then find

$$\begin{aligned}
\mathrm{Cut}_{p_1^2} T = -\,\mathrm{Disc}_{p_1^2}\, T &\cong \frac{2\pi}{p_1^2(z-\bar{z})}\Theta\left[\delta_{1-z} + \delta_{\mu_{12}} + \delta_{z\bar{z}-\mu_{12}}\right]\mathcal{T} \\
&= -\frac{2\pi}{p_1^2(z-\bar{z})}\Theta\delta_{1-\mu_{12}}\mathcal{T}, \\
\mathrm{Cut}_{p_2^2} T = -\,\mathrm{Disc}_{p_2^2}\, T &\cong -\frac{2\pi}{p_1^2(z-\bar{z})}\Theta\delta_{z\bar{z}-\mu_{12}}\mathcal{T}, \\
\mathrm{Cut}_{p_3^2} T = -\,\mathrm{Disc}_{p_3^2}\, T &\cong -\frac{2\pi}{p_1^2(z-\bar{z})}\Theta\delta_{1-z}\mathcal{T}.
\end{aligned} \tag{3.69}$$

For the p_1^2 channel cut, we used the fact that there is no branch point at $p_1^2 = 0$ to find a simpler relation.

The double cuts are computed in the regions

$$\begin{aligned}
R_2^{p_1^2,p_2^2} &: \quad p_1^2 > m_{12}^2\,, \quad p_2^2 > m_{12}^2\,, \quad p_3^2 < 0\,, \quad m_{12}^2 > 0\,,\\
R_2^{p_1^2,p_3^2} &: \quad p_1^2 > m_{12}^2\,, \quad p_2^2 < 0\,, \quad p_3^2 > 0\,, \quad m_{12}^2 > 0\,,\\
R_2^{p_2^2,p_3^2} &: \quad p_1^2 < 0\,, \quad p_2^2 > m_{12}^2\,, \quad p_3^2 > 0\,, \quad m_{12}^2 > 0\,.
\end{aligned} \tag{3.70}$$

Determining the signs of the symbol letters and their imaginary parts in each of these regions is straightforward for all double discontinuities, except for $\text{Cut}_{p_2^2,p_1^2}T$, in which case the imaginary part of $\bar{z}-\mu_{12}$ does not have a definite sign in the cut region. We showed how this issue could be addressed in section 3.4.2, where we also mentioned that the result can be cross-checked by comparing $\text{Cut}_{p_2^2,p_1^2}T$ and $\text{Cut}_{p_1^2,p_2^2}T$.

The full set of relations among cuts, discontinuities and the coproduct is

$$\begin{aligned}
\text{Cut}_{p_1^2,p_2^2}T &= \text{Disc}_{p_1^2,p_2^2}\,T \cong \frac{4\pi^2 i}{p_1^2(z-\bar{z})}\Theta\delta_{1-\mu_{12},\bar{z}-\mu_{12}}\mathcal{T}\,,\\
\text{Cut}_{p_2^2,p_1^2}T &= \text{Disc}_{p_2^2,p_1^2}\,T \cong \frac{-4\pi^2 i}{p_1^2(z-\bar{z})}\Theta\left[\delta_{z\bar{z}-\mu_{12},1-z}+\delta_{z\bar{z}-\mu_{12},\bar{z}}+\delta_{z\bar{z}-\mu_{12},\bar{z}-\mu_{12}}\right]\mathcal{T}\,,\\
\text{Cut}_{p_1^2,p_3^2}T &= \text{Disc}_{p_1^2,p_3^2}\,T \cong \frac{4\pi^2 i}{p_1^2(z-\bar{z})}\Theta\delta_{1-\mu_{12},1-z}\mathcal{T}\,,\\
\text{Cut}_{p_3^2,p_1^2}T &= \text{Disc}_{p_3^2,p_1^2}\,T \cong -\frac{4\pi^2 i}{p_1^2(z-\bar{z})}\Theta\delta_{1-z,\bar{z}-\mu_{12}}\mathcal{T}\,,\\
\text{Cut}_{p_2^2,p_3^2}T &= \text{Disc}_{p_2^2,p_3^2}\,T \cong \frac{4\pi^2 i}{p_1^2(z-\bar{z})}\Theta\delta_{z\bar{z}-\mu_{12},1-z}\mathcal{T}\,,\\
\text{Cut}_{p_3^2,p_2^2}T &= \text{Disc}_{p_3^2,p_2^2}\,T \cong \frac{4\pi^2 i}{p_1^2(z-\bar{z})}\Theta\delta_{1-z,\bar{z}-\mu_{12}}\mathcal{T}\,.
\end{aligned} \tag{3.71}$$

Using these results and the expressions given in appendix B.3.3, we indeed verify that $\text{Cut}_{p_1^2,p_2^2}T = \text{Cut}_{p_2^2,p_1^2}T$. We have also checked that all the relations are satisfied for all pairs of external channels.

3.5.7 Two-mass-hard box

We now look at the two-mass-hard box, a box integral (having massless propagators) with two adjacent external massless legs $p_3^2 = p_4^2 = 0$, and two massive ones. The symbol alphabet consists exclusively of linear functions of the invariants because we will only study the function up to terms that vanish when

$\epsilon = 0$ (at higher orders, having a rational symbol alphabet requires using variables like in eq. (2.29), see section B.4.6). Our main reason for including this example is that despite this apparent simplicity, understanding the relations between Cut, Disc and δ requires some care regarding the kinematic regions. Furthermore, the two-mass-hard box analysed here will also be needed for our two-loop calculations that follow, where it appears as a subdiagram in some cuts.

We use the result of ref. [98], with an additional factor of $ie^{\gamma_E \epsilon}$ inserted to match our conventions. In the euclidean region, the box is given by

$$\begin{aligned} B^h(s,t;p_1^2,p_2^2) &\equiv \frac{e^{\gamma_E\epsilon}}{\pi^{2-\epsilon}} \int d^{4-2\epsilon}k \; \frac{1}{k^2(k+p_2)^2(k+p_2+p_3)^2(k-p_1)^2} \\ &= ic_\Gamma \frac{(-p_1^2)^\epsilon(-p_2^2)^\epsilon}{(-t)^{1+2\epsilon}(-s)^{1+\epsilon}} \left[\frac{1}{\epsilon^2} + 2\mathrm{Li}_2\left(1-\frac{t}{p_1^2}\right) + 2\mathrm{Li}_2\left(1-\frac{t}{p_2^2}\right)\right] + \mathcal{O}(\epsilon)\,, \end{aligned} \tag{3.72}$$

where $s = (p_1+p_2)^2$ and $t = (p_2+p_3)^2$ and c_Γ is defined in eq. (A.12). In the following equations, we drop the $\mathcal{O}(\epsilon)$ terms. The coproduct (or symbol, which are almost equivalent for the weight 2 functions we are concerned with here) is evaluated order by order in the Laurent expansion in ϵ. At order $1/\epsilon^2$, it is trivial and there is clearly no discontinuity. At order $1/\epsilon$, the coproduct is simply the function itself,

$$\Delta_1\, B^h\big|_{1/\epsilon} = \qquad \frac{i}{st\epsilon}\left[\log(-p_1^2) + \log(-p_2^2) - \log(-s) - 2\log(-t)\right]. \tag{3.73}$$

At order ϵ^0, we are interested in the $\Delta_{1,1}$ term of the coproduct, which is given by

$$\begin{aligned} &\Delta_{1,1}\, B^h\big|_{\epsilon^0} = \\ &= \frac{i}{st}\left[\log(-p_1^2)\otimes\log(-p_2^2) + \log(-p_2^2)\otimes\log(-p_1^2) - \log(-p_1^2)\otimes\log(-s)\right. \\ &- \log(-s)\otimes\log(-p_1^2) - 2\log(-p_1^2)\otimes\log(-t) - 2\log(-t)\otimes\log(-p_1^2) \\ &-2\log\left(\frac{t}{p_1^2}\right)\otimes\log\left(1-\frac{t}{p_1^2}\right) + \log(-p_1^2)\otimes\log(-p_1^2) - \log(-p_2^2)\otimes\log(-s) \\ &- \log(-s)\otimes\log(-p_2^2) - 2\log(-p_2^2)\otimes\log(-t) - 2\log(-t)\otimes\log(-p_2^2) \\ &-2\log\left(\frac{t}{p_2^2}\right)\otimes\log\left(1-\frac{t}{p_2^2}\right) + \log(-p_2^2)\otimes\log(-p_2^2) + 2\log(-s)\otimes\log(-t) \\ &\left.+2\log(-t)\otimes\log(-s) + \log(-s)\otimes\log(-s) + 4\log(-t)\otimes\log(-t)\right]. \end{aligned} \tag{3.74}$$

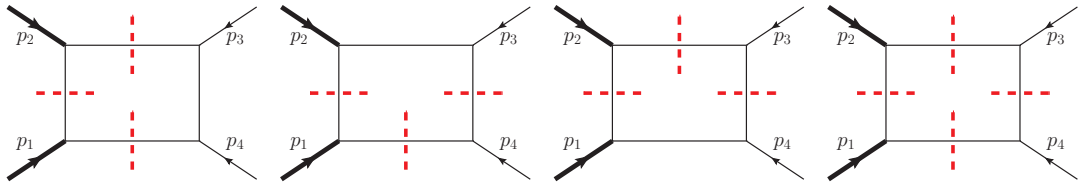

Figure 3.6: Cut integral diagrams for sequential discontinuities of the two-mass-hard box, where legs 3 and 4 have null momenta. (a) Channel pairs $(s, p_1^2), (s, p_2^2)$, or (p_1^2, p_2^2). (b) Channel pair (t, p_1^2). (c) Channel pair (t, p_2^2). (d) Channel pair (s, t).

Up to order $\mathcal{O}(\epsilon)$, the symbol alphabet can then be chosen to be

$$\mathcal{A}_h = \left\{p_1^2, p_2^2, t, s, t - p_1^2, t - p_2^2\right\} . \tag{3.75}$$

Discontinuity in the t-channel: The discontinuity of B^h in the t-channel, with $t > 0$ and all other invariants negative, can be straightforwardly computed according to the definition (2.34) starting with the expression for the function B^{2mh} in (3.72), obtaining:

$$\begin{aligned}\mathrm{Disc}_t B^h &= 4\pi c_\Gamma \frac{(-p_1^2)^\epsilon (-p_2^2)^\epsilon}{t^{1+2\epsilon}(-s)^{1+\epsilon}} \left[\frac{1}{\epsilon} + \log\left(1 - \frac{t}{p_1^2}\right) + \log\left(1 - \frac{t}{p_2^2}\right) + \mathcal{O}(\epsilon)\right] \\ &= -\frac{4\pi}{st}\left[\frac{1}{\epsilon} + \log\frac{(-p_1^2)(-p_2^2)}{(-s)t^2} + \log\left(1 - \frac{t}{p_1^2}\right) + \log\left(1 - \frac{t}{p_2^2}\right) + \mathcal{O}(\epsilon)\right] . \end{aligned} \tag{3.76}$$

Considering instead the coproduct relation (2.41) and using the coproduct entry given in eq. (3.74), we find

$$\begin{aligned}\delta_t B^h \cong \frac{i}{st}\Big[&-\frac{2}{\epsilon} - 2\log(-p_1^2) - 2\log\left(1 - \frac{t}{p_1^2}\right) - 2\log(-p_2^2) - 2\log\left(1 - \frac{t}{p_2^2}\right) \\ &+ 2\log(-s) + 4\log(-t) + \mathcal{O}(\epsilon)\Big], \end{aligned} \tag{3.77}$$

and thus $\mathrm{Disc}_t\, B^h \cong -2\pi i\, \Theta\, \delta_t B^h$, as expected.

Sequential discontinuities: Since the two-mass-hard box has four momentum channels, there are six pairs to consider as sequential discontinuities. Cutting any of the pairs of channels $(s, p_1^2), (s, p_2^2)$, or (p_1^2, p_2^2) cuts the same set of three propagators, as shown in fig. 3.6a, and gives the leading singularity . The result

of the integral in the respective kinematic regions is $-4\pi^2 i/(st)$, which matches the value computed from the coproduct, eq. (3.77), or the direct evaluation of discontinuities (we will compute these cuts explicitly in section 5.5.7).

Let us now consider the sequential discontinuities on the channel pair (t, p_i^2), where $i = 1$ or 2. For concreteness we focus on the case $i = 2$. We first discuss the relation of the discontinuity to the coproduct as in eq. (2.41); finally we will verify that the result is consistent with the iterated cut integral in the region where the latter is defined.

Specializing (2.41) to the case of interest, we have

$$\mathrm{Disc}_{t,p_2^2;R_2} B^h = \Theta \sum_{(x_1,x_2)\in\mathcal{A}_h^2} a_1(t,x_1)a_2(p_2^2,x_2)\delta_{x_1,x_2}B^h\,, \tag{3.78}$$

where R_1 is the region where $t > 0$ and $p_2^2 < 0$ and R_2 is the one where both $t > 0$ and $p_2^2 > 0$. The relevant letters for x_1 can a priori be t and $t - p_i^2$, however, by the first entry condition we know that $\delta_{t-p_i^2}B^h = 0$ so we only need to consider $x_1 = t$. We find:

$$a_1(t,t) = \mathrm{Disc}_{t;t>0}\log(-t - i0) = -2\pi i \tag{3.79}$$

For x_2 the relevant letters are p_2^2 and $t - p_2^2$, and both potentially contribute:

$$\begin{aligned} a_2(p_2^2,p_2^2) &= \mathrm{Disc}_{p_2^2;R_2}\log(-p_2^2 + i0) = 2\pi i \\ a_2(p_2^2,t-p_2^2) &= \mathrm{Disc}_{p_2^2;R_2}\log(t - p_2^2 + i0) = 2\pi i\theta(p_2^2 - t)\,. \end{aligned} \tag{3.80}$$

However using the coproduct of eq. (3.74) we have $\delta_{t,p_2^2}B^h = 0$, so we get

$$\mathrm{Disc}_{t,p_2^2;R_2} B^h = -(2\pi i)^2\theta(p_2^2 - t)\delta_{t,t-p_2^2}B^h = -\frac{8\pi^2 i}{st}\theta(p_2^2 - t)\,. \tag{3.81}$$

Next consider the sequential discontinuity in the reverse order:

$$\mathrm{Disc}_{p_2^2,t;R_2} B^h = \Theta \sum_{(x_1,x_2)\in\mathcal{A}_h^2} a_1(p_2^2,x_1)a_2(t,x_2)\delta_{x_1,x_2}B^h\,, \tag{3.82}$$

where R_1 is now the region where $p_2^2 > 0$ and $t < 0$ and R_2 is the one where both $t > 0$ and $p_2^2 > 0$. Taking into account the first entry condition, there is only one

relevant letter for the first discontinuity, $x_1 = p_2^2$, and we find:

$$a_1(p_2^2, p_2^2) = \mathrm{Disc}_{p_2^2;p_2^2>0} \log(-p_2^2 - i0) = -2\pi i\,. \tag{3.83}$$

For the second discontinuity x_2 can either be t or $t - p_i^2$ for $i = 1$ and 2.

$$\begin{aligned} a_2(t,t) &= \mathrm{Disc}_{t;R_2} \log(-t + i0) = 2\pi i \\ a_2(t, t-p_i^2) &= \mathrm{Disc}_{t;R_2} \log(p_i^2 - t + i0) = 2\pi i\,\theta(t - p_i^2)\,. \end{aligned} \tag{3.84}$$

Using the coproduct component in eq. (3.74) we find that $\delta_{p_2^2,t-p_2^2} B^h$ vanishes and we finally obtain:

$$\mathrm{Disc}_{p_2^2,t;R_2}\, B^h = -(2\pi i)^2 \left(\delta_{p_2^2,t} B^h + \delta_{p_2^2,t-p_2^2} B^h\right) = -\frac{8\pi^2 i}{st}\theta(p_2^2 - t)\,. \tag{3.85}$$

We thus obtain the same result irrespectively of the order in which the two discontinuities are taken,

$$\mathrm{Disc}_{t,p_2^2}\, B^h = \mathrm{Disc}_{p_2^2,t}\, B^h\,. \tag{3.86}$$

Consider now the cut diagrams in the channel pairs (t, p_1^2) and (t, p_2^2). This cut involves an on-shell massless three-point vertex, as shown in fig. 3.6, diagrams (b) and (c). For $D > 4$, as needed to regularise the infrared divergences of the integral, the integral over w vanishes

$$\mathrm{Cut}_{p_1^2,t} B^{2mh} = \mathrm{Cut}_{p_2^2,t} B^{2mh} = 0\,. \tag{3.87}$$

It should be emphasised that this result is in fact only valid for $t > p_2^2$, which is consistent with real external momenta (the complimentary region is unphysical; it can only be realised for complex external momenta). Given that the iterated cut $\mathrm{Cut}_{p_2^2,t}$ is only defined for $t > p_2^2$, where it was shown to vanish identically, and the discontinuities (3.81) and (3.85) also vanish in that region, we have verified that

$$\mathrm{Cut}_{p_2^2,t} B^{2mh} = \mathrm{Disc}_{p_2^2,t}\, B^{2mh} = -(2\pi i)^2 \Theta \left(\delta_{p_2^2,t} B^{2mh} + \delta_{p_2^2,t-p_2^2} B^{2mh}\right) = 0\,. \tag{3.88}$$

Exactly the same conclusion holds for the double discontinuity on p_1^2 and t.

Finally, a comment is due concerning the channel pair (s,t). This double discontinuity is excluded because the cuts cross in the sense described in the cutting rules of the previous section. Indeed the relation between Cut and Disc does not apply for crossed cuts because the second Disc operation would not have an unambiguous $i0$ prescription. Note however that in the coproduct, eq. (3.74), there are terms proportional to $\log(-s)\otimes\log(-t)$ and $\log(-t)\otimes\log(-s)$. If we were to compute the cut integral, it would be zero, not only because of the on-shell three-point vertices, but also because there is no real-valued momentum solution for any box with all four propagators on shell, even in $D=4$. We will see in chapter 5 a way to consistently compute these cuts.

3.5.8 Four-mass box

Let us now look at the four mass box. In $D=4$ dimensions, this diagram is very similar to the three-mass triangle because of its conformal symmetry [99]. We give the result for the uncut function in section B.4.8, eq. (B.123), computed as a parameter integral in what we believe is a new derivation of this result.

Here, our goal is to study its cuts and their relation with the discontinuities and the coproduct. When computing the cuts, we will see that the variables in terms of which the result is best written appear naturally. There are two different types of single unitarity cuts: cuts that isolate one vertex (in one of the p_i^2), and cuts that isolate a pair of vertices (in either the s or the t channels). We will look at one example of each configuration: the cut in the p_3^2 channel and the cut in the s channel. Because of the long list of arguments, we write $B(s,t;p_1^2,p_2^2,p_3^2,p_4^2)\equiv B^{4m}$.

Calculation of single unitarity cuts: Following the cutting rules we established in the previous section, and working in $D=4$, we have

$$\begin{aligned}\mathrm{Cut}_{p_3^2}B^{4m} =& 4\int d^4k\frac{\delta^+\left(k^2\right)\delta^+\left((k-p_3)^2\right)}{(k+p_2)^2(k+p_1+p_2)^2} \\ =& 4\int_0^\infty da_1\int_0^\infty da_2\,\delta\left(1-\sum_{i\in S}a_i\right)\int d^4k\frac{\delta^+\left(k^2\right)\delta^+\left((k-p_3)^2\right)}{\left((a_1+a_2)k^2+2k\cdot\eta+\beta^2\right)^2}\,,\end{aligned} \tag{3.89}$$

where in the last line we combined the two uncut propagators using Feynman parameters, and we have defined the four-vector η and the invariant β^2 as

$$\eta = a_1 p_2 + a_2(p_1 + p_2)\,, \qquad\qquad \beta^2 = a_1 p_2^2 + a_2 s\,.$$

Following the Cheng-Wu theorem, for which we provide a proof in section B.4.8, since the denominator of the integrand is homogeneous of degree 2 in (a_1, a_2), we may take S to be any nonempty subset of $\{1, 2\}$. As far as the integration of the cut loop momentum is concerned, we are in a situation similar to the one of the three-mass triangle, and we thus use a similar parametrisation of the momenta,

$$\begin{aligned} p_3 &= \sqrt{p_3^2}(1, 0, \mathbf{0}_2), \qquad \eta = \sqrt{\eta^2}(\alpha, \sqrt{\alpha^2 - 1}, \mathbf{0}_2), \\ k &= (k_0, |k|\cos\theta, |k|\sin\theta\ \mathbf{1}_2), \end{aligned}$$

where now α and η^2 are functions of the Feynman parameters. The integration over the cut loop-momentum can be done easily and we get

$$\begin{aligned} \mathrm{Cut}_{p_3^2} B^{4m} &= 2\pi \int_0^\infty da_1 \int_0^\infty da_2 \frac{\delta\left(1 - \sum_{i\in S} a_i\right)}{p_3^2\eta^2 + \beta^4 + 2\beta^2 p_3 \cdot \eta} \\ &= 2\pi \int_0^\infty da_1 \int_0^\infty da_2 \frac{\delta\left(1 - \sum_{i\in S} a_i\right)}{a_1^2 p_2^2 t + a_2^2 p_4^2 s + a_1 a_2 \left(st - p_1^2 p_3^2 + p_2^2 p_4^2\right)}\,. \end{aligned} \tag{3.90}$$

Choosing $S = \{2\}$ so that $a_2 = 1$, and changing variables to $y = a_1 \frac{p_2^2}{s}$,

$$\begin{aligned} \mathrm{Cut}_{p_3^2} B^{4m} &= \frac{2\pi}{st} \int_0^\infty dy \frac{1}{(Z + y)(\bar{Z} + y)} \\ &= -\frac{2\pi}{st} \frac{1}{Z - \bar{Z}} \log \frac{\bar{Z}}{Z}\,. \end{aligned} \tag{3.91}$$

where

$$\begin{aligned} Z &= \frac{1}{2}\left(1 + U - V + \sqrt{\lambda(1, U, V)}\right), \\ \bar{Z} &= \frac{1}{2}\left(1 + U - V - \sqrt{\lambda(1, U, V)}\right), \end{aligned} \tag{3.92}$$

with

$$U = \frac{p_2^2 p_4^2}{st}\,, \qquad V = \frac{p_1^2 p_3^2}{st}. \tag{3.93}$$

As for the three-mass triangle, Z and $\bar{Z}$ appear naturally in the calculation of the cut of the four-mass box diagram, and it is fair to say that this calculation is simpler than the evaluation of the uncut diagram.

The cut in the s-channel can be computed following exactly the same steps. We only quote the result,

$$\mathrm{Cut}_s B^{4m} = \frac{2\pi}{st}\frac{1}{Z-\bar{Z}}\left(\log\frac{1-Z}{1-\bar{Z}} + \log\frac{\bar{Z}}{Z}\right). \tag{3.94}$$

Discussion: As expected, we find that both cuts verify the relations we anticipated

$$\mathrm{Cut}_{p_3^2} B^{4m} = -\mathrm{Disc}_{p_3^2} B^{4m} \cong (2\pi i)\,\Theta\,\delta_{1-Z} B^{4m}, \tag{3.95}$$

and

$$\mathrm{Cut}_s B^{4m} = -\mathrm{Disc}_s B^{4m} \cong -(2\pi i)\,\Theta\,\left(\delta_Z B^{4m} + \delta_{1-Z} B^{4m}\right). \tag{3.96}$$

Similar results can be obtained for the other external massive channels of the box.

The analysis of multiple cuts is more complicated. Following the methods we have developed, the calculation of the three- and four-propagator cuts is not hard. The difficulty lies in identifying the correct region where the cuts and discontinuities should be related. Indeed, as we already saw in the previous example, identifying this kinematic region for box diagrams is not trivial. It becomes even harder in the case of the four-mass box, given the required change of variables to Z and $\bar{Z}$. This is a technical issue only, but makes this example not particularly enlightening as an illustration of the Disc-Cut-δ relations, so we will not discuss it further.

3.6 Two-loop three-point three-mass ladder

The two-loop, three-point, three-mass ladder diagram with massless internal lines, fig. 3.7, is finite in four dimensions [99]. In terms of the variables $z, \bar{z}$ defined

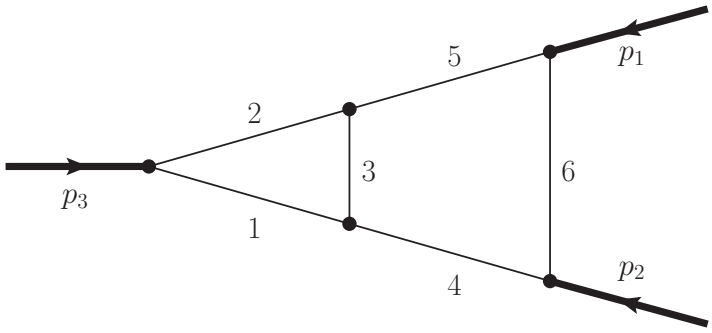

Figure 3.7: Two-loop three-mass ladder.

in eq. (2.29), it is given by a remarkably simple expression:

$$\begin{aligned} T_L(p_1^2,p_2^2,p_3^2) &\equiv -\frac{i}{\pi^4}\int d^4k_1 \int d^4k_2\, \frac{1}{k_1^2\,(p_3-k_1)^2(k_1+p_1)^2\,k_2^2\,(p_3-k_2)^2(k_1-k_2)^2} \\ &= i\left(p_1^2\right)^{-2}\frac{1}{(1-z)(1-\bar{z})(z-\bar{z})}F(z,\bar{z})\,, \end{aligned} \tag{3.97}$$

where we have defined the pure function

$$\begin{aligned} F(z,\bar{z}) =& 6\big[\mathrm{Li}_4\,(z)-\mathrm{Li}_4(\bar{z})\big]-3\log\,(z\bar{z})\,\big[\mathrm{Li}_3\,(z)-\mathrm{Li}_3(\bar{z})\big] \\ &+\frac{1}{2}\log^2(z\bar{z})\big[\mathrm{Li}_2(z)-\mathrm{Li}_2(\bar{z})\big]\,. \end{aligned} \tag{3.98}$$

Because the two-loop three-point ladder in four dimensions is given by weight-four functions, its coproduct structure is much richer than the one-loop cases of the preceding section. Since one of our goals is to match the entries in the coproduct to the cuts of the integral, we list below for later reference all the relevant components of the coproduct, of the form $\Delta_{\underbrace{1,\ldots,1}_{k\text{ times}},n-k}$. We have

$$\begin{aligned} \Delta_{1,3}(F(z,\bar{z})) &= \log(z\bar{z})\otimes\left[-3\,\mathrm{Li}_3(z)+3\,\mathrm{Li}_3(\bar{z})+\log(z\bar{z})\,\left(\mathrm{Li}_2(z)-\mathrm{Li}_2(\bar{z})\right)\right] \\ &\quad+\log((1-z)(1-\bar{z}))\otimes\frac{1}{2}\log z\log\bar{z}\log\frac{z}{\bar{z}}\,, \end{aligned} \tag{3.99}$$

$$\begin{aligned}\Delta_{1,1,2}(F(z,\bar{z})) = {} & \log((1-z)(1-\bar{z})) \otimes \log z \otimes \left(\log z \log \bar{z} - \frac{1}{2}\log^2 \bar{z}\right) \\ & - \log((1-z)(1-\bar{z})) \otimes \log \bar{z} \otimes \left(\log z \log \bar{z} - \frac{1}{2}\log^2 z\right) \\ & - \log(z\bar{z}) \otimes \log(1-z) \otimes \left(\log z \log \bar{z} - \frac{1}{2}\log^2 z\right) \\ & + \log(z\bar{z}) \otimes \log(1-\bar{z}) \otimes \left(\log z \log \bar{z} - \frac{1}{2}\log^2 \bar{z}\right) \\ & + \log(z\bar{z}) \otimes \log(z\bar{z}) \otimes [\mathrm{Li}_2(z) - \mathrm{Li}_2(\bar{z})] \,, \end{aligned} \tag{3.100}$$

$$\begin{aligned}\Delta_{1,1,1,1}(F(z,\bar{z})) = {} & \log((1-z)(1-\bar{z})) \otimes \log\frac{z}{\bar{z}} \otimes (\log\bar{z} \otimes \log z + \log z \otimes \log\bar{z}) \\ & - \log((1-z)(1-\bar{z})) \otimes \log z \otimes \log\bar{z} \otimes \log\bar{z} \\ & + \log((1-z)(1-\bar{z})) \otimes \log\bar{z} \otimes \log z \otimes \log z \\ & + \log(z\bar{z}) \otimes \log\frac{1-\bar{z}}{1-z} \otimes \log z \otimes \log\bar{z} + \log(z\bar{z}) \otimes \log\frac{1-\bar{z}}{1-z} \otimes \log\bar{z} \otimes \log z \\ & - \log(z\bar{z}) \otimes \log(1-\bar{z}) \otimes \log\bar{z} \otimes \log\bar{z} + \log(z\bar{z}) \otimes \log(1-z) \otimes \log z \otimes \log z \\ & - \log(z\bar{z}) \otimes \log(z\bar{z}) \otimes \log(1-z) \otimes \log z \\ & + \log(z\bar{z}) \otimes \log(z\bar{z}) \otimes \log(1-\bar{z}) \otimes \log\bar{z} \,. \end{aligned} \tag{3.101}$$

Notice that the first entry of $\Delta_{1,1,1,1}$ is (the logarithm of) a Mandelstam invariant, in agreement with the first entry condition.

In the rest of this section we evaluate the standard unitarity cuts of the ladder graph of fig. 3.7, which give the discontinuities across branch cuts of Mandelstam invariants in the time-like region. Our goal is, first, to relate these cuts to specific terms of $\Delta_{1,3}$ of $T_L(p_1^2, p_2^2, p_3^2)$, and, in the following section, to take cuts of these cuts and relate them to $\Delta_{1,1,2}$.

In contrast to the one-loop case, even if the uncut diagram is finite, individual cut diagrams are infrared divergent: even though $T_L(p_1^2, p_2^2, p_3^2)$ is finite in $D = 4$ dimensions, its unitarity cuts need to be computed in $D = 4 - 2\epsilon$ dimensions. The finiteness of $T_L(p_1^2, p_2^2, p_3^2)$ for $\epsilon = 0$ imposes cancellations between ϵ-poles of individual cut diagrams. These cancellations can be understood in the same way as the cancellation of infrared singularities between real and virtual corrections in scattering cross sections.

For practical reasons, the cut diagrams will be computed in the region $R^*_{\triangle}$,

where $\bar{z} = z^*$ and all the Mandelstam invariants are timelike. This restriction is consistent with the physical picture of amplitudes having branch cuts in the timelike region of their invariants. When comparing the results of cuts with δ, but particularly with Disc, we will be careful to analytically continue our result to the region where only the cut invariant is positive, as this is where Cut is to be compared with Disc.

Before we start computing the cut integrals, we briefly outline our approach to these calculations. We will compute the cuts of this two-loop diagram by integrating first over a carefully chosen one-loop subdiagram, with a carefully chosen parametrisation of the internal propagators. We make our choices according to the following rules, which were designed to simplify the calculations as much as possible:

- Always work in the center of mass frame of the cut channel p_i^2. The momentum p_i is taken to have positive energy ;
- The routing of the loop momentum k_1 is such that k_1 is the momentum of a propagator, and there is either a propagator with momentum $(p_i - k_1)$ or a subdiagram with $(p_i - k_1)^2$ as one of its Mandelstam invariants ;
- The propagator with momentum k_1 is always cut ;
- Whenever possible, the propagator with momentum $(p_i - k_1)$ is cut ;
- Subdiagrams are chosen so to avoid the square root of the Källén function as their leading singularity. This is always possible for this ladder diagram.

These rules, together with the parametrisation of the momenta

$$\begin{aligned} p_i &= \sqrt{p_i^2}(1, 0, \mathbf{0}_{D-2}), \qquad p_j = \sqrt{p_j^2}\left(\alpha, \sqrt{\alpha^2 - 1}, \mathbf{0}_{D-2}\right), \\ k_1 &= (k_{1,0}, |k_1|\cos\theta, |k_1|\sin\theta\ \mathbf{1}_{D-2}), \end{aligned} \tag{3.102}$$

where $\theta \in [0, \pi]$, $|k_1| > 0$, and $\mathbf{1}_{D-2}$ ranges over unit vectors in the dimensions transverse to p_i and p_j, make the calculation of these cuts particularly simple. It is easy to show that

$$\alpha\sqrt{p_i^2}\sqrt{p_j^2} = \frac{p_l^2 - p_i^2 - p_j^2}{2} \quad \text{and} \quad \sqrt{p_i^2}\sqrt{p_j^2}\sqrt{\alpha^2 - 1} = \frac{1}{2}\sqrt{\lambda(p_i^2, p_j^2, p_l^2)}\,. \tag{3.103}$$

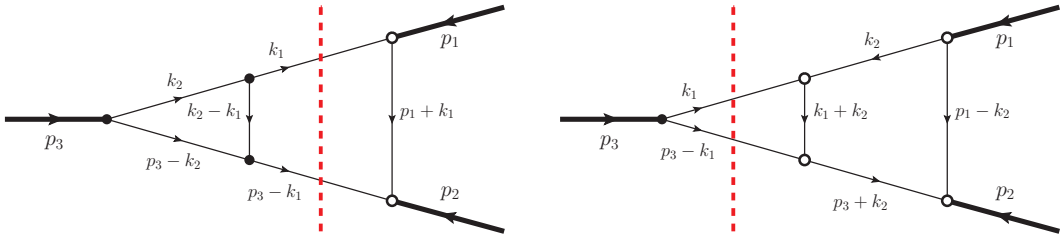

(a) Cut [45] (b) Cut [12]

Figure 3.8: Two-particle cuts in the p_3^2-channel.

The changes of variables

$$\cos\theta = 2x - 1 \quad \text{and} \quad k_{1,0} = \frac{\sqrt{p_i^2}}{2} y \,, \tag{3.104}$$

are also useful (the y variable is useful mainly when $(p_i - k_1)$ is not cut).

3.6.1 Unitarity cut in the p_3^2 channel

We present the computation of the cuts in the p_3^2 channel in some detail, in order to illustrate our techniques for the evaluation of cut diagrams outlined above. We follow the cut rules in section 3.2. We then collect the different contributions and check the cancellation of divergent pieces and the agreement with the term $\delta_{1-z}F(z,\bar{z})$ in eq. (3.99) as predicted in eq. (3.65c).

There are four cuts contributing to this channel,

$$\begin{aligned}\mathrm{Cut}_{p_3^2} T_L(p_1^2,p_2^2,p_3^2) = \\ = \Big(\mathrm{Cut}_{p_3^2,[45]} + \mathrm{Cut}_{p_3^2,[12]} + \mathrm{Cut}_{p_3^2,[234]} + \mathrm{Cut}_{p_3^2,[135]}\Big) T_L(p_1^2,p_2^2,p_3^2)\,,\end{aligned} \tag{3.105}$$

and our aim is to show that

$$\begin{aligned}\mathrm{Cut}_{p_3^2} T_L(p_1^2,p_2^2,p_3^2) &= -\,\mathrm{Disc}_{p_3^2}\, T_L(p_1^2,p_2^2,p_3^2) \\ &\cong -\,\Theta\,\frac{2\pi}{p_1^4}\frac{1}{(1-z)(1-\bar{z})(z-\bar{z})}\delta_{1-z}F(z,\bar{z}).\end{aligned} \tag{3.106}$$

Two-particle cuts: There are two two-particle cut diagrams contributing to the p_3^2-channel unitarity cut, $\mathrm{Cut}_{p_3^2,[45]} T_L(p_1^2,p_2^2,p_3^2)$ and $\mathrm{Cut}_{p_3^2,[12]} T_L(p_1^2,p_2^2,p_3^2)$, shown in fig. 3.8.

We start by considering the diagram in fig. 3.8a, which is very simple to compute because the cut completely factorises the two loop momentum integrations into a one-mass triangle and the cut of a three-mass triangle:

$$\begin{aligned}\mathrm{Cut}_{p_3^2,[45],R^*_\triangle} T_L(p_1^2,p_2^2,p_3^2) = -i &\left[\frac{e^{\gamma_E\epsilon}}{\pi^{2-\epsilon}}\int d^{4-2\epsilon}k_1 (2\pi)^2 \frac{\delta\left(k_1^2\right)\delta\left((p_3-k_1)^2\right)}{(k_1+p_1)^2-i0}\right] \\ &\left[\frac{e^{\gamma_E\epsilon}}{\pi^{2-\epsilon}}\int d^{4-2\epsilon}k_2 \frac{1}{k_2^2+i0}\frac{1}{(p_3-k_2)^2+i0}\frac{1}{(k_1-k_2)^2+i0}\right] \\ =& i\,T(p_3^2)\,\mathrm{Cut}_{p_3^2,R^*_\triangle} T(p_1^2,p_2^2,p_3^2)\,. \end{aligned} \tag{3.107}$$

We can find expressions for $T(p_3^2)$ and $\mathrm{Cut}_{p_3^2,R^*_\triangle} T(p_1^2,p_2^2,p_3^2)$ in sections B.1.1 and B.3.1. We note that the one-mass triangle is evaluated for space-like p_3^2, while in this calculation we have $p_3^2>0$, given that we are cutting in this channel. We can make sense of terms like $\log(-p_3^2)$ by recalling that given the $+i0$ prescription of the propagators contributing to the one-mass triangle, we have $p_3^2 = p_3^2 + i0$.

As expected, the result is divergent for $\epsilon\to 0$: the origin of the divergent terms is the one-loop one-mass triangle subdiagram. Expanding up to $\mathcal{O}(\epsilon)$, we get

$$\begin{aligned}&\mathrm{Cut}_{p_3^2,[45],R^*_\triangle} T_L(p_1^2,p_2^2,p_3^2) = \\ &= i\frac{(p_1^2)^{-2-2\epsilon}}{(1-z)(1-\bar z)(z-\bar z)}\left\{\frac{1}{\epsilon^2}f^{(-2)}_{[45]}(z,\bar z)+\frac{1}{\epsilon}f^{(-1)}_{[45]}(z,\bar z)+f^{(0)}_{[45]}(z,\bar z)\right\}+\mathcal{O}(\epsilon)\,.\end{aligned} \tag{3.108}$$

Expressions for the coefficients $f^{(i)}_{[45]}(z,\bar z)$ are given in appendix C.1.

We now go on to fig. 3.8b. We can see diagrammatically that the integration over k_2 is the (complex-conjugated) two-mass-hard box with external masses p_1^2 and p_2^2 and $s=p_3^2$, $t=(p_1+k_1)^2$. We give the result for this diagram up to the needed power of ϵ in eq. (B.105). More precisely, we have

$$\begin{aligned}&\mathrm{Cut}_{p_3^2,[12],R^*_\triangle} T_L(p_1^2,p_2^2,p_3^2) = \\ &= \frac{e^{\gamma_E\epsilon}}{\pi^{2-\epsilon}} i\int d^{4-2\epsilon}k_1 (2\pi)^2\delta\left(k_1^2\right)\delta\left((p_3-k_1)^2\right)\left(B^h(p_3^2,(p_1+k_1)^2;p_1^2,p_2^2)\right)^\dagger\,.\end{aligned} \tag{3.109}$$

To proceed, we parametrise the momenta as in eq. (3.102), with $(i,j)=(3,1)$.

Then, we rewrite the momentum integration as

$$\begin{aligned}\frac{e^{\gamma_E\epsilon}}{\pi^{2-\epsilon}}\int d^{4-2\epsilon}k_1(2\pi)^2\delta\left(k_1^2\right)\delta\left((p_3-k_1)^2\right) = \\ =&\frac{4\pi}{\Gamma(1-\epsilon)}\int dk_{1,0}\int d\left|\mathbf{k}_1\right|^2\left|\mathbf{k}_1\right|^{1-2\epsilon}\delta(k_{1,0}^2-\left|\mathbf{k}_1\right|^2)\delta(p_3^2-2p_3\cdot k_1)\\ &\int_{-1}^{1}d\cos\theta(1-\cos^2\theta)^{-\epsilon}\,.\end{aligned}$$

The two delta functions allow us to trivially perform the $k_{1,0}$ and $|\mathbf{k}_1|$ integrations. For the remaining integral, it is useful to change variables to $\cos\theta = 2x-1$, as in eq. (3.104), and we get,

$$(p_1+k_1)^2 = p_1^2\left(z-x(z-\bar{z})\right)\,.$$

We finally have

$$\begin{aligned}&\mathrm{Cut}_{p_3^2,[12],R_\triangle^*}T_L(p_1^2,p_2^2,p_3^2) = \\ =&2\pi\frac{c_\Gamma}{\Gamma(1-\epsilon)}(p_1^2)^{-2-2\epsilon}e^{-i\pi\epsilon}u_2^\epsilon u_3^{-1-2\epsilon}\int_0^1 dx\frac{x^{-\epsilon}(1-x)^{-\epsilon}}{(z-x(z-\bar{z}))^{1+2\epsilon}}\\ &\left[\frac{1}{\epsilon^2}+2\mathrm{Li}_2(1-z+x(z-\bar{z}))+2\mathrm{Li}_2\left(1-\frac{z-x(z-\bar{z})}{z\bar{z}}\right)\right]+\mathcal{O}(\epsilon)\,,\end{aligned}\tag{3.110}$$

where c_Γ is defined in eq. (A.12). The factor $e^{-i\pi\epsilon}$ was determined according to the $i0$ prescription of the invariants. After expansion in ϵ, all the integrals above are simple to evaluate in terms of multiple polylogarithms. We write this expression as:

$$\begin{aligned}&\mathrm{Cut}_{p_3^2,[12],R_\triangle^*}T_L(p_1^2,p_2^2,p_3^2) = \\ &= i\frac{(p_1^2)^{-2-2\epsilon}}{(1-z)(1-\bar{z})(z-\bar{z})}\left\{\frac{1}{\epsilon^2}f_{[12]}^{(-2)}(z,\bar{z})+\frac{1}{\epsilon}f_{[12]}^{(-1)}(z,\bar{z})+f_{[12]}^{(0)}(z,\bar{z})\right\}+\mathcal{O}(\epsilon)\,,\end{aligned}\tag{3.111}$$

and give the expressions for the coefficients $f_{[12]}^{(i)}(z,\bar{z})$ in appendix C.1.

Three-particle cuts: There are two three-particle cut diagrams contributing to the p_3^2-channel unitarity cut, $\mathrm{Cut}_{p_3^2,[234]}T_L(p_1^2,p_2^2,p_3^2)$ and $\mathrm{Cut}_{p_3^2,[135]}T_L(p_1^2,p_2^2,p_3^2)$, shown in fig. 3.9. As these two cuts are very similar, we only present the details for the computation of the cut in fig. 3.9a, and simply quote the result for fig. 3.9b.

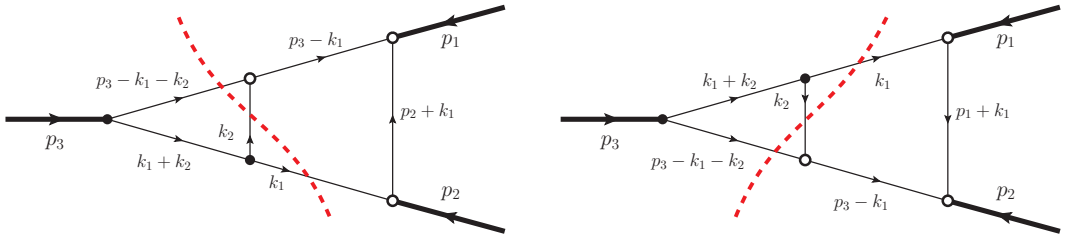

(a) Cut [234] (b) Cut [135]

Figure 3.9: Three-particle cuts in the p_3^2-channel.

In both cases, we note that the integration over k_2 is the cut in the $(p_3 - k_1)^2$-channel of a two-mass one-loop triangle, with masses p_3^2 and $(p_3 - k_1)^2$. More precisely, for the cut in fig. 3.9a we have

$$\begin{aligned}\text{Cut}_{p_3^2,[234],R_\triangle^*} T_L(p_1^2, p_2^2, p_3^2) =& \frac{e^{\gamma_E \epsilon}}{\pi^{2-\epsilon}} \int d^{4-2\epsilon} k_1 (2\pi) \frac{\delta\left(k_1^2\right)}{\left((p_2 + k_1)^2 - i0\right)\left((p_3 - k_1)^2 - i0\right)} \\ & \times \text{Cut}_{(p_3-k_1)^2} T\left(p_3^2, (p_3 - k_1)^2\right) . \end{aligned} \tag{3.112}$$

We take the result for the cut of the two mass triangle given in appendix B.2.1 and insert it into eq. (3.112),

$$\begin{aligned}&\text{Cut}_{p_3^2,[234],R_\triangle^*} T_L(p_1^2, p_2^2, p_3^2) = \\ &= 2\frac{e^{2\gamma_E \epsilon}}{\pi^{-\epsilon}} \frac{\Gamma(1-\epsilon)}{\epsilon\Gamma(1-2\epsilon)} \int d^{4-2\epsilon} k_1 \, \frac{\delta\left(k_1^2\right)}{(p_2 + k_1)^2} \frac{\theta\left((p_3 - k_1)^2\right)}{p_3 \cdot k_1} \left(\frac{1}{(p_3 - k_1)^2}\right)^{1+\epsilon} \theta(k_{1,0}) \,, \end{aligned} \tag{3.113}$$

where we have used the δ-function to set $k_1^2 = 0$, and we have dropped the $\pm i0$ of all propagators. We have included the θ-functions because the cut of the two-mass triangle is only nonzero when the $(p_3 - k_1)^2$-channel is positive. It is also important to recall that the positive energy flow across the cut requires $k_{1,0} > 0$, so we have included this θ-function explicitly. We use the parametrisation of eq. (3.102), with $(i, j) = (3, 2)$ and both changes of variables in eq. (3.104), since the propagator with momentum $(p_3 - k_1)$ is not cut. The two conditions imposed by the θ-functions imply that

$$0 \leq y \leq 1 \,. \tag{3.114}$$

We get

$$\begin{aligned}\mathrm{Cut}_{p_3^2,[234],R^*_\triangle} T_L(p_1^2,p_2^2,p_3^2) &= -\frac{2\pi e^{2\gamma_E\epsilon}\Gamma(1-\epsilon)}{\epsilon^2\Gamma(1-3\epsilon)}(p_1^2)^{-2-2\epsilon}\frac{u_3^{-1-2\epsilon}}{u_2} \\ &\int_0^1 dx\, x^{-\epsilon}(1-x)^{-1-\epsilon}\,{}_2F_1\left(1,1-2\epsilon;1-3\epsilon;1-\frac{z-x(z-\bar{z})}{u_2}\right).\end{aligned} \tag{3.115}$$

We can now expand the hypergeometric function into a Laurent series in ϵ using standard techniques [100], and we then perform the remaining integration order by order. As usual, we write the result in the form

$$\begin{aligned}&\mathrm{Cut}_{p_3^2,[234],R^*_\triangle} T_L(p_1^2,p_2^2,p_3^2) = \\ &= i\frac{(p_1^2)^{-2-2\epsilon}}{(1-z)(1-\bar{z})(z-\bar{z})}\left\{\frac{1}{\epsilon^2}f^{(-2)}_{[234]}(z,\bar{z})+\frac{1}{\epsilon}f^{(-1)}_{[234]}(z,\bar{z})+f^{(0)}_{[234]}(z,\bar{z})\right\}+\mathcal{O}(\epsilon)\,.\end{aligned} \tag{3.116}$$

The diagram of fig. 3.9b can be calculated following exactly the same steps, the only difference being that when using the parametrisation of eq. (3.102) we have $(i,j)=(3,1)$. The result is

$$\begin{aligned}&\mathrm{Cut}_{p_3^2,[135],R^*_\triangle} T_L(p_1^2,p_2^2,p_3^2) = -\frac{2\pi e^{2\gamma_E\epsilon}\Gamma(1-\epsilon)}{\epsilon^2\Gamma(1-3\epsilon)}(p_1^2)^{-2-2\epsilon}u_3^{-1-2\epsilon} \\ &\int_0^1 dx\, x^{-\epsilon}(1-x)^{-1-\epsilon}\,{}_2F_1\left(1,1-2\epsilon;1-3\epsilon;1-z+x(z-\bar{z})\right) \\ &= i\frac{(p_1^2)^{-2-2\epsilon}}{(1-z)(1-\bar{z})(z-\bar{z})}\left\{\frac{1}{\epsilon^2}f^{(-2)}_{[135]}(z,\bar{z})+\frac{1}{\epsilon}f^{(-1)}_{[135]}(z,\bar{z})+f^{(0)}_{[135]}(z,\bar{z})\right\}+\mathcal{O}(\epsilon)\,.\end{aligned} \tag{3.117}$$

Explicit expressions for the $f^{(i)}_{[234]}(z,\bar{z})$ and $f^{(i)}_{[135]}(z,\bar{z})$ are given in appendix C.1.

Summary and discussion. Let us now combine the results for each p_3^2-channel cut diagram and compare the total with Disc and the relevant terms in the coproduct. We observe the sum is very simple, compared to the expressions for each of the cuts.

Note that, as imposed by the fact that the two-loop ladder is finite in four dimensions, the sum of the divergent terms of each diagram vanishes. In fact, this cancellation happens in a very specific way: the sum of the two-particle cuts

cancels with the sum of the three-particle cuts. If we write

$$\frac{f^{(-2)}_{[45]} + f^{(-2)}_{[12]}}{\epsilon^2} + \frac{f^{(-1)}_{[45]} + f^{(-1)}_{[12]}}{\epsilon} \equiv \frac{f^{(-2)}_{\text{virt}}}{\epsilon^2} + \frac{f^{(-1)}_{\text{virt}}}{\epsilon^1}\,, \tag{3.118}$$

$$\frac{f^{(-2)}_{[234]} + f^{(-2)}_{[135]}}{\epsilon^2} + \frac{f^{(-1)}_{[234]} + f^{(-1)}_{[135]}}{\epsilon} \equiv \frac{f^{(-2)}_{\text{real}}}{\epsilon^2} + \frac{f^{(-1)}_{\text{real}}}{\epsilon^1}\,, \tag{3.119}$$

then this cancellation can be written as

$$f^{(-2)}_{\text{virt}} = -f^{(-2)}_{\text{real}} \quad \text{and} \quad f^{(-1)}_{\text{virt}} = -f^{(-1)}_{\text{real}}\,. \tag{3.120}$$

We call the divergent contribution of two particle cuts a *virtual contribution* because it is associated with divergences of loop diagrams, whereas the divergent contribution of three particle cuts, the *real contribution*, comes from integrating over a three-particle phase space. This cancellation is similar to the cancellation of infrared divergences for inclusive cross sections, although in this case we are not directly dealing with a cross section, but merely with the unitarity cuts of a single finite Feynman integral. A better understanding of these cancellations might prove useful for the general study of the infrared properties of amplitudes, and it would thus be interesting to understand how it generalises to other cases.

As expected, the sum of the finite terms does not cancel. We get

$$f^{(0)}_{[45]}(z,\bar{z}) + f^{(0)}_{[12]}(z,\bar{z}) + f^{(0)}_{[234]}(z,\bar{z}) + f^{(0)}_{[135]}(z,\bar{z}) = i\pi \log z \log \bar{z} \log \frac{z}{\bar{z}}\,. \tag{3.121}$$

Since all divergences have cancelled, we can set $\epsilon = 0$ and write the cut-derived discontinuity of the integral as

$$\text{Cut}_{p_3^2, R^*_\triangle} T_L(p_1^2, p_2^2, p_3^2) = -\frac{\pi (p_1^2)^{-2}}{(1-z)(1-\bar{z})(z-\bar{z})} \log z \log \bar{z} \log \frac{z}{\bar{z}}\,. \tag{3.122}$$

For comparison with Disc, we now analytically continue this result to the region $R^3_\triangle$ where only the cut invariant is positive: $p_3^2 > 0$ and $p_1^2, p_2^2 < 0$. In terms of the z and $\bar{z}$ variables, the region is: $z > 1 > \bar{z} > 0$, see table 2.1. None of the functions in eq. (3.122) has a branch cut in this region, and thus there is nothing to do for the analytic continuation and the result is valid in this region as it is

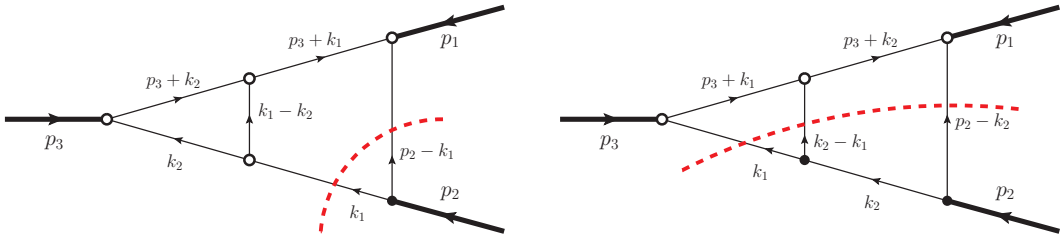

(a) Cut [46] (b) Cut [136]

Figure 3.10: Cuts in the p_2^2-channel

given above,

$$\mathrm{Cut}_{p_3^2,R^3_\triangle} T_L(p_1^2,p_2^2,p_3^2) = \mathrm{Cut}_{p_3^2,R^*_\triangle} T_L(p_1^2,p_2^2,p_3^2)\,.$$

This is consistent with the expectation that the discontinuity function would be real in the region where only the cut invariant is positive [21, 23].

The relations with Disc and δ are now easy to verify. As expected, we find,

$$\begin{aligned}\mathrm{Cut}_{p_3^2,R^3_\triangle} T_L(p_1^2,p_2^2,p_3^2) &= -\,\mathrm{Disc}_{p_3^2}\, T_L(p_1^2,p_2^2,p_3^2) \\ &\cong -2\pi\left(p_1^2\right)^{-2}\Theta\frac{1}{(1-z)(1-\bar z)(z-\bar z)}\delta_{1-z}F(z,\bar z)\,.\end{aligned} \tag{3.123}$$

We can write this equation diagrammatically as

$$\delta_{1-z}T_L(p_1^2,p_2^2,p_3^2) = \frac{1}{2\pi i}\Bigg($$

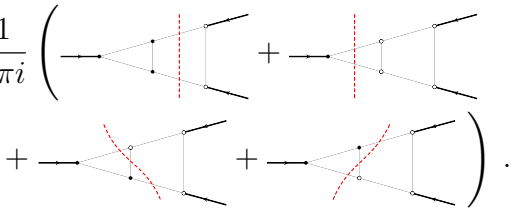

$$\Bigg)\,.$$

3.6.2 Unitarity cut in the p_2^2 channel

We now turn to the calculation of the cuts in the p_2^2 channel, in order to reproduce the $\delta_z T_L(p_1^2,p_2^2,p_3^2)$ entry of the coproduct in eq. (3.99) as predicted in eq. (3.65b). Only two cut diagrams contribute to this channel,

$$\mathrm{Cut}_{p_2^2} T_L(p_1^2,p_2^2,p_3^2) = \Big(\mathrm{Cut}_{p_2^2,[46]} + \mathrm{Cut}_{p_2^2,[136]}\Big) T_L(p_1^2,p_2^2,p_3^2)\,. \tag{3.124}$$

The computation of the two cuts diagrams follows the same strategy as before, i.e., we compute the cut of the two-loop diagram by integrating over a carefully chosen one-loop subdiagram.

Computation of the cut diagrams. We start with $\mathrm{Cut}_{p_2^2,[46]} T_L(p_1^2, p_2^2, p_3^2)$. As suggested by the momentum routing in fig. 3.10a, we identify the result of the k_2 integration with the complex conjugate of an uncut two-mass triangle, with masses $(p_3 + k_1)^2$ and p_3^2:

$$\begin{aligned}
&\mathrm{Cut}_{p_2^2,[46],R_\triangle^*} T_L(p_1^2, p_2^2, p_3^2) = \\
&= -i \frac{e^{\gamma_E \epsilon}}{\pi^{2-\epsilon}} \int d^{4-2\epsilon} k_1 (2\pi)^2 \frac{\delta\left(k_1^2\right) \delta\left((p_2 - k_1)^2\right)}{(p_3 + k_1)^2 - i\varepsilon} \left(T(p_3^2, (p_3 + k_1)^2)\right)^\dagger . \qquad (3.125)
\end{aligned}$$

Using the result for the triangle given in appendix B.2.1 and proceeding in the same way as with the p_3^2-channel cuts, we get (setting $(i, j) = (2, 3)$ in eq. (3.102))

$$\begin{aligned}
&\mathrm{Cut}_{p_2^2,[46],R_\triangle^*} T_L(p_1^2, p_2^2, p_3^2) = 2\pi \frac{c_\Gamma e^{\gamma_E \epsilon}}{\epsilon^2 \Gamma(1-\epsilon)} u_2^{-\epsilon} e^{-i\pi\epsilon} (p_1^2)^{-2-2\epsilon} \int_0^1 dx\, (1-x)^{-\epsilon} x^{-\epsilon} \\
&\frac{(u_3 + z - u_2 - x(z - \bar{z}))^{-\epsilon} - u_3^{-\epsilon}}{(u_3 + z - u_2 - x(z - \bar{z}))\,(z - u_2 - x(z - \bar{z}))} \\
&= i \frac{(p_1^2)^{-2-2\epsilon}}{(1-z)(1-\bar{z})(z-\bar{z})} \left\{ \frac{1}{\epsilon} f_{[46]}^{(-1)}(z, \bar{z}) + f_{[46]}^{(0)}(z, \bar{z}) \right\} + \mathcal{O}(\epsilon) , \qquad (3.126)
\end{aligned}$$

where c_Γ is defined in eq. (A.12).

The cut integral $\mathrm{Cut}_{p_2^2,[136]} T_L(p_1^2, p_2^2, p_3^2)$ is slightly more complicated. Using the routing of loop momenta of fig. 3.10b, we look at it as the k_1-integration over the cut of a three-mass box,

$$\begin{aligned}
&\mathrm{Cut}_{p_2^2,[136],R_\triangle^*} T_L(p_1^2, p_2^2, p_3^2) = \\
&\qquad = -\frac{e^{\gamma_E \epsilon}}{\pi^{2-\epsilon}} \int d^{4-2\epsilon} k_1 \frac{2\pi\delta\left(k_1^2\right)}{(p_3 + k_1)^2 - i\varepsilon} \mathrm{Cut}_t B\left(s, t; l_2^2, l_3^2, l_4^2\right) , \qquad (3.127)
\end{aligned}$$

where $\mathrm{Cut}_t B\left(s, t, l_2^2, l_3^2, l_4^2\right)$ is the t-channel cut of the three-mass box with masses l_i^2, for $i \in \{2, 3, 4\}$, $l_1^2 = 0$, $s = (l_1 + l_2)^2$ and $t = (l_2 + l_3)^2$. In our case:

$$l_2^2 = (p_3 + k_1)^2 - i0, \quad l_3^2 = p_1^2 - i0, \quad l_4^2 = p_2^2 + i0, \quad s = p_3^2 - i0, \quad t = (p_2 - k_1)^2 .$$

The result for the t-channel cut of the three-mass box is given in eq. (B.110) in the region where the uncut invariants are negative and t is positive. Since we work in the region where all the p_i^2 are positive, some terms in the expression (B.110) need to be analytically continued using the $\pm i0$ prescriptions given above. Using eq. (3.102) with $(i,j) = (2,3)$ and introducing the variables x and y according to eq. (3.104), we have:[6]

$$\begin{aligned}
\log(-s) &= \log p_1^2 + \log u_3 + i\pi\,, \\
(-l_2^2)^{-\epsilon} &= \left(e^{i\pi} p_1^2\right)^{-\epsilon} \left(u_3 + y\,(z - u_2 - x(z-\bar{z}))\right)^{-\epsilon}\,, \\
(-l_3^2)^{-\epsilon} &= \left(e^{i\pi} p_1^2\right)^{-\epsilon}\,, \\
\log\left(1 - \frac{l_4^2}{t}\right) &= \log y - \log(1-y) - i\pi\,, \\
\log\left(1 - \frac{l_2^2 l_4^2}{st}\right) &= \log\left(u_3 + z - u_2 - x(z-\bar{z})\right) + \log y - \log u_3 - \log(1-y) - i\pi\,.
\end{aligned}$$

Combining everything, $\mathrm{Cut}_{p_2^2,[136],R_\triangle^*} T_L(p_1^2, p_2^2, p_3^2)$ is given by

$$\begin{aligned}
&\mathrm{Cut}_{p_2^2,[136],R_\triangle^*} T_L(p_1^2, p_2^2, p_3^2) = \\
=&2\pi \frac{e^{2\gamma_E \epsilon}}{\Gamma(1-2\epsilon)} u_2^{-\epsilon} (p_1^2)^{-2-2\epsilon} \int_0^1 dx\,(1-x)^{-\epsilon} x^{-\epsilon} \int_0^1 dy\, y^{-2\epsilon} \\
&\frac{1}{u_3 + z - u_2 - x(z-\bar{z})} \frac{1}{u_3 + y\,(z - u_2 - x(z-\bar{z}))} \Bigg[2\log u_2 + \frac{2}{\epsilon} u_2^{-\epsilon} (1-y)^{-\epsilon} \\
&+ 2\log(1-y) - \frac{u_2^\epsilon}{\epsilon} (1-y)^\epsilon \left(u_3 + y\,(z - u_2 - x(z-\bar{z}))\right)^{-\epsilon} \\
&- 2\log\left(u_3 + z - u_2 - x(z-\bar{z})\right) \Bigg] + \mathcal{O}(\epsilon) \\
=&i \frac{(p_1^2)^{-2-2\epsilon}}{(1-z)(1-\bar{z})(z-\bar{z})} \left\{ \frac{1}{\epsilon} f_{[136]}^{(-1)}(z,\bar{z}) + f_{[136]}^{(0)}(z,\bar{z}) \right\} + \mathcal{O}(\epsilon)\,. \qquad (3.128)
\end{aligned}$$

Explicit results for $f_{[46]}^{(i)}(z,\bar{z})$ and $f_{[136]}^{(i)}(z,\bar{z})$ are given in appendix C.1.

Summary and discussion. Similarly to the p_3^2-channel cuts, we first analyze the cancellation of the singularities in the sum of the two cuts contributing to the

[6] Strictly speaking, this analytic continuation is valid for $\bar{z} = z^*$, with $\mathfrak{Re}(z) < 1$. For the case of $\mathfrak{Re}(z) > 1$, the factors of $i\pi$ are distributed in other ways among the different terms, but the combination of all terms is still the same.

p_2^2 channel, and check the agreement with $\delta_z T_L(p_1^2, p_2^2, p_3^2)$ given in eq. (3.99). In this case we only have single poles, and we see that the poles cancel, as expected:

$$f^{(-1)}_{[46]}(z,\bar{z}) + f^{(-1)}_{[136]}(z,\bar{z}) = 0\,. \tag{3.129}$$

This cancellation can again be understood as the cancellation between virtual (from cut [46]) and real contributions (from cut [136]).

Adding the finite contributions, we find

$$f^{(0)}_{[46]}(z,\bar{z}) + f^{(0)}_{[136]}(z,\bar{z}) = 2\pi i \Big\{ 3\big[\mathrm{Li}_3(\bar{z}) - \mathrm{Li}_3(z)\big] + \big(\log(z\bar{z}) - i\pi\big)\big[\mathrm{Li}_2(z) - \mathrm{Li}_2(\bar{z})\big] \Big\}\,. \tag{3.130}$$

Hence, the cut of the two-loop ladder in the p_2^2 channel is

$$\begin{aligned}\mathrm{Cut}_{p_2^2, R^*_\triangle} T_L(p_1^2, p_2^2, p_3^2) = &- \frac{2\pi (p_1^2)^{-2}}{(1-z)(1-\bar{z})(z-\bar{z})} \Big\{ 3\big[\mathrm{Li}_3(\bar{z}) - \mathrm{Li}_3(z)\big] \\ &+ \big(\log(z\bar{z}) - i\pi\big)\big[\mathrm{Li}_2(z) - \mathrm{Li}_2(\bar{z})\big] \Big\}\,.\end{aligned} \tag{3.131}$$

Since this result was computed in the region where all invariants are positive, we now analytically continue to the region $R^2_\triangle$ where $p_2^2 > 0$ and $p_1^2, p_3^2 < 0$. For the z and $\bar{z}$ variables, this corresponds to $1 > z > 0 > \bar{z}$, see table 2.1. The analytic continuation of the Li_2 and Li_3 functions is trivial, because their branch cuts lie in the $[1, \infty)$ region of their arguments. However, the continuation of $\log(z\bar{z})$ needs to be done with some care, since $(z\bar{z})$ becomes negative. We can determine the sign of the $i0$ associated with $(z\bar{z})$ by noticing that

$$\log\left(-\frac{p_2^2}{p_1^2 - i0}\right) = \log\left(-z\bar{z} - i0\right)\,,$$

where we associate a $-i0$ to p_1^2 because it is in the complex-conjugated region of the cut diagrams. We thus see that the $-i\pi$ term in eq. (3.131) is what we get from the analytic continuation of $\log(-z\bar{z} - i0)$ to positive $(z\bar{z})$. In region $R^2_\triangle$, we thus have

$$\begin{aligned}\mathrm{Cut}_{p_2^2, R^2_\triangle} T_L(p_1^2, p_2^2, p_3^2) = &- \frac{2\pi (p_1^2)^{-2}}{(1-z)(1-\bar{z})(z-\bar{z})} \Big\{ 3\big[\mathrm{Li}_3(\bar{z}) - \mathrm{Li}_3(z)\big] \\ &+ \log(-z\bar{z} - i\varepsilon)\big[\mathrm{Li}_2(z) - \mathrm{Li}_2(\bar{z})\big] \Big\}\,.\end{aligned} \tag{3.132}$$

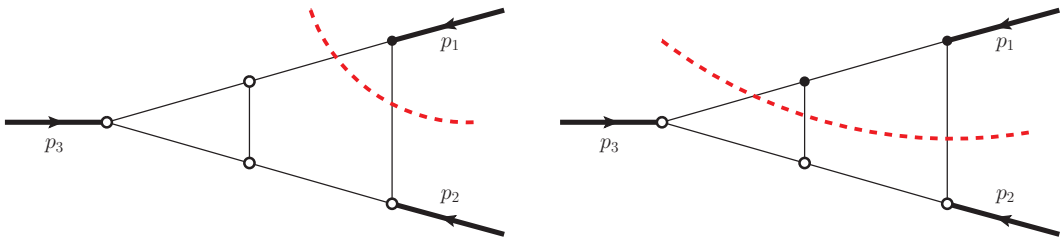

(a) Cut [56] (b) Cut [236]

Figure 3.11: Cuts in the p_1^2-channel

This agrees with the expectation that the discontinuity function should be real in the region where only the cut invariant is positive [21, 23]. Furthermore, we again observe the expected relations with Disc and δ,

$$\begin{aligned}\mathrm{Cut}_{p_2^2,R_\triangle^2} T_L(p_1^2,p_2^2,p_3^2) &= -\,\mathrm{Disc}_{p_2^2} T_L(p_1^2,p_2^2,p_3^2)\\ &\cong -2\pi\,\Theta\left(p_1^2\right)^{-2}\frac{1}{(1-z)(1-\bar{z})(z-\bar{z})}\delta_z F(z,\bar{z})\,. \end{aligned} \tag{3.133}$$

Diagrammatically, the relation can be written as follows:

$$\delta_z T_L(p_1^2,p_2^2,p_3^2) = \frac{1}{2\pi i}\left(\quad + \quad \right)\,. \tag{3.134}$$

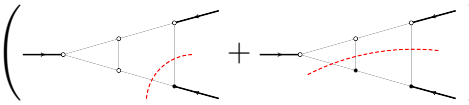

3.6.3 Unitarity cut in the p_1^2 channel

Given the symmetry of the three-point ladder, the cut in the p_1^2 channel shown in fig. 3.11 can be done in exactly the same way as the p_2^2 channel, so we will be brief in listing the results.

For the sum of the two cut integrals, the reflection symmetry can be implemented by exchanging p_1 and p_2 in eq. (3.131), along with transforming $z \to 1/\bar{z}$ and $\bar{z} \to 1/z$. The total cut integral is then

$$\begin{aligned}\mathrm{Cut}_{p_1^2,R_\triangle^*} T_L(p_1^2,p_2^2,p_3^2) = -\,&\frac{2\pi(p_1^2)^{-2}}{(1-z)(1-\bar{z})(z-\bar{z})}\Bigg\{3\left[\mathrm{Li}_3\left(\frac{1}{z}\right)-\mathrm{Li}_3\left(\frac{1}{\bar{z}}\right)\right]\\ &-\left(\log(z\bar{z})+i\pi\right)\left[\mathrm{Li}_2\left(\frac{1}{\bar{z}}\right)-\mathrm{Li}_2\left(\frac{1}{z}\right)\right]\Bigg\}\,. \end{aligned} \tag{3.135}$$

We now analytically continue p_2^2 and p_3^2 to the region $R_\triangle^1$ where we should match Cut with Disc. In this region, we have $\bar{z} < 0$ and $z > 1$, see 2.1. Similarly to the

previous case, we take $p_2^2 - i0$ to find that $\log(z\bar{z} - i0) \to \log(-z\bar{z}) - i\pi$, and thus

$$\begin{aligned}\mathrm{Cut}_{p_1^2, R^1_\triangle} T_L(p_1^2, p_2^2, p_3^2) = &- \frac{2\pi (p_1^2)^{-2}}{(1-z)(1-\bar{z})(z-\bar{z})} \Bigg\{ 3 \left[\mathrm{Li}_3\left(\frac{1}{z}\right) - \mathrm{Li}_3\left(\frac{1}{\bar{z}}\right) \right] \\ &- \log(-z\bar{z}) \left[\mathrm{Li}_2\left(\frac{1}{\bar{z}}\right) - \mathrm{Li}_2\left(\frac{1}{z}\right) \right] \Bigg\} \\ = &- \mathrm{Disc}_{p_1^2} T_L(p_1^2, p_2^2, p_3^2). \end{aligned} \tag{3.136}$$

In the last line, we have confirmed that the cut result agrees with a direct evaluation of the discontinuity of $T_L(p_1^2, p_2^2, p_3^2)$ in the region $R^1_\triangle$.

The δ discontinuity evaluated from the coproduct is simply related to the discontinuities in the p_2^2 and p_3^2 channels. Indeed, we can rewrite eq. (3.99) as

$$\begin{aligned}\Delta_{1,3}(F(z,\bar{z})) = &\log\left(-p_2^2\right) \otimes \delta_{p_2^2} F(z,\bar{z}) + \log\left(-p_3^2\right) \otimes \delta_{p_3^2} F(z,\bar{z}) \\ &+ \log\left(-p_1^2\right) \otimes \delta_{p_1^2} F(z,\bar{z}),\end{aligned}$$

where

$$\begin{aligned}&\delta_{p_2^2} F(z,\bar{z}) = \delta_z F(z,\bar{z})\,, \qquad \delta_{p_3^2} F(z,\bar{z}) = \delta_{1-z} F(z,\bar{z})\,, \\ &\delta_{p_1^2} F(z,\bar{z}) = -\delta_z F(z,\bar{z}) - \delta_{1-z} F(z,\bar{z})\,. \end{aligned} \tag{3.137}$$

Explicitly,

$$\begin{aligned}(-2\pi i)\delta_{p_1^2} T_L = &- \frac{2\pi (p_1^2)^{-2}}{(1-z)(1-\bar{z})(z-\bar{z})} \Bigg\{ 3\big[\mathrm{Li}_3(\bar{z}) - \mathrm{Li}_3(z)\big] \\ &+ \log(-z\bar{z})\big[\mathrm{Li}_2(z) - \mathrm{Li}_2(\bar{z})\big] + \frac{1}{2}\log z \log\bar{z} \log\frac{z}{\bar{z}} \Bigg\}, \end{aligned} \tag{3.138}$$

which agrees with $\mathrm{Disc}_{p_1^2} T_L$ from eq. (3.136) modulo π^2.

3.6.4 Double unitarity cuts

In this section we describe the computation of the sequences of two unitarity cuts corresponding to $\mathrm{Cut}_{p_1^2} \circ \mathrm{Cut}_{p_3^2}$ and $\mathrm{Cut}_{p_1^2} \circ \mathrm{Cut}_{p_2^2}$; see fig. 3.12 and fig. 3.13. All the cut integrals can be computed following similar techniques as the ones outlined in sections 3.6.1 and 3.6.2, so we will be brief and only comment on some special features of the computation. Details on how to compute the integrals can

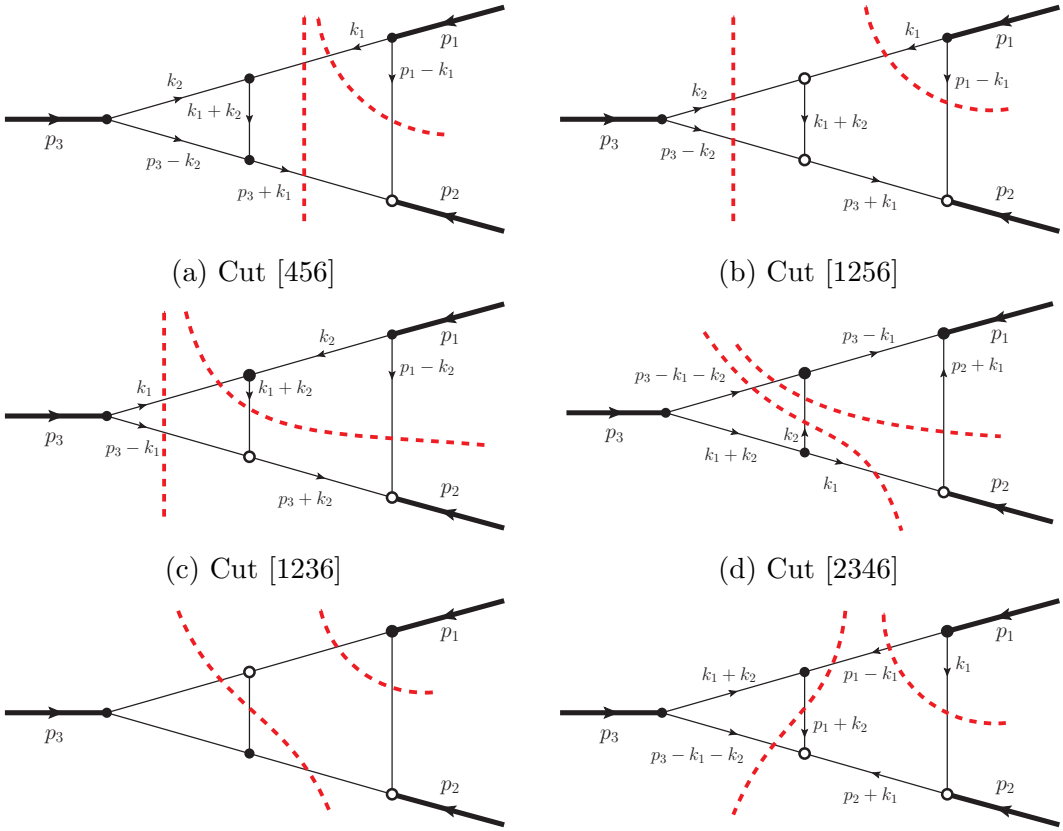

Figure 3.12: Cut diagrams contributing to the $\text{Cut}_{p_1^2} \circ \text{Cut}_{p_3^2}$ sequence of unitarity cuts.

be found in appendix C.2.1, and the explicit results for all the cuts in fig. 3.12 and fig. 3.13 are given in appendices C.2.2 and C.2.3 respectively.

First, we note that, since we are dealing with sequences of unitarity cuts, the cut diagrams correspond to the extended cutting rules introduced in section 3.2. In particular, in section 3.2 we argued that cut diagrams with crossed cuts should be discarded, and such diagrams are therefore not taken into account in our computation. (In this example, all possible crossed cut diagrams would vanish anyway, for the reason given next.)

Second, some of the cut integrals vanish because of energy-momentum constraints. Indeed the cut in fig. 3.12e vanishes in real kinematics because it contains a three-point vertex where all the connected legs are massless and on shell. Hence, the cut diagram cannot satisfy energy momentum conservation in real kinematics with $D > 4$. We will set this diagram to zero, and we observe

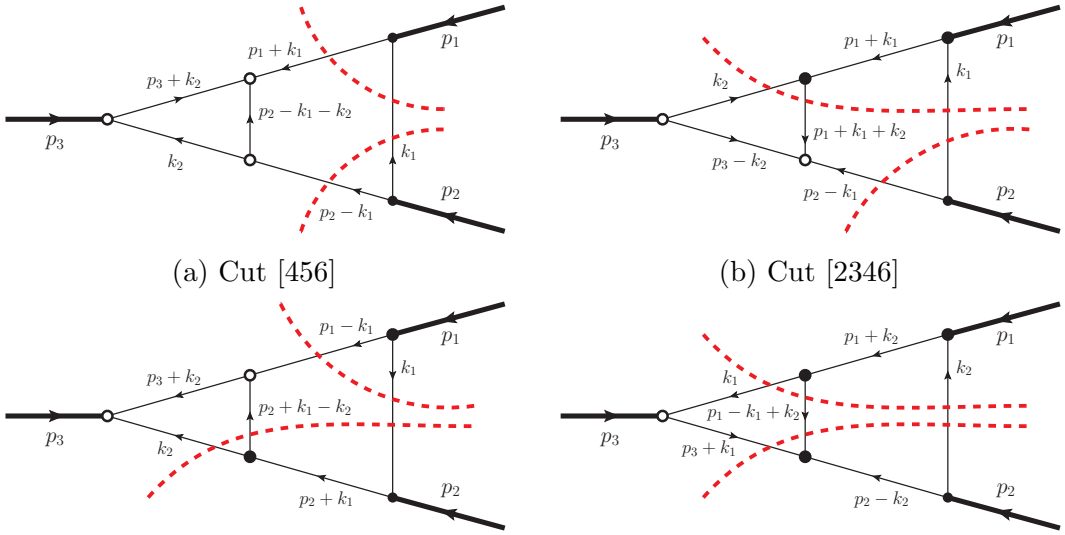

(a) Cut [456]

(b) Cut [2346]

(c) Cut [1356]

(d) Cut [1236]

Figure 3.13: Cut diagrams contributing to the $\text{Cut}_{p_1^2} \circ \text{Cut}_{p_2^2}$ sequence of unitarity cuts.

a posteriori that this is consistent with the other results, again supporting our approach of working in real kinematics.

We make one further remark on kinematic restrictions. Recall that the generalised cutting rules allow for all possible directions of energy flow across each cut (as illustrated in fig. 3.1 for the triangle). In this example of the ladder cut in channels p_1^2 and p_3^2, all diagrams except fig. 3.12b would vanish if the energy components of p_1 and p_3 had the same sign. However, it follows from the conditions of the cut region ($p_1^2, p_3^2 > 0,\ p_2^2 < 0$), in real kinematics, that the energy components of p_1 and p_3 must have opposite signs. Thus we will find that we always have nonvanishing contributions from all diagrams except fig. 3.12e. It is important to be aware of these types of restrictions on the existence of the cut region, since they do not necessarily show up explicitly in the cut integrals.

Let us now focus on the cuts that do not vanish. As we mentioned previously, the cuts are computed by integrating over carefully chosen one-loop subdiagrams. In particular, for simplicity we avoid integrating over three-mass triangles, cut or uncut, because the leading singularity of this diagram is the square root of the Källén function, which leads to integrands that are not directly integrable using the tools developed for multiple polylogarithms. In Tables 3.1 and 3.2 we summarise the preferred choices of subdiagrams for the first loop integration. We

Cut – computed in $R^{1,3}_{\triangle}$	One-loop subdiagram
$\mathrm{Cut}_{p_1^2,[56]} \circ \mathrm{Cut}_{p_3^2,[45]} = \mathrm{Cut}_{[456],R^{1,3}_{\triangle}}$	One-mass triangle, mass p_3^2, fig. 3.12a (this cut completely factorises).
$\mathrm{Cut}_{p_1^2,[56]} \circ \mathrm{Cut}_{p_3^2,[12]} = \mathrm{Cut}_{[1256],R^{1,3}_{\triangle}}$	Cut two-mass triangle, masses p_3^2 and $(p_3+k_1)^2$, in p_3^2 channel, fig. 3.12b.
$\mathrm{Cut}_{p_1^2,[236]} \circ \mathrm{Cut}_{p_3^2,[12]} = \mathrm{Cut}_{[1236],R^{1,3}_{\triangle}}$	Cut two-mass-hard box, masses p_1^2 and p_2^2, in $t=(p_1-k_1)^2$ channel, fig. 3.12c.
$\mathrm{Cut}_{p_1^2,[236]} \circ \mathrm{Cut}_{p_3^2,[234]} = \mathrm{Cut}_{[2346],R^{1,3}_{\triangle}}$	Cut two-mass triangle, masses p_3^2 and $(p_3-k_1)^2$, in $(p_3-k_1)^2$ channel, fig. 3.12d.
$\mathrm{Cut}_{p_1^2,[56]} \circ \mathrm{Cut}_{p_3^2,[135]} = \mathrm{Cut}_{[1356],R^{1,3}_{\triangle}}$	Cut two-mass triangle, masses p_3^2 and $(p_3-k_1)^2$, in $(p_3-k_1)^2$ channel, fig. 3.12f.

Table 3.1: Nonvanishing cuts contributing to the $\mathrm{Cut}_{p_1^2} \circ \mathrm{Cut}_{p_3^2}$ sequence of unitarity cuts.

observe that it is insufficient to define a cut integral by the subset of propagators that are cut. Indeed, some cut integrals in the two tables have the same cut propagators, but are computed in different kinematic regions due to the rules of section 3.2, leading to very different results.

Finally, depending on the cut integral and the kinematic region where the cut is computed, the integrands might become divergent at specific points, and we need to make sense of these divergences to perform the integrals. In the case where the integral develops an end-point singularity, we explicitly subtract the divergence before expanding in ϵ, using the technique known as the plus prescription. For example, if $g(y,\epsilon)$ is regular for all $y \in [0,1]$, then, for $\epsilon < 0$, we have:

$$\int_0^1 dy\, \frac{g(y,\epsilon)}{(1-y)^{1+\epsilon}} = \frac{g(1,\epsilon)}{\epsilon} + \int_0^1 dy\, \frac{g(y,\epsilon)-g(1,\epsilon)}{(1-y)^{1+\epsilon}}\,. \tag{3.139}$$

The remaining integral is manifestly finite, and we can thus expand in ϵ under the integration sign. However, we also encounter integrands which, at first glance, develop simple poles inside the integration region. A careful analysis however reveals that the singularities are shifted into the complex plane due to the Feynman $i0$ prescription for the propagators. As a consequence, the integral

Cut – computed in $R^{1,2}_{\triangle}$	One-loop subdiagram
$\mathrm{Cut}_{p_1^2,[56]} \circ \mathrm{Cut}_{p_2^2,[46]} = \mathrm{Cut}_{[456],R^{1,2}_{\triangle}}$	One-mass triangle, mass p_3^2, fig. 3.13a (this cut completely factorises).
$\mathrm{Cut}_{p_1^2,[236]} \circ \mathrm{Cut}_{p_2^2,[46]} = \mathrm{Cut}_{[2346],R^{1,2}_{\triangle}}$	Cut two-mass triangle, masses p_3^2 and $(p_1+k_1)^2$, in $(p_1+k_1)^2$ channel, fig. 3.13b.
$\mathrm{Cut}_{p_1^2,[56]} \circ \mathrm{Cut}_{p_2^2,[136]} = \mathrm{Cut}_{[1356],R^{1,2}_{\triangle}}$	Cut two-mass triangle, masses p_3^2 and $(p_2+k_1)^2$, in $(p_2+k_1)^2$ channel, fig. 3.13c.
$\mathrm{Cut}_{p_1^2,[236]} \circ \mathrm{Cut}_{p_2^2,[136]} = \mathrm{Cut}_{[1236],R^{1,2}_{\triangle}}$	Cut two-mass-hard box, masses p_1^2 and p_2^2, in $t=(p_1-k_1)^2$ channel, fig. 3.13d.

Table 3.2: Cuts contributing to the $\mathrm{Cut}_{p_1^2} \circ \mathrm{Cut}_{p_2^2}$ sequence of unitarity cuts.

develops an imaginary part, which can be extracted by the usual principal value prescription,

$$\lim_{\varepsilon\to 0} \frac{1}{a \pm i\varepsilon} = \mathrm{PV}\frac{1}{a} \mp i\pi\,\delta(a), \tag{3.140}$$

where PV denotes the Cauchy principal value, defined by

$$\mathrm{PV}\int_0^1 dy\,\frac{g(y)}{y-y_0} = \lim_{\eta\to 0}\left[\int_0^{y_0-\eta} dy\,\frac{g(y)}{y-y_0} + \int_{y_0+\eta}^1 dy\,\frac{g(y)}{y-y_0}\right], \tag{3.141}$$

where $g(y)$ is regular on $[0,1]$ and $y_0 \in [0,1]$. Note that the consistency throughout the calculation of the signs of the $i0$ of uncut propagators and subdiagram invariants, as derived from the conventions of the extended cutting rules of section 3.2 (see also appendix A), is a nontrivial consistency check of these cutting rules.

Summary and discussion

Let us now look at explicit results for $\mathrm{Cut}_{p_3^2,p_1^2} T_L$ and $\mathrm{Cut}_{p_2^2,p_1^2} T_L$. From the explicit calculations collected in Appendix C.2, we get

$$\mathrm{Cut}_{p_3^2,p_1^2} T_L\left(p_1^2,p_2^2,p_3^2\right) = \frac{4\pi^2 i (p_1^2)^{-2}}{(1-z)(1-\bar z)(z-\bar z)}\left(\log(z)\log(\bar z) - \frac{\log^2(z)}{2}\right), \tag{3.142}$$

and

$$\mathrm{Cut}_{p_2^2,p_1^2} T_L\left(p_1^2,p_2^2,p_3^2\right) = \frac{4\pi^2 i (p_1^2)^{-2}}{(1-z)(1-\bar{z})(z-\bar{z})}\Big(\log(z)\log(\bar{z}) - \frac{1}{2}\log^2(z) - \mathrm{Li}_2(z) + \mathrm{Li}_2(\bar{z})\Big). \tag{3.143}$$

Comparing with the coproduct in eq. (3.100), we verify from these results that the relations of eq. (3.20) between Cut and δ, as written in eqs. (3.66), are satisfied. We have confirmed by direct calculation from the original ladder function, eq. (3.97), that the Disc operation gives the expected results as well.

Diagrammatically, for the specific cuts considered above, we have

$$[\delta_{1-z,\bar{z}} + \delta_{1-z,1-z}] T_L(p_1^2,p_2^2,p_3^2) = \frac{1}{(2\pi i)^2}$$

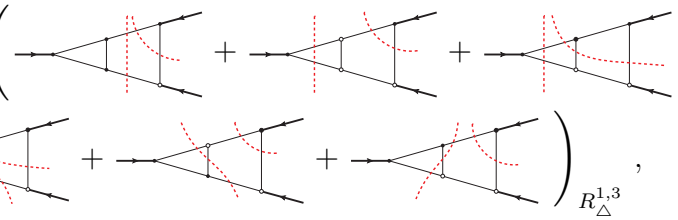

$$R_{\triangle}^{1,3},$$

and,

$$[\delta_{z,\bar{z}} + \delta_{z,1-z}]\, T_L(p_1^2,p_2^2,p_3^2) = \frac{1}{(2\pi i)^2}$$

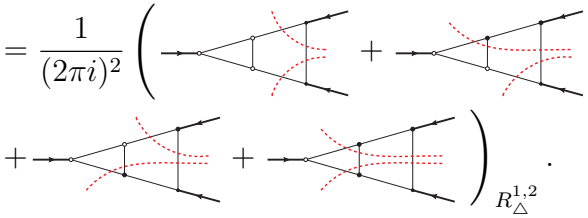

$$R_{\triangle}^{1,2}.$$

One could wonder about a sequence of three unitarity cuts in the three distinct channels of the ladder. As argued in Section 2.3.3, the region where one would hope to compute this triple cut has all $p_i^2 > 0$. Since F is only a function of the ratios of the p_i^2, this region is indistinguishable from the euclidean region, so the triple cut must vanish and contains no nontrivial information on the analytic structure of the function.

3.7 Summary and discussion

For the class of Feynman integrals with massless propagators that may be expressed in terms of the iterated integrals known as multiple polylogarithms, we have formulated precise relations between discontinuities across their physical branch cuts, their unitarity cuts, and their coproduct.

Taking a step beyond the familiar case of a single unitarity cut, in sections 3.2 and 3.3 we developed the concept of a sequence of unitarity cuts. To define this notion consistently, we extended the cutting rules of [21, 23] to accommodate multiple cuts in different channels or in a combination of channels and internal masses, in an appropriately chosen kinematic region. The cutting rules specify a unique prescription for complex conjugation of certain vertices and propagators, dictated by the channels on which cuts are taken. Importantly, the result does not depend on the order in which the cuts are applied (aside from the minor detail discussed below eq. (3.18)).

Having specified the definition of a sequence of unitarity cuts, we find the following correspondences, which we conjecture to be general, among

- the sum of all cut diagrams in the kinematic invariants $r_1, ..., r_k$, where the r_i can be either external channels or internal masses, which we denote by $\text{Cut}_{r_1,...,r_k}$;

- a sequence of discontinuity operations, which we denote by $\text{Disc}_{r_1,...,r_k}$;

- the weight $n-k$ cofactors of the terms in the coproduct of the form $\Delta_{1,1,...,1,n-k}$, where each of the k weight one entries of a specific term in $\Delta_{1,1,...,1,n-k}$ is associated with the r_i in a well defined manner.

The precise relations are given in section 3.4, and were illustrated by a variety of one—see section 3.5—and two-loop examples—see section 3.6. In establishing the relations given in section 3.4, we had to settle several small issues related to the order in which discontinuities are taken and the determination of the $i0$-prescription of symbol letters. We will not review them here, but it is important to have them in mind when determining the relations in specific examples. We also found an interesting result about cuts of massive propagators that isolate an external channel, see the discussion around eq. (3.19).

In sections 3.5.1 and 3.6, we explained the techniques we developed to compute cut diagrams. This was one of the most challenging parts of the work presented in this chapter, as techniques to compute cut diagrams are far less well developed than techniques to compute uncut diagrams. We note that individual cuts of multi-loop integrals that are themselves finite in four dimensions may be divergent when the internal propagators that are put on shell are massless. However, because the diagram is finite, the combination of cuts contributing to the unitarity cut in a given channel must be finite. This situation was encountered here upon taking unitarity cuts of the two-loop ladder graph, where we saw that the pattern of cancellation is similar to the familiar real-virtual cancellation mechanism in cross sections, although this example does not correspond to a cross section. Understanding this pattern of cancellation is useful for the general program of developing efficient subtraction procedures for infrared singularities, and it would be interesting to explore how this generalises for other multi-loop integrals.

Unfortunately, in this section we observed that unitarity cuts are not enough to describe the full structure of the coproduct of Feynman diagrams. This is perhaps most apparent in the two-loop example where we could not go deeper than $\Delta_{1,1,2}$. Another shortcoming of our method is that it does not allow cuts in crossed channels, which means we have no way of reproducing the iterated discontinuity on the s and t channels of a box diagram. Finally, we insisted on using real kinematics in computing the cut diagrams, and although it allowed us to reproduce the results computed with Disc, even in the two-loop case, it is known that cuts computed in complex kinematics capture information about the analytic structure of Feynman diagrams [4, 5, 9, 56, 57, 85, 86, 101]. It is of course interesting to understand if one can relax some of the rather strict conditions we imposed in a systematic way, and this question will be addressed in chapter 5.

However, before that, in the next chapter we will discuss the question of whether we can use the information obtained by computing cuts to reconstruct the uncut Feynman integral.

Chapter 4

Reconstruction from cut diagrams

4.1 Introduction

In the previous chapter we introduced computational tools to compute cut integrals, and we showed that extended cutting rules in real kinematics lead to consistent results. Furthermore, we argued that the entries in the coproduct of a Feynman integral can be related to its discontinuities and cut integrals. While these results are interesting in their own right, in this section we take a step further and put them to use: we present several ways of using the knowledge of (sequences of) cut integrals to reconstruct the original Feynman integral based on the knowledge of its cuts. The work presented here is covered in refs. [36, 37].

We motivate our approach by discussing the three-point functions with massless propagators and three external massive legs. It is obvious from the first-entry condition that if all cuts are known, we can immediately write down the coproduct component of weight $(1, n-1)$ of a pure integral of weight n. In particular, for the three-point functions with massless propagators, we immediately obtain

$$\begin{aligned} \Delta_{1,1}(\mathcal{T}(z,\bar{z})) &= \log(z\bar{z}) \otimes \delta_z \mathcal{T}(z,\bar{z}) + \log((1-z)(1-\bar{z})) \otimes \delta_{1-z} \mathcal{T}(z,\bar{z}) \,, \\ \Delta_{1,3}(F(z,\bar{z})) &= \log(z\bar{z}) \otimes \delta_z F(z,\bar{z}) + \log((1-z)(1-\bar{z})) \otimes \delta_{1-z} F(z,\bar{z}) \,, \end{aligned} \tag{4.1}$$

where $\mathcal{T}(z,\bar{z})$ is the one-loop triangle defined in eq. (B.53) and $F(z,\bar{z})$ the two-

loop ladder of eq. (3.98), and the quantities $\delta_z \mathcal{T}(z,\bar{z})$, $\delta_{1-z}\mathcal{T}(z,\bar{z})$, $\delta_z F(z,\bar{z})$ and $\delta_{1-z}F(z,\bar{z})$ are directly related to the discontinuities of the integral through eqs. (3.65). These components of the coproduct in turn determine the functions $\mathcal{T}(z,\bar{z})$ and $F(z,\bar{z})$ up to terms that vanish when acting with $\Delta_{1,1}$ and $\Delta_{1,3}$. We will see how this information can be recovered in the following.

Similarly, in eq. (3.66) we have shown how the double discontinuities of the two-loop ladder triangle are related to the entries in the coproduct. We can then immediately write

$$\Delta_{1,1,2}(F(z,\bar{z})) = \sum_{(x_1,x_2)\in\mathcal{A}^2_{\triangle}} \log x_1 \otimes \log x_2 \otimes \delta_{x_1,x_2} F(z,\bar{z})\,, \tag{4.2}$$

and the values of $\delta_{x_1,x_2}F(z,\bar{z})$ can be read off from eq. (3.66).[1] Thus, we see that the knowledge of *all* double discontinuities enables us to immediately write down the answer for the (1,1,2) component of the two-loop ladder triangle. Just as in the case of a single unitarity cut, this component of the coproduct determines $F(z,\bar{z})$ up to terms that vanish when acting with $\Delta_{1,1,2}$. In the following, we show how this ambiguity can be lifted.

While the previous application is trivial and follows immediately from the first-entry condition and the knowledge of the set of variables that can enter the symbol in these particular examples, it is less obvious that we should be able to reconstruct information about the full function by looking at a single unitarity cut, or at a specific sequence of two unitarity cuts. In the rest of this section we give evidence that this is true nevertheless (both for diagrams with massless or massive propagators).

The classic tool for determining a Feynman integral from its cuts is the *dispersion relation*, which expresses a given Feynman integral as the integral of its discontinuity across a certain branch cut. Traditionally used in the context of the study of strongly interacting theories, dispersion relations appear more generally as a consequence of the unitarity of the S-matrix, and of the analytic structure of amplitudes [20]. These relations are valid in perturbation theory, order by order

[1] As written, eq. (3.66) gives solutions for four of the sixteen functions, $\delta_{x_1,x_2}F(z,\bar{z})$. The remaining ones can be obtained trivially by imposing the first entry condition, so that $\delta_z F(z,\bar{z}) = \delta_{\bar{z}}F(z,\bar{z})$ and $\delta_{1-z}F(z,\bar{z}) = \delta_{1-\bar{z}}F(z,\bar{z})$, and by extending the kinematic analysis to regions in which $\bar{z} > z$, thus restoring the symmetry of the full function under exchange of z and $\bar{z}$.

in an expansion of the coupling constant. It was shown in refs. [18, 19, 21–23] that individual Feynman integrals can also be written as dispersive integrals. The fundamental ingredient in the proof of the existence of this representation is the largest time equation [21], which is also the basis of the cutting rules. In the first part of this section we review dispersion relations for Feynman integrals, illustrating them with the examples of the one-loop three-mass triangle integral and the two-loop three-point three-mass ladder integral. We used the same method to compute the one-loop triangles with three external masses and one or two massive propagators, but left that discussion for the appendix—see section B.3.

We then show we can use the modern Hopf algebraic language to determine the symbol of the integrals from either a single unitarity cut or a single sequence of unitarity cuts. We will present several methods for this reconstruction, both for diagrams with massless or massive propagators. Most of them require a previous knowledge of the symbol alphabet, so we present them mostly as an illustration of how the analytic strucutre of Feynman diagrams is constrained by the knowledge of its cuts.

The reconstructibility procedure presented here works for the full integral, and not for individual terms[2] in the Laurent expansion in ϵ. We therefore focus on examples which are finite in four dimensions, so that we can set $\epsilon = 0$.

Aside from the review on dispersive integrals, all the work presented here was done during my PhD, in collaboration with Ruth Britto, Claude Duhr, my supervisor Einan Gardi, and Hanna Grönqvist for the study of diagrams with internal masses.

4.2 Dispersion relations

Dispersion relations are a prescription for computing an integral from its discontinuity across a branch cut, taking the form

$$F(p_1^2, p_2^2, \ldots) = \frac{1}{2\pi i} \int_C \frac{ds}{s - (p_2^2 + i\varepsilon)} \, \rho(p_1^2, s, \ldots) \,, \tag{4.3}$$

[2] An example of an infrared divergent integral where the reconstructibility of individual terms in the Laurent expansion would fail is the two-mass-hard box: it is clear from eq. (3.76) that a cut in a single channel does not capture all terms of the symbol.

where

$$\rho(p_1^2, s, \ldots) = \mathrm{Disc}_{p_2^2} F(p_1^2, p_2^2, \ldots)\big|_{p_2^2=s} ,$$

as computed with eq. (2.34), and the integration contour C goes along that same branch cut. The above relation can be checked using eqs. (2.34) and (3.140).

We start with a simple generalisation of the above expression. Let

$$G(p_i^2) = r(p_i^2) F(p_i^2) ,$$

where $r(p_i^2)$ is a rational function of the Mandelstam invariants p_i^2. Then, because $G(p_i^2)$ and $F(p_i^2)$ have the same branch point and branch cut structure, $G(p_i^2)$ itself has a dispersive representation of the form eq. (4.3). This in turn provides an alternative representation for $F(p_i^2)$. Indeed, using that

$$\mathrm{Disc}_{p_2^2} G(p_1^2, p_2^2, \ldots) = r(p_1^2, p_2^2, \ldots) \, \mathrm{Disc}_{p_2^2} F(p_1^2, p_2^2, \ldots) ,$$

one gets:

$$F(p_1^2, p_2^2, \ldots) = \frac{1}{2\pi i} \frac{1}{r(p_1^2, p_2^2, \ldots)} \int_C \frac{ds}{s - (p_2^2 + i\varepsilon)} \, r(p_1^2, s, \ldots) \rho(p_1^2, s, \ldots) , \quad (4.4)$$

provided the integral on the right hand side is well defined, and where for simplicity we assumed $\rho(p_1^2, s, \ldots)$ has no poles in the integration region (if this is not the case, we need to add the contribution of the residues at those poles, as dictated by the residue theorem). Eq. (4.3) can be seen as a particular case of eq. (4.4), with $r(p_i^2) = 1$. If the integral in eq. (4.3) is not well defined, typically by becoming divergent at some endpoint of the integration region, a judicious choice of $r(p_i^2)$ can be made to find a dispersive representation for $F(p_i^2)$. These are called subtracted dispersion relations (see e.g. Appendix B in [102] for an example in the context of dispersive representations of Feynman integrals).

In light of the relation between discontinuities and cuts presented in this thesis, if $F(p_1^2, p_2^2, \ldots)$ is a Feynman integral, eq. (4.4) can also be written as:

$$\begin{aligned} &F(p_1^2, p_2^2, \ldots) = \\ &= -\frac{1}{2\pi i} \frac{1}{r(p_1^2, p_2^2, \ldots)} \int_C \frac{ds}{s - (p_2^2 + i\varepsilon)} \, r(p_1^2, s, \ldots) \left(\mathrm{Cut}_{p_2^2} F(p_1^2, p_2^2, \ldots) \right) \Big|_{p_2^2=s} . \end{aligned} \quad (4.5)$$

In order to illustrate the use of dispersion relations, we first look at the case

of the scalar three-mass triangle. Its p_2^2-channel cut was computed in eq. (B.56), and we recall it here expressed in terms of Mandelstam invariants,

$$\begin{aligned}&\mathrm{Cut}_{p_2^2} T(p_1^2, p_2^2, p_3^2) = \\ &\qquad = \frac{2\pi}{\sqrt{\lambda(p_1^2, p_2^2, p_3^2)}} \log\left(\frac{p_1^2 - p_2^2 + p_3^2 - \sqrt{\lambda(p_1^2, p_2^2, p_3^2)}}{p_1^2 - p_2^2 + p_3^2 + \sqrt{\lambda(p_1^2, p_2^2, p_3^2)}}\right) + \mathcal{O}(\epsilon). \end{aligned} \tag{4.6}$$

This leads to a dispersive representation for the three-mass triangle of the form ($r(p_i^2) = 1$):

$$\begin{aligned}&T(p_1^2, p_2^2, p_3^2) = \\ &= \frac{-1}{2\pi i} \int_0^\infty \frac{ds}{s - (p_2^2 + i\varepsilon)} \frac{2\pi}{\sqrt{\lambda(p_1^2, s, p_3^2)}} \log\left(\frac{p_1^2 - s + p_3^2 - \sqrt{\lambda(p_1^2, s, p_3^2)}}{p_1^2 - s + p_3^2 + \sqrt{\lambda(p_1^2, s, p_3^2)}}\right). \end{aligned} \tag{4.7}$$

Note that the integration contour runs along the real positive axis: it corresponds to the branch cut for timelike invariants of Feynman integrals with massless internal propagators. Already for this not too complicated diagram we see that the dispersive representation involves a rather complicated integration.

The main difficulty in performing the integral above comes from the square root of the Källén function, whose arguments depend on the integration variable. However, defining $x = s/p_1^2$, and introducing variables α and $\bar{\alpha}$ similar to eq. (2.29), which are are a particular case of the more general eq. (2.26), defined as

$$\alpha\bar{\alpha} = x \quad \text{and} \quad (1-\alpha)(1-\bar{\alpha}) = u_3\,, \tag{4.8}$$

or equivalently,

$$\alpha = \frac{1 + x - u_3 + \sqrt{\lambda(1, x, u_3)}}{2} \quad \text{and} \quad \bar{\alpha} = \frac{1 + x - u_3 - \sqrt{\lambda(1, x, u_3)}}{2}\,, \tag{4.9}$$

we can rewrite the dispersive integral as,

$$\begin{aligned}&T(p_1^2, p_2^2, p_3^2) = \\ &= \frac{i}{p_1^2} \int du_3 \int \frac{dx}{x - u_2} \frac{1}{\alpha - \bar{\alpha}} \log\frac{1-\alpha}{1-\bar{\alpha}}\, \delta\big(u_3 - (1-\alpha)(1-\bar{\alpha})\big)\, \theta(-x)\, \theta(u_3) \\ &= \frac{-i}{p_1^2} \int_0^1 d\alpha \int_{-\infty}^0 d\bar{\alpha} \frac{1}{\alpha\bar{\alpha} - u_2} \delta\big(u_3 - (1-\alpha)(1-\bar{\alpha})\big) \log\frac{1-\alpha}{1-\bar{\alpha}} \end{aligned}$$

$$= \frac{-i}{p_1^2}\frac{1}{z-\bar{z}}\int_0^1 d\alpha \left(\frac{1}{\alpha-\bar{z}} - \frac{1}{\alpha-z}\right)\Big[2\log(1-\alpha) - \log u_3\Big]\,, \tag{4.10}$$

where the integration region for α and $\bar{\alpha}$ is deduced from the region where the discontinuity is computed (see e.g. table 2.1). Written in this form, the remaining integration is trivial to perform in terms of polylogarithms, and we indeed recover the result of the three-mass triangle, eq. (B.51).

For the three-mass triangle, we can in fact take a second discontinuity and reconstruct the result through a double dispersion relation because the discontinuity function, eq. (4.6), has a dispersive representation itself [19, 94]. Note that this representation falls outside of what is discussed in ref. [22], and we are not aware of a proof of its existence from first principles. The double discontinuity is simply given, up to overall numerical and scale factors, by the inverse of the square root of the Källén function, see eq. (B.60). We obtain

$$\begin{aligned}
&T(p_1^2,p_2^2,p_3^2) = \\
&= -\frac{1}{(2\pi i)^2}\int\frac{dx}{x-u_2}\int\frac{dy}{y-u_3}\Big(\mathrm{Cut}_{p_3^2,p_2^2}\,T(p_1^2,p_2^2,p_3^2)\Big)\Big|_{u_2=x,u_3=y} \\
&= \frac{1}{(2\pi i)^2}\frac{4\pi^2 i}{p_1^2}\int\frac{dx}{x-u_2}\int\frac{dy}{y-u_3}\frac{1}{\sqrt{\lambda(1,x,y)}}\,\theta(-x)\,\theta(-y) \\
&= \frac{-i}{p_1^2}\int_1^\infty d\alpha\int_{-\infty}^0 d\bar{\alpha}\frac{1}{\alpha\bar{\alpha}-z\bar{z}}\frac{1}{(1-\alpha)(1-\bar{\alpha})-(1-z)(1-\bar{z})}\,.
\end{aligned} \tag{4.11}$$

The integral is trivial to perform[3] and leads to the correct result.

We now turn to the case of the two-loop ladder. As long as we are using suitable variables, from the point of view of dispersion relations it is trivial to go from the three-mass triangle to the two-loop ladder. The only new feature we need to deal with is a more complicated rational prefactor: instead of just having the inverse of the square root of the Källén function, it appears multiplied by $1/u_3$. This makes the dispersive integral over p_3^2 as written in eq. (4.3) non convergent. However, we can easily overcome this difficulty by setting $r(p_i^2) = p_3^2/p_1^2 = u_3$ in eq. (4.5). When considering a dispersive integral over p_2^2 this is not necessary for the convergence of the integral, but the same choice of $r(p_i^2)$ still simplifies

[3]We have redefined α and $\bar{\alpha}$ by replacing u_3 by y in eq. (4.9). Just as for the single dispersion integral, the integration region is deduced from the region where the double discontinuity is computed, $R_{2,3}$ in this case. Changing variables to $\beta = \frac{1}{\alpha}$ and $\gamma = \frac{1}{1-\bar{\alpha}}$ makes the integral particularly simple to evaluate.

the integrand and makes the calculation simpler. Having made this choice, and proceeding as with the three-mass triangle, the remaining integral is trivial to perform in terms of polylogarithms.

As an example, we consider the dispersive integral over p_3^2:

$$\begin{aligned} &T_L(p_1^2,p_2^2,p_3^2) = \\ &= -\frac{1}{2\pi i}\frac{1}{u_3}\int_{-\infty}^{0}\frac{dy}{y-u_3}\,y\int_0^{\infty}du_2\,\delta(u_2-\alpha\bar{\alpha})\left(\mathrm{Cut}_{p_3^2}T_L(p_1^2,p_2^2,p_3^2)\right)\Big|_{u_3=y} \\ &= \frac{i(p_1^2)^{-2}}{(z-\bar{z})(1-z)(1-\bar{z})}\int_0^1 d\bar{\alpha}\left(\frac{1}{\bar{\alpha}-\bar{z}}-\frac{1}{\bar{\alpha}-z}\right)\frac{1}{2}\log\bar{\alpha}\log\frac{u_2}{\bar{\alpha}}\log\frac{u_2}{\bar{\alpha}^2}\,, \end{aligned} \tag{4.12}$$

where the variables α and $\bar{\alpha}$ are similar to the ones defined in eq. (4.9) but with x replaced by u_2 and u_3 by y, and we used $\mathrm{Cut}_{p_3^2}T_L(p_1^2,p_2^2,p_3^2)$ as obtained from eq. (3.122). This integral does indeed reproduce the expected result, eq. (3.97).

Similarly to the one-loop three-mass triangle, the two-loop three-mass ladder also has a representation as a double dispersive integral. Given the variables we chose to work with it is more convenient to consider the double unitarity cut on p_2^2 and p_3^2. Using eq. (3.66), with the necessary prefactors as in eq. (3.97),

$$\mathrm{Cut}_{p_3^2,p_2^2}T_L(p_1^2,p_2^2,p_3^2) = -\frac{4\pi^2 i\,(p_1^2)^{-2}}{(1-z)(1-\bar{z})(z-\bar{z})}\left(\log z\log\bar{z}-\frac{1}{2}\log^2 z\right)\,,$$

from which we get:

$$\begin{aligned} &T_L(p_1^2,p_2^2,p_3^2) = \\ &= -\frac{1}{(2\pi i)^2}\frac{1}{u_3}\int_{-\infty}^{0}\frac{dx}{x-u_2}\int_{-\infty}^{0}\frac{dy}{y-u_3}\,y\left(\mathrm{Cut}_{p_3^2,p_2^2}T_L(p_1^2,p_2^2,p_3^2)\right)\Big|_{u_2=x,u_3=y} \\ &= -i\frac{(p_1^2)^{-2}}{u_3}\int_1^{\infty}d\alpha\int_{-\infty}^{0}d\bar{\alpha}\frac{\log\alpha\log\bar{\alpha}-\frac{\log^2\alpha}{2}}{(\alpha\bar{\alpha}-u_2)((1-\alpha)(1-\bar{\alpha})-u_3)}\,, \end{aligned} \tag{4.13}$$

where we again used $r(p_i^2)=u_3$ and exactly the same comments as the ones accompanying eq. (4.11) apply. The remaining integrals are trivial to perform, and we indeed recover the correct result, eq. (3.97). As far as we are aware, this is the first time such a representation of the two-loop three-mass ladder has been given.

We see that we can obtain the full result for the one-loop three-mass triangle and the two-loop three-point three-mass ladder from the knowledge of either

its single or double cuts. A fundamental ingredient necessary to perform the dispersive integral was the choice of variables in which to write the dispersive integral. While for the one-loop example we studied one might still consider performing the integration in terms of the Mandelstam invariants, for the two-loop ladder this does not seem feasible anymore given the complexity of the expression for the discontinuity in any of the channels when written in terms of the Mandelstam invariants. For these examples, choosing the variables of eq. (4.9), which we showed are naturally found by computing cuts, the increase in complexity in going from one to two loops is not as great as one might naïvely expect. More generally, although dispersive integrals are initially defined in terms of Mandelstam invariants, as in eq. (4.3), we expect them to become simpler when it is possible to change variables to letters in the symbol alphabet, eq. (2.26). Indeed, in terms of these variables the underlying structure of iterated integrals described in Section 2.2 becomes manifest.

We finish with a comment: we believe the dispersive representation for the three-mass triangle provides one of the simplest ways to compute the diagram to any order in the expansion of the dimensional regularisation parameter ϵ. While we only considered the leading order in eq. (4.10), following the same arguments we could as easily have written

$$T(p_1^2,p_2^2,p_3^2) = -i\frac{(p_1^2)^{-1-\epsilon}}{z-\bar{z}}\frac{e^{\gamma_E\epsilon}\Gamma(1-\epsilon)}{\Gamma(2-2\epsilon)}\int_0^1 d\alpha\left(\frac{1}{\alpha-\bar{z}}-\frac{1}{\alpha-z}\right)\frac{u_3-(1-\alpha)^2}{u_3} \left(\frac{\alpha(1-\alpha-u_3)}{1-\alpha}\right)^{-\epsilon}{}_2F_1\left(1,1-\epsilon;2-2\epsilon;\frac{u_3-(1-\alpha)^2}{u_3}\right) \quad (4.14)$$

where we used the D-dimensional result for the cut given in eq. (B.56). Integration over α and expansion in ϵ on the right hand side commute, and we are left at any order with one integration to perform. The expansion in ϵ of the hypergeometric function, although not trivial, has been automatised [100]. Aside from one overall rational prefactor that cancels the one remaining in the integrand, it will only produce polylogarithms and thus the remaining integration is trivial to perform in terms of multiple polylogarithms. The result will already be expressed as a function of the variables in terms of which this diagram is known to be most simply written.

We believe a deeper understanding of the connection between multiple cuts

and sequential discontinuities as defined in this thesis can provide a way to prove the existence of multiple dispersive representations. We expect they will in turn be useful in the actual calculation of Feynman integrals in cases where more traditional techniques fail.

4.3 Reconstruction of three-point functions with massless propagators

We now present purely algebraic methods to reconstruct the uncut three-mass one-loop triangle and three-mass two-loop ladder.

4.3.1 Reconstructing the coproduct from a single unitarity cut

As discussed above, Feynman diagrams can be fully recovered from unitarity cuts in a given channel through dispersion relations. These relations rely on two ingredients: the discontinuity of a function across a specific branch cut, and the position of that particular branch cut. Given the relations between the $(1, n-1)$ entries of the coproduct, discontinuities, and single unitarity cuts established in previous sections, it is clear that the full information about the Feynman integral is encoded in any one of these entries of the coproduct, since it contains the same information about the function as a dispersive representation. We should thus be able to reconstruct information about the full function by looking at a single cut in a given channel.

For simplicity, we work mainly at the level of the symbol in the rest of this section, keeping in mind that we lose information about terms proportional to π and zeta values in doing so. We will find that this information can easily be recovered in our examples. In a nutshell, we observe that if we combine the first entry condition and the results for the discontinuities with the integrability condition (2.17), we immediately obtain the symbol of the full function. In the following, we illustrate this procedure in the examples of the one-loop triangle and two-loop three-point ladder. Starting from the result for the unitarity cut in a single channel, the procedure to obtain the symbol of the full function can be formulated in terms of a simple algorithm, which involves two steps:

(i) Check if the tensor satisfies the integrability condition, and if not, add the relevant terms required to make the tensor integrable.

(ii) Check if the symbol obtained from the previous step satisfies the first entry condition, and if not, add the relevant terms. Then return to step (i).

We start by illustrating this procedure on the rather simple example of the three-mass triangle of Section B.3.1. From eq. (B.56), the symbol of the cut in the p_2^2 channel is

$$\frac{1-z}{1-\bar{z}}\,,$$

where we emphasise that the rational function is to be interpreted as the symbol of a logarithm. We note that the same exercise can be done using the cuts in other channels. Since we considered a cut in the p_2^2 channel, the first entry condition implies that we need to prepend $u_2 = z\bar{z}$ to the symbol of the discontinuity. Thus we begin with the tensor

$$(z\bar{z}) \otimes \frac{1-z}{1-\bar{z}}\,.$$

We then proceed as follows.

- Step (i): This tensor is not the symbol of a function, as it violates the integrability condition. To satisfy the integrability condition, we need to add the two terms

  $$(1-z)\otimes\bar{z} - (1-\bar{z})\otimes z\,.$$

  The full tensor is not the symbol of a Feynman diagram, since the two new terms do not satisfy the first entry condition.

- Step (ii): To satisfy the first entry condition, we add two new terms:

  $$(1-\bar{z})\otimes\bar{z} - (1-z)\otimes z\,.$$

  At this stage, the sum of terms obeys the first entry condition and the symbol obeys the integrability condition, so we stop our process.

Putting all the terms together, we obtain

$$\mathcal{S}(\mathcal{T}(z,\bar{z})) = z\bar{z}\otimes\frac{1-\bar{z}}{1-z} + (1-z)(1-\bar{z})\otimes\frac{z}{\bar{z}}, \tag{4.15}$$

which agrees with the symbol of the one-loop three mass triangle in $D = 4$ dimensions, eq. (B.54).

Note that we can easily integrate this symbol to the full function. Indeed, the cut computation has allowed us to determine the symbol, and hence also the symbol alphabet $\mathcal{A}_\triangle = \{z, \bar{z}, 1-z, 1-\bar{z}\}$. It is well known that the most general class of functions giving rise to this symbol alphabet and satisfying the first entry condition are the single-valued harmonic polylogarithms [103]. Up to overall normalisation, there is a unique single-valued harmonic polylogarithm of weight two that is odd under the exchange of z and $\bar{z}$, namely the function $\mathcal{P}_2(z)$ defined in eq. (B.52). We therefore immediately recover the analytic expression for $\mathcal{T}(z, \bar{z})$ given in section B.3.1.

While the previous example might seem too simple to be representative, we show next that the same conclusion still holds for the two-loop ladder. In the following we use our knowledge of the cut in the p_3^2 channel, eq. (3.122), and show that we can again reconstruct the symbol of the full integral $F(z, \bar{z})$. As for the one-loop example, the same exercise can be done using the cuts in other channels. Combining eq. (3.122) with the first entry condition, we conclude that $\mathcal{S}(F(z, \bar{z}))$ must contain the following terms:

$$\begin{aligned}&(1-z)(1-\bar{z})\otimes \\ &\left[z\otimes z\otimes \bar{z} + z\otimes \bar{z}\otimes z + \bar{z}\otimes z\otimes z - z\otimes \bar{z}\otimes \bar{z} - \bar{z}\otimes z\otimes \bar{z} - \bar{z}\otimes \bar{z}\otimes z\right] .\end{aligned} \tag{4.16}$$

If we follow the same steps as in the one-loop case, we can again reconstruct the symbol of the full function from the knowledge of the symbol of the cut in the p_3^2 channel alone. More precisely, we perform the following operations:

- Step (i): To obey the integrability condition, we must add to the expression above the following eight terms:

$$\begin{aligned}&+ z\otimes(1-\bar{z})\otimes z\otimes\bar{z} + z\otimes z\otimes(1-\bar{z})\otimes\bar{z} + z\otimes(1-\bar{z})\otimes\bar{z}\otimes z \\ &+ \bar{z}\otimes(1-z)\otimes z\otimes z - z\otimes(1-\bar{z})\otimes\bar{z}\otimes\bar{z} - \bar{z}\otimes(1-z)\otimes z\otimes\bar{z} \\ &- \bar{z}\otimes(1-z)\otimes\bar{z}\otimes z - \bar{z}\otimes\bar{z}\otimes(1-z)\otimes z\,.\end{aligned}$$

- Step (ii): The terms we just added violate the first entry condition. To restore it we must add eight more terms that combine with the ones above

to have Mandelstam invariants in the first entry,

$$
\begin{aligned}
&+ \bar{z} \otimes (1-\bar{z}) \otimes z \otimes \bar{z} + \bar{z} \otimes z \otimes (1-\bar{z}) \otimes \bar{z} + \bar{z} \otimes (1-\bar{z}) \otimes \bar{z} \otimes z \\
&+ z \otimes (1-z) \otimes z \otimes z - \bar{z} \otimes (1-\bar{z}) \otimes \bar{z} \otimes \bar{z} - z \otimes (1-z) \otimes z \otimes \bar{z} \\
&- z \otimes (1-z) \otimes \bar{z} \otimes z - z \otimes \bar{z} \otimes (1-z) \otimes z \,.
\end{aligned}
$$

- Step (i): The newly added terms violate the integrability condition. To correct it, we must add two new terms,

$$
z \otimes \bar{z} \otimes (1-\bar{z}) \otimes \bar{z} - \bar{z} \otimes z \otimes (1-z) \otimes z \,. \tag{4.17}
$$

- Step (ii): We again need to add terms that combine with the two above to have invariants in the first entry,

$$
\bar{z} \otimes \bar{z} \otimes (1-\bar{z}) \otimes \bar{z} - z \otimes z \otimes (1-z) \otimes z \,. \tag{4.18}
$$

At this point the symbol satisfies both the first entry and integrability conditions, and we obtain a tensor which agrees with the symbol for $F(z,\bar{z})$ in eq. (3.101).

Note that we can again easily promote the symbol to the full function. Indeed, the symbol alphabet $\mathcal{A}_{\triangle} = \{z, \bar{z}, 1-z, 1-\bar{z}\}$ combined with the first entry condition again implies that $F(z,\bar{z})$ can be expressed in terms of single-valued harmonic polylogarithms. Taking into account the antisymmetry under exchange of z and $\bar{z}$ we find that there is a one-parameter family of functions with the correct symbol,

$$
\begin{aligned}
F(z,\bar{z}) = {} & 6\big[\mathrm{Li}_4(z) - \mathrm{Li}_4(\bar{z})\big] - 3\log(z\bar{z})\big[\mathrm{Li}_3(z) - \mathrm{Li}_3(\bar{z})\big] \\
& + \frac{1}{2}\log^2(z\bar{z})\big[\mathrm{Li}_2(z) - \mathrm{Li}_2(\bar{z})\big] + c\,\mathcal{P}_2(z)\,,
\end{aligned} \tag{4.19}
$$

where c is a real constant (of weight two). This constant can be fixed by explicitly computing the discontinuity of the function $F(z,\bar{z})$ in the variable p_3^2, and imposing that the discontinuity agrees with the result for the cut integral (3.122), i.e., by requiring that (cf. eq. (3.123)),

$$
\mathrm{Disc}_{p_3^2} F(z,\bar{z}) = i\,(p_1^2)^2\,(1-z)(1-\bar{z})(z-\bar{z})\,\mathrm{Cut}_{p_3^2,R_{\triangle}^3} T_L(p_1^2,p_2^2,p_3^2)\,. \tag{4.20}
$$

It is easy to check that we must have $c = 0$. Note that if the free parameters in the solution multiply functions that vanish when a discontinuity in a given channel is taken, we can supplement this procedure by considering cuts in other channels. In this way we can fix the initial condition up to a polylogarithmic function that does not have any discontinuities, and must thus be a constant. This constant can easily be fixed by computing the value of the original Feynman integral numerically in a single point.

We finish with a comment. In these examples the integrability condition, eq. (2.17), was particularly simple to implement because none of the letters of the symbol alphabet depended on more than one independent variable, in this case z and $\bar{z}$. This is of course not true in general (even for these examples, at higher orders in ϵ the letter $(z - \bar{z})$ appears in the symbol alphabet), so implementing the integrability condition is in general more complicated than in the examples considered here.

4.3.2 Reconstructing the coproduct from double unitarity cuts

While the possibility of reconstructing the function from a single cut in a given channel might not be surprising, due to the fact that Feynman integrals can be written as dispersive integrals over the discontinuity in a given channel, we show in this section that in this particular case we are able to reconstruct the full answer for $\Delta_{1,1,2}F$ from the knowledge of just *one* sequential double cut, along with the symbol alphabet. Note that $\Delta_{1,1,2}F$ is completely equivalent to the symbol $\mathcal{S}(F)$. Indeed, the weight two part of $\Delta_{1,1,2}F$ is defined only modulo π, which is precisely the amount of information contained in the symbol.

Assuming that the symbol letters are drawn from the symbol alphabet already given previously, $\mathcal{A}_{\triangle} = \{z, \bar{z}, 1 - z, 1 - \bar{z}\}$, we can write $\Delta_{1,1,2}F$ in the following general form:

$$\Delta_{1,1,2}F = \sum_{(x_1,x_2)\in\mathcal{A}_{\triangle}^2} \log x_1 \otimes \log x_2 \otimes f_{x_1,x_2} \,,$$

where the f_{x_1,x_2} denote 16 a priori unknown functions of weight two (defined only modulo π^2). Imposing the first entry condition and the integrability condition in the first two entries of the coproduct gives the following constraints among

the f_{x_1,x_2}:

$$\begin{aligned}
&f_{z,z} = f_{\bar{z},z} = f_{z,\bar{z}} = f_{\bar{z},\bar{z}}\,,\\
&f_{1-z,z} = f_{1-\bar{z},z} = f_{z,1-\bar{z}} = f_{\bar{z},1-\bar{z}}\,,\\
&f_{z,1-z} = f_{\bar{z},1-z} = f_{1-z,\bar{z}} = f_{1-\bar{z},\bar{z}}\,,\\
&f_{1-z,1-z} = f_{1-\bar{z},1-z} = f_{1-z,1-\bar{z}} = f_{1-\bar{z},1-\bar{z}}\,,
\end{aligned} \tag{4.21}$$

which reduces the number of unknown functions to 4. Defining $\tilde{F}(z,\bar{z}) = F(\bar{z},z)$, we must require in addition that $\tilde{F}(z,\bar{z}) = -F(z,\bar{z})$ (because its leading singularity is likewise odd under this exchange), which gives further constraints. For instance,

$$f_{1-\bar{z},z} = -\tilde{f}_{1-z,\bar{z}}\,. \tag{4.22}$$

We can thus write

$$\begin{aligned}
&\Delta_{1,1,2}F =\\
&= \log(z\bar{z})\otimes\log(z\bar{z})\otimes f_{z,z} + \log((1-z)(1-\bar{z}))\otimes\log((1-z)(1-\bar{z}))\otimes f_{1-z,1-z}\\
&+ [\log(z\bar{z})\otimes\log(1-z) + \log((1-z)(1-\bar{z}))\otimes\log\bar{z}]\otimes f_{1-z,\bar{z}}\\
&- [\log(z\bar{z})\otimes\log(1-\bar{z}) + \log((1-z)(1-\bar{z}))\otimes\log z]\otimes \tilde{f}_{1-z,\bar{z}}\,.
\end{aligned} \tag{4.23}$$

Notice that up to this stage all the steps are generic: we have not used our knowledge of the functional form of any of the double cuts which determine the f_{x_1,x_2}, but only the knowledge of the set of variables entering its symbol and the antisymmetry of the leading singularity under the exchange of z and $\bar{z}$.

We now assume that we know the value of $\mathrm{Cut}_{p_3^2,p_2^2}F$, and thus by eq. (3.66f) we have determined that

$$\delta_{1-z,\bar{z}}F = -\log z\log\bar{z} + \frac{1}{2}\log^2 z\,. \tag{4.24}$$

Next, we have to require that eq. (4.23) be integrable in the second and third component. Assuming again that we only consider symbols with letters drawn from the set $\mathcal{A}_\triangle$, we use eq. (4.24) and impose the integrability condition eq. (2.17), and we see that the symbols of the two unknown functions in eq. (4.23)

are uniquely fixed,

$$\begin{aligned}\mathcal{S}(f_{z,z}) &= -z\otimes(1-z)+\bar{z}\otimes(1-\bar{z}) = \mathcal{S}(\mathrm{Li}_2(z)-\mathrm{Li}_2(\bar{z}))\,,\\ \mathcal{S}(f_{1-z,1-z}) &= 0\,,\end{aligned}$$

in agreement with eq. (3.100).

Note that once again we can easily integrate the symbol to the full function by an argument similar to the one presented in Section 4.3.1: the most general function having the correct symbol is again given by eq. (4.19), and the constant c can easily be shown to vanish by requiring the function to have the correct double discontinuity, i.e., by imposing that

$$\mathrm{Disc}_{p_3^2,p_2^2} F(z,\bar{z}) = -i\,(p_1^2)^2\,(1-z)(1-\bar{z})(z-\bar{z})\,\mathrm{Cut}_{p_3^2,p_2^2} T_L(p_1^2,p_2^2,p_3^2)\,. \quad (4.25)$$

We stress that the fact that we can reconstruct $\Delta_{1,1,2}F$ from a single sequence of cuts is not related to the specific sequence we chose. For example, if we had computed only $\mathrm{Cut}_{p_1^2,p_2^2}F$ and thus determined that $-f_{z,\bar{z}} - f_{1-z,\bar{z}} = -\mathrm{Li}_2(z) + \mathrm{Li}_2(\bar{z}) + \log z \log\bar{z} - \frac{1}{2}\log^2 z$, the integrability condition would fix the remaining two free coefficients in a similar way. Finally, we could consider $\mathrm{Cut}_{p_3^2,p_1^2}F$, but since this cut is obtained by a simple change of variables from $\mathrm{Cut}_{p_3^2,p_2^2}F$ through the reflection symmetry of the ladder, it is clear that integrability fixes the full symbol once again.

Let us briefly consider the analogous construction for the one-loop triangle, where the f_{x_1,x_2} are simply constant functions. The analog of eq. (4.23) above is

$$\begin{aligned}&\Delta_{1,1}\mathcal{T} =\\ &f_{z,z}\,(\log(z\bar{z})\otimes\log(z\bar{z})) + f_{1-z,1-z}\,(\log((1-z)(1-\bar{z}))\otimes\log((1-z)(1-\bar{z})))\\ &+ f_{1-z,\bar{z}}\,[\log(z\bar{z})\otimes\log(1-z)+\log((1-z)(1-\bar{z}))\otimes\log\bar{z}]\\ &+ f_{1-\bar{z},z}\,[\log(z\bar{z})\otimes\log(1-\bar{z})+\log((1-z)(1-\bar{z}))\otimes\log z]\,. \end{aligned} \quad (4.26)$$

A specific double cut, without loss of generality say $\mathrm{Cut}_{p_3^2,p_2^2}$, gives a constant value for $f_{1-z,\bar{z}}$, as seen from eq. (B.60) and eq. (3.66f). We have a consistent solution with $f_{1-z,\bar{z}} = -f_{1-\bar{z},z} = -1$ and $f_{z,z} = f_{1-z,1-z} = 0$, which is indeed the $\Delta_{1,1}$ of the triangle, obtained by a consistent completion algorithm as in the previous subsection.

While it is quite clear that the reason why the algorithm of section 4.3.1 converged was the existence of a dispersive representation of Feynman integrals, we do not know whether the existence of a double dispersive representation is a necessary condition for the reconstruction based on the knowledge of $\Delta_{1,1,2}$ done in this section to work, although it does seem reasonable that it would be the case.

In closing, we notice that in this example, the integrability condition eq. (4.21) implies that $\text{Cut}_{p_i^2,p_j^2} = \text{Cut}_{p_j^2,p_i^2}$, through the relations listed in eq. (3.66). It would be interesting to see whether there is a general link between the integrability of the symbol and the permutation invariance of a sequence of cuts.

4.4 Reconstruction of three-point functions with massive propagators

In [37], similar methods to the ones described above to reconstruct uncut functions with massless propagators were developed for one-loop triangles with internal masses. When internal masses are present, the reconstruction process is less algorithmic, and requires some knowledge of the type of symbol letters that can appear in order to construct a general ansatz for the symbol. This ansatz is then constrained by the information obtained from cuts. We describe how the ansatz is constructed for a variety of examples, and then how the uncut function is reconstructed from its symbol.

4.4.1 Constructing and constraining an ansatz for the symbol

Our general strategy is the following. We observe that the symbol alphabets of the scalar triangles we are investigating follow a pattern. With some experience, we are able to write an ansatz for their symbol, in terms of unknown numerical coefficients. Then, by imposing the knowledge of one channel cut, the first-entry condition, the integrability condition, the absence of trivial terms (of the form $x \otimes x$) and the symmetries of the function, we are able to fix all of the unknown coefficients. We now give more specific rules for each of the steps just mentioned.

We start by explaining how to build the ansatz. First, we recall that if

the diagram is a function of n invariants, the pure functions we are concerned with in this section are functions of $n-1$ dimensionless variables only. For concreteness, we always choose to normalise our variables by an external invariant. The procedure starts by listing the possible first entries. These are completely fixed by the first-entry condition—see sec. 2.3.2. Listing the second entries is more difficult than listing the first entries. It can however be done based on the knowledge of a cut integral, and, for the letters that do not appear in channel cuts, by the empirical observations we list below.

Listing the second entries: We always start from a single cut in an external channel. We observe the presence of the following terms in the set of second entries:

- All letters of the symbol alphabet of the channel cut taken as the known starting point ;
- Differences of internal masses, or their equivalents in terms of w_1 and $\bar{w}_1$—see eq. (2.33) ;
- For triangles with two external invariants, ratios of external invariants. In our examples, this is just p_2^2/p_3^2. For the examples with three external massive channels where we must use the variables z and $\bar{z}$ (see (2.29)), this condition is replaced by the presence of the letters z, $\bar{z}$, $(1-z)$ and $(1-\bar{z})$.

The terms generated through the above rules are added as cofactors of all the first entries, each multiplied by an undetermined numerical coefficient. For the first entry corresponding to the cut assumed to be known, these coefficients are of course fixed by the cut result. For the other first entries, they must be determined from additional considerations, according to the procedure we now describe.

Fixing the coefficients: We fix all coefficients according to the following steps:

1) We discard integrable terms of the form $x \otimes x$, as they are not needed in order to construct a minimal integrable symbol ;
2) Since the first-entry condition involves the original Mandelstam invariants, the dimensionless variables appearing in the symbol should be expanded when imposing this condition. Notably, we sometimes normalise the

invariants by a variable p_i^2 with a nonzero mass threshold, so that p_i^2 should not ultimately appear as a first entry by itself, although it shows up superficially in the expansion of the dimensionless variables. Thus, all of the second-entry cofactors of this p_i^2 should combine to give zero ;

3) We use the integrability condition, eq. (2.17), to fix the remaining parameters ;

These three rules are already highly constraining and indeed sufficient for most examples. If they are not, in particular in cases where we use the z, $\bar{z}$, w_1, and $\bar{w}_1$ variables, they can be complemented by the following:

4) Impose antisymmetry under $z \leftrightarrow \bar{z}$ and symmetry under $w_1 \leftrightarrow \bar{w}_1$. Indeed, the Feynman integrals are functions of the invariants only and must thus be symmetric under these transformations. When z and $\bar{z}$ are necessary, there is an antisymmetric rational prefactor, and so the pure function must be antisymmetric as well ;

5) If there is a symmetry under the exchange of the legs with momenta p_2 and p_3, impose symmetry under the simultaneous transformations $z \to 1 - \bar{z}$, $\bar{z} \to 1 - z$, $w_1 \to 1 - \bar{w}_1$, $\bar{w}_1 \to 1 - w_1$.

We now illustrate these rules in some examples. The example in appendix B.1.2 is trivial and the one in appendix B.1.3 divergent, so we will not address them. The next-simplest example is $T(p_1^2, 0, 0; m_{12}^2, m_{23}^2, 0)$—see appendix B.1.4—and we now show how to construct the ansatz for this case. We normalise the internal masses by p_1^2, giving the dimensionless variables $m_{12}^2/p_1^2 \equiv \mu_{12}$ and $m_{23}^2/p_1^2 \equiv \mu_{23}$, and we assume knowledge of the p_1^2 cut, eq. (B.15). Applying the rules given above for writing the ansatz, we get

$$\begin{aligned}
&\log(\mu_{12} - 1) \otimes [\log(\mu_{23} - 1 - \mu_{12}) - \log(\mu_{23})] \\
&\quad + \log(\mu_{12}) \otimes [a_1 \log(\mu_{23} - 1 - \mu_{12}) + a_2 \log(\mu_{23}) + a_3 \log(\mu_{12} - \mu_{23})] \\
&\quad + \log(\mu_{23}) \otimes [b_1 \log(\mu_{23} - 1 - \mu_{12}) + b_2 \log(\mu_{23}) + b_3 \log(\mu_{12} - \mu_{23})] \,, \qquad (4.27)
\end{aligned}$$

where we reintroduce the redundant 'log' for clarity of the equations. Our task is now to fix the coefficients a_i and b_i. In this case, using rules 1), 2) and 3) above fixes all coefficients, and we reproduce the symbol in eq. (B.14).

An example of similar complexity is the triangle $T(0, p_2^2, p_3^2; m_{12}^2, 0, 0)$, appendix B.2.3. We choose to normalise by p_2^2, and define the variables $m_{12}^2/p_2^2 \equiv \mu$ and $p_3^2/p_2^2 \equiv u$. We assume knowledge of the p_2^2 cut, eq. (B.45). According to the above steps, the general ansatz for the symbol reads:

$$\begin{aligned}
&\log(\mu-1)\otimes\{\log(u)+\log(\mu)-\log(\mu+u-1)\}\\
&\quad\log(u)\otimes\{a_1\log(u)+a_2\log(\mu)+a_3\log(\mu+u-1)\}\\
&+\log(\mu)\otimes\{b_1\log(u)+b_2\log(\mu)+b_3\log(\mu+u-1)\}
\end{aligned}\tag{4.28}$$

Our task is now to fix the coefficients a_i and b_i. As in the previous example, rules 1), 2) and 3) are sufficient and we reproduce the symbol in eq. (B.44).

As a final example of our rules to build the ansatz, we look at the most complicated case we address, $T(p_1^2, p_2^2, p_3^2; m_{12}^2, 0, m_{13}^2)$, given in appendix B.3.4. This requires using the variables z, $\bar{z}$, w_1 and $\bar{w}_1$. We assume knowledge of the p_1^2 cut, eq. (B.72). Following our rules, the ansatz is

$$\begin{aligned}
&\log(w_1(1-\bar{w}_1))\otimes\Big[\log(z-w_1)-\log(z-\bar{w}_1)-\log(\bar{z}-w_1)+\log(\bar{z}-\bar{w}_1)\Big]\\
&+\log(z\bar{z}-w_1\bar{w}_1)\otimes\Big[a_1\log(z-w_1)+a_2\log(z-\bar{w}_1)+a_3\log(\bar{z}-w_1)\\
&\qquad+a_4\log(\bar{z}-\bar{w}_1)+a_5\log(z)+a_6\log(\bar{z})+a_7\log(1-z)\\
&\qquad+a_8\log(1-\bar{z})+a_9\log(w_1\bar{w}_1-(1-w_1)(1-\bar{w}_1))\Big]\\
&+\log((1-z)(1-\bar{z})-(1-w_1)(1-\bar{w}_1))\otimes\Big[a_i\to b_i\Big]+\log(w_1\bar{w}_1)\otimes\Big[a_i\to c_i\Big]\\
&+\log(1-w_1)(1-\bar{w}_1)\otimes\Big[a_i\to d_i\Big],
\end{aligned}\tag{4.29}$$

and we must now determine the coefficients a_i, b_i, c_i and d_i. Interestingly, also for this case all we need are rules 1), 2) and 3) to fix all coefficients.

For all other triangles listed in appendix B, building the ansatz can be done in a similar way as illustrated above. We now list the rules we must apply to fix the coefficients of the ansatz of the remaining examples (for all cases, we assume knowledge of the p_1^2 cut):

- $T(p_1^2, 0, 0; m_{12}^2, 0, m_{13}^2)$, appendix B.1.5. Rules 1), 2) and 3) are sufficient ;
- $T(p_1^2, 0, 0; m_{12}^2, m_{23}^2, m_{13}^2)$, appendix B.1.6. Rules 1), 2), 3), 4) and 5) are needed ;

- $T(p_1^2, p_2^2, p_3^3; m_{12}^2, 0, 0)$, appendix B.3.3. Rules 1), 2) and 3) are sufficient.

4.4.2 Reconstructing the full function from the symbol

We now explain how we integrate the symbol to get the full function. Although integrating a symbol is in general an unsolved problem, it is a simple problem for weight two functions where a complete basis is even known to exist in terms of classical polylogarithms, see e.g. [53]. Once we have found a function that matches our symbol, all that remains to be done is fixing terms that are invisible to the symbol, in our case weight-one functions multiplied by π and terms proportional to ζ_2.

Powers of π are typically generated by analytic continuation and appear multiplied by i. Working in the Euclidean region where the function is real and away from any branch cut avoids this problem.

To fix the terms proportional to ζ_2, we can use two strategies. The first, which always works, is to evaluate the integrated symbol numerically at a single point and compare it to a numerically integrated Feynman parametrisation of the diagram. The difference must be a rational number multiplied by ζ_2, which completely determines our function. Alternatively, when possible, we can use the symmetries of the diagram to check if terms proportional to ζ_2 are allowed.

As examples, consider $T(p_1^2, 0, 0; 0, m_{23}^2, 0)$ and $T(p_1^2, p_2^2, p_3^2; m_{12}^2, 0, 0)$. In the first case, there is no symmetry consideration to fix terms proportional to ζ_2, and we must thus rely on numerical comparisons. In the second example, there is a rational prefactor antisymmetric under $z \leftrightarrow \bar{z}$, and thus the pure function must be antisymmetric under this transformation (the full function must be symmetric). This forbids the existence of terms proportional to ζ_2.

4.5 Summary and discussion

In this chapter, we have shown how the information obtained from the calculation of cuts of Feynamn integrals can be used to reconstruct the (symbol of the) full uncut function. This can be done either at the function level, by solving a dispersive integral, or at the symbol level, by purely algebraic manipulations on the symbol tensor or by using the cuts to constrain an ansatz of the symbol tensor.

We noticed that dispersion integrals which look complicated when written in terms of Mandelstam invariants become simple when written in terms of variables which make the symbol alphabet rational. The dispersion integral then falls naturally into the class of iterated integrals amenable to Hopf algebra techniques. This is of course consistent with the fact that each dispersion integral is expected to raise the transcendental weight of the function by one: it is the opposite operation to taking the discontinuity of the function across its branch cut. We first made this observation in the case of the three-mass triangle and two-loop three-point ladder [36], and we then used it to find an efficient way to compute the three-mass triangle with one or two internal masses [37]—see section B.3. Although dispersive integration is not a common method for the calculation of Feynman integrals, we believe these examples show that it can be a powerful method to compute them even in non-trivial cases.

We next presented purely algebraic ways to reconstruct the three-point three-mass triangle and two-loop ladder with massless propagators from the knowledge of a single set of cuts, along with the symbol alphabet. This was achieved by using two main constraints: the integrability of the symbol and the first-entry condition. More precisely, we showed how to reconstruct the symbol of the full integral from the knowledge of a single unitarity cut in one of the channels. We also showed that in the case of the two-loop ladder (and the much simpler one-loop triangle) it is possible to reconstruct all the terms of the $\Delta_{1,1,2}$ component of the coproduct of the uncut integral, and then the full function, from the knowledge of a single sequence of double cuts.

Finally, we showed how channel cuts highly constrain the symbol of triangles with internal masses. Indeed, we were able to completely constrain a general ansatz for the symbol of each triangle (except the fully massive triangle) using the knowledge of a single channel cut, the integrability condition and the symmetries of the functions. However, building the ansatz is more complicated than in the absence of internal masses, and we have had to postulate rules that determine how to construct symbol letters not appearing in channel cuts. These rules are obtained empirically and are specific to the class of diagrams we are studying. Once the symbol is known, we explain how to reconstruct the function by fixing terms invisible to the symbol. It would be interesting to see whether reconstruction can also be done starting from cuts in internal masses.

Aside from the dispersive integration method, it is not clear to us how general the reconstruction procedures presented in this section are. Indeed, they were mostly developed on a case by case basis, and rely on some outside knowledge, such as the symbol alphabet. This is particularly obvious in the reconstruction of diagrams with internal masses, section 4.4. Independently of this, we believe the results presented here are interesting because they show how much the analytic structure of Feynman integrals is constrained by the knowledge of a single one of its unitarity cuts.

Chapter 5

Cuts of one-loop diagrams as residues in complex kinematics

5.1 Introduction

Over the last decade, the calculation of one-loop amplitudes has been revolutionised by the so-called generalised unitarity approach [4, 5, 85, 86]. Building on the observation made in [2] that one-loop Feynman integrals with complicated numerators can be reduced to scalar ones, it was shown that any one-loop amplitude in four dimensions can be decomposed into a basis of scalar one-loop diagrams consisting of boxes, triangles, bubbles and tadpoles—see [90] for a review of this subject. In a nutshell, the idea of generalised unitarity is that the coefficients in this expansion can be extracted by projecting the amplitude onto this basis, and this is done by matching the discontinuities of the amplitude with the discontinuities of the basis integrals [4]. For instance, because triangles, bubbles and tadpoles have no quadruple cuts, the quadruple cuts of the amplitude project out its box contributions. Quadruple cuts have thus been very useful and powerful in the framework of generalised unitarity, although how to correctly interpret them has not always been clear.

Generalised unitarity is a very large subject, useful in both phenomenological studies or more theoretical investigations on the structure of quantum field theories. It is not the subject of this thesis, so we will not discuss it further. We simply wish to point out that because cuts can be used as projection operators to compute loop amplitudes, the last decade saw a renewed interest in the

development of methods to compute and interpret them [7–11, 14–17, 28, 56, 57, 101, 104–115]. On the subject of generalised unitarity, we benefited from reading the reviews [87–90].

In chapter 3 we generalised the notion of unitarity cut of a Feynman diagram [18–21] to allow for multiple unitarity cuts in different kinematic channels, both for diagrams with massless [36] or massive [37] propagators. However, we noted that this generalisation might not be enough to describe all the components of the coproduct of Feynman integrals. For instance, since we were looking at cuts as discontinuities on kinematic channels, we insisted on having a well-defined relation between cuts and discontinuities. Because of this, we excluded what we called crossed channel cuts, i.e. cuts on channels that do not define separate regions in a diagram, such as the cuts in the s and t channels of the box. However, these are exactly the quadruple cuts that we know play an important role in generalised unitarity.

In this chapter, we aim at finding a definition of cut that allows us to capture as much as possible of the analytic structure of Feynman integrals. In particular we will be able to give a concrete interpretation to quadruple cuts of boxes.

The four-propagator cut of a box should be very simple to compute for $\epsilon = 0$. Indeed, considering a box in $D = 4$ dimensions we have four integration variables and four propagators. If the four propagators are replaced by Dirac δ-functions, then the four integration variables are completely localised, which makes the integration trivial. Let's see how this is done in some more detail for the boxes with no internal masses (the generalisation to the case with internal masses is easy).

In $D = 4$, the box integral is given by

$$B(s,t;p_1^2,p_2^2,p_3^2,p_4^2) = \frac{1}{\pi^2}\int d^4k \frac{1}{k^2(p_2-k)^2(p_1+p_2-k)^2(k+p_3)^2}. \tag{5.1}$$

It is convenient to use so-called dual variables x_{jk}. We start by defining x_j through $p_j = x_j - x_{j+1}$, where the indices are defined cyclically. Then, we define $x_{jk}^2 = (x_j - x_k)^2$. Finally, if we define $k = x_0 - x_1$, we can rewrite the box integral as

$$B(s,t;p_1^2,p_2^2,p_3^2,p_4^2) = \frac{1}{\pi^2}\int d^4x_0 \frac{1}{x_{01}^2 x_{02}^2 x_{03}^2 x_{04}^2}. \tag{5.2}$$

The four-propagator cut is now computed by replacing all $\left(x_{0j}^2\right)^{-1}$ by $2\pi\delta\left(x_{0j}^2\right)$

(we will not attempt to justify the choice of normalisation for this cut for now, and leave the precise definition of this type of cut to the following section):

$$\mathrm{Cut}_4[B(s,t;p_1^2,p_2^2,p_3^2,p_4^2)] = 2^4\pi^2 \int d^4x_0 \delta\left(x_{01}^2\right) \delta\left(x_{02}^2\right) \delta\left(x_{03}^2\right) \delta\left(x_{04}^2\right). \tag{5.3}$$

To make it clearer that the four integrations are localised by the four Dirac δ-functions, we change variables to $s_j = x_{0j}^2$, in terms of which

$$\mathrm{Cut}_4[B(s,t;p_1^2,p_2^2,p_3^2,p_4^2)] = 2^4\pi^2 \left(\prod_{j=1}^{4} \int ds_j \delta(s_j)\right) \frac{1}{J}, \tag{5.4}$$

where

$$J = \det\left(\frac{\partial s_j}{\partial x_{0,\mu}}\right) = \det\left(2x_{0j,\mu}\right). \tag{5.5}$$

After some algebra, we find

$$J = 4\sqrt{\det\left(x_{jk}^2 - s_j^2 - s_k^2\right)}. \tag{5.6}$$

We finally get

$$\mathrm{Cut}_4[B(s,t;p_1^2,p_2^2,p_3^2,p_4^2)] = 4\pi^2 \left(\sqrt{\det\left(x_{jk}^2\right)}\right)^{-1}. \tag{5.7}$$

In this expression, x_{jk}^2 is the well known Cayley matrix which appears in the calculation of Feynman integrals (see e.g. [90]). We can specialise this expression for the different types of boxes, and find

$$\begin{aligned}
&\mathrm{Cut}_4[B(s,t)] = \mathrm{Cut}_4[B(s,t;p_1^2)] = \mathrm{Cut}_4[B^h(s,t;p_1^2,p_2^2)] = \frac{4\pi^2}{st}, \\
&\mathrm{Cut}_4[B^e(s,t;p_1^2,p_2^2)] = \mathrm{Cut}_4[B(s,t;p_1^2,p_2^2,p_3^2)] = \frac{4\pi^2}{st - p_1^2 p_3^2}, \\
&\mathrm{Cut}_4[B(s,t;p_1^2,p_2^2,p_3^2,p_4^2)] = \frac{4\pi^2}{st\sqrt{\lambda(1,U,V)}},
\end{aligned} \tag{5.8}$$

where U and V are defined in eq. (3.93). We thus see we can find a non-zero value we can associate with the maximal cut of a box, even for the fully massless case, where the maximal cut isolates four massless three-point vertices.

Unfortunately, it is not clear how to generalise the above procedure in a

consistent way beyond $\epsilon = 0$. Furthermore, while performing the different changes of variables it is hard to keep track of what the correct integration contour is, preventing a consistent generalisation of this method to the case where not all propagators are cut. In this section, our goal is to find a definition of cut diagrams which is consistent with the definition given in chapter 3, reproduces the above result for maximal cuts, and allows to compute cuts of arbitrary one-loop diagrams with any subset of cut propagators to all orders in ϵ.

We should mention that techniques to compute generalised cuts of one-loop amplitudes in D-dimensions have been developed elsewhere, see e.g. [9, 101, 105, 106]. In [9], the authors follow a procedure which is very common in generalised unitarity methods: the loop momentum is a $4 - 2\epsilon$ vector, but the external momenta are kept in exactly four dimensions. The advantage of this choice is that the spinor-helicity formalism (see e.g. [116] and references therein) can be used for the four-dimensional components, and the remaining -2ϵ integrations are performed separately. As with the method above, it is not trivial to generalise when going to higher orders in ϵ and/or when some of the propagators are not cut.

We finish with a comment on the quadruple cuts of boxes we computed above. Putting aside normalisation factors, comparing these results with the expressions for the boxes given in section B.4, we see the maximal cuts of the boxes are related to their rational prefactor, which is known to be related to the so-called *leading singularities* of Feynman integrals [56, 57]. Once we have settled our normalisation for computing this type of cut in a well defined way, we will define the maximal cut computed at $\epsilon = 0$ to be the leading singularity of the diagram. We note the above method can always be used to easily compute the leading singularities of diagrams with n propagators in n dimensions up to normalisation conventions. It is not hard to see that the answer will always be proportional to the inverse of the square-root of the determinant of the Cayley matrix.

All the work presented in this chapter was done during my PhD. The framework to compute cuts as residues in complex kinematics presented below was developed by myself, although I greatly benefited from discussions with and comments from Ruth Britto, Claude Duhr and my supervisor Einan Gardi. Most of the work presented in this chapter constitutes new results which, as far as I am aware, have not been published elsewhere.

5.2 Definition of cuts in Minkowski space

We will consider the m-propagator cut of a one-loop diagram with n propagators in $D = d - 2\epsilon$ dimensions, where d is an even number such that $d - 2 < n \leq d$. In this section, cuts will be computed in Minkowski space-time. We define the uncut diagram as:

$$I_n\left(\{p_j \cdot p_k\}; \{m_j^2\}\right) = \frac{e^{\gamma_E \epsilon}}{i\pi^{\frac{D}{2}}} \int d^D k \frac{1}{\left(k^2 - m_{n-1}^2\right)} \prod_{j=0}^{n-2} \frac{1}{(k - q_j)^2 - m_j^2}\,. \tag{5.9}$$

We note there is a change of normalisation with respect to what was done in the previous chapters, see appendix A for a summary of our conventions. We will in general not explicitly write the variables on which I_n depends.

In eq. (5.9), the q_j are combinations of the external momenta p_l:

$$q_j = \sum_{l=1}^{n} c_{jl} p_l, \qquad\qquad c_{jl} \in \{-1, 0, 1\}.$$

The numbering of the q_j does not follow any particular order, but a distinction is made between the ones that will not be cut (with $m - 2 < j \leq n - 2$) and the m propagators that will be (the others). For $m \geq 2$, q_0 is required to be such that $q_0^2 \neq 0$. This is a very mild requirement, and if it cannot be met the cut vanishes, see section 5.4.1. For single propagator cuts this is not required, but we postpone the discussion of this type of cuts to section 5.3.

The choice of varying the number of space-time dimensions with the number of propagators ensures that I_n is a pure function of weight $d/2$, i.e., it saturates the upper bound of eq. (2.25). This is mainly relevant for the next chapter, and most of the discussion in this chapter is independent of this choice (all but the discussion of sections 5.4.2 and 5.4.3). We should note that there are well established relations between diagrams computed in different space-time dimensions [117], and thus our choice can be seen as a choice of a basis for one-loop Feynman diagrams (although in this thesis we will not attempt to prove this basis is complete).

5.2.1 Parametrisation of the momenta and change of variables

We work in the centre of mass of q_0 and parametrise the q_j as:

$$q_0 = (q_{00}, \mathbf{0}_{D-1}), \quad q_1 = (q_{10}, q_{11}, \mathbf{0}_{D-2}), \quad q_j = (q_{j0}, \ldots, q_{jj}, \mathbf{0}_{D-j}). \tag{5.10}$$

For the loop momentum, we use polar coordinates:

$$k = k_0 \left(1, \beta\cos\theta_1, \ldots, \beta\cos\theta_{n-2}\left(\prod_{j=1}^{n-3}\sin\theta_j\right), \beta\left(\prod_{j=1}^{n-2}\sin\theta_j\right)\mathbf{1}_{D-n}\right) \tag{5.11}$$

where we made explicit the angles that will be relevant in the n propagators of the diagram, and the remaining angles can be trivially integrated.

With this parametrisation, the dot products of the internal momentum with the q_j become

$$\begin{aligned} &q_0 \cdot k = k_0 q_{00}, \quad q_0 \cdot k = k_0(q_{10} - q_{11}\beta\cos\theta_1), \\ &q_j \cdot k = k_0\left(q_{j0} - q_{j1}\beta\cos\theta_1 - \beta\sum_{\alpha=2}^{j} q_{j\alpha}\cos\theta_\alpha\prod_{\gamma=1}^{\alpha-1}\sin\theta_\gamma\right). \end{aligned} \tag{5.12}$$

Performing the trivial angular integrals, the integration measure is

$$\int d^D k = \frac{2\pi^{\frac{D-n+1}{2}}}{\Gamma\left(\frac{D-n+1}{2}\right)}\int dk_0 k_0^{D-1}\int d\beta\beta^{D-2}\left(\prod_{j=1}^{n-2}\int_0^\pi d\theta_j \sin^{D-2-j}\theta_j\right). \tag{5.13}$$

We now change variables according to

$$\cos\theta_j = 2x_j - 1 \quad \Rightarrow \quad d\cos\theta_j = 2dx_j \text{ and } \sin\theta_j = 2\sqrt{x_j(1-x_j)}, \tag{5.14}$$

for any $1 \leq j \leq n-2$. The propagators can then be written as

$$(k - q_j)^2 - m_j^2 = -A_j + B_j x_j, \tag{5.15}$$

where the A_j and B_j are functions of $k_0, \beta, x_1, \ldots, x_{j-1}$ and of the external

invariants, given by:

$$\begin{aligned}
A_0 =& 2k_0 q_{00} + m_0^2 - k^2 - q_0^2, \quad B_0 = 0, \\
A_1 =& 2k_0 \left(q_{10} + q_{11}\beta\right) + m_1^2 - k^2 - q_1^2, \quad B_1 = 4\beta k_0 q_{11}, \\
A_j =& 2k_0 \left[q_{j0} - \beta \sum_{\alpha=1}^{j-1} q_{j\alpha}(2x_\alpha - 1) \left(\prod_{\gamma=1}^{\alpha-1} 2\sqrt{x_\gamma(1-x_\gamma)} \right) \right. \\
& \left. + \beta q_{jj} \left(\prod_{\gamma=1}^{j-1} 2\sqrt{x_\gamma(1-x_\gamma)} \right) \right] + m_j^2 - q_j^2 - k^2, \\
B_j =& 2^{j+1} k_0 \beta q_{jj} \left(\prod_{\beta=1}^{j-1} \sqrt{x_\beta(1-x_\beta)} \right) = \frac{2q_{jj}}{q_{j-1j-1}} \sqrt{x_{j-1}(1-x_{j-1})} B_{j-1},
\end{aligned} \tag{5.16}$$

where the last relation holds for $j > 1$. We will in general not write the variables on which the A_j and B_j depend, as it is usually a rather long list that makes the equations hard to read. Finally, we also define $x_{j,p}$ as

$$x_{j,p} = \frac{A_j}{B_j}, \tag{5.17}$$

which is the point at which the propagator $(k - q_j)^2 - m_j^2$ vanishes.

We again stress that $A_j \equiv A_j(k_0, x_1, \ldots, x_{j-1})$ and $B_j \equiv B_j(k_0, x_1, \ldots, x_{j-1})$, which means the $x_{j,p}$ are also functions of these variables (and of the kinematic invariants on which I_n depends),

$$x_{j,p} \equiv x_{j,p}(k_0, x_1, \ldots, x_{j-1}). \tag{5.18}$$

As for A_j and B_j, we will in general not explicitly write the variables on which the $x_{j,p}$ depend for clarity of the expressions. Finally, we note that in terms of the $x_{j,p}$,

$$(k - q_j)^2 - m_j^2 = B_j \left(x_j - x_{j,p}\right). \tag{5.19}$$

We finish with a comment: the main advantage of our parametrisation is that to each propagator with momentum $(k - q_j)^2 - m_j^2$, for $j \geq 3$, it associates a single new variable x_j.

5.2.2 Uncut integral

The uncut integral is

$$I_n = \frac{2^{1+\sum_{j=1}^{n-2}(D-2-j)}\pi^{\frac{1-n}{2}}e^{\gamma_E\epsilon}}{\Gamma\left(\frac{D-n+1}{2}\right)}\int dk_0\int d\beta\frac{k_0^{D-1}\beta^{D-2}}{(k^2-m_{n-1}^2)((k-q_0)^2-m_0^2)} \left(\prod_{j=1}^{n-2}\int_0^1 dx_j\frac{(x_j(1-x_j))^{\frac{D-3-j}{2}}}{B_j\left(x_j-x_{jp}\right)}\right). \tag{5.20}$$

Out of the $n-2$ integrals over the x_j, we want to perform the last $n-m$. The others are not integrated over, as they are the ones corresponding to propagators that will be cut. We thus define the function $\tilde{f}_m\left(k_0,\beta,x_1,\ldots,x_{m-2}\right)$ which is the result of these $(n-m)$ integrations, as

$$\tilde{f}_m\left(k_0,\beta,x_1,\ldots,x_{m-2}\right) = 2^{\sum_{j=m-1}^{n-2}(D-2-j)}\left(\prod_{j=m-1}^{n-2}\int_0^1 dx_j\frac{(x_j(1-x_j))^{\frac{D-3-j}{2}}}{B_j\left(x_j-x_{jp}\right)}\right), \tag{5.21}$$

where we only wrote the dependence of $\tilde{f}_m$ on integration variables.

We then have

$$I_n = \frac{2^{1+\sum_{j=1}^{m-2}(D-2-j)}\pi^{\frac{1-n}{2}}e^{\gamma_E\epsilon}}{\Gamma\left(\frac{D-n+1}{2}\right)}\int dk_0\int d\beta\frac{k_0^{D-1}\beta^{D-2}}{(k^2-m_{n-1}^2)((k-q_0)^2-m_0^2)} \left(\prod_{j=1}^{m-2}\int_0^1 dx_j\frac{(x_j(1-x_j))^{\frac{D-3-j}{2}}}{B_j\left(x_j-x_{jp}\right)}\right)\tilde{f}_m\left(k_0,\beta,x_1,\ldots,x_{m-2}\right). \tag{5.22}$$

We will in general not write the variables on which $\tilde{f}_m\left(k_0,\beta,x_1,\ldots,x_{m-2}\right)$ depends. In this expression, the integrals that are left to be computed correspond to the m propagators we will be cutting.

5.2.3 Definition of cuts as residues — $\mathcal{C}_m$

We now give our definition of an m-propagator cut. This definition is based on the observation that, for a function $g(x)$ behaving well enough around $x=a$,

$$\int_{a_1}^{a_2} dx g(x)\delta(x-a) = \mathrm{Res}_{x=a}\frac{g(x)}{(x-a)} = g(a), \tag{5.23}$$

for $a_1 \leq a \leq a_2$. Instead of replacing cut propagators by delta functions as we did in chapter 3, we will compute cuts by evaluating residues of propagators at their poles. The advantage of this method is that while the replacement of the propagator by a Dirac δ-function will only give a contribution if $a_1 \leq a \leq a_2$, the replacement by a residue is easily extended to any a taking values anywhere in the complex plane.

We choose our normalisations tailored to the needs of chapter 6. This is true in particular for the factors of ± 1 and the powers of (2π). We define $\mathcal{C}_m$ as:

$$\mathcal{C}_m\left[I_n\right] \equiv (-1)^m (2\pi)^{\left\lfloor \frac{m}{2} \right\rfloor} \frac{2^{1+\sum_{j=1}^{m-2}(D-2-j)} e^{\gamma_E \epsilon}}{\pi^{\frac{n-1}{2}} \Gamma\left(\frac{D-n+1}{2}\right)} \mathrm{Res}_{k_0}\left[\mathrm{Res}_{\beta}\left[\mathrm{Res}_{x_1}\left[...\left[\mathrm{Res}_{x_{m-2}}\right.\right.\right.\right.$$
$$\left.\left.\left.\left.\left[\frac{|k_0|^{D-1}\,|\beta|^{D-2}}{(k^2-m_{n-1}^2)((k-q_0)^2-m_0^2)}\left(\prod_{j=1}^{m-2}\frac{|x_j(1-x_j)|^{\frac{D-3-j}{2}}}{|B_j|\,(x_j-x_{jp})}\right)\tilde{f}_m\right]\right]...\right]\right]\right]. \quad (5.24)$$

In this expression, $\lfloor x \rfloor$ denotes the 'floor function', which to each real number x associates the greatest integer smaller or equal to x. The residues are taken at $k_0 = k_{0,p}$, $\beta = \beta_p$, and $x_j = x_{j,p}$. The $x_{j,p}$ were defined above, but we recall they correspond to the poles of the propagators, are functions of the kinematic invariants, and more importantly of the integration variables,

$$x_{j,p} \equiv x_{j,p}(k_0, x_1, \ldots, x_{j-1}). \quad (5.25)$$

We must now define β_p and $k_{0,p}$.

The propagator of momentum k is quadratic in β and thus has two zeros,

$$\beta^{\pm} = \pm\sqrt{1 - \frac{m_{n-1}^2}{k_0^2}}. \quad (5.26)$$

By convention we take the residue at $\beta_p = \beta^+$. The propagator of momentum $(k - q_0)$ is linear in k_0 after imposing $\beta = \beta_p$,

$$(k-q_0)^2 - m_0^2 = -2q_{00}k_0 + q_0^2 + m_{m-1}^2 - m_0^2,$$

and $k_{0,p}$ is its zero. In the absence of internal masses, $\beta_p = 1$ and $k_{0,p} = \frac{q_{00}}{2}$.

Before proceeding with the evaluation of the residues in the expression above, we make some comments on this expression:

- this definition of cut is in principle also valid for single propagator cuts. However, the choice of parametrisation of the loop momentum makes it hard to evaluate them in practice. Below, in section 5.3, we give an equivalent definition of cuts more suitable to the evaluation of single propagator cuts ;

- the factor of $(-1)^m$ is included to have expressions consistent with what is needed for the work presented in chapter 6 ;

- the factor of $(2\pi)^{\lfloor \frac{m}{2} \rfloor}$ is included to have expressions without overall factors of π, as needed for the next chapter ;

- in general, the poles $x_{j,p}$ are complex numbers, and in particular not between 0 and 1. This is why this is a cut in complex kinematics. If we can choose real external kinematics such that all $x_j \in [0,1]$, then the cut is computable in real kinematics. Requiring this we recover the theta functions we had in the relation between cuts, discontinuities and the coproduct of the previous chapter, see e.g. eq. (3.66).

5.2.4 Evaluation of the residues and formal solution

We start by discussing the two-propagator cut, a special case of eq. (5.24) with $m = 2$. For this, we write

$$\begin{aligned}\left(k^2 - m_{n-1}^2\right)\left((k-q_0)^2 - m_0^2\right) =& 2\left|k_0\right|^2 \left|q_{00}\right| \left(\beta - \beta_p\right)\left(\beta + \beta_p\right) \\ & \left(k_0 - \frac{q_0^2 + m_{n-1}^2 - m_0^2}{2q_{00}}\right),\end{aligned} \tag{5.27}$$

so that eq. (5.24) becomes

$$\mathcal{C}_2[I_n] = \frac{e^{\gamma_E \epsilon} \pi^{\frac{3-n}{2}}}{\Gamma\left(\frac{D-n+1}{2}\right)} \frac{\left|k_{0,p}\right|^{D-3} \left|\beta_p\right|^{D-3}}{\left|q_{00}\right|} f_2. \tag{5.28}$$

In this expression, f_2 is $\tilde{f}_2(k_{0,p}, \beta_p)$, where $\tilde{f}_2$ is defined in eq. (5.21). We will in general use f_m to denote the function $\tilde{f}_m$ evaluate at the pole of all its arguments,

$$f_m \equiv \tilde{f}_m\left(k_{0,p}, \beta_p, x_{1,p}, \ldots, x_{m-2,p}\right). \tag{5.29}$$

Let's now look at eq. (5.24) for $m \geq 3$. We start by noting that

$$B_j = 2^{j+1} k_0 \beta q_{jj} \left(\prod_{\gamma=1}^{j-1} \sqrt{x_\gamma (1-x_\gamma)} \right)$$

$$\Rightarrow \quad \prod_{j=1}^{m-2} |B_j| = \frac{2^{\sum_{j=1}^{m-2}(j+1)}}{|k_0 \beta|^{2-m}} \left(\prod_{j=1}^{m-2} |q_{jj}| \right) \left(\prod_{j=1}^{m-3} |(x_j(1-x_j))|^{\frac{m-2-j}{2}} \right) . \tag{5.30}$$

Using this result,

$$\prod_{j=1}^{m-2} \frac{|(x_j(1-x_j))|^{\frac{D-3-j}{2}}}{|B_j|\,(x_j - x_{jp})} = \frac{2^{-\sum_{j=1}^{m-2}(j+1)}}{(|k_0|\,|\beta|)^{m-2}} \prod_{j=1}^{m-2} \frac{|(x_j(1-x_j))|^{\frac{D-1-m}{2}}}{|q_{jj}|\,(x_j - x_{jp})}. \tag{5.31}$$

We stress that, importantly, in the last line the power of the $x_j(1-x_j)$ factors is now independent of j.

As we will see, it is convenient to first evaluate the residue at $x_{m-2} = x_{m-2,p}$,

$$\mathrm{Res}_{x_{m-2}=x_{m-2,p}} \left[\left(\prod_{j=1}^{m-2} \frac{|(x_j(1-x_j))|^{\frac{D-3-j}{2}}}{|B_j|\,(x_j - x_{jp})} \right) \tilde{f}_m \right] = \frac{2^{-\sum_{j=1}^{m-2}(j+1)}}{(|k_0|\,|\beta|)^{m-2}}$$
$$\left(\prod_{j=1}^{m-3} \frac{|(x_j(1-x_j))|^{\frac{D-1-m}{2}}}{|q_{jj}|\,(x_j - x_{jp})} \right) \frac{|(x_{m-2,p}(1-x_{m-2,p}))|^{\frac{D-1-m}{2}}}{|q_{m-2,m-2}|} \tilde{f}_m(x_{m-2,p}).$$

On the right-hand-side, we wrote one of the arguments of $\tilde{f}_m\,(k_0, \beta, x_1, \ldots, x_{m-2})$ explicitly to stress that we had set $x_{m-2} = x_{m-2,p}$ when taking the residue associated with this variable.

We now use

$$|x_{m-2,p}(1-x_{m-2,p})|^{\frac{D-1-m}{2}} = \left(\frac{|A_{m-2}(B_{m-2} - A_{m-2})|}{\left|B_{m-2}^2\right|} \right)^{\frac{D-1-m}{2}}$$
$$= \frac{|A_{m-2}(B_{m-2} - A_{m-2})|^{\frac{D-1-m}{2}}}{(2^{m-1}\,|k_0|\,|\beta|\,|q_{m-2,m-2}|)^{D-1-m}} \left(\prod_{j=1}^{m-3} (x_j(1-x_j))^{\frac{1+m-D}{2}} \right)$$

to get

$$\mathrm{Res}_{x_{m-2}}\left(\prod_{j=1}^{m-2}\frac{|x_j(1-x_j)|^{\frac{D-3-j}{2}}}{|B_j|\,(x_j-x_{jp})}\right)f_m=\frac{2^{\frac{m(m+1)-2D(m-1)}{2}}}{(|k_0|\,|\beta|)^{D-3}}$$
$$\left(\prod_{j=1}^{m-3}\frac{1}{|q_{jj}|\,(x_j-x_{jp})}\right)\frac{|A_{m-2}(B_{m-2}-A_{m-2})|^{\frac{D-1-m}{2}}}{|q_{m-2,m-2}|^{D-m}}\tilde{f}_m(x_{m-2,p}).$$

Putting everything together,

$$\mathcal{C}_m\left[I_n\right]=(-1)^m\frac{2^{2-D}(2\pi)^{\lfloor\frac{m}{2}\rfloor}e^{\gamma_E\epsilon}}{\pi^{\frac{n-1}{2}}\Gamma\left(\frac{D-n+1}{2}\right)}\frac{|q_{m-2,m-2}|^{1+m-D}}{\left(\prod_{j=0}^{m-2}|q_{jj}|\right)}\mathrm{Res}_{k_0}\left[\mathrm{Res}_{\beta}\left[...\left[\mathrm{Res}_{x_{m-3}}\right.\right.\right.$$
$$\left.\left.\left.\left[\left(\prod_{j=1}^{m-1}\frac{1}{(x_j-x_{jp})}\right)\frac{|A_{m-2}(B_{m-2}-A_{m-2})|^{\frac{D-1-m}{2}}}{(\beta-\beta_p)\left(k_0-\frac{q_0^2+m_{n-1}^2-m_0^2}{2q_{00}}\right)}\tilde{f}_m(x_{m-2,p})\right]\right]...\right]\right]. \quad (5.32)$$

We observe that by evaluating the residue at $x_{m-2}=x_{m-2,p}$ we cancelled the Jacobians of k_0, β and all the x_j with $j<m-2$, and the remaining residues are trivial to evaluate.

We thus get a formal solution to $\mathcal{C}_m\left[I_n\right]$ valid for $m>2$:

$$\mathcal{C}_m\left[I_n\right]=(-1)^m\frac{2^{2-D}(2\pi)^{\lfloor\frac{m}{2}\rfloor}e^{\gamma_E\epsilon}}{\pi^{\frac{n-1}{2}}\Gamma\left(\frac{D-n+1}{2}\right)}\frac{|A_{m-2,p}(B_{m-2,p}-A_{m-2,p})|^{\frac{D-1-m}{2}}}{|q_{m-2,m-2}|^{D-m-1}\left(\prod_{j=0}^{m-2}|q_{jj}|\right)}f_{m,p}. \quad (5.33)$$

In this expression,

$$A_{m-2,p}\equiv A_{m-2}\left(k_{0,p},\beta_p,x_{1p},\ldots,x_{m-3,p}\right)$$
$$B_{m-2,p}\equiv B_{m-2}\left(k_{0,p},\beta_p,x_{1p},\ldots,x_{m-3,p}\right)$$
$$f_{m,p}\equiv\tilde{f}_m\left(k_{0,p},\beta_p,x_{1p},\ldots,x_{m-2,p}\right)$$

are now functions of the external invariants only. To make the expression more explicit, we recall that m is the number of cut propagators, n the total number of propagators, and $D=d-2\epsilon$ the dimensions, where d is an even number such that $d-2<n\leq d$. Examples of eq. (5.33) applied to some simple examples will be given below.

A particularly interesting case of eq. (5.33) is when all propagators are cut,

i.e. $m = n$, which we call the *maximal cut*. In this limit,

$$\mathcal{C}_n\left[I_n\right] = (-1)^n \frac{2^{2-D}(2\pi)^{\lfloor \frac{n}{2} \rfloor} e^{\gamma_E \epsilon}}{\pi^{\frac{n-1}{2}} \Gamma\left(\frac{D-n+1}{2}\right)} \frac{\left|A_{n-2,p}(B_{n-2,p} - A_{n-2,p})\right|^{\frac{D-1-n}{2}}}{\left|q_{n-2,n-2}\right|^{D-1-n} \left(\prod_{j=0}^{n-2} |q_{jj}|\right)}, \tag{5.34}$$

where we have set $f_{n,p} = 1$ as follows from eq. (5.21).

We take this opportunity to define a concept which we have been using loosely up to know, the leading singularity of Feynman integrals. From now on, we will define the leading singularity of a Feynman integral I_n, which we will denote LS, to be its maximal cut, computed at $\epsilon = 0$:

$$\mathrm{LS}\left[I_n\right] \equiv \mathcal{C}_n^{(0)}\left[I_n\right]. \tag{5.35}$$

Here the superscript (0) means we take the ϵ^0 coefficient of the ϵ-expansion of $\mathcal{C}_n\left[I_n\right]$. This definition fails when maximal cuts are zero, but this is a very minor issue and we will explain how to overcome it in section 6.4.

We finish with a comment on notation. It will often be necessary to specify which propagators are cut. For one-loop diagrams, we can identify each propagator by the external legs they connect. For a diagram with n propagators, each propagator is thus identified by a pair $(j, j+1)$, where $j = 1, \ldots, n$ and the indices are defined cyclically. The order in which the indices appear is irrelevant. We will then write[1]

$$\mathcal{C}_{m,[(j_1,j_1+1),\ldots,(j_m,j_m+1)]} \tag{5.36}$$

for the m propagator cut where the propagators $(j_1, j_1+1), \ldots, (j_m, j_m+1)$ are cut. We recall that the parametrisation of section 5.2.1 is to be chosen in agreement with the propagators that are being cut. For maximal cuts, there is no ambiguity so we will never write the cut propagators explicitly.

[1]This notation is not suitable for single cuts of bubbles, but those cases are simple enough that there should not be any ambiguity.

5.2.5 Examples

We now give a few examples to make eqs. (5.28), (5.33) and (5.34) more concrete. These are very simple examples, simply aimed at illustrating the use of the results we obtained above. More interesting and non-trivial examples will be addressed in section 5.5, where we compute cuts of one-loop diagrams with three, four or five propagators. Some of the results presented there are new results, as far as we are aware.

$I_2(p^2)$: We start with the two propagator cut of the bubble with massless propagators, $I_2(p^2)$, evaluated in $D = 2 - 2\epsilon$. According to the parametrisation of section 5.2.1, we have

$$q_0 = \sqrt{p^2}(1, \mathbf{0}_{D-1}). \tag{5.37}$$

Given that both propagators are massless, $\beta_p = 1$ and $k_{0,p} = \sqrt{p^2}/2$. We can then use eq. (5.28) to get

$$\mathcal{C}_2\left[I_2(p^2)\right] = 2\frac{e^{\gamma_E\epsilon}\Gamma(1-\epsilon)}{\Gamma(1-2\epsilon)}\left|p^2\right|^{-1-\epsilon}, \tag{5.38}$$

where we set $f_2 = 1$ as this is a maximal cut of the bubble. In the kinematic region consistent with a cut in the p^2-channel, we have $p^2 > 0$. Reinstating the necessary factors of π and i—see appendix A, in particular the discussion around eqs. (A.10) and (A.11)—we recover the result we would have got by applying the cutting rules of the previous section,

$$\text{Cut}_{p^2}\left[\text{Bub}(p^2)\right] = 2\pi\mathcal{C}_2\left[I_2(p^2)\right] = 4\pi\frac{e^{\gamma_E\epsilon}\Gamma(1-\epsilon)}{\Gamma(1-2\epsilon)}\left(p^2\right)^{-1-\epsilon}. \tag{5.39}$$

$I_2(p^2; m_0^2, m_1^2)$: We now look at the bubble with internal masses m_0^2 and m_1^2, $I_2(p^2; m_0^2, m_1^2)$. The parametrisation of the external momentum is the same as for the massless case—see eq. (5.37)—but we now have

$$k_{0,p} = \frac{p^2 + m_0^2 - m_1^2}{2\sqrt{p^2}}, \qquad \beta_p = \frac{\sqrt{p^2}}{2}\sqrt{\lambda\left(1, \mu_0, \mu_1\right)}, \tag{5.40}$$

where as usual $\lambda(a,b,c) = a^2 + b^2 + c^2 - 2ab - 2ac - 2bc$ is the Källén function and $\mu_i = m_i^2/p^2$. As above, we set $f_2 = 1$ in eq. (5.28) to get

$$\mathcal{C}_2\left[I_2(p^2; m_0^2, m_1^2)\right] = 2\frac{e^{\gamma_E \epsilon}\Gamma(1-\epsilon)}{\Gamma(1-2\epsilon)}\left|p^2\right|^{-1-\epsilon}\left(\sqrt{\lambda\left(1,\mu_0,\mu_1\right)}\right)^{-1-2\epsilon}, \tag{5.41}$$

which also matches the result for the channel cut we would have obtained from the cutting rules of the previous chapter, after multiplying by a factor of 2π.

$I_3(p_1^2; m_{23}^2)$: As a last example, we consider the triangle with one external massive leg, p_1^2, and one internal massive propagator connecting the external legs 2 and 3, of mass m_{23}^2. As this is a diagram with $n = 3$, it is evaluated in $D = 4 - 2\epsilon$. We start by evaluating its two-propagator cut, $\mathcal{C}_{2,[(12),(13)]}I_3(p_1^2; m_{23}^2)$. Given that in this case there is no ambiguity in which two propagators are cut (there is only one non-vanishing two-propagator cut), we will drop the subscript identifying the cut propagators for simplicity of notation. We parametrise the external momenta as

$$p_1 = q_0 = \sqrt{p_1^2}(1, \mathbf{0}_{D-1}), \qquad p_2 = -q_1 = -\frac{\sqrt{p_1^2}}{2}\left(1, -1, \mathbf{0}_{D-2}\right). \tag{5.42}$$

The propagators are

$$\frac{1}{k^2}, \quad \frac{1}{(k-q_0)^2} \quad \text{and} \quad \frac{1}{(k-q_1)^2 - m_{23}^2}, \tag{5.43}$$

and because the propagators of momentum k and $(k - q_0)$ are massless we have $\beta_p = 1$ and $k_{0,p} = \sqrt{p_1^2}/2$. We can compute the quantities $A_{1,p}$ and $B_{1,p}$ as defined in eq. (5.16), and we get

$$A_{1,p} = m_{23}^2 \qquad B_{1,p} = -p_1^2. \tag{5.44}$$

Finally, we will also need $f_{2,p}$ as defined in eq. (5.21),

$$f_{2,p} = -\frac{2^{1-2\epsilon}}{m_{23}^2}\frac{\Gamma^2(1-\epsilon)}{\Gamma(2-2\epsilon)}\,{}_2F_1\left(1, 1-\epsilon; 2-2\epsilon; -\frac{p_1^2}{m_{23}^2}\right). \tag{5.45}$$

We note that $f_{2,p}$ is away from branch cuts in the natural kinematic region where this cut is to be evaluated, $p_1^2 > 0$ and $m_{23}^2 > 0$. It is now straightforward to use

eq. (5.28) to get

$$\mathcal{C}_2\left[I_3(p_1^2;m_{23}^2)\right] = -\frac{e^{\gamma_E\epsilon}\Gamma(1-\epsilon)}{\Gamma(2-2\epsilon)}\frac{\left|p_1^2\right|^{-\epsilon}}{m_{23}^2}\,{}_2F_1\left(1,1-\epsilon;2-2\epsilon;-\frac{p_1^2}{m_{23}^2}\right), \tag{5.46}$$

which, after multiplication by a factor of (-2π), agrees with the result already quoted in eq. (B.7) for $\text{Cut}_{p_1^2}\left[T(p_1^2;m_{23}^2)\right]$.

For this diagram, we can also evaluate the three-propagator cut. We have already given all necessary ingredients, so we can just replace them in eq. (5.34) with $m=3$ to get

$$\mathcal{C}_3\left[I_3(p_1^2;m_{23}^2)\right] = -\frac{e^{\gamma_E\epsilon}}{\Gamma(1-\epsilon)}\left|p_1^2\right|^{-1+\epsilon}\left|m_{23}^2(p_1^2+m_{23}^2)\right|^{-\epsilon}, \tag{5.47}$$

which in the relevant kinematic region ($p_1^2 > 0$ and $m_{23}^2 < 0$) and after multiplication by a factor of $(4\pi^2 i)$ agrees with the result for $\text{Cut}_{p_1^2,m_{23}^2}\left[T(p_1^2;m_{23}^2)\right]$ quoted in eq. (B.9).

5.3 Alternative definition in Euclidean space

5.3.1 General formulation

Unfortunately, the definition of cut given in eq. (5.24) is not convenient to compute single propagator cuts, which are the simplest cuts one could think of. The reason for this is perhaps best illustrated by an example, so let's look at what happens for the tadpole of mass m^2 computed in $2-2\epsilon$ dimensions,

$$I_1 = \frac{e^{\gamma_E\epsilon}}{i\pi^{1-\epsilon}}\int d^{2-2\epsilon}k\frac{1}{k^2-m^2}. \tag{5.48}$$

According to the parametrisation of section 5.2.1, we would write the propagator as

$$k^2-m^2 = k_0^2(1-\beta^2)-m^2,$$

and we would then associate the single propagator cut with a residue of this propagator. The reason why this parametrisation is not the most practical is already apparent: although we only have one propagator, we needed two variables to parametrise it, k_0 and β_0. We could in theory proceed by choosing to take a

residue on either k_0 or β, and then performing the integral in the remaining variable[2]. In practice, we found this integral not easy to compute even for the simplest Feynman diagrams.

However, one would expect that the single propagator cut of a tadpole should be very simple to compute. Indeed, there should be a choice of variables in terms of which the propagator is parametrised by a single variable, and the remaining $1-2\epsilon$ variables can be integrated trivially. Then, the cut would correspond to taking the residue associated with the variable parametrising the propagator. We recall that this was the main advantage of the parametrisation chosen in section 5.2.1: to each propagator of momentum q_j with $j > 0$ is associated a single variable x_j, and the cut of this propagator is the residue on this variable.

As it turns out, there is a parametrisation very similar to that of section 5.2.1 that associates a variable to each propagator, but it requires to first perform a Wick rotation from Minkowski to Euclidean space. Let us then redo the exercise that led us to eq. (5.33) in this new parametrisation. We define a set of Euclidean momenta in D dimensions in terms of their Minkowski counterparts as

$$\begin{aligned} k^E &= (-ik_0, k_1, \dots, k_{D-1}) \\ q_j^E &= (-iq_{j0}, q_{j1}, \dots, q_{jj}, \mathbf{0}_{D-j}) \equiv \left(q_{j0}^E, \dots, q_{jj}^E, \mathbf{0}_{D-j}\right), \end{aligned} \tag{5.49}$$

satisfying

$$\left(k^E\right)^2 = -k^2 \qquad \left(q_j^E\right)^2 = -q_j^2 \qquad k^E \cdot q_j^E = -k \cdot q_j. \tag{5.50}$$

Given that k^E is now a vector in Euclidean space, we can parametrise it as

$$k^E = \left|k^E\right| \left(\cos\theta_0, \cos\theta_1 \sin\theta_0, \dots, \cos\theta_{n-2} \left(\prod_{j=0}^{n-3} \sin\theta_j\right), \left(\prod_{j=0}^{n-2} \sin\theta_j\right) \mathbf{1}_{D-n} \right) \tag{5.51}$$

where $\mathbf{1}_{D-n}$ is a unit vector in the $D-n$ remaining components, which can be

[2]The reason why cuts with two or more propagators can be computed with the parametrisation of section 5.2.1 is that this remaining integration is also replaced by a residue, as was done in eq. (5.28): the integrations on the variables k_0 and β are localised by taking the residues associated with the propagators $k^2 - m_{n-1}^2$ and $(k-q_0)^2 - m_0^2$.

trivially integrated to get

$$\int d^D k^E = \frac{\pi^{\frac{D-n+1}{2}}}{\Gamma\left(\frac{D-n+1}{2}\right)} \int d\left|k^E\right|^2 \left(\left|k^E\right|^2\right)^{\frac{D-2}{2}} \left(\prod_{j=0}^{n-2} \int_0^\pi d\theta_j \sin^{D-2-j}\theta_i\right). \quad (5.52)$$

In practice, this means that by going from Minkowski to Euclidean space we traded the integration over β to an integration over an extra angle θ_0, as can be seen by comparing this expression with the equivalent in Minkowski space, eq. (5.13).

We can now proceed as we did for the angular integrals in Minkowski space: for each angle θ_j, change variables to $x_j = (\cos\theta_j + 1)/2$, and associate a variable x_j to the propagator with momentum $(k - q_j)$,

$$-\left((k-q_j)^2 - m_j^2\right) = (k^E - q_j^E)^2 + m_j^2 = -A_j^E + B_j^E x_j.$$

Unlike what happened in the Minkowski parametrisation, we now have $B_0^E \neq 0$. For any $j \geq 0$,

$$\begin{aligned} A_j^E = 2\left|k^E\right| \Bigg[& \sum_{\alpha=0}^{j-1} q_{j\alpha}^E (2x_\alpha - 1) \left(\prod_{\gamma=0}^{\alpha-1} 2\sqrt{x_\gamma(1-x_\gamma)}\right) \\ & -2^j q_{jj}^E \left(\prod_{\gamma=0}^{j-1} \sqrt{x_\gamma(1-x_\gamma)}\right)\Bigg] - m_j^2 - (q_j^E)^2 - \left|k^E\right|^2, \\ B_j^E = -2^{j+2}\left|k^E\right| q_{jj}^E & \left(\prod_{\beta=0}^{j-1} \sqrt{x_\beta(1-x_\beta)}\right), \end{aligned} \quad (5.53)$$

and we also define $x_{j,p}^E = A_j^E / B_j^E$. Finally, as required, the propagator with momentum k now only depends on one of the integration variables,

$$k^2 - m_{n-1}^2 = -\left(\left|k^E\right|^2 + m_{n-1}^2\right).$$

The uncut integral with n propagators can then be written as

$$I_n = (-1)^n \frac{2^{\sum_{j=0}^{m-2}(D-2-j)} \pi^{\frac{1-n}{2}} e^{\gamma_E \epsilon}}{\Gamma\left(\frac{D-n+1}{2}\right)} \int d\left|k^E\right|^2 \frac{\left(\left|k^E\right|^2\right)^{\frac{D-2}{2}}}{\left|k^E\right|^2 + m_{n-1}^2} \left(\prod_{j=0}^{m-2} \int_0^1 dx_j \frac{(x_j(1-x_j))^{\frac{D-3-j}{2}}}{B_j^E \left(x_j - x_{jp}\right)} \right) \tilde{f}_m^E \left(\left|k^E\right|, x_0, x_1, \ldots, x_{m-2}\right), \quad (5.54)$$

where $\tilde{f}_m^E$ is defined as in eq. (5.21) with B_j replaced by B_j^E and $x_{j,p}$ by $x_{j,p}^E$.

We are now ready to define what we mean by a m-propagator cut in this new parametrisation. The equivalent of eq. (5.24) is

$$\mathcal{C}_m^E [I_n] \equiv (-1)^m (2\pi)^{\lfloor \frac{m}{2} \rfloor} \frac{2^{\sum_{j=0}^{m-2}(D-2-j)} e^{\gamma_E \epsilon}}{\pi^{\frac{n-1}{2}} \Gamma\left(\frac{D-n+1}{2}\right)} \mathrm{Res}_{|k^E|^2} \left[\mathrm{Res}_{x_0} \left[\ldots \left[\mathrm{Res}_{x_{m-2}} \left[\frac{\left|\left|k^E\right|^2\right|^{\frac{D-2}{2}}}{\left|k^E\right|^2 + m_{n-1}^2} \left(\prod_{j=0}^{m-2} \frac{|x_j(1-x_j)|^{\frac{D-3-j}{2}}}{\left|B_j^E\right| \left(x_j - x_{jp}^E\right)} \right) \tilde{f}_m \right] \right] \ldots \right] \right], \quad (5.55)$$

where the residues are evaluated at $x_j = x_{j,p}^E$ and $\left|k^E\right|^2 = \left|k^E\right|_p^2$, which is the zero of the propagator of momentum k. As for the equivalent relation in Minkowski space, eq. (5.24), the normalisations were chosen to match what is needed for the work presented in chapter 6.

For $m = 1$, eq. (5.55) gives a very simple expressions:

$$\mathcal{C}_1^E [I_n] = -\frac{e^{\gamma_E \epsilon}}{\pi^{\frac{n-1}{2}} \Gamma\left(\frac{D-n+1}{2}\right)} \left|m_{n-1}^2\right|^{\frac{D-2}{2}} f_1^E, \quad (5.56)$$

where $f_1^E = \tilde{f}_1^E \left(\left|k^E\right|^2 = -m_{n-1}^2\right)$. For $m \geq 2$, we can go through the same exercise of section 5.2.4 to get

$$\mathcal{C}_m^E [I_n] = (-1)^m \frac{2^{2-D} (2\pi)^{\lfloor \frac{m}{2} \rfloor} e^{\gamma_E \epsilon}}{\pi^{\frac{n-1}{2}} \Gamma\left(\frac{D-n+1}{2}\right)} \frac{\left|A_{m-2,p}^E (B_{m-2,p}^E - A_{m-2,p}^E)\right|^{\frac{D-1-m}{2}}}{\left|q_{m-2,m-2}^E\right|^{D-1-m} \left(\prod_{j=0}^{m-2} \left|q_{jj}^E\right|\right)} f_{m,p}^E. \quad (5.57)$$

Although eqs. (5.24) and (5.55) are equivalent, we will prefer the definition of

cut given in eq. (5.55) for all but single propagator cuts, and only rely on eq. (5.55) to define single propagator cuts. Indeed working in Euclidean space often makes it harder to handle expressions for cuts of more complicated diagrams. We will however show in some simple examples that eqs. (5.24) and (5.55) give consistent results.

5.3.2 Examples

We now illustrate the computation of single propagator cuts using eq. (5.55), and show that for double cuts of bubbles we get results consistent with the ones obtained from eq. (5.24). As with the examples of section 5.2, these are simply an illustration of the above expressions, and we leave the computation of cuts of more interesting diagrams to section 5.5.

$I_1(m^2)$: We start by looking at the diagram that motivated the alternative definition of cut in Euclidean space, the tadpole with internal mass m^2 in $D = 2 - 2\epsilon$ dimensions. As promised, the single propagator cut is now trivial to evaluate. Indeed, we can use eq. (5.56) with $n = 1$ and set $f_1^E = 1$, as this is a maximal cut, to get

$$\mathcal{C}_1^E\left[I_1\right] = -\frac{e^{\gamma_E \epsilon}}{\Gamma\left(1-\epsilon\right)}\left|m^2\right|^{-\epsilon}. \tag{5.58}$$

Multiplying by a factor of (2π), this reproduces the results one would expect by computing the discontinuity of the tadpole in the relevant kinematic region, $m^2 < 0$. Indeed, following the cutting rules of the previous section, we would have found

$$\mathrm{Cut}_{m^2}\left[\mathrm{Tad}(m^2)\right] = -2\pi\frac{e^{\gamma_E \epsilon}}{\Gamma\left(1-\epsilon\right)}\left(-m^2\right)^{-\epsilon}. \tag{5.59}$$

$I_2(p^2)$: We now show that eqs. (5.24) and (5.55) give the same result for the double cut of the bubble with massless propagators. We use eq. (5.57) with $m = n = 2$, and $D = 2 - 2\epsilon$. It is easy to see that for this case $q_{00}^E = -i\sqrt{p^2}$, $A_{0,p}^E = -(q_{00}^E)^2$ and $B_{0,p}^E = 0$ so we get

$$\begin{aligned}\mathcal{C}_2^E\left[I_2(p^2)\right] &= 2e^{\gamma_E \epsilon}\frac{2^{2\epsilon}\sqrt{\pi}}{\Gamma\left(\frac{1-2\epsilon}{2}\right)}\left|q_{00}^E\right|^{-2-2\epsilon} \\ &= 2e^{\gamma_E \epsilon}\frac{\Gamma(1-\epsilon)}{\Gamma\left(1-2\epsilon\right)}\left|p^2\right|^{-1-\epsilon},\end{aligned} \tag{5.60}$$

which is consistent with the result given above.

$I_2(p^2; m_1^2)$: As a final example, we look at the cuts of the bubble with one internal massive propagator in $D = 2 - 2\epsilon$. In this case, $q_{00}^E = -i\sqrt{p^2}$, $|k_E|_p = \pm i m_1$, $A_0 = (\sqrt{p^2} \pm m_1)^2$ and $B_0 = \pm m_1 \sqrt{p^2}$. For the single cut, we also need $f_{1,p}^E$ as defined in eq. (5.21),

$$f_{1,p}^E = -\frac{2^{-2\epsilon}}{\left(\sqrt{p^2} \pm m_1\right)^2} \frac{\Gamma^2\left(\frac{1-2\epsilon}{2}\right)}{\Gamma(1-2\epsilon)} \, {}_2F_1\left(1, \frac{1-2\epsilon}{2}; 1-2\epsilon; \frac{\pm m_1\sqrt{p^2}}{\left(\sqrt{p^2} \pm m_1\right)^2}\right).$$

From eq. (5.56), we then get

$$\mathcal{C}_1^E\left[I_2(p^2; m_1^2)\right] = \frac{e^{\gamma_E \epsilon}}{\Gamma(1-\epsilon)} \frac{|m^2|^{-\epsilon}}{(\sqrt{p^2} \pm m_1)^2} \, {}_2F_1\left(1, \frac{1-2\epsilon}{2}; 1-2\epsilon; \frac{\pm m_1\sqrt{p^2}}{\left(\sqrt{p^2} \pm m_1\right)^2}\right).$$

Upon expansion of the hypergeometric function, it can be checked that once the factors of (2π) have been adjusted to match conventions, this rather complicated and inelegant result is consistent with the one obtained from the cutting rules of the previous chapter in the region $p^2 < m^2 < 0$,

$$\mathrm{Cut}_{m_1^2}\left[\mathrm{Bub}(p^2; m_1^2)\right] = 2\pi \frac{e^{\gamma_E \epsilon}}{\Gamma(1-\epsilon)} \frac{(-m^2)^{-\epsilon}}{p^2} \, {}_2F_1\left(1, 1+\epsilon; 1-\epsilon; \frac{m^2}{p^2}\right). \quad (5.61)$$

Finally, we also have all ingredients to compute the double cut of this bubble. Using eq. (5.57),

$$\mathcal{C}_2^E\left[I_2(p^2; m_1^2)\right] = 2e^{\gamma_E \epsilon} \frac{\Gamma(1-\epsilon)}{\Gamma(1-2\epsilon)} \left|p^2\right|^{\epsilon} \left|p^2 - m_1^2\right|^{-1-2\epsilon}, \quad (5.62)$$

which reproduces the $m_0^2 \to 0$ limit of eq. (5.41), and is also consistent with the result obtained by the cutting rules of the previous chapter,

$$\mathrm{Cut}_{p^2}\left[\mathrm{Bub}(p^2; m_1^2)\right] = 4\pi e^{\gamma_E \epsilon} \frac{\Gamma(1-\epsilon)}{\Gamma(1-2\epsilon)} \left(p^2\right)^{\epsilon} \left(p^2 - m_1^2\right)^{-1-2\epsilon}, \quad (5.63)$$

computed in the region where $0 < m^2 < p^2$.

5.4 General results on cuts of one-loop Feynman diagrams

In this section, we will look at some results that can be derived from the general expressions we have given for the m-propagator cut of one-loop Feynman diagrams, eqs. (5.24) and (5.55). We will start by determining which cuts can vanish for specific choices of kinematic configurations. Then we will show a relation between the first order in the ϵ-expansion of the maximal and next-to-maximal cuts (i.e., with $n-1$ cut propagators) of finite diagrams with an even number of propagators. This relation will play a very important role in the work presented in the next chapter. Finally, we will make a brief comment on the form of maximal cuts.

5.4.1 Vanishing cuts in complex kinematics

In the previous chapter, as in refs. [36, 37], we interpreted cuts of Feynman diagrams as discontinuities on kinematic channels or internal masses. This allowed us to argue that some cuts should vanish. For instance, the single propagator cut of a massless propagator should be zero, because it could not correspond to the discontinuity on any internal mass. As another example, if the two-propagator cut of a one-loop diagram selected a massless external channel, then it had to vanish as the function had no discontinuities associated to that cut. In this analysis, we restricted ourselves to the use of *real kinematics*, which meant that if a cut isolated a three-point vertex with three on-shell massless particles, then it had to vanish. This hypothesis was enough to obtain the relations between discontinuities, cuts and certain coproduct entries, but we also commented that we expected a generalisation of the cutting rules might be necessary to describe other coproduct entries. As we will see in the following chapter, the definition of cut given in the section above allows to do this. However, if we allow ourselves to go beyond real kinematics as we have done above, can we still identify vanishing cuts simply by looking at a cut diagram? Although some cuts we would previously set to zero are no longer vanishing, in the following we argue that it is possible, and identify which cuts of one loop Feynman diagrams can vanish.

Consider a general one-loop integral with n propagators. We now examine its

cuts, and look for which configurations of internal and external masses one finds a vanishing result.

One-propagator cuts: We start by single propagator cuts, for which we can use eq. (5.56). Provided $f^E_{1,p}$ does not behave as $\left|m^2_{n-1}\right|^{\frac{D-2}{2}}$ as $\left|m^2_{n-1}\right| \to 0$, the single cut will vanish if the mass of the cut propagator is zero, which agrees with the behaviour we would have expected from the relation between cuts and discontinuities. Let us then show that $f^E_{1,p}$ is analytic for $\left|k^E\right|^2 = m^2_{n-1} = 0$. In this limit, eq. (5.53) gives

$$A^E_{j,p}(|k_E| = 0) = -m_j^2 - \left(q_j^E\right)^2, \qquad B^E_{j,p}(|k_E| = 0) = 0, \qquad \text{for } j \geq 1. \tag{5.64}$$

We thus have

$$f^E_{1,p} = \pi^{\frac{n-1}{2}} \frac{\Gamma\left(\frac{D-n+1}{2}\right)}{\Gamma\left(\frac{D}{2}\right)} \left(\prod_{j=0}^{n-2} \frac{1}{-A^E_j(|k_E| = 0)} \right), \tag{5.65}$$

which shows $f^E_{1,p}$ is analytic at $\left|k^E\right|^2 = m^2_{n-1} = 0$.

Two-propagator cuts: For two propagator cuts, we also rely on the definition of cuts in Euclidean space, eq. (5.55), as the parametrisation in Minkowski is only valid for $q_0^2 \neq 0$. We will show that the double cut vanishes if $q_0^E = 0$, i.e., if the double cut selects a massless external channel. From eq. (5.57), the double cut is

$$\mathcal{C}^E_2\left[I_n\right] = (-1)^m \frac{2^{2-D}(2\pi)e^{\gamma_E \epsilon}}{\pi^{\frac{n-1}{2}}\Gamma\left(\frac{D-n+1}{2}\right)} \left|q^E_{00}\right|^{2-D} \left|A^E_{0,p}(B^E_{0,p} - A^E_{0,p})\right|^{\frac{D-2}{2}} f^E_{2,p}. \tag{5.66}$$

If $q^E_{00} = 0$, then $B^E_j = 0$ for all $j \geq 0$. This means all integrations in $f^E_{2,p}$ can be done trivially, as they were for $f^E_{1,p}$ above, and $f^E_{2,p}$ is analytic in this limit. We can thus conclude that the double cut vanishes if $q_0^2 = -(q_0^E)^2 = 0$. Again, this is in agreement with the relation between two-propagator cuts of one-loop diagrams and discontinuities on external channels discussed in the previous chapter.

Three-propagator cuts: We now look at three-propagator cuts. For these cuts, we can use the Minkowski space formulation of eqs. (5.24) and (5.33),

$$\mathcal{C}_3\left[I_n\right] = -\frac{2^{2-D}(2\pi)e^{\gamma_E\epsilon}}{\pi^{\frac{n-1}{2}}\Gamma\left(\frac{D-n+1}{2}\right)}\left|q_{11}\right|^{4-D}\frac{\left|A_{1,p}(B_{1,p}-A_{1,p})\right|^{\frac{D-4}{2}}}{\left|q_{00}\right|\left|q_{11}\right|}f_{3,p}. \tag{5.67}$$

By definition, we know $q_{11} \neq 0$, see section 5.2.1. To consider a triple cut, we must have at least three propagators, and so there is at least one massive external channel which we can identify with q_0^2. We thus also have $q_{00} \neq 0$. Finally, $f_{3,p}$ is non-zero for general kinematics (i.e., when all the q_j and m_j^2 are independent of each other). We thus see that the triple cut can vanish if and only if $A_{1,p} = 0$ or $A_{1,p} = B_{1,p}$, where $A_{1,p}$ and $B_{1,p}$ are given in eq. (5.16),

$$A_{1,p} = 2k_{0,p}(q_{10} + q_{11}\beta_p) + m_1^2 - k^2 - q_1^2, \qquad B_{1,p} = 4\beta_p k_{0,p} q_{11}. \tag{5.68}$$

To have $A_{1,p} = 0$ or $A_{1,p} = B_{1,p}$, we must have $k^2 = m_1^2 = q_1^2 = 0$, which in turn implies that $\beta_p = 1$ and $q_{10}^2 - q_{11}^2 = 0$. This last equation has two solutions,

$$\begin{aligned} q_{10} = q_{11} \quad &\Rightarrow \quad A_{1,p} = B_{1,p}, \\ q_{10} = -q_{11} \quad &\Rightarrow \quad A_{1,p} = 0. \end{aligned} \tag{5.69}$$

Physically, the configurations where the triple cut vanishes correspond exactly to what would have been expected from real kinematics: the triple cut is zero if it isolates a vertex with three massless on-shell legs. The two solutions correspond to the fact that the sign of the q_{11} component of q_1 is arbitrary. To finish our proof that the cut is zero in this configuration, we must also check that $f_{3,p}$ is analytic in this limit: we can use exactly the same argument as for $f_{1,p}^E$ above, because in this case all $B_{j,p}$ with $j \geq 2$ vanish (they are proportional to $\sqrt{x_{1,p}(1-x_{1,p})}$), which makes all the integrations in $f_{3,p}$ trivial.

In summary, for three particle cuts we can still rely on arguments from real kinematics to identify which cut diagrams vanish. As an example, the triple cut of the triangle with no internal massive propagators and one or two external massive channels will vanish.

Four or more propagator cuts: We now discuss the case where four or more propagators are cut. We start by looking at the four-propagator cut. Setting

$m = 4$ in eq. (5.33),

$$\mathcal{C}_4\left[I_n\right] = \frac{2^{2-D}(2\pi)^2 e^{\gamma_E \epsilon}}{\pi^{\frac{n-1}{2}}\Gamma\left(\frac{D-n+1}{2}\right)} \left|q_{22}\right|^{5-D} \frac{\left|A_{2,p}(B_{2,p}-A_{2,p})\right|^{\frac{D-5}{2}}}{\left|q_{00}\right|\left|q_{11}\right|\left|q_{22}\right|} f_{4,p}. \tag{5.70}$$

For the same reason as for the three-propagator cut, the quadruple cut will vanish if and only if $A_{2,p} = 0$ or $A_{2,p} = B_{2,p}$. Recalling that $x_{1,p} = A_{1,p}/B_{1,p}$, with $B_{1,p}$ as given above, we have

$$\begin{aligned} B_{2,p} &= 2\frac{q_{22}}{q_{11}} B_{1,p}\sqrt{x_{1,p}(1-x_{1,p})} = 2\frac{q_{22}}{q_{11}}\sqrt{A_{1,p}(B_{1,p}-A_{1,p})} \\ A_{2,p} &= 2k_{0,p}q_{20} - \frac{q_{21}}{2q_{11}}(2A_{1,p}-B_{1,p}) + \frac{q_{22}}{q_{11}}\sqrt{A_{1,p}(B_{1,p}-A_{1,p})} + m_2^2 - k^2 - q_2^2. \end{aligned} \tag{5.71}$$

The naïve guess to find a kinematic configuration where the quadruple cut could vanish would be to require any of the three-propagator cuts obtained by cutting one fewer propagator of such diagram to be zero, i.e., that any of the triple cuts would isolate a vertex with three massless legs. This can be realised in the above expressions by setting $A_{1,p} = 0$ and $k^2 = 0$, in which case

$$\begin{aligned} B_{2,p} &= 0 \\ A_{2,p} &= 2k_{0,p}(q_{20}+q_{21}) - q_2^2. \end{aligned} \tag{5.72}$$

where we have also set m_2^2 to be zero, which we are of course free to do. As for the triple cut, we can also require that $q_2^2 = 0$. We would then have a vanishing quadruple cut if $q_{20} + q_{21} = 0$. However, these two conditions cannot be satisfied at the same time: since by definition $q_{22} \neq 0$,

$$q_2^2 = 0 \quad \Rightarrow \quad q_{22}^2 = q_{20}^2 - q_{21}^2 \neq 0 \quad \Rightarrow \quad q_{20} + q_{21} \neq 0. \tag{5.73}$$

We thus conclude that the quadruple cut of a one-loop diagram cannot vanish for a general kinematic configuration. As an example, which we will explore in more detail below, the quadruple cut of the massless box is not zero, and can be computed using eq. (5.70) to all orders in ϵ. This result contradicts our intuition from the previous chapter in two ways. First, if we restricted ourselves to real kinematics this cut would vanish because it isolates a massless vertex (in fact, four massless vertices). Second, we got used to thinking of iterated cuts as iterated

discontinuities, but once we have taken the first cut, say on the s-channel of the box, the second cut, say on the t-channel, is a cut on a channel that does not have a well defined $i0$-prescription according to the rules of the previous chapter, which means we could not compute its double discontinuity. In that spirit, the only value that would make sense to assign to such a cut would be zero. We will however see that the quadruple cut can still be interpreted in some sense as a discontinuity on s and t.

We conjecture that the same conclusion holds for any number of cut propagators $m \geq 4$, for exactly the same reasons. We will give both direct and indirect evidence to support this conjecture. The direct evidence will be given in the next section where we will compute the five-propagator cut of the pentagon, and the indirect evidence in the next chapter where we will argue that maximal cuts are related to the homogeneous terms of the differential equations satisfied by Feynman diagrams.

To summarise this subsection, one-, two- and three-propagator cuts, computed in complex kinematics according to the definitions in eqs. (5.24) and (5.55), can also be understood from the perspective of the relation between cuts and discontinuities we developed in the previous section. One- and two-propagator cuts vanish if they do not correspond to a discontinuity on an internal mass or an external channel, and three-propagator cuts will vanish if they isolate a vertex with three massless legs. If four or more propagator are cut, the cuts will never vanish for general kinematics.

5.4.2 Maximal and next-to-maximal cuts of a diagram with an even number of propagators

We now look at an interesting relation between maximal and next-to-maximal cuts of diagrams with an even number n of propagators, computed in $d = n$ dimensions. This relation will play an important role in the discussion of the following chapter.

We start with an observation on the weight of Feynman integrals. As already mentioned, requiring that the space-time dimensions vary with the number of propagators as we do in eq. (5.9) guarantees that all one-loop Feynman diagrams are functions of weight $d/2$ (more precisely, a pure function once normalised to

its leading singularity, as defined in eq. (5.35)). It then follows that the m-propagator cut of a Feynman diagram as defined in eq. (5.24) is a function of weight $d/2 - \lceil m/2 \rceil$, where $\lceil x \rceil$ is the 'ceiling function' that associates a real number x to the smallest integer greater or equal to x. In particular, this means that the next-to-maximal and maximal cuts of a diagram with an even number of propagators are functions of weight 0, i.e., they are rational functions for $\epsilon = 0$. Note that this means that next-to-maximal and maximal cuts cannot be divergent.

We will now show that if the next-to-maximal cuts exist, i.e., if they are not zero for the reasons given in section 5.4.1, they are equal to each other and proportional to the maximal cut at $\epsilon = 0$. Furthermore, the proportionality constant is independent of the diagram.

We start by evaluating the maximal cut at $\epsilon = 0$. We can use eq. (5.34) and, because we are considering diagrams with an even number of propagators, set $D = n$:

$$\mathcal{C}_n^{(0)}\left[I_n\right] = 2^{2-\frac{n}{2}} \left|A_{n-2,p}(B_{n-2,p} - A_{n-2,p})\right|^{-\frac{1}{2}} \prod_{j=0}^{n-3} \left|q_{jj}\right|^{-1}, \tag{5.74}$$

where $\mathcal{C}_n^{(0)}\left[I_n\right]$ denotes the order ϵ^0 term in the ϵ-expansion of $\mathcal{C}_n\left[I_n\right]$.

The next-to-maximal cuts can be written in the form

$$\mathcal{C}_{n-1}^{(0)}\left[I_n\right] = -\frac{2^{2-\frac{n}{2}}}{2\pi} f_{n-1,p}^{(0)} \prod_{j=0}^{n-3} \left|q_{jj}\right|^{-1}, \tag{5.75}$$

where the superscript (0) has the same meaning as above. Note that while the maximal cut is unique, there are n different next-to-maximal cuts. However, they can all be written in this form, so we will not distinguish between them. Because the next-to-maximal cuts are not divergent, we can compute $f_{n-1,p}^{(0)}$ by setting $\epsilon = 0$ and $m = n - 1$ in eq. (5.21):

$$f_{n-1,p}^{(0)} = \int_0^1 d\,x \frac{(x(1-x))^{-\frac{1}{2}}}{(B_{m-2,p}x - A_{m-2,p})} = \pi \left|A_{n-2,p}(B_{n-2,p} - A_{n-2,p})\right|^{-\frac{1}{2}}. \tag{5.76}$$

We thus find that

$$\mathcal{C}_{n-1}^{(0)}\left[I_n\right] = -\frac{1}{2}\mathcal{C}_n^{(0)}\left[I_n\right] + \mathcal{O}(\epsilon). \tag{5.77}$$

This shows that for any one-loop diagram with an even number of propagators there is a relation between the next-to-maximal and the maximal cuts: the $\mathcal{O}(\epsilon^0)$ coefficients in the ϵ-expansion of all existing next-to-maximal cuts (i.e., non-vanishing according to the discussion in section 5.4.1) are equal to each other, and equal to minus one-half times the $\mathcal{O}(\epsilon^0)$ coefficient of the maximal cut.

As an example, consider the box diagram with one internal massive propagator, and four external massless legs. Following the discussion of section 5.4.1, this diagram has a single non-vanishing triple cut, the one where the massive propagator and the two adjacent ones are cut. According to eq. (5.77), we expect the first term in the ϵ-expansion of this cut to be minus one-half times the first term in the ϵ-expansion of the quadruple cut. In the next section, we will verify this by explicit calculation.

5.4.3 Brief comment on maximal cuts

We finish this section on general properties of cuts of one-loop diagrams with a brief comment on maximal cuts. Our formal solution for the m-propagator cut of a diagram with n propagators, given explicitly in eq. (5.33), is of the form

$$\mathcal{C}_m\left[I_n\right] = \mathcal{N}(\epsilon)\mathcal{R}(p_j \cdot p_k; m_l^2)\mathcal{X}(p_j \cdot p_k; m_l^2; \epsilon) f_{m,p}(p_j \cdot p_k; m_l^2; \epsilon), \tag{5.78}$$

where:

- $\mathcal{N}$ is a prefactor independent of the kinematic invariants ;
- $\mathcal{R}$ is a rational function of the invariants independent of ϵ ;
- $\mathcal{X}$ is a function of the invariants and of ϵ, with a very simple ϵ dependence of the form x^ϵ, giving only powers of simple logarithms upon expansion ;
- $f_{m,p}$ is a function of the invariants and of ϵ, obtained by integrating the uncut propagators, with a complicated ϵ dependence, producing non-trivial polylogarithms upon expansion.

For the maximal cut, $f_{n,p}(p_j \cdot p_k; m_l^2; \epsilon) = 1$, and we have

$$\mathcal{C}_n\left[I_n\right] = \mathcal{N}(\epsilon)\mathcal{R}(p_j \cdot p_k; m_l^2)\mathcal{X}(p_j \cdot p_k; m_l^2; \epsilon), \tag{5.79}$$

which means that, aside from a prefactor independent of the kinematic invariants, the ϵ dependence of the maximal cut is of the form x^ϵ. Because of this, maximal cuts will play a special role in the discussion of the next chapter.

5.5 New results for cuts in complex kinematics

When introducing our formulation for cuts of one-loop diagrams in sections 5.2 and 5.3, we illustrated the formulae we obtained by showing they gave the expected results for some trivial examples. We now apply them to more complicated diagrams. We first look once more at our favourite example, the one-loop three-mass triangle, to show we recover the results we already obtained previously. We then go on to compute cuts of a variety of box diagrams. We will not explore the one- and two-propagator cuts, as their calculation does not require the tools introduced in this chapter: the calculation is essentially the same as for triangles, but requires the evaluation of more complicated integrals. We will evaluate the next-to-maximal cuts to illustrate how they can vanish depending on the kinematic configuration. The maximal cuts of boxes will be the first example of a cut that could not have been computed through the methods of the previous chapters. Finally, we compute the maximal cut of the pentagon with no internal or external masses, which gives more evidence that cuts of four or more propagators do not vanish even if they isolate a vertex connecting three massless legs.

5.5.1 Three-mass triangle

We will consider the double and triple cuts of the triangle with three external massive legs of masses p_1^2, p_2^2 and p_3^2 in $D = 4 - 2\epsilon$ dimensions, which we already analysed in sections 3.5.1 and 3.5.5. These cuts are computable in real kinematics, so this example shows that the definition of cut as residues given in this chapter reproduces the results computed with the more standard techniques of the previous chapter when both methods give non-vanishing results.

In this case, eq. (5.9) is

$$I_3(p_1^2, p_2^2, p_3^2) = \frac{e^{\gamma_E \epsilon}}{i\pi^{2-\epsilon}} \int d^{4-2\epsilon}k \frac{1}{k^2} \frac{1}{(k-q_0)^2} \frac{1}{(k-q_1)^2}, \tag{5.80}$$

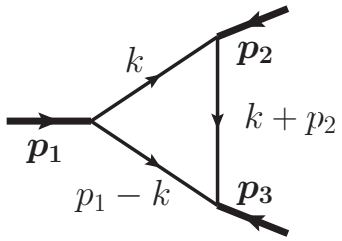

Figure 5.1: Parametrisation for the triangle with three external masses.

and we choose $q_0 = p_1$ and $q_1 = -p_2$, which is consistent with cutting the propagator (12), of momentum k, and (13), of momentum $(p_1 - k)$, see fig. 5.1. Working out the kinematics,

$$q_0 = \sqrt{p_1^2}(1, \mathbf{0}_{D-1}), \qquad q_1 = \frac{\sqrt{p_1^2}}{2}\left(1 + u_2 - u_3, -\sqrt{\lambda(1, u_2, u_3)}, \mathbf{0}_{D-2}\right). \quad (5.81)$$

Under the conditions $k_0 = \frac{\sqrt{p_1^2}}{2}$, $\beta = 1$, we have $A_{1,p}$ and $B_{1,p}$—see eq. (5.16):

$$A_{1,p} = p_1^2(1-z)\bar{z}, \qquad B_{1,p} = -p_1^2(z-\bar{z}), \qquad x_{1,p} = -\frac{(1-z)\bar{z}}{z-\bar{z}}. \quad (5.82)$$

This parametrisation is suitable for the p_1^2-channel cut, so we now show we do recover the expected result from eq. (5.28) with $n = 3$,

$$\mathcal{C}_{2,[(12),(13)]}\left[I_3(p_1^2, p_2^2, p_3^2)\right] = \frac{e^{\gamma_E \epsilon}}{\Gamma(1-\epsilon)}\left(\frac{\sqrt{p_1^2}}{2}\right)^{1-2\epsilon}\frac{f_{2,p}}{\sqrt{p_1^2}}, \quad (5.83)$$

in the region where $p_1^2 > 0$. $f_{2,p}$ is obtained from eq. (5.21) with $n = 3$,

$$\begin{aligned} f_{2,p} &= -\frac{2^{1-2\epsilon}}{p_1^2(z-\bar{z})}\int_0^1 dx_1 \frac{(x_1(1-x_1))^{-\epsilon}}{x_1 - x_{1p}} \\ &= -\frac{2^{1-2\epsilon}}{p_1^2 \bar{z}(1-z)}\frac{\Gamma^2(1-\epsilon)}{\Gamma(2-2\epsilon)}\,{}_2F_1\left(1, 1-\epsilon; 2-2\epsilon; -\frac{z-\bar{z}}{(1-z)\bar{z}}\right). \end{aligned} \quad (5.84)$$

Putting everything together,

$$\begin{aligned} &\mathcal{C}_{2,[(12),(13)]}\left[I_3(p_1^2, p_2^2, p_3^2)\right] = \\ &\qquad = -\frac{e^{\gamma_E\epsilon}\Gamma(1-\epsilon)}{\Gamma(2-2\epsilon)}\frac{(p_1^2)^{-1-\epsilon}}{(1-z)\bar{z}}\,{}_2F_1\left(1, 1-\epsilon; 2-2\epsilon; -\frac{z-\bar{z}}{(1-z)\bar{z}}\right), \end{aligned} \quad (5.85)$$

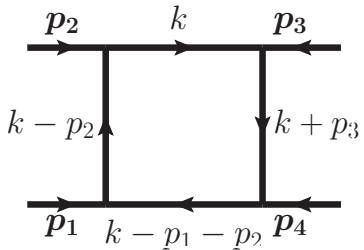

Figure 5.2: Parametrisation for the general box diagram. For each of the boxes we consider, some of the masses have to be put to zero.

which reproduces the result of eq. (B.55), which was computed as a unitarity cut using the methods of chapter 3, once multiplied by a factor of (-2π). In appendix A, eq. (A.10), we explain in detail how this factor can be determined.

We can also compute the maximal cut of this triangle, for which we use eq. (5.34) with $n = 3$,

$$\begin{aligned}\mathcal{C}_3\left[I_3(p_1^2,p_2^2,p_3^2)\right] =& \frac{2^{-1+2\epsilon}e^{\gamma_E\epsilon}}{\Gamma\left(1-\epsilon\right)}\frac{\left|q_{11}^{2\epsilon-1}\right|}{|q_{00}|}\left|A_{1,p}(B_{1,p}-A_{1,p})\right|^{-\epsilon}\\ =& -\frac{e^{\gamma_E\epsilon}}{\Gamma(1-\epsilon)}\frac{(p_1^2)^{-1-\epsilon}}{(z-\bar{z})^{1-2\epsilon}}\left|z\bar{z}(1-z)(1-\bar{z})\right|^{-\epsilon}, \end{aligned} \tag{5.86}$$

which reproduces the result of eq. (B.58) once factors of (2π) and i have been adjusted.

5.5.2 Triple and quadruple cut of the 0-mass box

We now look at the triple and quadruple cuts of the 0-mass box in $4-2\epsilon$ dimensions,

$$I_4(s,t) = \frac{e^{\gamma_E\epsilon}}{i\pi^{2-\epsilon}}\int d^{4-2\epsilon}k\frac{1}{k^2(k-(p_1+p_2))^2(k-p_2)^2(k+p_3)^2} \tag{5.87}$$

where $s=(p_1+p_2)^2$ and $t=(p_2+p_3)^2$. We parametrise the momenta as follows (see fig. 5.2 with all masses set to zero):

$$\begin{aligned} q_0 = p_1+p_2 &= \sqrt{s}\left(1,\mathbf{0}_{D-1}\right), \quad q_1 = p_2 = \frac{\sqrt{s}}{2}\left(1,-1,\mathbf{0}_{D-2}\right)\\ q_2 = -p_3 &= \frac{\sqrt{s}}{2}\left(1,-1-2r,2\sqrt{-r(1+r)},\mathbf{0}_{D-3}\right), \end{aligned}$$

$$k = k_0 \left(1, \cos\theta_1, \sin\theta_1 \cos\theta_2, \sin\theta_1 \sin\theta_2 \mathbf{1}_{D-4}\right), \tag{5.88}$$

where $r = t/s$.

The triple cut for which this parametrisation is suitable, $\mathcal{C}_{3,[(12),(23),(14)]}\left[I_4(s,t)\right]$, isolates a vertex with three massless particles (we can easily check $x_{1,p} = 0$), and following the discussion of section 5.4.1 it must thus vanish. In fact, by symmetry this is true for any triple cut and we can write more generally

$$\mathcal{C}_3\left[I_4(s,t)\right] = 0. \tag{5.89}$$

The quadruple cut is a maximal cut so we can use eq. (5.34) with $n = 4$ and $D = 4 - 2\epsilon$,

$$\mathcal{C}_4\left[I_4(s,t)\right] = \frac{e^{\gamma_E \epsilon}\Gamma(1-\epsilon)}{\Gamma\left(1-2\epsilon\right)} \frac{\left|q_{22}\right|^{2\epsilon}}{\left|q_{00}\right|\left|q_{11}\right|} \left|A_{2,p}(B_{2,p} - A_{2,p})\right|^{-\frac{1+2\epsilon}{2}}, \tag{5.90}$$

where $A_{2,p}$ and $B_{2,p}$ are evaluated at $x_1 = x_{1,p} = 0$, and thus become very simple:

$$A_{2,p} = -t, \quad \text{and} \quad B_{2,p} = 0. \tag{5.91}$$

We then get

$$\mathcal{C}_4 I_4(s,t) = 2\frac{e^{\gamma_E \epsilon}\Gamma(1-\epsilon)}{\Gamma\left(1-2\epsilon\right)} \frac{s^{-\epsilon} t^{-\epsilon} (s+t)^{\epsilon}}{st}, \tag{5.92}$$

where we chose to be in the region where $s, t > 0$, as this cut is symmetric in these two variables.

This is the first cut we computed with the definition of cut given in eq. (5.24) that we would not have been able to compute using the method of chapter 3. It would thus be interesting to have some check of this result. The first check we can do is to check whether the coefficient of order ϵ^0 matches the rational prefactor of this diagram [56, 57], and it is easy to see that it does. Indeed, up to normalisation factors it also matches the result we have computed in eq. (5.8). However, we claim our method should give the quadruple cut to all orders in ϵ, so we would like to check higher orders in ϵ are correct as well. We now show how this can be done.

The uncut box is given in eq. (B.91). Because this diagram only depends on two variables, its analytic structure should be simple to understand: by symmetry

of the diagram and of its quadruple cut, it is reasonable to expect that

$$\delta_{s,t} I_4(s,t) = \delta_{t,s} I_4(s,t) = \pm \mathcal{C}_4 I_4(s,t), \tag{5.93}$$

and this relation should hold to all orders in ϵ. We can thus compute the symbol of eq. (B.91), and check that its $\delta_{s,t}$ agrees with the symbol of eq. (5.92) order by order in ϵ. We have checked that the equality holds up to ϵ^4, with a plus sign in eq. (5.93).

Note that this means we can identify the quadruple cut of the box with the double discontinuity on s and t up to an overall sign. Indeed, there is no way to correctly determine the sign in eq. (5.93): after the first discontinuity has been taken, the variable on which the second discontinuity is taken does not have a well defined $i0$ prescription. This is why we have excluded this type of cuts from the discussion of chapter 3.

5.5.3 Triple and quadruple cut of the 1-mass box

The triple and quadruple cuts of the 1-mass box in $4-2\epsilon$ are also very easily computable. We have

$$I_4(s,t;p_4^2) = \frac{e^{\gamma_E \epsilon}}{i\pi^{2-\epsilon}} \int d^{4-2\epsilon}k \frac{1}{k^2 (k-(p_1+p_2))^2 (k-p_2)^2 (k+p_3)^2}. \tag{5.94}$$

The momenta are parametrised as:

$$\begin{aligned}
q_0 = p_1 + p_2 &= \sqrt{s}\,(1, \mathbf{0}_{D-1})\,, \quad q_1 = p_2 = \frac{\sqrt{s}}{2}\,(1, -1, \mathbf{0}_{D-2})\,, \\
q_2 = -p_3 &= \frac{s - p_4^2}{2\sqrt{s}} \left(1, \frac{1-\mu+2r}{\mu-1}, 2\frac{\sqrt{r(\mu-1-r)}}{1-\mu}, \mathbf{0}_{D-3}\right), \\
k &= k_0\,(1, \cos\theta_1, \sin\theta_1 \cos\theta_2, \sin\theta_1 \sin\theta_2 \mathbf{1}_{D-4})\,,
\end{aligned} \tag{5.95}$$

where we defined $r = t/s$ and $\mu = p_4^2/s$—see fig. 5.2 with the relevant masses set to zero.

As for the zero-mass box, all triple cuts are zero because of the discussion of section 5.4.1. For the quadruple cut, we can use eq. (5.90). It turns out that the

quantities $A_{2,p}$ and $B_{2,p}$ are equal to the ones of the zero-mass box,

$$A_{2,p} = -t, \quad \text{and} \quad B_{2,p} = 0. \tag{5.96}$$

Putting everything together, we find

$$\mathcal{C}_4\left[I_4(s,t;p_4^2)\right] = 2\frac{e^{\gamma_E\epsilon}\Gamma(1-\epsilon)}{\Gamma(1-2\epsilon)}\frac{s^{-\epsilon}t^{-\epsilon}(s+t-p_4^2)^{\epsilon}}{st}, \tag{5.97}$$

which in the $p_4^2 \to 0$ limit reproduces eq. (5.92) as it should. We can perform the same checks on this result as we did for eq. (5.92). We observe it matches the result in eq. (5.8), up to normalisation factors and at order $\epsilon = 0$. Furthermore, by symmetry we expect the quadruple cut to match $\delta_{s,t}I_4(s,t;p_4^2)$ to all orders in ϵ. This can be checked explicitly from the expression for the one-mass box, eq. (B.92), and we have done so up to ϵ^4.

5.5.4 Triple and quadruple cut of the 2-mass-easy box

We now look at the triple and quadruple cuts of the 2-mass-easy box in $4-2\epsilon$ dimensions,

$$I_4^e(s,t;p_2^2,p_4^2) = \frac{e^{\gamma_E\epsilon}}{i\pi^{2-\epsilon}}\int d^{4-2\epsilon}k\frac{1}{k^2(k-(p_1+p_2))^2(k-p_2)^2(k+p_3)^2}. \tag{5.98}$$

The momenta are parametrised as follows (see fig. 5.2 with the relevant masses set to zero):

$$\begin{aligned}
q_0 &= p_1+p_2 = \sqrt{s}\,(1,\mathbf{0}_{D-1}), \qquad q_1 = p_2 = \left(\frac{s+p_2^2}{2\sqrt{s}}, \frac{s-p_2^2}{2\sqrt{s}}, \mathbf{0}_{D-2}\right)\\
q_2 &= -p_3 = \frac{s-p_4^2}{2\sqrt{s}}\left(1, \frac{2s(p_2^2+p_4^2-s-t)}{(p_2^2-s)(s-p_4^2)} - 1,\right.\\
&\qquad \left. 2\frac{\sqrt{s(s+t-p_2^2-p_4^2)(p_2^2p_4^2-st)}}{(s-p_2^2)(s-p_4^2)}, \mathbf{0}_{D-3}\right)\\
k &= k_0\,(1, \cos\theta_1, \sin\theta_1\cos\theta_2, \sin\theta_1\sin\theta_2\mathbf{1}_{D-4})\,.
\end{aligned} \tag{5.99}$$

It is easy to see that all triple cuts isolate a three-point massless vertex, so they all vanish. For the quadruple cut, we use eq. (5.90) but now $A_{2,p}$ and $B_{2,p}$

are given by

$$A_{2,p} = \frac{st - p_2^2 p_4^2}{p_2^2 - s}, \quad \text{and} \quad B_{2,p} = 0. \tag{5.100}$$

Putting everything together,

$$\mathcal{C}_4 \left[I_4^e(s,t;p_2^2,p_4^2) \right] = 2 \frac{e^{\gamma_E \epsilon} \Gamma(1-\epsilon)}{\Gamma(1-2\epsilon)} \frac{(s+t-p_2^2-p_4^2)^\epsilon}{(st-p_2^2 p_4^2)^{1+\epsilon}}. \tag{5.101}$$

As expected, the limit $p_2^2 \to 0$ reproduces eq. (5.97), and the limit $p_2^2, p_4^2 \to 0$ reproduces eq. (5.92). The $\epsilon = 0$ limit of this expression is also consistent with the result computed in eq. (5.8). To check that the symbol of this expression is consistent with the appropriate truncation of the coproduct to higher order in ϵ, we use the result for the uncut two-mass-easy box in eq. (B.93). There is however a difference between this example and the previous two: the relevant truncation is no longer $\delta_{s,t} I_4^e(s,t;p_2^2,p_4^2)$, which is zero, but rather $\delta_{s,st-p_2^2p_4^2} I_4^e(s,t;p_2^2,p_4^2)$. Indeed, looking at a selection of box diagrams, we observe that the coproduct entry that is reproduced by the quadruple cut is of the form $\delta_{s,\Xi}$ where Ξ is (one-half times) the leading singularity of the box in question as defined in eq. (5.35). We have no deeper understanding of this observation but note that $\delta_{s,st-p_2^2p_4^2}$ reduces to $\delta_{s,t}$ in the limits corresponding to the zero-mass and one-mass boxes, so there is some consistency between the three examples. We have verified the agreement up to $\mathcal{O}(\epsilon^4)$.

5.5.5 Triple and quadruple cut of the 0-mass box with one internal mass

We now look at the triple and quadruple cuts of the 0-mass box with one internal massive propagator between external legs 1 and 2, of mass m_{12}^2, in $4-2\epsilon$ dimensions,

$$I_4(s,t;m_{12}^2) = \frac{e^{\gamma_E \epsilon}}{i\pi^{2-\epsilon}} \int d^{4-2\epsilon}k \frac{1}{k^2 (k-p_1+p_2)^2 ((k-p_2)^2 - m_{12}^2)(p_3+k)^2}. \tag{5.102}$$

We can use the same parametrisation of the external momenta as for the 0-mass box given in eq. (5.88)—see also fig. 5.2 with the relevant masses set to zero—which is consistent with a two-propagator cut in the s-channel, and a three-propagator cut which also cuts the massive propagator. The coefficients $A_{j,p}$ and

$B_{j,p}$ are different because of the internal mass,

$$\begin{aligned}
&A_{1,p} = m_1^2 = s\mu_{12}, \qquad B_{1,p} = -s, \qquad x_{1p} = -\mu_{12},\\
&A_{2,p} = s(-\mu_{12} - r - 2\mu_{12}r + 2\sqrt{\mu_{12}r(1+\mu_{12})(1+r)}) \equiv -s\bar{\alpha},\\
&B_{2,p} = 4s\sqrt{\mu_{12}r(1+\mu_{12})(1+r)} \equiv s(\alpha - \bar{\alpha}), \qquad x_{2p} = -\frac{\bar{\alpha}}{\alpha - \bar{\alpha}}.
\end{aligned} \tag{5.103}$$

where $r = t/s$, $\mu_{12} = m_{12}^2/s$ and α and $\bar{\alpha}$ were defined to have more compact and easy-to-handle expressions. It is useful to notice that $\alpha\bar{\alpha} = (\mu - r)^2$ and that the integral is symmetric under $\alpha \leftrightarrow \bar{\alpha}$.

This is our first example of a box for which the triple cut does not vanish. Indeed, $x_{1,p} \notin \{0, 1\}$. To compute this cut, we need to compute $f_{3,p}$, as defined in eq. (5.21). After some algebra, we see that the integral that must be evaluated is

$$\int_0^1 dx_2 \frac{(x_2(1-x_2))^{-1/2-\epsilon}}{x_2\alpha + (1-x_2)\bar{\alpha}}.$$

It is convenient to use the $\alpha \leftrightarrow \bar{\alpha}$ symmetry of this expression to find a better behaved integral representation of this integral (this is not necessary, but facilitates the expansion of the final result). We note that

$$\int_0^1 dx_2 \frac{(x_2(1-x_2))^{-1/2-\epsilon}}{x_2\alpha + (1-x_2)\bar{\alpha}} = \int_0^1 dx_2 \frac{(x_2(1-x_2))^{-1/2-\epsilon}}{(1-x_2)\alpha + x_2\bar{\alpha}}$$

and so

$$\begin{aligned}
\int_0^1 dx_2 \frac{(x_2(1-x_2))^{-1/2-\epsilon}}{x_2\alpha + (1-x_2)\bar{\alpha}} &= \frac{\alpha + \bar{\alpha}}{2s} \int_0^1 dx_2 \frac{(x_2(1-x_2))^{-1/2-\epsilon}}{\alpha\bar{\alpha} + x_2(1-x_2)(\alpha-\bar{\alpha})^2}\\
&= \frac{2^{2\epsilon-1}(\alpha+\bar{\alpha})}{\alpha\bar{\alpha}} \frac{\sqrt{\pi}\Gamma(1/2-\epsilon)}{\Gamma(1-\epsilon)} {}_2F_1\left(1, \frac{1}{2} - \epsilon; 1-\epsilon; -\frac{(\alpha-\bar{\alpha})^2}{4\alpha\bar{\alpha}}\right).
\end{aligned}$$

Using this result,

$$f_{3,p} = \frac{\alpha + \bar{\alpha}}{2\alpha\bar{\alpha}s} \frac{\sqrt{\pi}\Gamma\left(\frac{1-\epsilon}{2}\right)}{\Gamma(1-\epsilon)} {}_2F_1\left(1, \frac{1}{2} - \epsilon; 1-\epsilon; -\frac{(\alpha-\bar{\alpha})^2}{4\alpha\bar{\alpha}}\right). \tag{5.104}$$

From eq. (5.33), with $m = 3$ and $n = 4$, we get

$$\mathcal{C}_3\left[I_4(s,t;m_{12}^2)\right] = -\frac{2^{-1+2\epsilon}e^{\gamma_E\epsilon}}{\sqrt{\pi}\Gamma\left(\frac{1-\epsilon}{2}\right)} \frac{|q_{11}|^{2\epsilon-1}}{|q_{00}|} f_{3,p} \left|A_{1,p}\left(B_{1,p} - A_{1,p}\right)\right|^{-\epsilon}, \tag{5.105}$$

which for this particular case becomes,

$$\begin{aligned}
&\mathcal{C}_{3,[(12),(23),(14)]}\left[I_4(s,t;m_{12}^2)\right] = \\
&= -\frac{e^{\gamma_E\epsilon}\left|s\right|^{-2+\epsilon}}{2\Gamma\left(1-\epsilon\right)}\left|m_{12}^2(s+m_{12}^2)\right|^{-\epsilon}\frac{\alpha+\bar{\alpha}}{\alpha\bar{\alpha}}\,{}_2F_1\left(1,\frac{1}{2}-\epsilon;1-\epsilon;-\frac{(\alpha-\bar{\alpha})^2}{4\alpha\bar{\alpha}}\right) \\
&=\frac{1}{s(m_{12}^2-t)}\Bigg\{1+\epsilon\Bigg(-2\log\left(\frac{s\left(t-m_{12}^2\right)}{t\left(m_{12}^2+s\right)}\right)-\log\left(m_{12}^2+s\right) \\
&\quad -\log\left(-m_{12}^2\right)+\log(s)\Bigg)\Bigg\}+\mathcal{O}(\epsilon^2).
\end{aligned} \tag{5.106}$$

This result could have been computed using the methods of the previous chapter, and we have checked that the two methods agree in the region where $s > 0$ and $t < m_{12}^2 < 0$.

Upon expansion and substitution of α and $\bar{\alpha}$ by their expressions in terms of invariants, it is a non-trivial check of our result that there are no square roots remaining. Indeed, we know that the symbol alphabet of this diagram is rational when written in terms of (ratios of) Mandelstam invariants and internal masses, as can be seen explicitly in eq. (B.95). As a side comment, in chapter 6 we will argue that one can guess if the alphabet of a box diagram is rational when written in terms of the kinematic invariants by looking at the different diagrams obtained by pinching some of the propagators of the box: if any of them requires a more complicated parametrisation, so will the box. We easily see this is not the case for this example.

As a final check of eq. (5.106), we can verify it is consistent with $\delta_{s,m_{12}^2} I_4(s,t;m_{12}^2)$ using the result for $I_4(s,t;m_{12}^2)$ in eq. (B.95). Higher orders in the expansion can be found in the accompanying `MATHEMATICA` package.

We now look at the quadruple cut. We can use eq. (5.90) for which all ingredients have already been given. We find

$$\mathcal{C}_4\left[I_4(s,t;m_{12}^2)\right] = 2\frac{e^{\gamma_E\epsilon}\Gamma(1-\epsilon)}{\Gamma\left(1-2\epsilon\right)}s^{-1-\epsilon}t^{\epsilon}(s+t)^{\epsilon}(t-m_{12})^{-1-2\epsilon}. \tag{5.107}$$

This expression passes the usual checks: the massless limit reproduces eq. (5.92), and it matches $\delta_{s,m_{12}^2-t} I_4(s,t;m_{12}^2)$ up to ϵ^3, the order to which we have evaluated $I_4(s,t;m_{12}^2)$. Furthermore, this is the first example for which we can check that the relation in eq. (5.77) holds: it is easy to see that the finite terms of eqs. (5.106)

and (5.107) do agree with it.

5.5.6 Triple and quadruple cut of the 0-mass box with two adjacent internal masses

We now look at the triple and quadruple cuts of the 0-mass box with two adjacent internal masses in $4-2\epsilon$ dimensions,

$$\begin{aligned} &I_4(s,t;m_{12}^2,m_{23}^2) = \\ &= \frac{e^{\gamma_E\epsilon}}{\pi^{2-\epsilon}}\int d^{4-2\epsilon}k \frac{1}{k^2((k-p_1+p_2)^2-m_{23}^2)((k-p_2)^2-m_{12}^2)(p_3+k)^2}. \end{aligned} \tag{5.108}$$

We will use the same parametrisation as for the the 0-mass box and the previous example, see fig. 5.2 with the relevant masses set to zero. Because the propagator of momentum $(k-q_0)$ is massive, the pole of the residue of k_0 is now at $k_{0,p} = \frac{s-m_{23}^2}{2\sqrt{s}}$. The coefficients $A_{j,p}$ and $B_{j,p}$ are given by

$$\begin{aligned} &A_{1,p} = m_{12}^2 = s\mu_{12}, \qquad B_{1,p} = m_{23}^2 - s = s(\mu_{23}-1), \qquad x_{1,p} = \frac{\mu_{12}}{\mu_{23}-1}, \\ &A_{2,p} = s(-\mu_{12}-r-2\mu_{12}r+r\mu_{23}+2\sqrt{\mu_{12}r(1+\mu_{12}-\mu_{23})(1+r)}) \equiv -s\bar{\delta}, \\ &B_{2,p} = 4s\sqrt{\mu_{12}r(1+\mu_{12}-\mu_{23})(1+r)} \equiv s(\delta-\bar{\delta}), \qquad x_{2,p} = -\frac{\bar{\delta}}{\delta-\bar{\delta}}, \end{aligned} \tag{5.109}$$

where $r = t/s$ and $\mu_{ij} = m_{ij}^2/s$. The quantities δ and $\bar{\delta}$ were defined for convenience and simplicity of the expressions. It is useful to notice that $\delta\bar{\delta} = (\mu_{12}+r(\mu_{23}-1))^2$.

The parametrisation we chose is consistent with the triple cut where the propagators (12), (23) and (14) are cut. Proceeding as in the previous example,

$$\begin{aligned} &\mathcal{C}_{3,[(12),(23),(14)]}\left[I_4(s,t;m_{12}^2,m_{23}^2)\right] = \\ &= -\frac{e^{\gamma_E\epsilon}\left|s\right|^{-2+\epsilon}}{2\Gamma\left(1-\epsilon\right)}\left|m_{12}^2(s+m_{12}^2-m_{23}^2)\right|^{-\epsilon}\frac{\delta+\bar{\delta}}{\delta\bar{\delta}}\,{}_2F_1\left(1,\frac{1}{2}-\epsilon;1-\epsilon;-\frac{(\delta-\bar{\delta})^2}{4\delta\bar{\delta}}\right) \\ &= \frac{1}{s\left(m_{12}^2-t\right)+m_{23}^2t}\Bigg\{1+\epsilon\Bigg(-2\log\left(\frac{-m_{12}^2s-m_{23}^2t+st}{t\left(m_{12}^2-m_{23}^2+s\right)}\right) \\ &-\log\left(m_{12}^2-m_{23}^2+s\right)-\log\left(-m_{12}^2\right)+\log(s)\Bigg)\Bigg\}+\mathcal{O}(\epsilon^2). \end{aligned} \tag{5.110}$$

The same comments as below eq. (5.106) apply: the same result could have been computed with the methods of chapter 3 in the kinematic region where $s > m_{23}^2$ and $t < m_{12}^2 < 0$, all square roots disappear upon expansion and substitution of δ and $\bar{\delta}$ (as for the previous box, we can check all triangles obtained by contracting one of the propagators have a rational symbol alphabet when written in terms of ratios of kinematic invariants), and this expression reproduces $\delta_{s,m_{12}^2} I_4(s,t;m_{12}^2,m_{23}^2)$, which we can compute using eq. (B.99). Furthermore, we can check the $m_{23}^2 \to 0$ limit of the unexpanded expression agrees with the result in eq. (5.106). Higher orders in the expansion can be found in the accompanying `MATHEMATICA` package.

There is another non-vanishing triple cut we can compute, $\mathcal{C}_{3,[(12),(23),(34)]}\left[I_4\right]$, which would correspond to a double discontinuity on t and m_{23}^2 in the language of the previous section. We could re-parametrise the momenta to have a parametrisation consistent with this triple cut, and go through the same exercise as above. However, it is easier to notice that $\mathcal{C}_{3,[(12),(23),(14)]}$ and $\mathcal{C}_{3,[(12),(23),(34)]}$ are related by symmetry:

$$\mathcal{C}_{3,[(12),(23),(34)]}\left[I_4(s,t;m_{12}^2,m_{23}^2)\right] = \mathcal{C}_{3,[(12),(23),(14)]}\left[I_4(t,s;m_{23}^2,m_{12}^2)\right]. \quad (5.111)$$

To finish with this example, the quadruple cut is given by

$$\mathcal{C}_4\left[I_4(s,t;m_{12}^2,m_{23}^2)\right] = 2\frac{e^{\gamma_E\epsilon}\Gamma(1-\epsilon)}{\Gamma(1-2\epsilon)}(s+t)^{\epsilon}(s(t-m_{12})-m_{23}^2 t)^{-1-2\epsilon}. \quad (5.112)$$

This expression passes the usual checks: the massless limit reproduces eqs. (5.92) and (5.107), and it matches $\delta_{s,s(t-m_{12})-m_{23}^2 t} I_4(s,t;m_{12}^2)$ up to ϵ^2, the order to which we have evaluated $I_4(s,t;m_{12}^2,m_{23}^2)$. As for the previous examples, we can check that eqs. (5.110)), (5.111)) and (5.112)) are in agreement with the relation in eq. (5.77).

5.5.7 Triple and quadruple cut of the 2-mass-hard box

As our last box example, we look at the triple and quadruple cuts of the 2-mass-hard box in $4-2\epsilon$ dimensions,

$$I_4^h(s,t;p_1^2,p_2^2) = \frac{e^{\gamma_E\epsilon}}{\pi^{2-\epsilon}}\int d^{4-2\epsilon}k \frac{1}{k^2(k-(p_1+p_2))^2(k-p_2)^2(k+p_3)^2}. \quad (5.113)$$

We choose a parametrisation consistent with a first cut in the s channel and a second cut in the propagator (12), see fig. 5.2 with the relevant masses set to zero:

$$\begin{aligned} q_0 =& p_1 + p_2 = \sqrt{s}\,(1, \mathbf{0}_{D-1})\,, \qquad q_1 = p_2 = \sqrt{p_2^2}\left(\alpha, \sqrt{\alpha^2-1}, \mathbf{0}_{D-2}\right), \\ q_2 =& -p_3 = \beta\left(1, \gamma, \sqrt{1-\gamma^2}, \mathbf{0}_{D-3}\right), \\ k =& k_0\,(1, \cos\theta_1, \sin\theta_1\cos\theta_2, \sin\theta_1\sin\theta_2 \mathbf{1}_{D-4})\,. \end{aligned} \tag{5.114}$$

After working out the kinematics,

$$q_1 = \sqrt{s}\left(\frac{1-u_1+u_2}{2}, \frac{\sqrt{\lambda}}{2}, \mathbf{0}_{D-2}\right), \quad q_2 = \frac{\sqrt{s}}{2}\left(1, \gamma, \sqrt{1-\gamma^2}, \mathbf{0}_{D-3}\right), \tag{5.115}$$

where

$$u_i = \frac{p_i^2}{s}, \quad \gamma = \frac{1-u_1-u_2+2r}{\sqrt{\lambda}}, \quad r = \frac{t}{s}, \quad \lambda = \lambda(1, u_1, u_2).$$

We will use the by now usual z and $\bar{z}$ defined as $u_1 = z\bar{z}$ and $u_2 = (1-z)(1-\bar{z})$, see also section B.4.6.

We start by computing the $A_{j,p}$ and $B_{j,p}$ coefficients:

$$\begin{aligned} A_{1,p} &= sz(1-\bar{z}), \quad B_{1,p} = s(z-\bar{z}), \\ A_{2,p} &= s\left(\frac{1+\gamma}{2} - \gamma x_1 + \sqrt{1-\gamma^2}\sqrt{x_1(1-x_1)}\right) \equiv s\chi, \\ B_{2,p} &= 2s\sqrt{1-\gamma^2}\sqrt{x_1(1-x_1)} = s(\chi - \bar{\chi}). \end{aligned} \tag{5.116}$$

The poles of the propagators are at:

$$x_{1,p} = \frac{z(1-\bar{z})}{z-\bar{z}}, \quad x_{2,p} = \frac{1+\gamma-2\gamma x_1 + 2\sqrt{1-\gamma^2}\sqrt{x_1(1-x_1)}}{4\sqrt{1-\gamma^2}\sqrt{x_1(1-x_1)}} = \frac{\chi}{\chi-\bar{\chi}},$$

where χ and $\bar{\chi}$, introduced for convenience, satisfy $\chi\bar{\chi} = \frac{r^2}{(z-\bar{z})^2}$.

By the arguments of section 5.4.1, there is a single non-vanishing triple cut, the cut of propagators (12), (14) and (23). We are by now familiar with this type

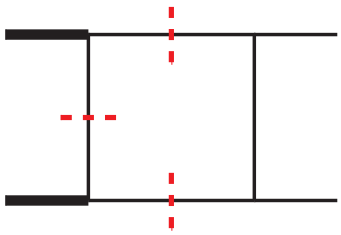

(a) Three-propagator cut

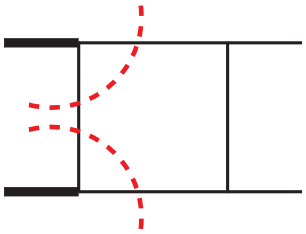

(b) Cut in p_1^2 and p_2^2

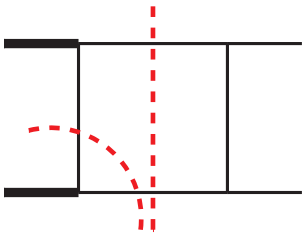

(c) Cut in s and p_1^2

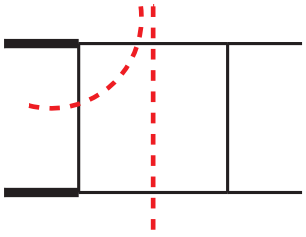

(d) Cut in s and p_2^2

Figure 5.3: Different interpretations of the non-vanishing triple cut of the two-mass-hard box.

of calculation, so we simply quote the result:

$$\begin{aligned}
&\mathcal{C}_{3,[(12),(23),(14)]}\left[I_4^h(s,t;p_1^2,p_2^2)\right] = \\
&= -\frac{e^{\gamma_E\epsilon}\,|s|^{-2+\epsilon}}{2\Gamma\,(1-\epsilon)}\frac{|z\bar{z}(1-z)(1-\bar{z})|^{-\epsilon}}{|z-\bar{z}|^{1-2\epsilon}}\frac{\chi+\bar{\chi}}{\chi\bar{\chi}}\,{}_2F_1\left(1,\frac{1}{2}-\epsilon;1-\epsilon;-\frac{(\chi-\bar{\chi})^2}{\chi\bar{\chi}}\right) \\
&= \frac{1}{s^2 r}\Bigg\{-1+\epsilon\Bigg(-2\log(r-z\bar{z}+\bar{z})+2\log(-r)+\log(s) \\
&+\log\left(-\frac{(1-z)\bar{z}}{z(1-\bar{z})}\right)\Bigg)\Bigg\}+\mathcal{O}(\epsilon^2).
\end{aligned} \tag{5.117}$$

As the previous two triple cuts of boxes we computed, this cut could have been computed with the methods of the previous chapter. However, this is the first time that a three-propagator cut—see fig. 5.3a—can have different interpretations as discontinuities. Indeed, it can correspond to a discontinuity on p_1^2 and p_2^2—see fig. 5.3b—to a discontinuity on s and p_1^2—see fig. 5.3c—or to a discontinuity on s and p_2^2—see fig. 5.3d. These three discontinuities must thus be related by analytic continuation (in our expression, we chose to compute it in the region where $p_1^2, s > 0$ and $p_2^2, t < 0$). More importantly, following the relation between cuts, discontinuities and coproduct entries, this implies many relations between

coproduct entries. For instance, from $\text{Disc}_{p_1^2,p_2^2} = \text{Disc}_{p_2^2,p_1^2}$, we get

$$\delta_{\bar{z},1-z} I_4^h(s,t;p_1^2,p_2^2) = \delta_{1-z,\bar{z}} I_4^h(s,t;p_1^2,p_2^2) = -\mathcal{C}_{3,[(12),(23),(14)]} I_4^h(s,t;p_1^2,p_2^2) \mod \pi.$$

From $\text{Disc}_{s,p_1^2} = \text{Disc}_{s,p_2^2}$, which must hold by symmetry, we get

$$\begin{aligned}
&(\delta_{s,\bar{z}} - \delta_{z,\bar{z}} - \delta_{1-z,\bar{z}} - \delta_{x,\bar{z}})\, I_4^h(s,t;p_1^2,p_2^2) = \\
&\quad = (\delta_{s,1-z} - \delta_{z,1-z} - \delta_{1-z,1-z} - \delta_{x,1-z})\, I_4^h(s,t;p_1^2,p_2^2) \\
&\quad = \mathcal{C}_{3,[(12),(23),(14)]} I_4^h(s,t;p_1^2,p_2^2) \mod \pi
\end{aligned}$$

We also get some relations from $\text{Disc}_{p_1^2,s}$ and $\text{Disc}_{p_2^2,s}$ but these would involve other symbol letters so we will not go into that detail here. Indeed, we simply wanted to illustrate once more through a new example that the analytic structure of Feynman integrals is highly constrained by their cuts.

We finish this example with the quadruple cut, for which we can use eq. (5.90). Using

$$\begin{aligned}
&q_{22}^2 = s\frac{(r+z-z\bar{z})(z\bar{z}-r-\bar{z})}{(z-\bar{z})^2}, \quad q_{00}q_{11} = \frac{s(z-\bar{z})}{2}, \\
&A_2(B_2-A_2) = -s^2\frac{r^2}{(z-\bar{z})^2}
\end{aligned}$$

the quadruple cut is

$$\mathcal{C}_4\left[I_4^h(s,t;p_1^2,p_2^2)\right] = 2\frac{e^{\gamma_E\epsilon}\Gamma(1-\epsilon)}{\Gamma(1-2\epsilon)}\frac{s^{-1-\epsilon}(-r)^{-1-2\epsilon}}{|(r+z-z\bar{z})(z\bar{z}-r-\bar{z})|^{-\epsilon}}. \tag{5.118}$$

This expression passes all the usual checks. In particular, it agrees with

$$\mathcal{C}_4\left[I_4^h(s,t;p_1^2,p_2^2)\right] = (\delta_{s,r} - \delta_{z,r} - \delta_{1-z,r} - \delta_{r,r})\, I_4^h(s,t;p_1^2,p_2^2) \mod \pi,$$

as it should, given the relation between the quadruple cut and the double discontinuity $\text{Disc}_{s,t}\left[I_4^h(s,t;p_1^2,p_2^2)\right]$. We can also check the agreement of eqs. (5.117) and (5.118) in the perspective of eq. (5.77).

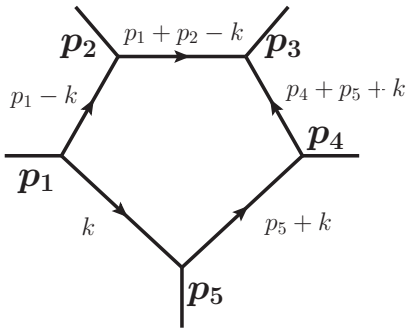

Figure 5.4: Parametrisation for the massless pentagon.

5.5.8 Maximal cut of the massless pentagon

As a final example, we examine the maximal cut of the massless pentagon in $D = 6 - 2\epsilon$ dimensions. Through this example, we wish to illustrate two main points. The first is to show that it is possible to have a non-vanishing cut that isolates a vertex with three massless legs in a diagram with an odd number of cut propagators. The second is to point out a subtlety in the usage of eq. (5.16).

We start with some notation. In the usual way, we define

$$s_{jk} = (p_j + p_k)^2 = 2p_j \cdot p_k. \tag{5.119}$$

The pentagon depends on five independent dimensionful variables. As usual, we can factor out a scale that carries the dimensions of the integral, and the non-trivial part of the integral is a function of four dimensionless variables. We choose

$$r_{ij} = \frac{s_{ij}}{s_{12}}, \text{ with } ij = 23, 34, 45, 15. \tag{5.120}$$

We parametrise the momenta as follows, see fig. 5.4:

$$\begin{aligned}
q_0 &= p_1 + p_2 = \sqrt{s_{12}}\,(1, \mathbf{0}_{D-1})\,, \qquad q_1 = p_1 = \frac{\sqrt{s_{12}}}{2}\,(1, 1, \mathbf{0}_{D-2})\,, \\
q_2 &= -(p_4 + p_5) = \sqrt{s_{12}}\left(1 + r_{45}, 1 + 2r_{23} - r_{45}, -2\sqrt{r_{23}(r_{45} - 1 - r_{23})}, \mathbf{0}_{D-3}\right), \\
q_3 &= -p_5 = -\sqrt{s_{12}}\left(\gamma_0, \gamma_1, \gamma_2, \sqrt{\gamma_0^2 - \gamma_1^2 - \gamma_2^2}, \mathbf{0}_{D-4}\right),
\end{aligned} \tag{5.121}$$

where

$$\gamma_0 = \frac{r_{34}-1}{2}, \qquad \gamma_1 = \frac{r_{34}-1-2r_{15}}{2},$$
$$\gamma_2 = \frac{-r_{15}-2r_{23}r_{15}+r_{45}r_{15}-r_{23}+r_{23}r_{34}-r_{34}r_{45}}{2\sqrt{-r_{23}\,(1+r_{23}-r_{45})}}.$$

To compute the maximal cut, we will need to evaluate $A_{3,p}$ and $B_{3,p}$. We can start by noticing that once the propagators (12), (23) and (15) have been cut we have isolated two three-point massless vertices. Following the discussion of section 5.4.1, we have $x_{1,p} \in \{0,1\}$, which implies $\sqrt{x_{1,p}(1-x_{1,p})} = 0$. One could then be tempted to say that

$$\prod_{j=1}^{2} \sqrt{x_{j,p}(1-x_{j,p})} = 0, \tag{5.122}$$

This product appears in both $A_{3,p}$ and $B_{3,p}$. However, this is not the case, because $x_{2,p}$ is itself a function of $x_{1,p}$. Being more careful, we have

$$\prod_{j=1}^{2} \sqrt{x_{j,p}(1-x_{j,p})} = \frac{\sqrt{A_{1,p}(B_{1,p}-A_{1,p})}}{B_{1,p}} \frac{\sqrt{A_{2,p}(B_{2,p}-A_{2,p})}}{B_{2,p}},$$

where

$$B_{2,p} = \frac{2q_{22}}{q_{11}}\sqrt{x_{1,p}(1-x_{1,p})}B_{1,p} = \frac{2q_{22}}{q_{11}}\sqrt{A_{1,p}(B_{1,p}-A_{1,p})}$$

and thus

$$\prod_{j=1}^{2} \sqrt{x_{j,p}(1-x_{j,p})} = \frac{q_{11}}{2q_{22}B_{1,p}}\sqrt{A_{2,p}(B_{2,p}-A_{2,p})},$$

which does not vanish if $\sqrt{x_{1,p}(1-x_{1,p})} = 0$, i.e., if $A_{1,p} = 0$ or $A_{1,p} = B_{1,p}$.

As a side comment, we note there is no contradiction between the point we make here and the discussion of section 5.4.1. There, we used the fact that

$$\sqrt{x_{1,p}(1-x_{1,p})}\prod_{j=2}^{2} \sqrt{x_j(1-x_j)} \tag{5.123}$$

vanishes to argue that $f_{3,p}$ was analytic if $x_{1,p} \in \{0,1\}$. The difference is that in one case, eq. (5.122), we are considering products of $x_{j,p}$ which are related for different values of j, $x_{j,p} = x_{j,p}(k_{0,p}, x_{1,p}, \ldots, x_{j-1,p})$, and in the other, section

5.4.1, a product of integration variables, which are unrelated to $x_{1,p}$.

Let us then write explicitly the coefficients $A_{1,p}$, $A_{2,p}(x_{1,p})$, $A_{3,p}(x_{1,p}, x_{2,p})$, $B_{1,p}$, $B_{2,p}(x_{1,p})$ and $B_{3,p}(x_{1,p}, x_{2,p})$, which we will need for the maximal cut of the pentagon:

$$\begin{aligned}
A_{1,p} &= 2k_{0,p}\left(q_{10} + q_{11}\beta_p\right) + m_1^2 - k_p^2 - q_1^2, \\
A_{2,p} &= 2k_{0,p}q_{20} - \frac{q_{21}}{2q_{11}}\left(2A_{1,p} - B_{1,p}\right) + \frac{q_{22}}{q_{11}}\sqrt{A_{1,p}\left(B_{1,p} - A_{1,p}\right)} + m_2^2 - k_p^2 - q_2^2, \\
A_{3,p} &= 2k_{0,p}q_{30} - \frac{q_{31}}{2q_{11}}\left(2A_{1,p} - B_{1,p}\right) - \frac{q_{33}}{2q_{22}}\left(2A_{2,p} - B_{2,p}\right) \\
&\quad + \frac{q_{33}}{q_{22}}\sqrt{A_{2,p}\left(B_{2,p} - A_{2,p}\right)} + m_3^2 - k_p^2 - q_3^2,
\end{aligned} \tag{5.124}$$

and

$$\begin{aligned}
B_{1,p} &= 4\beta_p k_{0,p}q_{11}, \quad B_{2,p} = 2\frac{q_{22}}{q_{11}}\sqrt{A_{1,p}\left(B_{1,p} - A_{1,p}\right)}, \\
B_{3,p} &= 2\frac{q_{33}}{q_{22}}\sqrt{A_{2,p}\left(B_{2,p} - A_{2,p}\right)}.
\end{aligned} \tag{5.125}$$

For the case we are interested in and with the parametrisation we chose, $\beta_p = 1$, $k_p^2 = q_1^2 = m_1^2 = 0$, and so $A_{1,p} = B_{1,p} = 4k_0q_{11} = s_{12}$, which means $x_{1,p} = 1$ as expected. The remaining coefficients are

$$\begin{aligned}
A_{2,p} &= -s_{12}r_{23}, \qquad B_{2,p} = 0, \qquad B_{3,p} = \frac{s_{12}\sqrt{\Delta}}{\left(1 + r_{23} - r_{45}\right)}, \\
A_{3,p} &= s_{12}\frac{r_{23} - r_{15} - r_{23}r_{34} + r_{15}r_{45} + r_{34}r_{45} + \sqrt{\Delta}}{2\left(1 + r_{23} - r_{45}\right)},
\end{aligned} \tag{5.126}$$

where

$$\begin{aligned}
\Delta \equiv{}& 2r_{15}\left(r_{23}\left(r_{34} + \left(r_{34} + 1\right)r_{45} - 1\right) - r_{34}\left(r_{45} - 1\right)r_{45}\right) \\
&+ r_{15}^2\left(r_{45} - 1\right)^2 + \left(r_{23}\left(r_{34} - 1\right) - r_{34}r_{45}\right)^2.
\end{aligned} \tag{5.127}$$

We can then use eq. (5.34) with $n = 5$ and $D = 6 - 2\epsilon$,

$$\mathcal{C}_5\left[I_5\right] = -\frac{2^{-2+2\epsilon}e^{\gamma_E\epsilon}}{\Gamma(1-\epsilon)}\left|q_{33}\right|^{2\epsilon}\frac{\left|A_{3,p}(B_{3,p} - A_{3,p})\right|^{-\epsilon}}{\left|q_{00}\right|\left|q_{11}\right|\left|q_{22}\right|\left|q_{33}\right|}. \tag{5.128}$$

After some algebra,

$$|q_{33}| = \frac{1}{2}\sqrt{s_{12}}\frac{\sqrt{\Delta}}{\sqrt{r_{23}(r_{23}-r_{45}+1)}}, \qquad |q_{00}|\,|q_{11}|\,|q_{22}|\,|q_{33}| = \frac{s_{12}^2}{4}\sqrt{\Delta},$$
$$|A_{3,p}(B_{3,p}-A_{3,p})| = s_{12}^2\left|\frac{r_{15}r_{34}r_{45}}{r_{23}-r_{45}+1}\right|. \tag{5.129}$$

Putting all ingredients together, we get the remarkably simple expression

$$\mathcal{C}_5\left[I_5\right] = -\frac{e^{\gamma_E\epsilon}}{\Gamma(1-\epsilon)}s_{12}^{-2-\epsilon}\frac{\left|r_{15}r_{23}r_{34}r_{45}\right|^{-\epsilon}}{\left(\sqrt{\Delta}\right)^{1-2\epsilon}}. \tag{5.130}$$

As expected, we get a non-zero result for this five-propagator cut. As we will see in the next chapter, this is in agreement with the fact that the differential equation for the pentagon has an homogeneous term. Given that we have not actually computed the massless pentagon, there are not many checks we can do on this result. However, its leading order does reproduce the expected result as it is proportional to the inverse of the square-root of the determinant of the Cayley matrix, as we argued in the introduction to this chapter, section 5.1, and has the correct symmetries (the cut should be symmetric under exchange of any of the channels).

5.6 Summary and discussion

In this chapter, we have given a new definition of cut diagrams. The definition we presented in eq. (5.24), the central result of this chapter, is consistent with the cutting rules of chapter 3 when both methods give non-zero results, which is of course something we wanted to preserve. However, in this chapter we addressed the fact that the definition of Cut given in chapter 3 was not general enough to be able to reproduce important features of the analytic structure of Feynman integrals. In particular, we could not compute maximal cuts of a massless box, but we are now able to do so.

It was important to make this generalisation such that it would apply to any one-loop Feynman diagram, with any number of cut propagators, and to any order in ϵ, unlike the brute-force method we described in the introduction to this

chapter, section 5.1.

We gave two formulations of our new cut method, one in Minkowski space and one in Euclidean space. These two formulations are consistent, but the one in Euclidean space is more suitable to compute single-propagator cuts. For any other type of cut, we prefer the formulation in Minkowski space as the expressions are easier to handle and interpret.

Having formal solutions for the m-propagator cut of a diagram with n propagators allowed us to establish some general results about cuts of Feynman diagrams in section 5.4. In particular, we characterised all cuts that can vanish, established a relation between maximal and next-to-maximal cuts for diagrams with an even number of propagators, and we commented on the general functional form of maximal cuts. All these observations will play an important role in the work presented in the next chapter.

Then, in section 5.5 we computed cuts of some non-trivial Feynman diagrams. These results illustrate the formalism for cuts we developed in the previous sections, and the general observations of section 5.4. Some of the cuts we computed are new results, as far as we are aware. We considered the three-mass triangle to show the consistency with the definition of Cut in chapter 3, and then a selection of box integrals we would not have been able to fully analyse with the cutting rules of chapter 3. All the results we obtained here for cuts of boxes will be used in the next chapter. Finally, we checked the maximal cut of the pentagon was not zero in agreement with the discussion of section 5.4.1.

The main motivation for the development of the formalism in this chapter was to find a procedure to compute cut Feynman diagrams that was general enough to capture all the contributions appearing in the right entries of the coproduct of Feynman integrals. In the next chapter, we will see this is indeed achieved by the definition proposed in eq. (5.24).

While we restricted our definition to one-loop diagrams, we are of course interested in generalising the formalism we developed here to Feynman diagrams beyond one loop. We do not foresee any major obstacles in this generalisation, but have not yet explored this issue in detail.

Chapter 6

Diagrammatic representation of the coproduct of one-loop Feynman diagrams

6.1 Introduction

In the previous chapters, we discussed the relation between multiple unitarity cuts and iterated discontinuities, and showed how these were related to coproduct entries. Then we showed how one could give a more general definition of Cut, defined by sequentially evaluating the residues associated to the m cut propagators in the complex plane, which we called $\mathcal{C}_m$. This allowed us to compute cuts that were beyond the reach of the methods developed to compute unitarity cuts.

We believe these results to be important in their own right. However, the reason why we studied this problem in the first place was that this was a step towards a more ambitious goal: to establish a completely diagrammatic representation of the coproduct of Feynman integrals. The idea that such a representation could exist was first introduced to us by Claude Duhr. The initial idea was motivated by the Landau conditions [18], which we now review briefly.

Following [18], we write a general l-loop scalar Feynman diagram with n propagators as

$$F = \int d^D k_1 \ldots \int d^D k_l \frac{1}{A_1 \ldots A_n}, \tag{6.1}$$

where A_i are the propagators,

$$A_i = q_i^2 - m_i^2. \tag{6.2}$$

The propagators can now be combined using Feynman parameters,

$$\frac{1}{A_1 \dots A_n} = (n-1)! \int_0^\infty dx_1 \dots \int_0^\infty dx_n \frac{\delta\left(1 - \sum_{i=1}^n x_i\right)}{\left(\sum_{i=1}^n x_i A_i\right)^n}. \tag{6.3}$$

Discontinuities are of course generated by the poles of the denominator (one can check that in the euclidean region, as defined in section 2.3.2, the denominator is positive definite and thus we are away from any branch cuts). Landau shows that a necessary condition for a singularity to be generated is that either

$$x_i = 0\,, \qquad \text{or} \qquad A_i = 0\,. \tag{6.4}$$

There are thus two types of sources of discontinuities. The first kind, where we set $x_i = 0$, corresponds to a situation where the propagator A_i does not contribute. Diagrammatically, this is equivalent to contracting the propagator A_i, which means we obtain a diagram with less propagators. Hence, this source of discontinuity is associated with simpler diagrams. The other source of discontinuities corresponds to setting $A_i = 0$. This is the condition we are more familiar with, where a propagator is put on-shell. These singularities are intrinsically associated with the diagram we are investigating.

In summary, according to the Landau conditions there are two graphical operations one can perform on a Feynman graph that capture their discontinuity structure: either we cut edges or we contract edges. We thus wanted to understand if by using these two graphical operations we could construct a completely graphical representation of the coproduct of Feynman diagrams.

It quickly became clear to us that studying a general Feynman diagram might be too ambitious, so we decided to focus on one-loop integrals. We first intended to only look at diagrams with no internal masses, building on the work presented in [36], but after studying diagrams with internal masses in [37] we decided to try to address all one-loop scalar diagrams. This turned out to be a wise choice, as including internal masses was fundamental to understanding the general structure of the coproduct of one-loop integrals.

In this chapter, we will then show how to construct a completely graphical representation of the coproduct of Feynman graphs. Following our brief review of the Landau conditions, the ingredients will be Feynman diagrams themselves, and cuts of Feynman diagrams as defined in the previous chapter. It turns out to be possible to construct the graphical coproduct through purely graphical operations on Feynman graphs. Once this is done, one may map the graphs to the functions they evaluate to, and recover the familiar coproduct on polylogarithms introduced in chapter 2, order by order in ϵ .

In fact, we can show that we can construct not only a coproduct but a complete Hopf algebra on Feynman graphs. In this thesis, we will not give the full construction of the Hopf algebra, as it would require introducing several concepts (such as the counit and the antipode) that would go beyond the scope of this thesis. This will be presented in a separate paper [118]. Here, we will simply show how to construct the coproduct of the Hopf algebra of one-loop Feynman graphs.

Because this construction is a rather abstract exercise, we believe it is useful to start by motivating it by looking at an example, so we first investigate bubble diagrams. Having introduced most of the ideas in section 6.2, we hope the abstract formulation of section 6.3 will be more transparent. Then, in section 6.4 we make the connection between the graphical coproduct and the coproduct of MPLs. In this section, we also check that the graphical coproduct correctly reproduces the coproduct of Feynman integrals in a variety of non-trivial examples. Finally, in sections 6.5 and 6.6 we look at the consequences of the diagrammatic coproduct for the study of discontinuities and differential equations of Feynman integrals, which will allow us to make some indirect checks of the validity of our construction. These last two sections illustrate how the graphical coproduct can have practical applications in the calculation of Feynman diagrams.

We should mention that Hopf algebras have been seen to be useful in several aspects of particle physics and quantum field theories [119–123]. While we were researching what we present in this chapter, we were were made aware through private communications that Francis Brown is working on related subjects with encouraging results. Aside from the usual collaborators, we also benefited from discussions with Erik Panzer.

All the work presented here was done during my PhD, in collaboration with Ruth Britto, Claude Duhr, and my supervisor Einan Gardi. As far as we are aware, this is new work that has not been published elsewhere at the time of writing.

6.2 Motivation — Bubble diagrams

The next sections of this chapter will be rather formal. We have thus decided to have an introductory section which motivates the idea of the chapter by looking at three different types of bubble diagrams (with 0, 1 or 2 massive propagators). The presentation in this section follows the way we arrived at the more abstract formulation of the next sections. We believe keeping in mind the reasons why we started exploring this subject is important, particularly if one wants to generalise what we present here beyond one-loop diagrams.

We are looking for a completely diagrammatic representation of the coproduct of these three bubble diagrams. Our main guiding principles for the construction of such representations will be the first-entry condition presented in 2.3.2, the fact that discontinuities act in the first entry of the coproduct, eq. (2.21b), and the fact that the coproduct of a function of weight n has two trivial components of weight $(n,0)$ and $(0,n)$. Using these ideas, we will write a conjecture for a diagrammatic coproduct, which we can then check by explicitly comparing the coproduct of the functions the bubble diagrams evaluate to with what is predicted by their diagrammatic representation.

6.2.1 Diagrammatic coproduct of bubble diagrams

Zero-mass bubble, $I_2(p^2)$: We start with the bubble with no internal masses, $I_2(p_2^2)$, which according to our conventions is given by

$$I_2(p^2) = -2c_\Gamma \frac{(-p^2)^{-1-\epsilon}}{\epsilon}\,, \tag{6.5}$$

for which the ϵ expansion is trivial.

From the discussion of chapters 2 and 3, we already know that

$$\mathcal{C}_2\left[I_2\left(p^2\right)\right] = -\delta_{p^2} I_2(p^2) = 2\frac{e^{\gamma_E \epsilon}\Gamma(1-\epsilon)}{\Gamma(1-2\epsilon)}(p^2)^{-1-\epsilon}, \tag{6.6}$$

where the result for the cut is written in the natural region for this cut, i.e., $p^2 > 0$. By the first entry condition, we know that the weight one cofactors of all coproduct entries of the form $(1, n)$ of the massless bubble are $\log(-p^2)$ (we included a minus sign to have the logarithm well defined in the euclidean region). This means all weight n cofactors are trivially related to $\delta_{p^2} I_2(p^2)$, and we now have a diagrammatic representation of the rightmost cofactor of terms of weight $(1, n)$ in the coproduct of the bubble.

We would also like to have a diagrammatic interpretation of the weight one cofactor. Because of the relation between discontinuities and the coproduct, which we recall states that discontinuities operators only act in the first entry, or more formally

$$\Delta \operatorname{Disc} = (\operatorname{Disc} \otimes \mathrm{id})\Delta\,, \tag{6.7}$$

we expect that the diagrams in the first entry should have the same discontinuity structure as a Feynman diagram. The obvious guess is that it is a Feynman diagram. More specifically, in the very simple case we are looking at, it is easy to guess that this should be the bubble itself: indeed, this is a diagram whose expansion produces powers of logarithms and nothing else, and in particular a $\log(-p^2)$ at order ϵ^0.

Let us then suppose that the coproduct of the zero-mass bubble is given by the zero-mass bubble in the first entry and the cut bubble in the second entry, and that this is true to all orders in ϵ. It is obvious that this naïve choice does not work because both diagrams contribute a factor of $2/p^2$, which is the leading order of the double cut of the bubble. This problem can be solved in three different ways: either we normalise the cut bubble appearing in the right cofactor of the coproduct, or we normalise the uncut bubble appearing in the left cofactor of the coproduct, or we choose to only work with normalised diagrams everywhere. For reasons we will highlight below, the first option is not viable in general. The other two options are. Normalising the diagram appearing in the left cofactor of the coproduct would be the ideal solution as the diagrammatic coproduct would then encode the maximum information about the function. However, for practical purposes we choose to normalise all diagrams, cut or uncut: this will allow us to have a simpler mapping between diagrams and the functions they represent. To be completely precise, all diagrams are normalised to the leading order of their maximal cut (to their leading singularity). Note that this is a minor detail, as

one can always reinstate the correct normalisation at the end of all manipulations done with the coproduct.

Let us then write

$\Delta\left($  $\right) =$  $\otimes$ 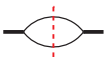 , (6.8)

where

 $= \dfrac{I_2(p^2)}{\mathrm{LS}\left[I_2\left(p^2\right)\right]},$ (6.9)

and

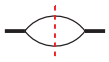 $= \dfrac{\mathcal{C}_2\left[I_2\left(p^2\right)\right]}{\mathrm{LS}\left[I_2\left(p^2\right)\right]} = \dfrac{e^{\gamma_E \epsilon}\Gamma(1-\epsilon)}{\Gamma(1-2\epsilon)}(p^2)^{-\epsilon},$ (6.10)

where

$$\mathrm{LS}\left[I_2\left(p^2\right)\right] = \frac{2}{p^2} \tag{6.11}$$

is the order ϵ^0 term in the ϵ-expansion of $\mathcal{C}_2\left[I_2\left(p^2\right)\right]$, i.e, the leading singularity of the zero-mass bubble as defined in eq. (5.35). This is a rational function, given that $\mathcal{C}_2\left[I_2\left(p^2\right)\right]$ is a weight 0 function.

Note that strictly speaking the operator Δ in eq. (6.8) is not the same as the coproduct of polylogarithms introduced in section 2 because it is acting on a diagram rather than on a function. However, in this section we will use the same symbol in the same way that we associate the diagrams on the right to the functions they evaluate to. In the next two sections we will make this distinction more precise.

We can show that eq. (6.8) is correct by evaluating both sides order by order in the dimensional regularisation parameter. Let's see this explicitly for the first orders:

- $\mathcal{O}(\epsilon^{-1})$: the coefficient of this order in the Laurent expansion is of weight 0, and so its coproduct should have only one term, $1 \otimes 1$ given our choice of normalising all diagrams. From eq. (6.8),

$\Delta\left($  $\right) =$ $\otimes$  $+$  $\otimes$ 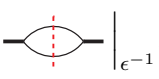 . (6.12)

We have

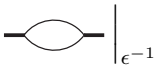 $= 1,$ (6.13)

and

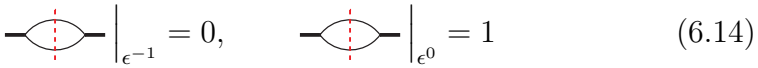

$$= 0, \qquad = 1 \tag{6.14}$$

so eq. (6.12) is

$$(1 \otimes 1) = (1 \otimes 1)\,. \tag{6.15}$$

- $\mathcal{O}(\epsilon^0)$: the coefficient of this order in the Laurent expansion is of weight 1, and so its coproduct should have only two terms, of weight $(1,0)$ and $(0,1)$. From eq. (6.8),

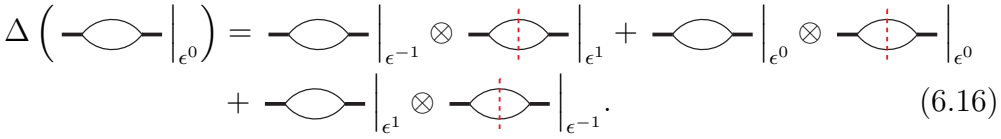

$$\Delta\left(\quad\right) = \quad \otimes \quad + \quad \otimes \quad + \quad \otimes \quad . \tag{6.16}$$

The last term vanishes because of eq. (6.14). For the other two, we need

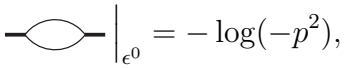

$$= -\log(-p^2), \tag{6.17}$$

and

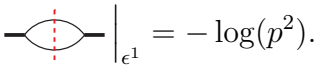

$$= -\log(p^2). \tag{6.18}$$

Then, eq. (6.16) becomes

$$-\left(1 \otimes \log(p^2) + \log(-p^2) \otimes 1\right) = -\left(1 \otimes \log(p^2) + \log(-p^2) \otimes 1\right) \tag{6.19}$$

where on the left-hand side we used the fact that the second entries of the coproduct are defined modulo π.

- $\mathcal{O}(\epsilon)$: the coefficient of this order in the Laurent expansion is of weight 2, and so its coproduct should have three terms, of weight $(2,0)$, $(1,1)$ and $(0,2)$. From eq. (6.8),

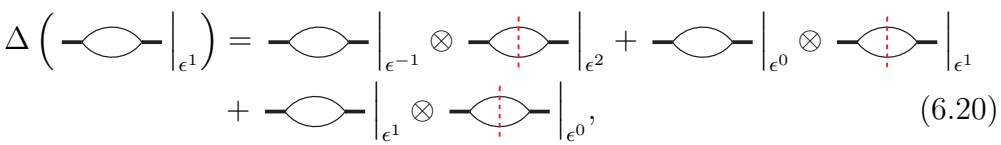

$$\Delta\left(\quad\right) = \quad \otimes \quad + \quad \otimes \quad + \quad \otimes \quad , \tag{6.20}$$

where we only wrote terms not vanishing because of eq. (6.14). We need

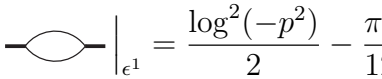

$$= \frac{\log^2(-p^2)}{2} - \frac{\pi^2}{12}, \tag{6.21}$$

and

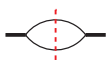

$$= \frac{1}{2}\left(\log^2(p^2) - \frac{\pi^2}{2}\right). \tag{6.22}$$

The left-hand side of eq. (6.20) is

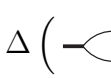

$$= \frac{1}{2}\Bigg(1 \otimes \log^2(p^2) + 2\log(-p^2) \otimes \log(p^2) + \left(\log^2(-p^2) - \frac{\pi^2}{6}\right) \otimes 1\Bigg). \tag{6.23}$$

For the right-hand side,

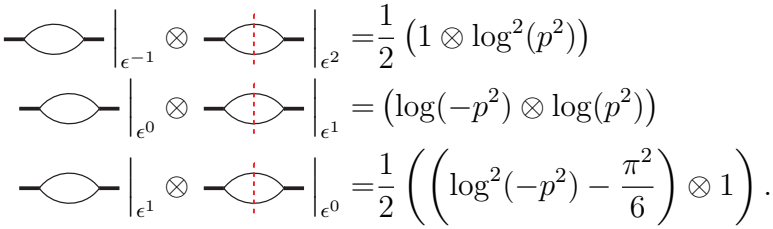

$$= \frac{1}{2}\left(1 \otimes \log^2(p^2)\right)$$

$$= \left(\log(-p^2) \otimes \log(p^2)\right)$$

$$= \frac{1}{2}\left(\left(\log^2(-p^2) - \frac{\pi^2}{6}\right) \otimes 1\right). \tag{6.24}$$

In both cases we used the fact that the second entries of the coproduct are defined modulo π. Comparing the two sides, we see that eq. (6.20) is indeed correct.

Higher orders in ϵ of eq. (6.16) can be checked in exactly the same way, and we have verified its validity up to order ϵ^4.

To finish with this example, we comment on a feature which will reappear in the general formulation of the diagrammatic representation of the coproduct regarding the trivial coproduct entries (of the form $F \otimes 1$ and $1 \otimes F$, of respective weights $(n, 0)$ and $(0, n)$ for a function F of weight n). Given the diagrammatic representation in eq. (6.8) and the ϵ expansion of eq. (6.10), it is clear that the trivial coproduct entry of weight $(n, 0)$, at order ϵ^{n-1}, will be given by the term

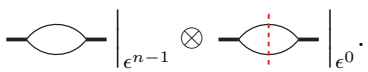

(6.25)

It is however less clear how the other trivial coproduct entry of weight $(0, n)$ is reproduced, as the diagram itself does not appear in the second entry. Looking at the explicit check of the conjecture above, we see it is generated by the terms of the form

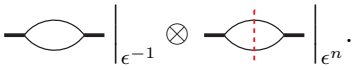

(6.26)

Indeed, one can easily check this kind of term is the only one generating a contribution of the required weight. Another way to write this observation, is

$$I_2^{(n)}(p^2) = \mathcal{C}_2^{(n+1)}\left[I_2(p^2)\right] \mod i\pi \tag{6.27}$$

While this might seem a rather trivial observation for this simple example, we will see that its generalisation to more complicated cases will lead to a very interesting result.

One-mass bubble, $I_2(p^2;m^2)$: According to our conventions, the bubble with one massive propagator is given by

$$I_2(p^2;m^2) = -\frac{e^{\gamma_E\epsilon}\Gamma(1+\epsilon)}{\epsilon}\left(m^2-p^2\right)^{-1-\epsilon}\,{}_2F_1\left(-\epsilon,1+\epsilon;1-\epsilon;\frac{p^2}{p^2-m^2}\right). \tag{6.28}$$

It has two different non-vanishing cuts. A one-propagator cut,

$$\mathcal{C}_1\left[I_2(p^2;m^2)\right] = -\frac{e^{\gamma_E\epsilon}}{\Gamma(1-\epsilon)}\frac{(-m^2)^{-\epsilon}}{p^2}\,{}_2F_1\left(1,1+\epsilon;1-\epsilon;\frac{m^2}{p^2}\right), \tag{6.29}$$

and a two-propagator cut,

$$\mathcal{C}_2\left[I_2(p^2;m^2)\right] = 2\frac{e^{\gamma_E\epsilon}\Gamma(1-\epsilon)}{\Gamma(1-2\epsilon)}\left(p^2\right)^{\epsilon}\left(p^2-m^2\right)^{-2\epsilon-1}, \tag{6.30}$$

where the results for the cuts are written in their natural regions: $p^2 < m^2 < 0$ for the single propagator cut, and $0 < m^2 < p^2$ for the two-propagator cut.

We can now play the same game as for the massless bubble. Following the discussion of chapters 2 and 3, we know that

$$\begin{aligned}\mathcal{C}_1\left[I_2(p^2;m^2)\right] &= -\delta_{m^2}I_2(p^2;m^2)\\ \mathcal{C}_2\left[I_2(p^2;m^2)\right] &= -\delta_{m^2-p^2}I_2(p^2;m^2),\end{aligned} \tag{6.31}$$

which means we have a diagrammatic interpretation for the cofactors of weight n of all terms of the form $(1,n)$ in the coproduct of the one-mass bubble. The weight one cofactors are $\log(m^2)$ or $\log(m^2-p^2)$. $\log(m^2)$ is most naturally generated by the expansion of a tadpole of mass m^2. $\log(m^2-p^2)$ is generated by a one-mass bubble, but as we know—see section 2.3.2— this diagram also generates $\log(m^2)$

as a first entry. It is thus not as obvious which diagram to choose to reproduce the first-entries $\log(m^2 - p^2)$.

However, using the expression for the tadpole,

$$I_1(m^2) = -\frac{e^{\gamma_E \epsilon}\Gamma(1+\epsilon)}{\epsilon}(m^2)^{-\epsilon}, \tag{6.32}$$

one can easily check that the combination

$$\frac{I_1(m^2)}{\mathrm{LS}\left[I_1\left(m^2\right)\right]} + \frac{1}{2}\left(\frac{I_2(p^2;m^2)}{\mathrm{LS}\left[I_2(p^2;m^2)\right]}\right) \tag{6.33}$$

has only $\log(m^2 - p^2)$ as first entry in the coproduct, which is what we want to appear with $\mathcal{C}_2\left[I_2(p^2;m^2)\right]$ in the second entry.

Let us come back to the comment on the normalisation of diagrams we made above eq. (6.8). We now see why it would not have been consistent to normalise the cut diagrams appearing in the right cofactor and not normalise the uncut diagrams appearing in the left cofactor. In general, while we can have different types of diagrams in the first entry, each with their own leading singularity, in the second entry we always take cuts of the same diagram, the one whose coproduct we are studying. Had we not normalised the diagrams appearing in the leftmost cofactor, we would have generated different combinations of rational factors. Clearly, our choice of normalising all diagrams avoids this issue.

As for the zero-mass bubble, we define

$$= \frac{I_1(m^2)}{\mathrm{LS}\left[I_1\left(m^2\right)\right]} = -I_1(m^2), \tag{6.34a}$$

$$= \frac{I_2(p^2;m^2)}{\mathrm{LS}\left[I_2\left(p^2;m^2\right)\right]}, \tag{6.34b}$$

$$= \frac{\mathcal{C}_1\left[I_2\left(p^2;m^2\right)\right]}{\mathrm{LS}\left[I_2\left(p^2;m^2\right)\right]}, \tag{6.34c}$$

$$= \frac{\mathcal{C}_2\left[I_2\left(p^2;m^2\right)\right]}{\mathrm{LS}\left[I_2\left(p^2;m^2\right)\right]}, \tag{6.34d}$$

where we recall

$$\mathcal{C}_1\left[I_1\left(m^2\right)\right] = -\frac{e^{\gamma_E \epsilon}}{\Gamma(1-\epsilon)}(-m^2)^{-\epsilon}, \tag{6.35}$$

in the natural region of this cut, and

$$\mathrm{LS}\left[I_2\left(p^2;m^2\right)\right] = \frac{2}{p^2-m^2}. \tag{6.36}$$

We can now make a guess for what the diagrammatic representation of the coproduct of the bubble with one internal mass should be:

Δ  $=$ $\otimes$  $+$  $\otimes$  . (6.37)

As for the zero-mass bubble, we can check the validity of this expression order by order in ϵ. Using eqs. (6.28), (6.29) and (6.30), see also the `MATHEMATICA` package in [38], we have done so up to weight 4 (order ϵ^3), and thus believe it to be valid to all orders in ϵ.

Instead of the details in the checks, we will show eq. (6.37) is consistent through some observations. First, since we claim eq. (6.37) to be valid to all orders in ϵ, it should reproduce eq. (6.8) for $m^2 \to 0$. This is trivial to check: tadpoles and single propagator cut vanish in this limit, and so we recover eq. (6.8).

Second, as for the massless bubble, the trivial term of the coproduct of weight $(n,0)$ is reproduced by

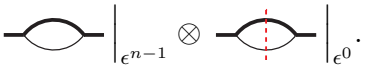 (6.38)

This implies that the tadpole contributions at this weight must vanish, i.e.,

 (6.39)

which can only happen if,

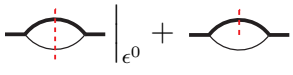 (6.40)

This is exactly the relations we found between maximal and next-to-maximal cuts of diagrams with an even number of propagators in section 5.4.2.

Finally, the other trivial component of the coproduct, of weight $(0,n)$, is now

generated by the poles of tadpoles and bubbles. Indeed, noticing that

$$\left(\quad + \frac{1}{2} \right) \Big|_{\epsilon^{-1}} = \Big|_{\epsilon^{-1}} = 1, \tag{6.41}$$

one can then check that

$$I_2^{(n)}(p^2;m^2) = \mathcal{C}_1^{(n+1)}\left[I_2^{(n)}(p^2;m^2)\right] + \mathcal{C}_2^{(n+1)}\left[I_2^{(n)}(p^2;m^2)\right] \mod i\pi. \tag{6.42}$$

Notice that we used the fact that because only the one-mass bubble appears in this relation, we are free to not normalise any of the terms to the leading singularity of this integral.

Two-mass bubble, $I_2(p^2;m_1^2,m_2^2)$: According to our conventions, the bubble with two massive propagator is given by

$$\begin{aligned} &I_2(p^2;m_1^2,m_2^2) = \\ &= -\frac{e^{\gamma_E\epsilon}\Gamma(1+\epsilon)}{\epsilon}\frac{(-p^2)^{-1-\epsilon}}{(w_1-\bar{w}_1)^{1+\epsilon}}\left[w_1^{-\epsilon}\,{}_2F_1\left(-\epsilon,1+\epsilon;1-\epsilon;\frac{w_1}{w_1-\bar{w}_1}\right)\right. \\ &\left.-(w_1-1)^{-\epsilon}\,{}_2F_1\left(-\epsilon,1+\epsilon;1-\epsilon;\frac{w_1-1}{w_1-\bar{w}_1}\right)\right] \end{aligned} \tag{6.43}$$

This diagram has three different non-vanishing cuts. A single propagator cut on the mass m_1^2,

$$\mathcal{C}_{1,[1]}\left[I_2(p^2;m_1^2,m_2^2)\right] = \frac{e^{\gamma_E\epsilon}}{\Gamma(1-\epsilon)}\frac{(-p_1^2)^{-1-\epsilon}}{w_1(w_1\bar{w}_1)^{\epsilon}}\,{}_2F_1\left(1,1+\epsilon;1-\epsilon;\frac{\bar{w}_1}{w_1}\right), \tag{6.44}$$

a single propagator cut on the mass m_2^2,

$$\begin{aligned} &\mathcal{C}_{1,[2]}\left[I_2(p^2;m_1^2,m_2^2)\right] = \\ &=\frac{e^{\gamma_E\epsilon}}{\Gamma(1-\epsilon)}\frac{(-p_1^2)^{-1-\epsilon}(1-w_1)^{-\epsilon}}{(w_1-\bar{w}_1)^{1+\epsilon}}\,{}_2F_1\left(-\epsilon,1+\epsilon;1-\epsilon;\frac{w_1-1}{w_1-\bar{w}_1}\right), \end{aligned} \tag{6.45}$$

and a two propagator cut,

$$\mathcal{C}_2\left[I_2(p^2;m_1^2,m_2^2)\right] = 2\frac{e^{\gamma_E\epsilon}\Gamma(1-\epsilon)}{\Gamma(1-2\epsilon)}(p^2)^{-1-\epsilon}(w_1-\bar{w}_1)^{-1-2\epsilon}. \tag{6.46}$$

All results are written in the natural region for the corresponding discontinuity, and we use an obvious notation to distinguish the two single propagator cuts. The leading singularity we normalise the diagrams by is

$$\mathrm{LS}\left[I_2(p^2; m_1^2, m_2^2)\right] = \frac{2}{p^2(w_1 - \bar{w}_1)}. \tag{6.47}$$

Given the diagrammatic representations of the coproduct of the zero and one-mass bubbles in eqs. (6.8) and (6.37), we can make an educated guess for what the diagrammatic coproduct of the two-mass bubble should be. The simplest guess we can make that is consistent in the limit of vanishing propagator masses and that preserves the symmetry under the exchange of the two masses is:

Δ 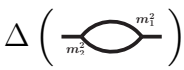 = 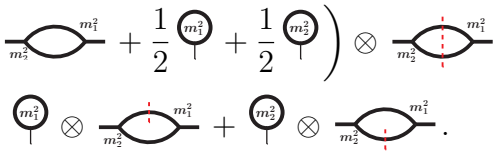

 . (6.48)

We recall all diagrams are normalised to their leading singularity.

As for the other two examples above, we can then check the validity of this relation order by order in ϵ, and we have done so up to weight 4 (i.e., order ϵ^3). We should stress the two-mass bubble is already not a trivial function, as can be seen by expanding eq. (6.43), and so it is highly non-trivial that a relation like eq. (6.48) would hold true to order ϵ^3 by accident.

As for the one-mass bubble, we can make some consistency checks on eq. (6.48). We already commented that it agrees with eqs. (6.8) and (6.37) in the appropriate massless limit, so we now look at the trivial coproduct components. Correctly reproducing the component $(n, 0)$ requires

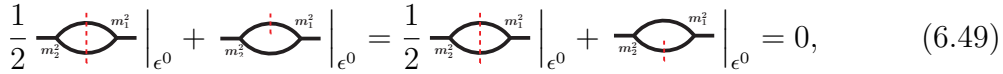 (6.49)

which is the equivalent for the two-mass bubble of the constraint we derived in eq. (6.39) for the one-mass bubble. This is the relation we found in section 5.4.2: for diagrams with an even number of propagators, at leading order in ϵ, all non-vanishing next-to-maximal cuts are equal to minus one-half of the maximal cut. The $(0, n)$ component is reproduced by the poles of the diagrams appearing in the first entry. However, unlike what happened in the previous two examples,

because the two-mass bubble is finite only the poles of tadpoles contribute. The relation between cut and uncut diagrams equivalent to eq. (6.42) is now

$$I_2^{(n)}(p^2;m_1^2,m_2^2) = \mathcal{C}_{1,[1]}^{(n+1)}\left[I_2^{(n)}(p^2;m_1^2,m_2^2)\right] + \mathcal{C}_{1,[2]}^{(n+1)}\left[I_2^{(n)}(p^2;m_1^2,m_2^2)\right] + \mathcal{C}_2^{(n+1)}\left[I_2^{(n)}(p^2;m_1^2,m_2^2)\right] \mod i\pi. \tag{6.50}$$

Because the two-mass bubble is finite, we can also check that the singularities introduced by the tadpoles in eq. (6.48) cancel. This requires

$$\mathcal{C}_{1,[1]}^{(0)}\left[I_2^{(n)}(p^2;m_1^2,m_2^2)\right] + \mathcal{C}_{1,[2]}^{(0)}\left[I_2^{(n)}(p^2;m_1^2,m_2^2)\right] + \mathcal{C}_2^{(0)}\left[I_2^{(n)}(p^2;m_1^2,m_2^2)\right] = 0,$$

which is indeed true, and can be seen as the $n = -1$ case of the previous relation.

6.2.2 Towards a general formulation

It turns out that the different mass configurations of the bubble topology already teach us a great deal about the diagrammatic representation of the coproduct of one-loop diagrams. We now summarise the main points we established by looking at this example.

First, in the construction of the diagrammatic coproduct itself, we see there is a relation between the propagators that are cut and the ones appearing in the corresponding first entry. For one-propagator cuts, the corresponding first entry is the diagram obtained by contracting the uncut propagator. However, there is an unequal treatment of cuts with an even or an odd number of cut propagators. Indeed, following what happens for single cuts, one might be tempted to say that the first entry corresponding to a two propagator cut should be the bubble itself, and not the combination of bubbles and tadpoles we see in eqs. (6.37) and (6.48). One way to see this naïve generalisation cannot be correct is to look at the trivial coproduct entry of weight $(n, 0)$. As is clear from the examples of the one- and two-mass bubble, the tadpole must appear in the first entry corresponding to the two-propagator cut for it to be correctly reproduced, see the discussion above eq. (6.39). This implies the constraint in eq. (6.40) for the one-mass bubble and the equivalent for the two-mass bubble, eq. (6.49). One way to make sense of this combination is to say that the first entry of a cut with an even number of propagators is obtained by contracting the uncut propagators and adding all

diagrams with an extra contraction multiplied by 1/2. While it is just a guess at this stage, we will confirm this is indeed the correct interpretation when looking at box diagrams.

Second, one might wonder about the origin of the factor of 1/2, and whether in the generalisation to more complicated diagrams one should allow this coefficient to take other values. When looking at the bubbles, we highlighted the connection between this factor and the relations between next-to-maximal and maximal cuts of diagrams with an even number of propagators we established in section 5.4.2. There, we showed this relation holds for diagrams with any even number of propagators, and we thus see that there is no reason to expect any other coefficient when considering more complicated topologies. We note this is also connected to the previous point: for any other value of this parameter, the trivial coproduct entry of weight $(n, 0)$ would not be correctly reproduced.

Finally, in all our examples we commented on a relation between cut and uncut diagrams which allowed us to correctly reproduce the other trivial coproduct component of weight $(0, n)$. According to eqs. (6.27), (6.42) and (6.50), the uncut diagram at a given order in ϵ is given by the sum of all one- and two-propagator cuts at the next order in ϵ. This observation has to remain valid for more complicated topologies for a diagrammatic representation of the coproduct to exist, because the uncut diagram itself will never appear in the second entry (we know the second entries correspond to discontinuity functions, i.e., to cuts)[1]. Furthermore, if an uncut diagram is finite, we also need a relation between the leading orders of cuts to cancel the singularities introduced by the divergent tadpoles and/or bubbles in the first entry.

All these observations show that Feynman diagrams and their cuts have to satisfy many constraints for a diagrammatic representation of their coproduct to exist, and it is thus highly non-trivial that such a representation would exist. In the next sections we conjecture that it does exist for any one-loop diagram, and give substantial evidence supporting our claim.

[1]We note this relation is consistent in terms of weight. Let's assume the uncut diagram has weight n. Then in the perspective of chapters 2 and 3, one and two-propagator cuts correspond to single discontinuities and are thus functions of weight $n-1$ (we normalise by the factor of π generated by taking the discontinuity). The coefficient of order j in the Laurent expansion in ϵ of the uncut function will have weight $j+n$, and so will the coefficient of order $j+1$ in the Laurent expansion of the cuts

6.2.3 Coassociativity of the diagrammatic coproduct

Strictly speaking, in the examples above we only showed that the tensor obtained by the action of the coproduct operator on the functions Feynman diagrams evaluate to can be given a diagrammatic interpretation. More precisely, we have not shown that the action of Δ on a diagram, as in eq. (6.48), has the same properties as a coproduct. Indeed, as we already mentioned, there is an abuse of notation in using the same symbol Δ to describe the coproduct that acts on polylogarithms and the coproduct that acts on diagrams. We will eventually see this is justified when we map them to each other.

We now show how one can see that the diagrammatic coproduct is coassociative, which we means that

$$(\mathrm{id} \otimes \Delta)\,\Delta = (\Delta \otimes \mathrm{id})\,\Delta\,, \tag{6.51}$$

i.e., acting with the coproduct operator in the first or second entry of the coproduct entry gives the same result. We recall this is crucial for iterations of the coproduct to be well defined (as for instance its maximal iteration, the symbol). We will only show it for the two-mass bubble, because we know that the other mass configurations can be obtained by taking the appropriate massless limit.

$(\Delta \otimes \mathrm{id})\,\Delta$: We start by acting with Δ in the first entries of eq. (6.48), which means Δ is acting on uncut diagrams, either tadpoles or bubbles. We know how Δ acts on a bubble, and the way it acts on the tadpole is by now easy to guess:

Δ  =  $\otimes$  . (6.52)

We then have

$(\Delta \otimes \mathrm{id})\,\Delta$ 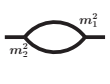 = 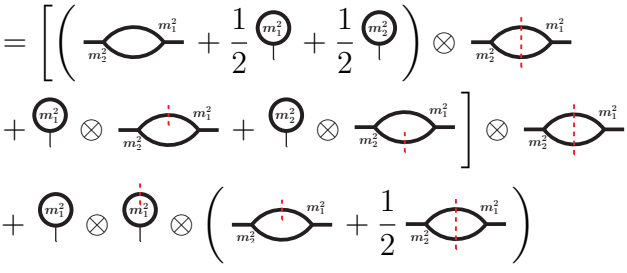

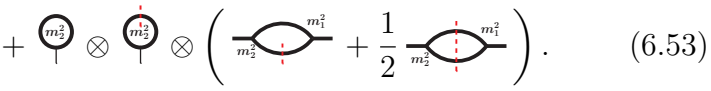

(6.53)

(id ⊗ Δ) Δ: We now want to act with Δ on the second entry of eq. (6.48), for which we must know how the coproduct acts on cut diagrams. We follow the same reasoning as for the uncut diagram. For the second entries, we list all further cuts of the cut diagram we are considering. The corresponding first entry is then obtained by pinching all uncut propagators, and adding one-half times the diagrams with an extra propagator contracted in case of an even number of cuts in the second entry. The propagators that were cut in the cut diagram under consideration remain cut in the first entry[2]. We now give some examples. For the cut in the mass m_1^2,

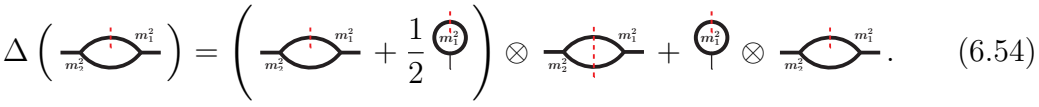

(6.54)

For the cut in the mass m_2^2, the equivalent expression holds. For the cut in the external channel, which is a maximal cut,

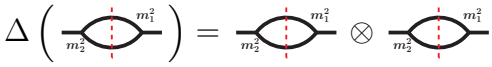

(6.55)

Comparing these expressions with eq. (6.48), we see that there is a quicker way to get the diagrammatic representation of the coproduct of cut diagrams once the diagrammatic representation of the uncut diagram has been determined: all terms that do not have the propagators that will be cut in the first entry are discarded, and in the terms that have them they are cut.

Let us briefly go back on the issue of normalisation discussed above eq. (6.8). We now see why we chose to normalise all diagrams to the first order in the ϵ expansion of the maximal cut. Had we not done this and chosen the other alternative of keeping the normalisation in diagrams appearing on the rightmost entry of the coproduct, we would have had to introduce a different notation distinguishing cut diagrams appearing on the rightmost coproduct entry or any other entry. To make the connection between diagrams and functions more direct,

[2]Discontinuity operators only act on the first entry of the coproduct, so the first entries of the diagrammatic coproduct of a cut diagram must have the same discontinuity structure as the cut diagram. We thus claim the first entries of the diagrammatic coproduct of a cut diagram will be a diagram with the same cut propagators.

we chose to normalise all diagrams.

Before we check that with this procedure of obtaining the diagrammatic coproduct of cut diagrams we find the same result as in eq. (6.53), we make a comment on maximal cuts. From eq. (6.55), we see the coproduct of the maximal cut is trivial: the same diagram appears in the first and the second entry. According to our rules this will be the case for any maximal cut, and objects having this type of coproduct are called group-like. It is easy to see that a function of the form x^ϵ is group-like, as implied by eq. (2.12). The diagrammatic coproduct of a maximal cut is thus in accordance with the discussion in section 5.4.3, where we argued maximal cuts had precisely this functional form.

We now evaluate the action of $(\mathrm{id}\otimes\Delta)\Delta$ on the two-mass bubble to compare it with eq. (6.53). According to eq. (6.54) and eq. (6.55), we have

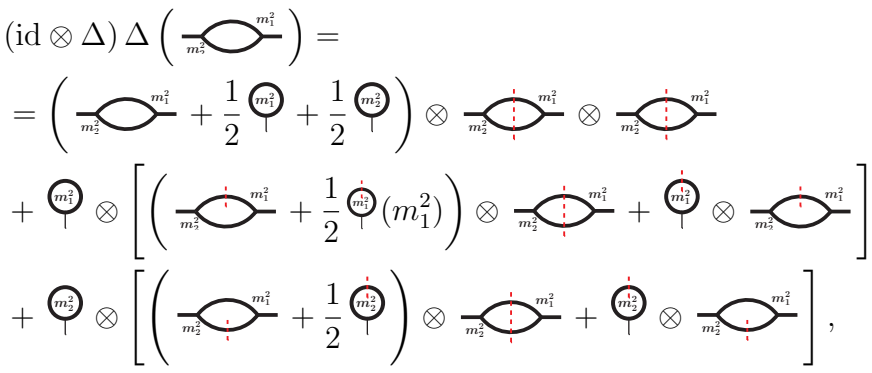

(6.56)

which matches eq. (6.53).

We have thus shown that

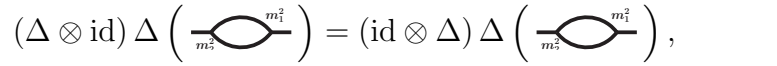

(6.57)

which means the graphical coproduct of the two-mass bubble diagram is coassociative. By taking the appropriate massless limits, we can easily check this is true for the bubbles with zero or one internal masses as well.

6.3 Graphical coproduct of one-loop Feynman graphs

We now discuss the diagrammatic coproduct in a more abstract and general way. In this section, all diagrams should be thought of just as graphs. Our goal will be to show that one can define a coproduct on the space of one-loop Feynman graphs. One can in fact go further and show that one can define a Hopf algebra on the space of one-loop Feynman graphs. However, this requires introducing several new structures that we would not use in the following sections, so in this thesis we simply show how a coproduct can be defined. The more complete construction will be presented in a separate paper [118]. In the next section, the graphical coproduct constructed here will be mapped to the coproduct of polylogarithms we are used to.

6.3.1 General formulation

Definition of Feynman graph: A Feynman graph G is defined by the following properties:

- A set of vertices V_G ;
- A set of edges E_G, each incident on exactly two vertices (the two vertices can coincide, and multiple edges can be incident on the same pair of vertices). These are called internal edges ;
- A set of half-edges E_G^{ext}, each incident on exactly one vertex. These are called external legs ;
- To each internal edge $e \in E_G$, we associate a real number m_e^2 which we call the mass squared ;
- To each external leg $e \in E_G^{\text{ext}}$, we associate a D-dimensional vector p_e which we call momentum, subject to momentum conservation,

$$\sum_{e \in E_G^{\text{ext}}} p_e = 0. \tag{6.58}$$

Feynman graphs are Poincaré invariant: if two Feynman graphs differ only by the assignment of the external momenta, or if these are related by a Lorentz transformation, the two graphs are equivalent. Furthermore, if two external legs e_1 and e_2 of momentum p_1 and p_2 respectively are incident in the same vertex, they can be replaced by a single external leg incident on the same vertex but with momentum $p_1 + p_2$.

Contraction of internal edges: An obvious operation one can define on a Feynman graph is the contraction of a subset of its internal edges. If $S \subseteq E_G$, G/S is the Feynman graph obtained by contracting all edges in S. For instance,

$$G/\varnothing = G \qquad \text{and} \qquad G/E_G = 0, \tag{6.59}$$

where 0 denotes the empty graph and $\varnothing$ and empty set. For future use, we define G_S as the Feynman graph where all edges except those in S have been contracted, $G_S = G/\bar{S}$. For instance,

$$G_{E_G} = G \qquad \text{and} \qquad G_{\varnothing} = 0. \tag{6.60}$$

Cut Feynman graph: A *cut Feynman graph* is a pair (G, C), where G is a Feynman graph, and C is a subset of the internal edges of G, i.e. $C \subseteq E_G$. An edge in C is called a cut edge. (G, E_G) is called a maximal cut (all internal edges are cut) and $(G, \varnothing) = G$ is called an uncut graph[3]. The contraction operation is extended to cut Feynman graphs:

$$\text{If } S \subseteq E_G\,, \qquad (G, C)/S = \begin{cases} (G/S, C) & \text{if } C \cap S = \varnothing \\ 0 & \text{otherwise} \end{cases}\,. \tag{6.61}$$

So far the discussion was valid for any Feynman graph. From now on we focus on one-loop graphs.

[3]In this notation, the next-to-maximal cuts we mentioned previously are $(G, E_G/e)$ for $e \in E_G$. There are $|E_G|$ different next-to-maximal cuts, where $|E_G|$ denotes the cardinality of E_G.

Definition of Δ: Let $\mathcal{P}$ denote the (free) $\mathbb{Q}$-algebra generated by one-loop cut Feynman graphs. We define an algebra morphism $\Delta : \mathcal{P} \to \mathcal{P} \otimes \mathcal{P}$ acting on cut graphs as

$$\Delta(G, C) = \sum_{\substack{C \subseteq I \subseteq E_G \\ I \neq \varnothing}} \left((G_I, C) + a_I \sum_{e \in I/C} (G_{I/e}, C) \right) \otimes (G, I), \tag{6.62}$$

where

$$a_I = \begin{cases} \frac{1}{2} & \text{if } |I| \text{ even} \\ 0 & \text{otherwise} \end{cases} . \tag{6.63}$$

$|I|$ denotes the cardinality of the set I.

Maximal cuts: It is easy to show that according to this definition of Δ maximally cut Feynman graphs are group-like. For this, we note that

$$E_G \subseteq I \subseteq E_G \Rightarrow I = E_G \qquad \text{and} \qquad E_G / E_G = \varnothing, \tag{6.64}$$

so that there is only one term surviving in eq. (6.62), which has $I = E_G$. As already noted above, $G_{E_G} = G$, and we thus have

$$\Delta(G, E_G) = (G, E_G) \otimes (G, E_G) \tag{6.65}$$

as expected.

Coassociativity of Δ: For the algebra morphism defined in eq. (6.62) to be a coproduct it must be coassociative. We now show that with the definition of Δ given above, $(\mathrm{id} \otimes \Delta)\,\Delta = (\Delta \otimes \mathrm{id})\,\Delta$. This proof was first proposed to us by Erik Panzer in a private communication.

We start with $(\mathrm{id} \otimes \Delta)\,\Delta$. Acting with Δ on the cofactor (G, I) in eq. (6.62):

$$\begin{aligned} (\mathrm{id} \otimes \Delta)\,\Delta(G, C) = \sum_{\substack{C \subseteq I \subseteq E_G \\ I \neq \varnothing}} \sum_{\substack{I \subseteq J \subseteq E_G \\ J \neq \varnothing}} & \left((G_I, C) + a_I \sum_{e \in I/C} (G_{I/e}, C) \right) \\ & \otimes \left((G_J, I) + a_J \sum_{f \in J/I} (G_{J/f}, I) \right) \otimes (G, J). \end{aligned} \tag{6.66}$$

For later use, it is convenient to make the substitution $I \leftrightarrow J$ in the above expression, which is just a renaming of the sets we sum over. We also note that

$$\sum_{\substack{C\subseteq I\subseteq E_G \\ I\neq\varnothing}} \sum_{\substack{I\subseteq J\subseteq E_G \\ J\neq\varnothing}} \longrightarrow \sum_{\substack{C\subseteq J\subseteq E_G \\ J\neq\varnothing}} \sum_{\substack{J\subseteq I\subseteq E_G \\ I\neq\varnothing}} = \sum_{\substack{C\subseteq I\subseteq E_G \\ I\neq\varnothing}} \sum_{\substack{C\subseteq J\subseteq I \\ J\neq\varnothing}}$$

and we finally get

$$\begin{aligned}(\mathrm{id}\otimes\Delta)\,\Delta(G,C) = \sum_{\substack{C\subseteq I\subseteq E_G \\ I\neq\varnothing}} \sum_{\substack{C\subseteq J\subseteq I \\ J\neq\varnothing}} \left((G_J,C) + a_J \sum_{e\in J/C} (G_{J/e},C)\right) \\ \otimes \left((G_I,J) + a_I \sum_{f\in I/J} (G_{I/f},J)\right) \otimes (G,I). \end{aligned} \tag{6.67}$$

To compute $(\Delta\otimes\mathrm{id})\,\Delta$, we will need the following expressions, easily obtained from eq. (6.62),

$$\begin{aligned}\Delta(G_I,C) &= \sum_{\substack{C\subseteq J\subseteq I \\ J\neq\varnothing}} \left((G_J,C) + a_J \sum_{e\in J/e} (G_{J/e},C)\right) \otimes (G_I,J) \\ \Delta(G_{I/f},C) &= \sum_{\substack{C\subseteq J\subseteq I/f \\ J\neq\varnothing}} \left((G_J,C) + a_J \sum_{e\in J/e} (G_{J/e},C)\right) \otimes (G_{I/f},J).\end{aligned}$$

We then have (in eq. (6.62), the name of the edges in I/C summed over is now f instead of e):

$$\begin{aligned}&(\Delta\otimes\mathrm{id})\,\Delta(G,C) = \\ &= \sum_{\substack{C\subseteq I\subseteq E_G \\ I\neq\varnothing}} \sum_{\substack{C\subseteq J\subseteq I \\ J\neq\varnothing}} \left((G_J,C) + a_J \sum_{e\in J/C} (G_{J/e},C)\right) \otimes (G_I,J)\otimes(G,I) \\ &+ \sum_{\substack{C\subseteq I\subseteq E_G \\ I\neq\varnothing}} \sum_{\substack{C\subseteq J\subseteq I/f \\ J\neq\varnothing}} \sum_{f\in I/C} a_I \left((G_J,C) + a_J \sum_{e\in J/C} (G_{J/e},C)\right) \otimes (G_{I/f},J)\otimes(G,I).\end{aligned} \tag{6.68}$$

It is clear the first term on the right-side of the above equation matches the

contribution of the (G_I, J) term appearing in the middle cofactor of eq. (6.67). For the remaining contribution, we can notice the following equivalence of conditions

$$(f \in I/C \quad \wedge \quad C \subseteq J \subseteq I/f) \quad \Leftrightarrow \quad (f \in I/J \quad \wedge \quad C \subseteq J \subseteq I)\,. \tag{6.69}$$

The last line in eq. (6.68) then becomes

$$\sum_{\substack{C \subseteq I \subseteq E_G \\ I \neq \emptyset}} \sum_{\substack{C \subseteq J \subseteq I \\ J \neq \emptyset}} \sum_{f \in I/J} a_I \left((G_J, C) + a_J \sum_{e \in J/C} (G_{J/e}, C) \right) \otimes (G_{I/f}, J) \otimes (G, I),$$

which matches the remaining contributions of eq. (6.67).

We have thus proven that Δ as defined in eq. (6.62) is coassociative. We note that nothing in this proof depends on the specific form of the coefficient a_I in eq. (6.62), but we have set it to that particular value because it is the one that matches the coproduct of Feynman integrals.

The Hopf algebra of one-loop graphs: It turns out that the algebra $\mathcal{P}$ has a much richer algebraic structure than what we discussed here. It can be shown that starting from the algebra $\mathcal{P}$ one can define a counit and an antipode, which together with the coproduct Δ defined in eq. (6.62) turn $\mathcal{P}$ into a Hopf algebra (strictly speaking the Hopf algebra it is not $\mathcal{P}$, but rather an algebra constructed from $\mathcal{P}$). Showing this would require introducing more notation and proving several non-trivial results. Because it will not be used in the remainder of this thesis we will not do it here and the full construction of this Hopf algebra will be presented elsewhere [118].

6.3.2 Examples

To make eq. (6.62) more concrete, we now illustrate it for uncut and cut Feynman graphs with up to four internal edges. Cut edges will be denoted by a dashed red line. We will see we recover the diagrammatic coproduct of tadpoles and bubbles already determined above.

$|E_G| = 1$: For one internal edge, eq. (6.62) is trivial. When the edge is uncut,

(6.70)

This is the same as we obtained in eq. (6.52).

When the edge is cut,

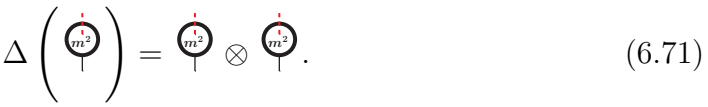

(6.71)

$|E_G| = 2$: We already studied the case with two internal edges in the previous section. We now show we get the same result from eq. (6.62). When $|C| = 0$,

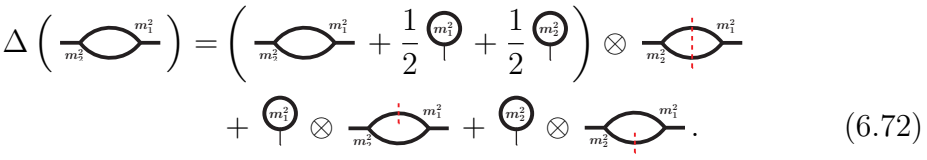

(6.72)

There are two different graphs with $|C| = 1$. They are similar, so we only consider one:

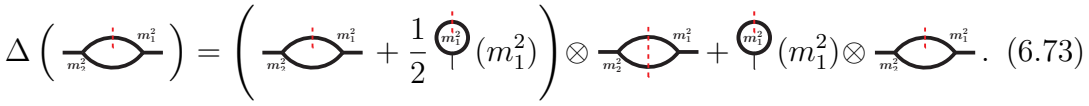

(6.73)

The maximal cut, with $|C| = 2$, gives

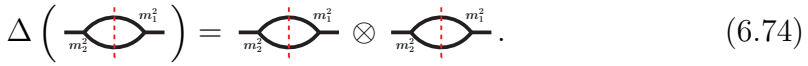

(6.74)

This is exactly the same diagrammatic coproduct we had already established in the previous section.

$|E_G| = 3$: For $|C| = 0$,

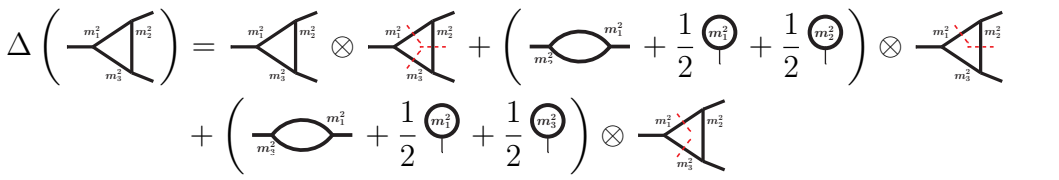

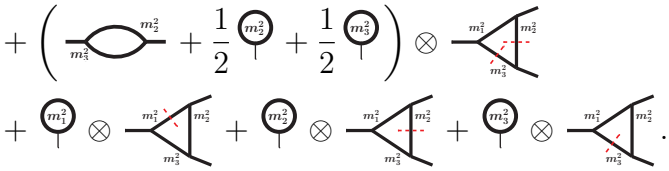

(6.75)

For $|C| = 1$, there are three similar graphs. We only consider one:

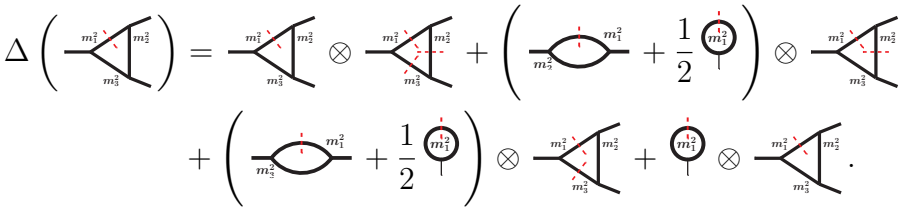

(6.76)

For $|C| = 2$, there are three similar graphs. We only consider one:

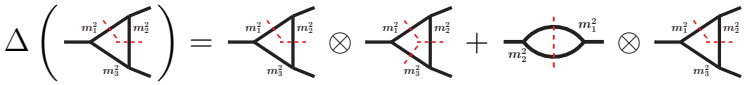

(6.77)

Finally, the maximal cut with $|C| = 3$:

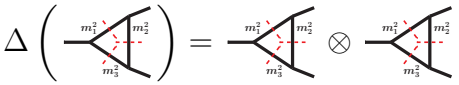

(6.78)

$|E_G| = 4$: For $|C| = 0$,

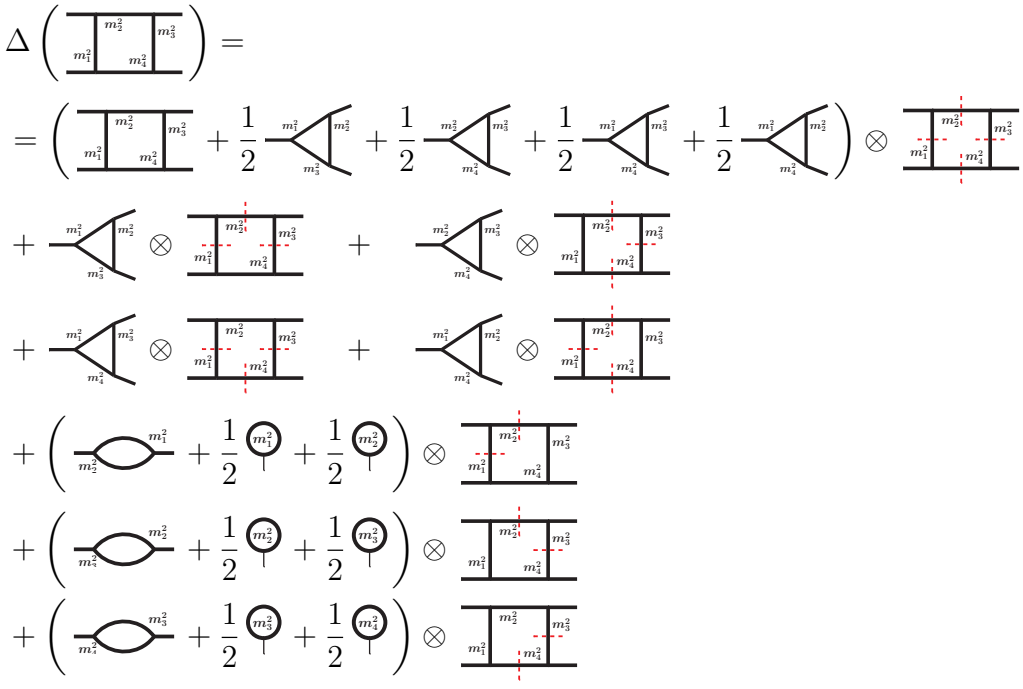

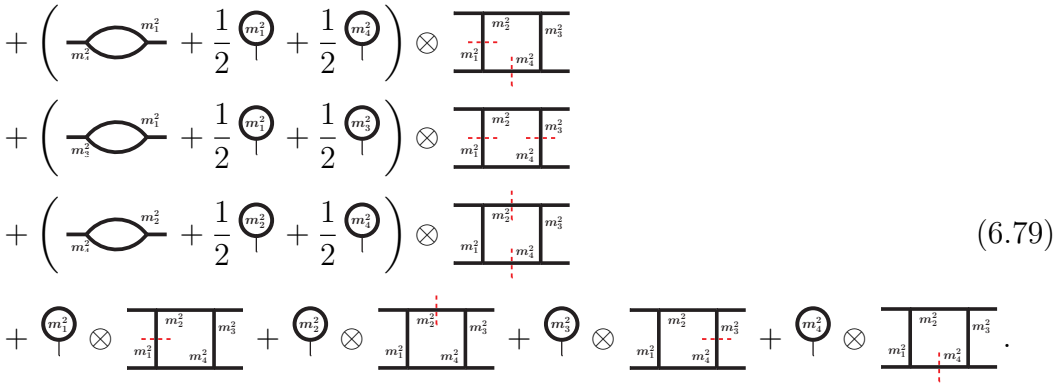

(6.79)

For $|C| = 1$, there are four similar graphs. We only consider one:

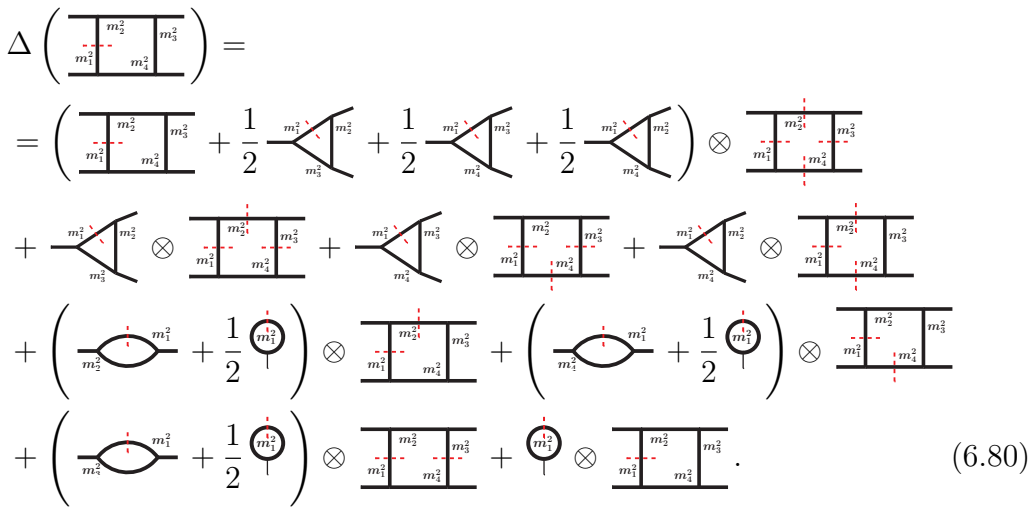

(6.80)

For $|C| = 2$, there are six similar graphs. We only consider one:

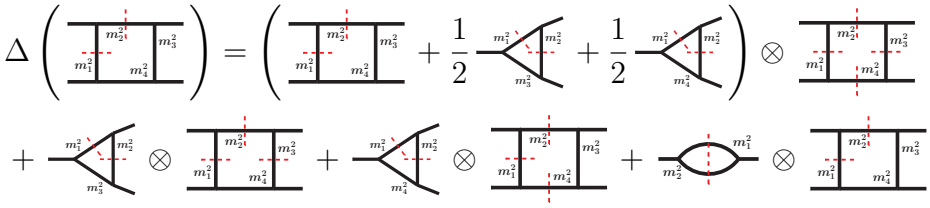

(6.81)

Note that out of the six graphs with $|C| = 2$, two are special in that they do not cut adjacent edges (these are the cuts in the s and t channels of the box). However, this fact changes nothing in eq. (6.62) and the structure of the graphical coproduct of these two terms is similar to the other four.

For $|C| = 3$, there are four similar graphs. We only consider one:

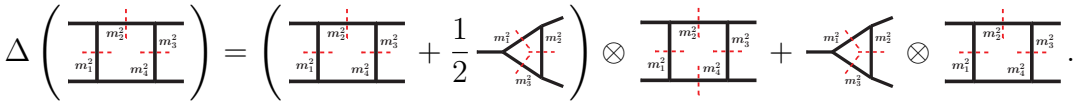

(6.82)

Finally, the maximal cut with $|C| = 4$:

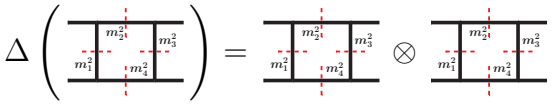

(6.83)

These examples illustrate eq. (6.62). Graphs with more edges are better suited to be studied with the help of a computer given the number of terms generated by eq. (6.62).

6.4 Diagrammatic coproduct of one-loop Feynman diagrams

In the previous section we saw how one could define a purely graphical coproduct on $\mathcal{P}$, the $\mathbb{Q}$-algebra generated by one-loop cut Feynman graphs, as defined below eq. (6.60). Of course, we are interested in what the implications of this structure are for the functions Feynman diagrams evaluate to. We will thus define how we map Feynman graphs to Feynman integrals, and then we will discuss some consequences of the underlying graphical coproduct. We will finish with some examples illustrating our main points.

6.4.1 The graphical coproduct and the coproduct of MPLs

Mapping between graphs and Feynman integrals: Let us then define the mapping between the graphs of the previous section and the MPLs Feynman integrals evaluate to. This map is quite straightforward.

A Feynman graph with n-external legs (after combining the half-edges incident

on the same vertex) and n-propagators (previously called internal edges) is computed according to the rules of chapter 5, summarised in appendix A below eq. (A.8), but normalised to their leading singularity as defined in eq. (5.35). For instance:

$$\begin{aligned}
&\text{  } = \frac{I_1(m^2)}{\mathrm{LS}[I_1(m^2)]}\,, \qquad \text{  } = \frac{I_2(p^2;m_1^2,m_2^2)}{\mathrm{LS}[I_2(p^2;m_1^2,m_2^2)]}\,,\\
&\text{  } = \frac{I_3(p_1^2,p_2^2,p_3^2;m_1^2,m_2^2,m_3^2)}{\mathrm{LS}[I_3(p_1^2,p_2^2,p_3^2;m_1^2,m_2^2,m_3^2)]}\,,\\
&\text{ 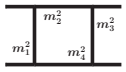 } = \frac{I_4(p_1^2,p_2^2,p_3^2,p_4^2;m_1^2,m_2^2,m_3^2,m_4^2)}{\mathrm{LS}[I_4(p_1^2,p_2^2,p_3^2,p_4^2;m_1^2,m_2^2,m_3^2,m_4^2)]}.
\end{aligned} \tag{6.84}$$

We recall I_n is computed according to

$$I_n\left(\{p_j\cdot p_k\}\,;\{m_j^2\}\right) = \frac{e^{\gamma_E\epsilon}}{i\pi^{\frac{D}{2}}}\int d^Dk \frac{1}{\left(k^2-m_{n-1}^2+i0\right)}\prod_{j=0}^{n-2}\frac{1}{(k-q_j)^2-m_j^2+i0}\,. \tag{6.85}$$

All cuts are computed according to the rules of the previous chapter, and each is normalised to its leading singularity. For instance,

$$\text{  } = \frac{\mathcal{C}_{1,[1]}[I_2(p^2;m_1^2,m_2^2)]}{\mathrm{LS}[I_2(p^2;m_1^2,m_2^2)]}. \tag{6.86}$$

Finally, the coproduct Δ acting on graphs introduced in the previous section is simply mapped to the coproduct Δ acting on MPLs introduced in chapter 2.

Let us now make a comment on the connection between graphs and the Feynman integrals they correspond to, evaluated in dimensional regularisation. We recall we formulated the graphical coproduct for graphs with massive propagators and massive external legs. However, if we claim eq. (6.62) to be valid in dimensional regularisation, it should still hold if we take some of the masses to zero. In this context, there are two interesting limits we can consider: the limit where all internal propagators and external legs are massive and generic, and the limit where all internal propagators and external legs are massless (strictly speaking, for triangles and bubbles we have to keep respectively one and two massive external legs to get a non-trivial diagram).

In the first case, we expect the Feynman integrals to evaluate to complicated

MPLs, depending on a large number of variables. The fact that there is an underlying graphical coproduct imposes strong constraints on these functions, but the connection between the coproduct on graphs and MPLs is straightforward according to the rules given above. For instance, looking at eq. (6.79) we see that the graphical coproduct has a rich structure which allows for the complex analytic structure one expects to be associated with this type of functions.

In the other limit, we have very simple functions depending on a small number of variables. Correspondingly, we expect that the graphical coproduct will have a simple structure, with only a few terms. It is a highly non-trivial observation that the graphical coproduct introduced in the previous section is consistent with dimensional regularisation. Because of this, many contributions of the graphical coproduct can vanish (for instance, because in that limit they would correspond to a scaleless integral, vanishing in dimensional regularisation). As we will see, despite the graphical operations having been defined in the fully massive case, even the coproduct of divergent diagrams is correctly reproduced by the graphical coproduct.

One could wonder whether we could have used other regularisation procedures. Unfortunately, we did not have time to explore this possibility, but it would certainly be an interesting subject to study.

ϵ-expansion of the diagrammatic coproduct: Although we claim the diagrammatic coproduct is valid in dimensional regularisation, which means we can think of the diagrams appearing in it as functions of ϵ, the validity of eq. (6.62) must be checked order by order in ϵ because the coproduct on functions is defined for the MPLs appearing in the Laurent expansion of the diagrams. As we know by now—see the discussion in section 2.2.2—the coefficients of each order in ϵ are functions of increasing weight. Moreover, we also know that for each weight n, there are several coproduct components we must check, of the form $(k, n-k)$ for each $k = 0, \ldots, n$.

This means when checking eq. (6.62) we must do two expansions: first an expansion in ϵ, and then, at each order in ϵ, an expansion in the different coproduct components for that specific weight. Understanding these expansions in detail, in particular which diagrams appearing in eq. (6.62) contribute at which order to a particular coproduct entry at a given power in ϵ is important, so we

now give some details about them. We explain the expansion for a fully massive diagram F with n even, with the uncut and cut diagrams computed according to the definitions of chapter 5. The discussion can easily be generalised to other cases, with n odd and/or some masses set to zero.

We start with some notation. Let us define the set of all propagators of F by $\{e_1, \ldots, e_n\}$. The ϵ-expansion of the uncut diagram (which we normalise to its leading singularity) is

$$F = \sum_{j=0} \epsilon^j f_j \,. \tag{6.87}$$

Since F is computed according to the eq. (5.9), we know it has weight $\omega = n/2$. This means the weights of the coefficients in its ϵ-expansion are

$$w\left(f_j\right) = \omega + j \,. \tag{6.88}$$

We now discuss its cuts. The maximal cut $\mathcal{C}_n[F]$ has weight 0, which means the coefficients in its ϵ-expansion, $\mathcal{C}_n^{(j)}[F]$ have weight

$$w\left(\mathcal{C}_n^{(j)}[F]\right) = j \,. \tag{6.89}$$

The next-to-maximal cuts also have weight 0. We denote the cut where all propagators but propagator e_j are cut by $\mathcal{C}_{n/\{e_j\}}[F]$, and thus have

$$w\left(\mathcal{C}_{n/\{e_j\}}^{(j)}[F]\right) = j \,. \tag{6.90}$$

More generally, a cut where k propagators are cut, $\mathcal{C}_k[F]$ with $0 < k \leq n$, has weight $\omega - \lceil k/2 \rceil$, which means

$$w\left(\mathcal{C}_k^{(j)}[F]\right) = \omega - \left\lceil \frac{k}{2} \right\rceil + j. \tag{6.91}$$

We can now determine the weight of all the contributions appearing in the second entry of the diagrammatic coproduct.

For the first entries, where uncut diagrams appear, we also introduce some definitions. We define $\mathfrak{Tad}(e_j)$ as the tadpole obtained by contracting all propagators of F the but the propagator e_j, with $0 < j \leq n$, normalised to its leading singularity. Tadpoles are functions of weight 1 which start at order

ϵ^{-1}, so we have

$$\mathfrak{Tad}(e_j) = \text{  }(e_j) = \sum_{l=-1} \epsilon^l \mathfrak{tad}_l(e_j) \qquad \text{with} \qquad w\left(\mathfrak{tad}_l(e_j)\right) = 1 + l. \tag{6.92}$$

with obvious notation for the argument of the diagram.

We then define $\mathfrak{Bub}(e_j, e_k)$, with $0 < j < k \leq n$ which avoids double counting, as the combination

$$\mathfrak{Bub}(e_j, e_k) = \text{ 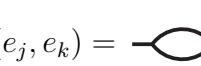 }(e_j, e_k) + \frac{1}{2}\text{}(e_j) + \frac{1}{2}\text{}(e_k), \tag{6.93}$$

with obvious notation for the arguments of the diagrams. This is a function of weight 1 which starts at order ϵ^{-1}, so we have

$$\mathfrak{Bub}(e_j, e_k) = \sum_{l=-1} \epsilon^l \mathfrak{bub}_l(e_j, e_k) \qquad \text{with} \qquad w\left(\mathfrak{bub}_l(e_j, e_k)\right) = 1 + l. \tag{6.94}$$

We proceed similarly for triangles, which are finite weight 2 functions.

$$\mathfrak{Tri}(e_i, e_j, e_k) = \text{  }(e_i, e_j, e_k), \tag{6.95}$$

where $0 < i < j < k \leq n$, with

$$\mathfrak{Tri}(e_i, e_j, e_k) = \sum_{l=0} \epsilon^l \mathfrak{tri}_l(e_i, e_j, e_k) \qquad \text{with} \qquad w\left(\mathfrak{tri}_l(e_i, e_j, e_k)\right) = 2 + l. \tag{6.96}$$

For the box terms, we define $\mathfrak{Box}(e_i, e_j, e_k, e_m)$, with $0 < i < j < k < m \leq n$, which are finite weight 2 functions, defined as

$$\begin{aligned}\mathfrak{Box}(e_i, e_j, e_k, e_m) = {} & \text{ 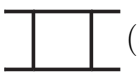 }(e_i, e_j, e_k, e_m) + \frac{1}{2}\text{ 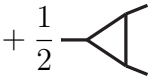 }(e_i, e_j, e_k) \\ & + \frac{1}{2}\text{  }(e_i, e_j, e_m) + \frac{1}{2}\text{  }(e_i, e_k, e_m) + \frac{1}{2}\text{ 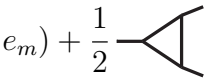 }(e_j, e_k, e_m),\end{aligned} \tag{6.97}$$

with

$$\mathfrak{Box}(e_i, e_j, e_k, e_m) = \sum_{l=0} \epsilon^l \mathfrak{box}_l(e_i, e_j, e_k), \tag{6.98}$$

and

$$w\left(\mathfrak{box}_l(e_i, e_j, e_k, e_m)\right) = 2 + l. \tag{6.99}$$

We define similar function for pentagons and hexagons. For pentagons, which are finite weight 3 functions,

$$\mathfrak{Pent} = \sum_{l=0} \epsilon^l \mathfrak{pent}_l \qquad \text{with} \qquad w\left(\mathfrak{pent}_l\right) = 3 + l, \tag{6.100}$$

where we did not write explicitly the propagators. For hexagons, we take the usual combination of the hexagon and one-half times the pentagons obtained by contracting each of the propagators. These are also a finite weight 3 function,

$$\mathfrak{Hex} = \sum_{l=0} \epsilon^l \mathfrak{hex}_l \qquad \text{with} \qquad w\left(\mathfrak{hex}_l\right) = 3 + l, \tag{6.101}$$

where we did not write explicitly the propagators.

Similar functions can be defined for diagrams with more propagators. The only ones we will need for our discussion are

$$\mathfrak{F} = \sum_{l=0} \epsilon^l \mathfrak{f}_l \qquad \text{with} \qquad w\left(\mathfrak{f}_l\right) = \omega + l \tag{6.102}$$

as the usual combination of F and the diagrams obtained by contracting one propagator. We also define

$$\mathfrak{F}^{(e_j)} = \sum_{l=0} \epsilon^l \mathfrak{f}_l^{(e_j)} \qquad \text{with} \qquad w\left(\mathfrak{f}_l^{(e_j)}\right) = \omega + l \tag{6.103}$$

for the diagrams obtained by contracting the propagator e_j of F.

Let us then go back to the check of the diagrammatic coproduct of F. We will consider the coefficient of order ϵ^j of the ϵ-expansion of F, which we recall has weight $\omega + j$. The different coproduct entries at this weight are:

- $\boldsymbol{(0, \omega + j)}$: The only diagrams appearing in the first entry with a weight 0 coefficient in their ϵ-expansion are $\mathfrak{Tad}$ and $\mathfrak{Bub}$ at order ϵ^{-1}. This means the left cofactor contributes at order $j_L = -1$, and so the right cofactor must contribute at order $j_R = j + 1$. This is consistent with the coefficient of the one- and two-propagator cuts at order ϵ^{j+1} having weight $\omega + j$.

- $\boldsymbol{(1, \omega + j - 1)}$: Again, the only diagrams appearing in the first entry with a weight 1 coefficient in their ϵ-expansion are $\mathfrak{Tad}$ and $\mathfrak{Bub}$ at order ϵ^0. This means the left cofactor contributes at order $j_L = 0$, and so the right cofactor

must contribute at order $j_R = j$. This is consistent with the coefficient of the one- and two-propagator cuts at order ϵ^j having weight $\omega + j - 1$.

- $\boldsymbol{(2, \omega + j - 2)}$: There are two different contributions to this coproduct entry.

  First, we have a contribution from the coefficient of order ϵ^1 in the ϵ-expansion of $\mathfrak{Tad}$ and $\mathfrak{Bub}$. Since the left cofactor contributes at order $j_L = 1$, the right cofactor must contribute at order $j_R = j - 1$. This is consistent with the coefficient of the one- and two-propagator cuts at order ϵ^{j-1} having weight $\omega + j - 2$.

  Second, we have a contribution from the coefficient of order ϵ^0 in the ϵ-expansion of $\mathfrak{Tri}$ and $\mathfrak{Box}$. Since the left cofactor contributes at order $j_L = 0$, the right cofactor must contribute at order $j_R = j$. This is consistent with the coefficient of the three- and four-propagator cuts at order ϵ^j having weight $\omega + j - 2$.

- $\boldsymbol{(3, \omega + j - 3)}$: There are three different contributions to this coproduct entry.

  First, we have a contribution from the coefficient of order ϵ^2 in the ϵ-expansion of $\mathfrak{Tad}$ and $\mathfrak{Bub}$. Since the left cofactor contributes at order $j_L = 2$, the right cofactor must contribute at order $j_R = j - 2$. This is consistent with the coefficient of the one- and two-propagator cuts at order ϵ^{j-2} having weight $\omega + j - 3$.

  Second, we have a contribution from the coefficient of order ϵ^1 in the ϵ-expansion of $\mathfrak{Tri}$ and $\mathfrak{Box}$. Since the left cofactor contributes at order $j_L = 1$, the right cofactor must contribute at order $j_R = j - 1$. This is consistent with the coefficient of the three- and four-propagator cuts at order ϵ^{j-1} having weight $\omega + j - 3$.

  Third, we have a contribution from the coefficient of order ϵ^0 in the ϵ-expansion of $\mathfrak{Pent}$ and $\mathfrak{Hex}$. Since the left cofactor contributes at order $j_L = 0$, the right cofactor must contribute at order $j_R = j$. This is consistent with the coefficient of the three- and four-propagator cuts at order ϵ^j having weight $\omega + j - 3$.

- $\boldsymbol{(k, \omega + j - k)}$: For any $3 < k < n$ we follow the same procedure as for the cases above. As k increases, more and more topologies start contributing.

- $\boldsymbol{(\omega + j, 0)}$: The only contributions in the right cofactor which have a weight 0 coefficient are the maximal and next-to-maximal cuts of F taken at order ϵ^0. This means $j_R = 0$, which implies $j_L = j$, which is consistent with the ϵ^j coefficients of $\mathfrak{F}$ and $\mathfrak{F}^{(e_j)}$ having weight $\omega + j$. We note that, given the relation obtained in section 5.4.2, we find

$$\mathfrak{f}_j \otimes \mathcal{C}_n^{(0)}[F] + \sum_{k=1,\dots,n} \mathfrak{f}_j^{(e_k)} \otimes \mathcal{C}_{n/e_k}^{(0)}[F] = f_j \otimes 1, \tag{6.104}$$

  which is the correct result for the trivial coproduct component of weight $(\omega + j, 0)$.

It is straightforward to generalise this discussion to diagrams with an odd number of propagators or to diagrams which are divergent. Understanding these expansions was important to perform the checks of the graphical coproduct we present in section 6.4.2.

Pole cancellation identity and the first-entry condition revisited: Given the graphical coproduct and the mapping to Feynman integrals we have established, let us now revisit what were our main guiding principles to introduce the diagrammatic coproduct for uncut Feynman diagrams in section 6.2. We recall there were three main guiding principles: *(i)* the fact that the discontinuity operator only acts in the first entry of the coproduct which implied having diagrams with the same analytic structure as Feynman diagrams in the first entry ; *(ii)* correctly reproducing the trivial components of the coproduct of weight $(0, n)$ and $(n, 0)$; and *(iii)* satisfying the first entry condition.

Point *(i)* is satisfied by construction of the graphical coproduct, eq. (6.62). We also note that the generalisation for cut diagrams is also satisfied: the propagators cut in the graph whose coproduct is being computed are always cut in the diagrams appearing in the first entry of the graphical coproduct.

Let us now see how the principle *(ii)* is satisfied. We start with the easiest, the component of weight $(n, 0)$. As shown in eq. (6.104), it is easy to see that this term is reproduced by the contribution of the graphical coproduct corresponding to the

maximal cut. For diagrams with an odd number of propagators, see e.g. eq. (6.75), the term appears by itself and there is nothing to add. For diagrams with an even number of propagators, see e.g. eq. (6.79), we can just follow the discussion that led us to eq. (6.104).

In section 6.2, we also argued that the component of weight $(0, n)$ was reproduced because of a relation between uncut graphs and their one- and two-propagator cuts, which we recall involved the singularities of bubbles and/or tadpoles. We now show this is true for a general finite diagram with all propagators massive. The proof presented here is a straightforward generalisation of an unpublished proof by Claude Duhr, which was obtained for the case where all propagators are massless. We start by noting that

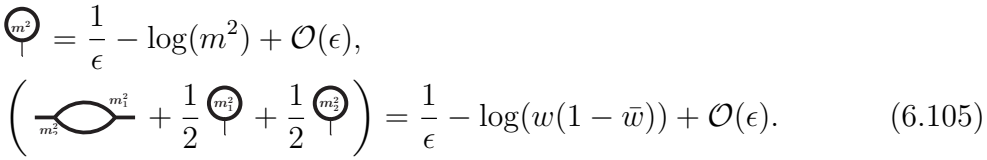

(6.105)

For an uncut graph evaluating to a finite function, it is easy to see that all other combinations of graphs appearing in the left cofactor of eq. (6.62)—the $\mathfrak{Tri}$, $\mathfrak{Box}$, $\mathfrak{Pent}$ and $\mathfrak{Hex}$ above—will be finite. In other words, given the mapping of graphs to the functions they evaluate to, we see that on the right-hand side of eq. (6.62) we have introduced a potentially divergent contribution which we can schematically write as

$$\frac{1}{\epsilon}\left(\sum(\text{one-propagator cuts}) + \sum(\text{two-propagator cuts})\right). \tag{6.106}$$

From chapter 3, we know that one-propagator cuts always correspond to discontinuities in internal masses, and two-propagator cuts to discontinuities in external channels. The divergent contribution can then be rewritten (schematically) in a similar form as above,

$$\frac{1}{\epsilon}\left(\sum(\text{internal mass discontinuities}) + \sum(\text{channel discontinuities})\right). \tag{6.107}$$

To understand the cancellation of the bubble/tadpole singularities we must thus try to relate discontinuities in internal masses and discontinuities in external channels to the original function.

Let us then prove the following result:

If $F(r_1, \ldots, r_{m+1})$ is a function obtained by integrating a l-loop Feynman integral (that evaluates to MPLs), depending on $m+1$ dimensionful quantities r_γ, then

$$\sum_{\gamma=1}^{m+1} \frac{1}{2\pi i} \operatorname{Disc}_{r_\gamma} F_k = l F_{k-1} \mod i\pi, \tag{6.108}$$

and we are particularly interested in the case $l = 1$.

Proof: To prove this result, we assume r_{m+1} to be an internal mass (squared), but the proof is equally valid if it is any kinematic invariant. We can then write

$$F(r_1, \ldots, r_{m+1}) = (r_{m+1} - i0)^{-l\epsilon} f(\rho_1, \ldots, \rho_m) \tag{6.109}$$

where ρ_γ are n dimensionless variables defined as $\rho_\gamma = r_\gamma / r_{m+1}$ for $1 \leq \gamma \leq n$. We assumed r_{m+1} positive and gave it a $(-i0)$-prescription because it is an internal mass and we work in the euclidean region of F. We then define F_k and f_k as the coefficients in the Laurent series of F and f. Using

$$\sum_k F_k \epsilon^k = (r_{m+1})^{-l\epsilon} \sum_k f_k \epsilon^k \tag{6.110}$$

we find that

$$F_k = \sum_{j=0}^{k} \frac{(-l)^j}{j!} \log^j(r_{m+1}) f_{k-j}. \tag{6.111}$$

We now define $\tau_{k,\gamma}$ as

$$\tau_{k,\gamma} \equiv \frac{1}{2\pi i} \operatorname{Disc}_{r_\gamma} f_k = \frac{1}{2\pi i} \operatorname{Disc}_{\rho_\gamma} f_k, \tag{6.112}$$

where the discontinuity is taken according to the definitions of chapters 2 and 3. We can then find

$$\frac{1}{2\pi i} \operatorname{Disc}_{r_\gamma} F_k = \sum_{j=0}^{k} \frac{(-l)^j}{j!} \log^j(r_{m+1}) \tau_{k-j,\gamma} \quad \text{for} \quad 1 \leq \gamma \leq n. \tag{6.113}$$

For r_{m+1}, we must be more careful as there are two contributions:

$$\begin{aligned}\frac{1}{2\pi i}\operatorname{Disc}_{r_{m+1}} F_k =& \sum_{j=0}^{k} \frac{(-l)^j}{j!} \frac{\operatorname{Disc}_{r_{m+1}}\left[\log^j(r_{m+1})\right]}{2\pi i} f_{k-j} \\ &+ \sum_{j=0}^{k} \frac{(-l)^j}{j!} \log^j(r_{m+1}) \frac{\operatorname{Disc}_{r_{m+1}}\left[f_{k-j}\right]}{2\pi i} \\ =& l \sum_{j=1}^{k} \frac{(-l)^{j-1}}{(j-1)!} \log^{j-1}(r_{m+1}) f_{k-j} \\ &- \sum_{\gamma=1}^{n} \sum_{j=0}^{k} \frac{(-l)^j}{j!} \log^j(r_{m+1}) \tau_{k-j,\gamma} \end{aligned} \tag{6.114}$$

We thus have

$$\sum_{\gamma=1}^{n+1} \frac{1}{2\pi i} \operatorname{Disc}_{r_\gamma} F_k = l \sum_{j=0}^{k-1} \frac{(-l)^j}{j!} \log^j(r_{m+1}) f_{k-1-j} = l F_{k-1} \mod i\pi, \tag{6.115}$$

which proves eq. (6.108).

The result in eq. (6.108) is valid modulo $i\pi$ because the function and its discontinuities are not evaluated in the same region. Being careful with factors of $\pm i$ and powers of 2π, we can easily check that this condition is equivalent to the statement that the sum of the one- and two-propagator cuts at order ϵ^k is equal to the function at order ϵ^{k-1}, up to analytic continuation.

This is quite a powerful result. If F is finite, for $k = 0$ it implies the cancellation of the poles introduced by the bubble/tadpole contributions. For $k > 0$, it guarantees all the coproduct entries of weight $(0, n)$ are correctly reproduced by the rules of the graphical coproduct.

Finally, we comment on principle *(iii)*, i.e., we comment on the first-entry condition from the perspective of the graphical coproduct. For this, it is worth keeping in mind the discussion above about how coproduct entries of weight $(1, w + j - 1)$ are reproduced by the graphical coproduct. According to our rules, we know that a diagram with n propagators has weight $\lceil n/2 \rceil$. This means that in the graphical coproduct of an uncut diagram the only terms of weight one in the first entry are tadpoles and bubbles, or, more precisely, the order ϵ^0 coefficient of the Laurent expansion of tadpoles and bubbles. The first-entry condition

stating that internal masses appear in the first entry of the coproduct is now a simple consequence of the graphical coproduct entries with a tadpole in the first entry and a one-propagator cut in the second entry. The first-entry condition corresponding to a channel cut is obtained from the terms with two-propagator cuts. For the fully massive case, the first-entry is the $\log(w(1-\bar{w}))$ appearing in eq. (6.105), which we already encountered in eq. (2.45) and the discussion below, where we argued it corresponded to the same condition as the physical mass threshold.

To finish this discussion, we make a comment on what happens when internal or external masses vanish. As already argued above, eq. (6.62) is consistent with dimensional regularisation. This means we are free to take kinematic invariants to zero, in which case some diagrams might become divergent in the infrared.

By infrared power counting (see e.g. [124]) diagrams with $n \geq 5$ propagators as defined in eq. (5.9) are finite independently of whether internal propagators and external legs are massive or not. However, boxes, triangles and bubbles can be divergent in the infrared, and tadpoles are divergent in the ultraviolet. Despite this, we claim that all combinations of uncut diagrams appearing in the first entry of eq. (6.62) are always finite except for bubbles and tadpoles. In other words, all the functions $\mathfrak{Tri}$ and $\mathfrak{Box}$ defined above that can appear in the first entry of the diagrammatic coproduct are finite, independently of the mass configurations.

This can be proved by examining all possibly divergent mass configurations, as there is a finite number of cases to check. To see that no divergences are introduced by triangles appearing by themselves, all we need to check is that divergent triangles correspond to vanishing three-propagators cuts (see section 5.4.1). For boxes, all one needs to check is that the combination of boxes and triangles appearing in the first entry of the four-propagator cuts in eq. (6.62) is always of order ϵ^0, independently of the configurations of the masses.

This means that if we want to study the trivial coproduct components and the first-entry condition for diagrams which do not have all propagators and all external legs massive, whether they are finite or not, we still only need to examine the contributions of bubbles and tadpoles.

Let us say we take all internal masses to zero. Then there are no tadpole contributions in eq. (6.62) because they become scaleless integrals. First entries

corresponding to two-propagator cuts are now divergent, not because of the poles of tadpoles, but because the massless bubble is divergent. One might naïvely think our discussion above of how poles of tadpoles and bubble were necessary to reproduce the weight $(0, n)$ components of the coproduct is no longer valid. However, we now have

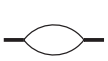 $= \frac{1}{\epsilon} - \log(-p^2) + \mathcal{O}(\epsilon),$ (6.116)

and it is the contribution of this pole that will reproduce the weight $(0, n)$ components. This can be proved in exactly the same way as we did for the case where there were no internal masses. The first entry condition is a trivial consequence of the graphical coproduct in this case.

In the intermediate case where some propagators are massive and some massless, we might have two-propagator cuts whose corresponding first-entry is a bubble with only one massive propagator. This case can be treated in the same way as the massless or the fully massive ones once we realise that singularities now come from

 $= \frac{1}{\epsilon} - \log(m^2) + \mathcal{O}(\epsilon),$

$\left($  $+ \frac{1}{2}$ $\right) = \frac{1}{\epsilon} - \log(m^2 - p^2) + \mathcal{O}(\epsilon).$ (6.117)

In this case also the first entry condition is a trivial consequence of the graphical coproduct, both for internal masses and external channels.

6.4.2 Examples

In the previous sections, we have given a very formal definition of a coproduct on one-loop graphs, established its connection to Feynman integrals, and then made several comments on the structure of the graphical coproduct to show it was consistent with the action of the coproduct of MPLs on the functions Feynman integrals evaluate to. We now illustrate all these points through some concrete examples.

We have already studied the tadpole, eq. (6.52), and all bubbles, eqs. (6.8), (6.37) and (6.48). The graphical coproduct of their cuts was also discussed in section 6.2.3. We will thus now focus on triangles and boxes. We believe there

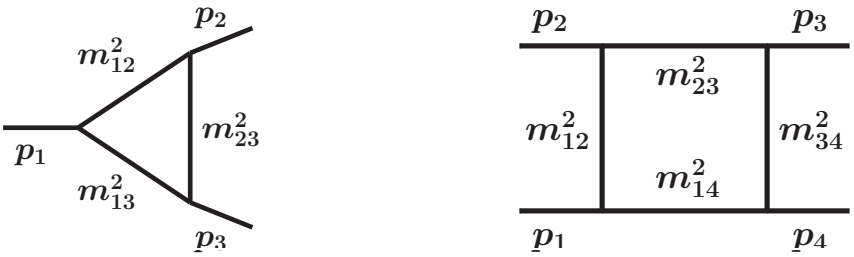

Figure 6.1: Notation for external legs and and internal masses for general triangles and boxes.

is a large enough variety of mass configurations for these topologies to provide ample evidence of the validity of eq. (6.62) for any one-loop diagram. In the following sections, we will see that the fully massless pentagon and hexagon are also consistent with eq. (6.62).

For each example, we will highlight which properties of the diagrammatic coproduct they illustrate. We have not checked it for the fully massive triangle or the fully massive box—see fig. 6.1—which would be the natural examples to explore given that the graphical coproduct was formulated for diagrams with generic internal and external masses. Unfortunately, in both cases, we have not found a parametrisation which would give a rational symbol alphabet, and this makes checking the diagrammatic coproduct very complicated. We will thus restrict ourselves to simpler (but already non-trivial) examples for which we have such a parametrisation.

When checking eq. (6.62) for a specific diagram, we recall there are two expansions, one in the dimensional regularisation parameter ϵ and one in the different coproduct components at a given weight, see the discussion below eq. (6.103). We must check the consistency of each term in this double expansion between the right-hand-side and the left-hand-side of eq. (6.62). All the examples were checked at least up to weight 3 (i.e., order ϵ^1 for triangles and boxes), when all diagrams contribute at least as weight 1 functions. The simplest examples were checked to higher weights.

We will not write the kinematic dependence of the diagrams in cases where it is obvious. If two cuts are related by symmetry, we only present the coproduct of one of them. We do not give expressions for the cuts for any of the examples. Some can be found in appendix B, but all relevant expressions have been collected in the accompanying `MATHEMATICA` package [38]. For all examples below, we refer

to the notation of fig. 6.1 to assign each invariant to a specific propagator or external legs.

$I_3(p_1^2, 0, 0; 0, 0, 0)$: We start by examining the triangle with a single external massive leg. From eq. (6.75) and equations below, we find

Δ 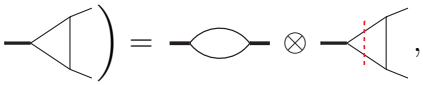 , (6.118)

Δ 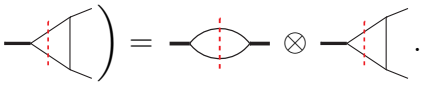 . (6.119)

This is a trivial example, very similar to the bubble with no internal masses, for which explicit expressions can be found in section B.1.1. It nevertheless warrants discussion because of the following observation concerning triangle integrals. In eq. (6.84), we said Feynman graphs were mapped to the corresponding Feynman integral normalised to the first order in the ϵ expansion of its maximal cut. However, as discussed in section 5.4.1, maximal cuts of triangles can vanish if they do not have enough masses. This happens in the example we are currently examining, as can be seen by the fact that the triple cut contribution is absent for the diagrammatic coproduct. Of course, this poses a problem to normalise the uncut and two-propagator cut diagram.

Fortunately, triangle diagrams have a particularity: their maximal cut, when non-zero, is independent of the internal masses (this is not true for bubbles—compare eqs. (6.10), (6.30) and (6.46)—or boxes—compare eqs. (5.92) and (5.107)). This means we can determine the normalisation for triangles with a given configuration of external channels by looking at any configuration of internal masses making the integral finite. For a triangle with one external massive leg, the simplest example is $I_3(p_1^2, 0, 0; 0, m_{23}^2, 0)$, from which we find

$$\mathrm{LS}[I_3(p_1^2, 0, 0; 0, 0, 0)] \equiv \mathcal{C}_3^{(0)}[I_3(p_1^2, 0, 0; 0, m_{23}^2, 0)] = -\frac{1}{p_1^2}. \tag{6.120}$$

All diagrams with one massive external leg and a vanishing triple cut will be normalised by this factor.

Finally, this diagram demonstrates that even if the massless limit of eq. (6.62)

gives rise to singularities, it still gives the correct coproduct. As we already mentioned previously, because the triple cut is zero this divergent triangle does not appear by itself in the first entry of the diagrammatic coproduct. We note that in this case the singularity introduced by the bubble is necessary to have the same degree of singularity on both sides of the relation.

$I_3(p_1^2, 0, 0; m_{12}^2, 0, 0)$: We now look at the triangle with one external massive leg and one adjacent massive propagator. We find

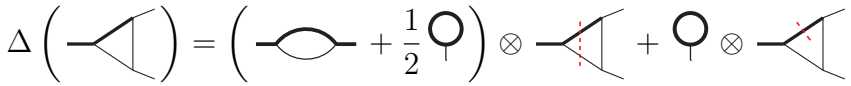

(6.121)

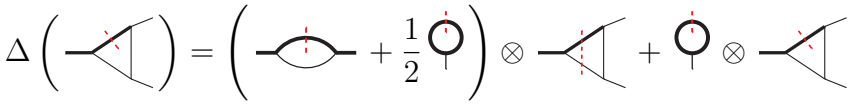

(6.122)

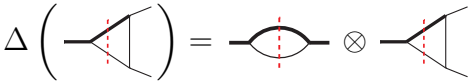

(6.123)

This example is also simple, and very similar to the bubble with one internal mass. Explicit expressions can be found in section B.1.3. As the previous example, its maximal cut vanishes and so we use the same trick to find the leading singularity.

$I_3(p_1^2, 0, 0; 0, m_{23}^2, 0)$: We now look at the triangle with one external massive leg and one massive propagator not adjacent to it. We find

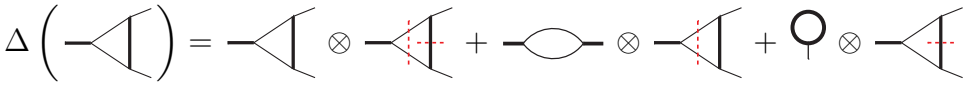

(6.124)

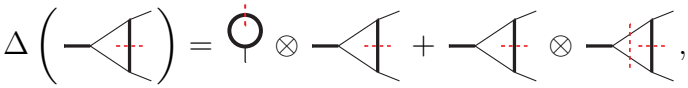

(6.125)

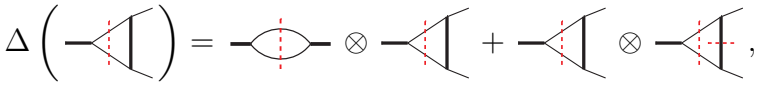

(6.126)

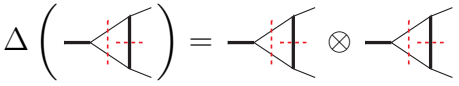

(6.127)

This example—explicit expressions can be found in section B.1.2—is interesting for two reasons. First, it is this diagrams we used to extract the normalisation factor for the previous two diagrams as it is the simplest diagram with one external massive leg having a non-vanishing triple cut. Second, this diagram illustrates how a tadpole can appear by itself if the massive propagator is not attached to any massive external channel, consistently with eq. (6.62).

$\boldsymbol{I_3(p_1^2, 0, 0; m_{12}^2, 0, m_{13}^2)}$**:** We now look at the triangle with one external massive leg and two adjacent massive propagators. We find

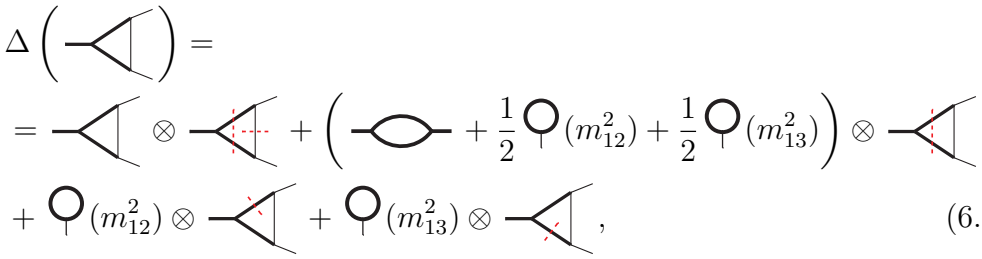

(6.128)

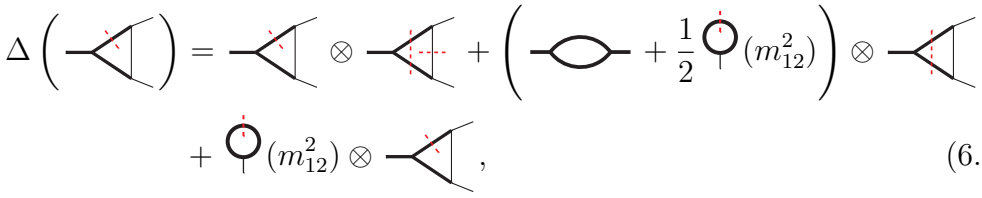

(6.129)

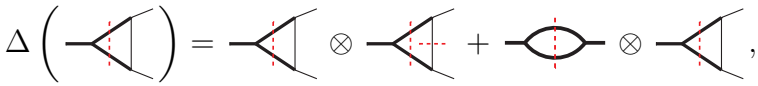

(6.130)

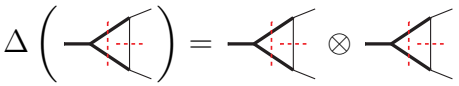

(6.131)

This diagram is interesting because it is the simplest triangle requiring variables as the w_1 and $\bar{w}_1$ defined in eq. (2.33) to get a rational symbol alphabet. Explicit

expressions can be found in section B.1.5. In that sense, it is similar to the bubble with two internal massive propagators. However, it has a very specific feature that we did not encounter in any other triangle: its non-vanishing maximal cut has no interpretation as an iterated discontinuity. This shows the diagrammatic conjecture contains more information than what we would get by simply analysing the discontinuities of Feynman diagrams as we did in chapters 2 and 3.

$I_3(p_1^2, 0, 0; m_{12}^2, m_{23}^2, m_{13}^2)$: As a last example of a triangle with one external massive leg, we look at the case where all internal propagators are massive. We find

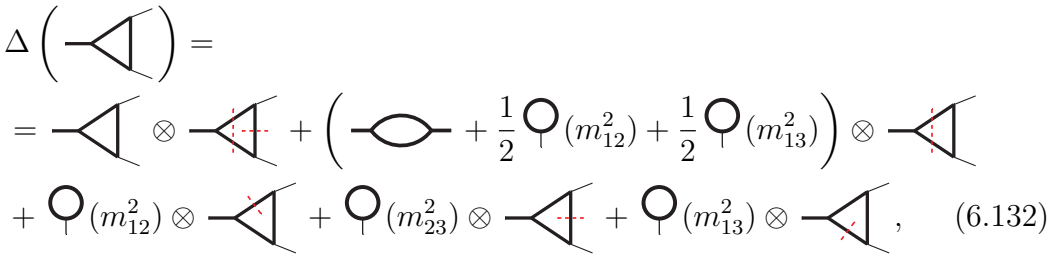

(6.132)

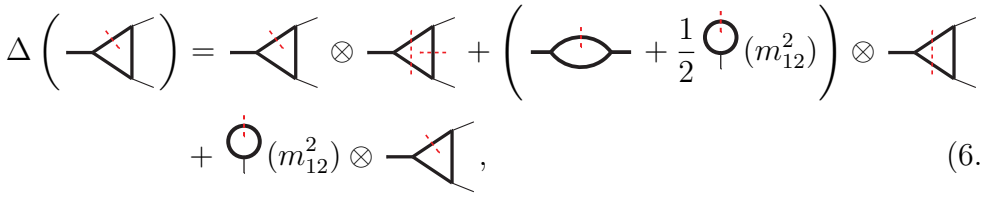

(6.133)

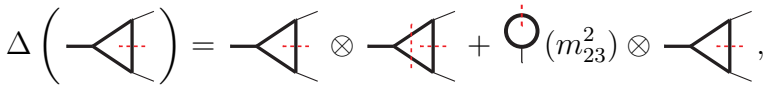

(6.134)

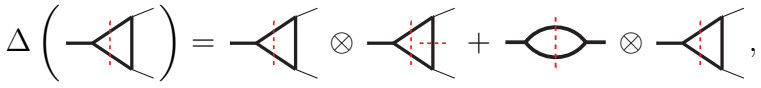

(6.135)

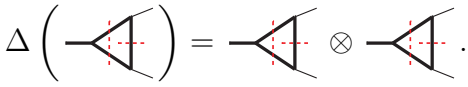

(6.136)

This diagram is included because it is the most general diagram with one external massive leg. Explicit expressions can be found in section B.1.6. All previous examples can be obtained as the massless limit of this case.

$I_3(0, p_2^2, p_3^2; 0, m_{23}^2, 0)$: We now start exploring diagrams with two external massive legs. As a first example, we look at the case with a single internal massive propagator adjacent to the two massive external legs. We find

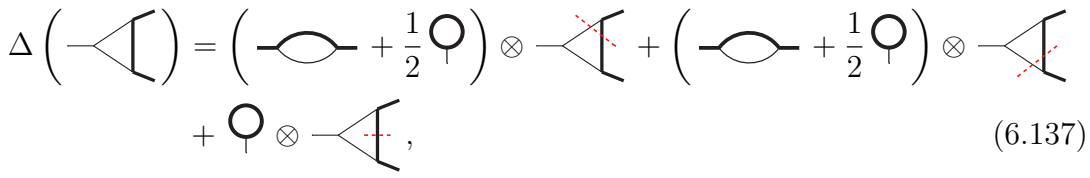

(6.137)

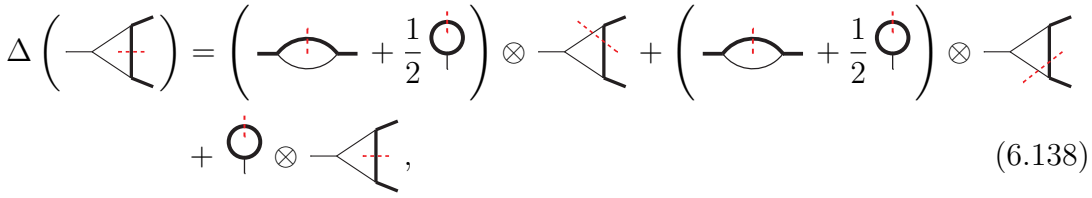

(6.138)

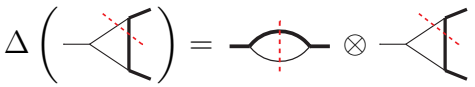

(6.139)

This is the only triangle with one internal massive propagator and two external massive legs that is not finite. Explicit expressions can be found in section B.2.2. It also has a vanishing triple cut: to find the leading singularity we use the same trick as for diagrams with one external massive propagators and extract the normalisation factor by looking at a case with more massive propagators (as the next example). We note the same has to be done for the triangle with two external masses and no massive propagators.

$I_3(0, p_2^2, p_3^2; m_{12}^2, m_{23}^2, 0)$: We then look at the triangle two internal massive legs, where one of the massive propagators is adjacent to the two external massive legs. Explicit expressions for this diagram can be found in the accompanying

`MATHEMATICA` package [38]. We find

Δ 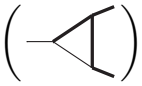 =

= 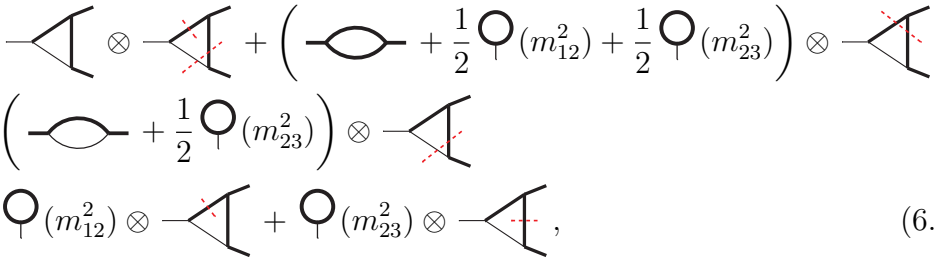

(6.140)

Δ 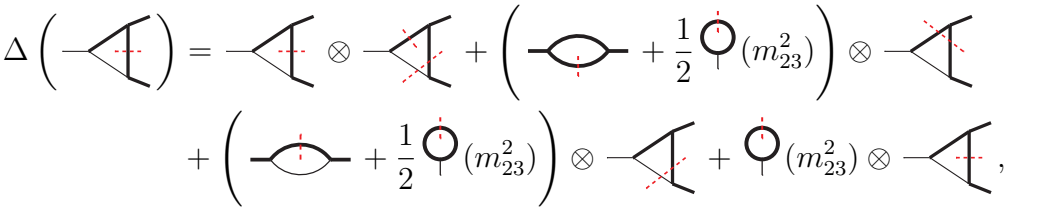

(6.141)

Δ 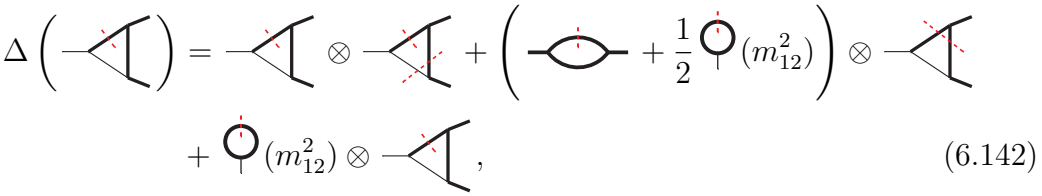

(6.142)

Δ 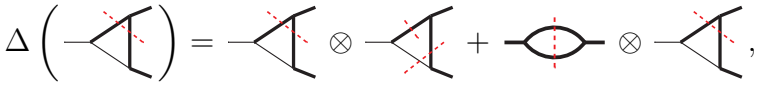

(6.143)

Δ 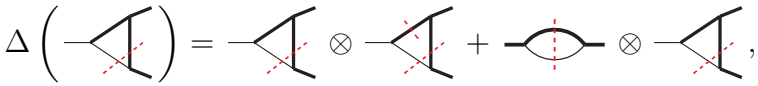

(6.144)

Δ 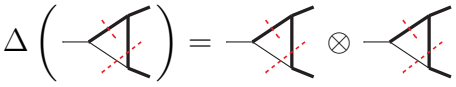

(6.145)

This is the most complicated example we will examine with two-massive external legs. We stress that this diagram evaluates to a rather complicated combination of MPLs [38], and in that sense is a highly non-trivial check of the graphical coproduct we introduce.

We have also analysed the example with two external massive legs and three internal propagators, for which we have found a parametrisation making the symbol alphabet rational. We have not included this example because the functions get rather complicated and do not teach us anything new about the diagrammatic coproduct.

$I_3(p_1^2, p_2^2, p_3^2; 0, 0, 0)$: As a final example of the diagrammatic coproduct for triangles, we examine the triangle with three massive external legs and massless propagators for which explicit expressions can be found in section B.3.1. We find

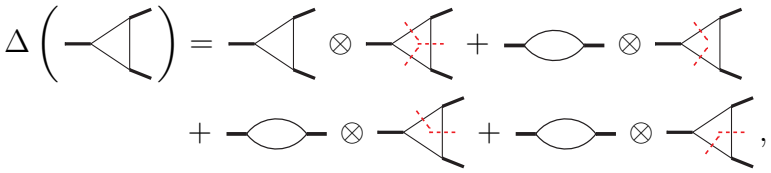

(6.146)

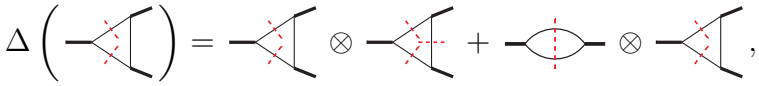

(6.147)

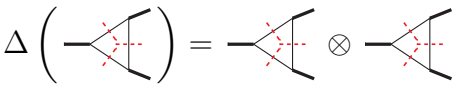

(6.148)

Although by this point it seems a rather trivial example, we could not not include our favourite example. It was also important for us when we started looking at the diagrammatic representation of the coproduct because it was the first example for which we understood the diagrammatic representation of all coproduct components. Finally, it helped us understand how the singularities introduced by bubbles cancel and reproduce the weight $(0, n)$ coproduct components, as we argued in the previous section.

We will not look at diagrams with three external massive legs and any number of massive propagators because they do not teach us anything new. For the cases

with one or two internal masses, we have a parametrisation in terms of which the symbol alphabet is rational, see appendix B.3. For the fully massive case, we did not find such a parametrisation.

$I_4(s,t)$: We now explore box diagrams. We start with the simplest one, the fully massless box. Explicit expressions for this diagram can be found in the accompanying `MATHEMATICA` package [38]. From eq. (6.79), we find

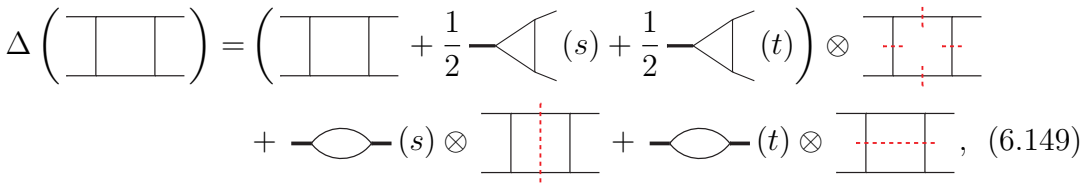

(6.149)

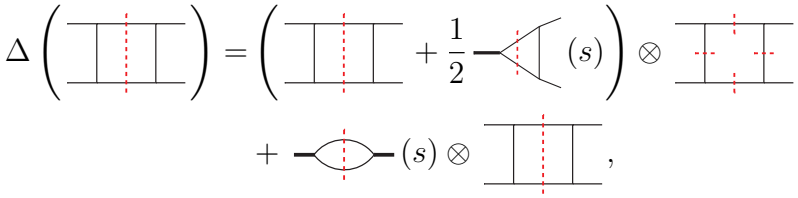

(6.150)

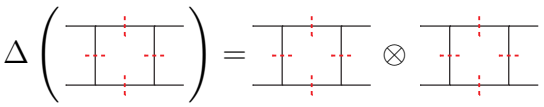

(6.151)

The massless box was important for us to understand that we could not avoid including maximal cuts of boxes. The reason for this is simple to see: had we not included the maximal cut, there would only be bubbles in the leftmost entry of the coproduct, which cannot reproduce the non-trivial analytic structure of the massless box (in particular, the symbol letter $(s+t)$ would never appear in the leftmost entries if that were the case).

This is also the first example were we can see that the first entry corresponding to the quadruple cut is finite, which requires a cancellation between double and single poles of the box and triangles. We recall this is important to ensure only bubbles and tadpoles are singular in the left entry of the diagrammatic coproduct, as this is needed for the components of weight $(0,n)$ to be correctly reproduced.

$I_4^e(s,t;p_1^2,0,p_3^2,0)$ — two-mass-easy: We now look at the simplest of the box topologies with two massive external legs, the two-mass-easy box. Explicit expressions for this diagrams can be found in the accompanying `MATHEMATICA` package [38]. We find

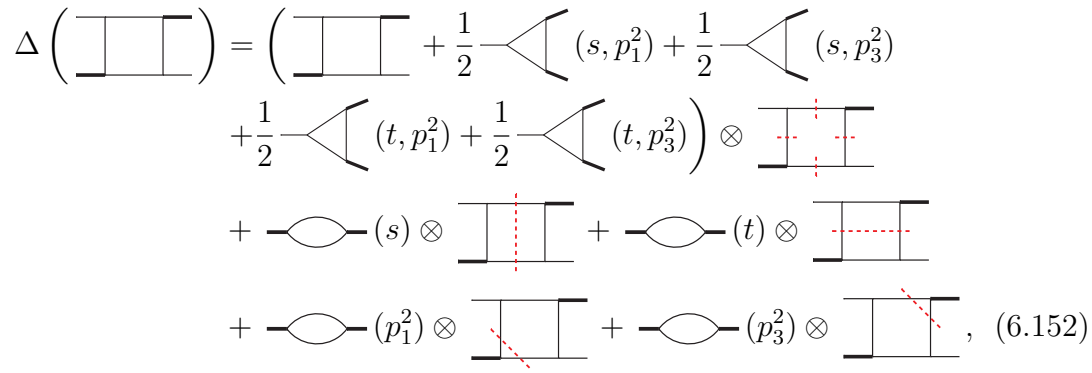

(6.152)

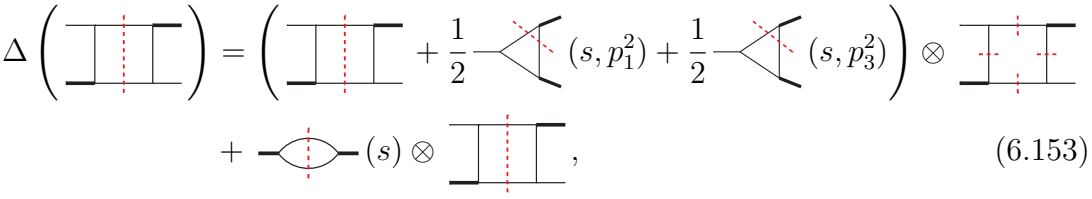

(6.153)

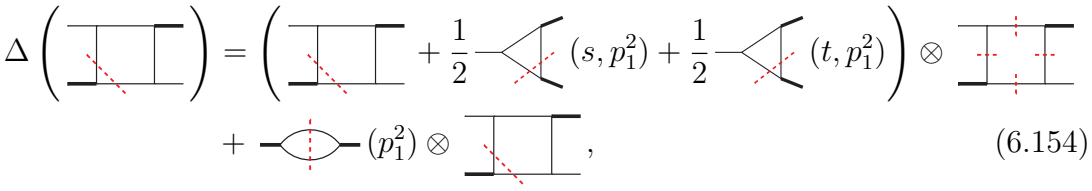

(6.154)

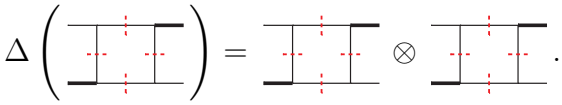

(6.155)

We present this example to contrast it with the following one. Indeed, we know the two-mass-easy box is simpler than the two-mass-hard box, as their names suggest. The reason for this is apparent from the perspective of the diagrammatic coproduct: unlike what happens for the two-mass-hard box, all the single propagator contractions of the two-mass-easy box give rise to simple triangles with two-massive external legs. We know these have a vanishing triple

cut, and therefore all triple cuts of the two-mass-easy box vanish.

As for the fully massless box, we can check the first entry corresponding to the maximal cut of this box is finite because the pole of the box cancels with the poles of the the four different triangles.

To finish, we note that the box with a single external massive leg can be obtained trivially from this example by sending e.g. p_3^2 to zero.

$I_4^h(s,t;p_1^2,p_2^2,0,0)$ — two-mass-hard: We now look at the hardest of the box topologies with two massive external legs, the two-mass-hard box. Explicit expressions for this diagrams can be found in the accompanying `MATHEMATICA` package [38]. We find

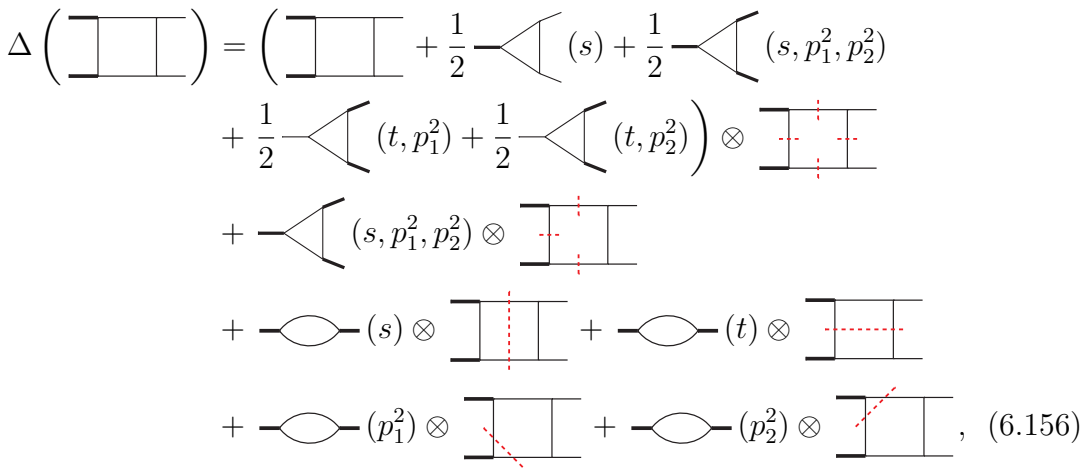

(6.156)

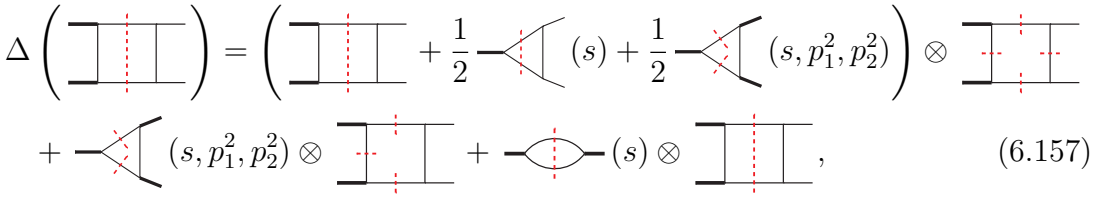

(6.157)

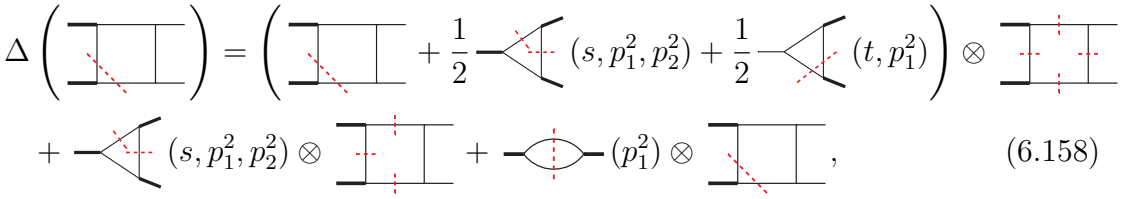

(6.158)

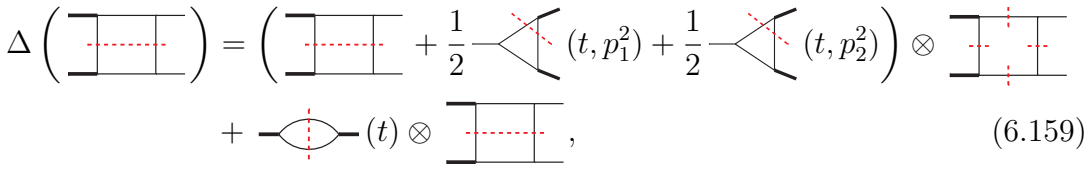

(6.159)

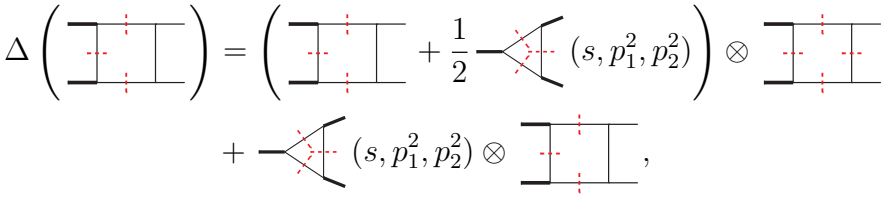

(6.160)

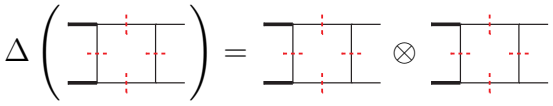

(6.161)

As we mentioned in the previous example, the two-mass-hard box has a more complicated structure. This can be seen by the fact that the contraction of one of its propagators gives rise to a triangle with three external masses, which, in contrast to the one- and two-mass triangles, has a non-vanishing maximal cut, see e.g. eq. (6.146). Related to this three-mass triangle, we also have the corresponding non-vanishing triple cut of the box appearing in the diagrammatic coproduct. Note that the appearance of the three-mass triangle in the coproduct means we expect we will need to use variables like the z and $\bar{z}$ defined in eq. (2.29) to get a rational symbol alphabet.

By looking at the diagrammatic coproduct of this function we can even predict these variables will only be needed at order ϵ^1. Let us apply the general discussion below eq. (6.103) to this particular example. We start by noting that as expected the first entry corresponding to the maximal cut is finite, and will thus only contribute at order ϵ^0. The same is true for the triple cut contribution. This means the order ϵ^{-2} and ϵ^{-1} coefficients of the two-mass-hard box are completely determined by the terms with bubbles in the first entry, and should thus be very simple (i.e., logarithms of (ratios of) invariants). At order ϵ^0, we start to get contributions from the terms with triple and quadruple cuts. However, because of the discussion in section 5.4.2, we know the contribution of the three-mass

triangle must cancel at leading order since it appears both with the triple and the quadruple cuts. We linked the necessity of using the z and $\bar{z}$ variables to the contribution of the three-mass triangle, and we are now seeing this contribution only starts at order ϵ^1. We thus expect only to need those variables starting from that order.

This example was checked up to weight 4, i.e. order ϵ^2, where it is already a rather complicated function [38]. We view this as one of the most important checks of the diagrammatic representation of the coproduct we propose, as it would be very unlikely that it would match by accident in such a complicated example.

This is the most complicated box with no massive propagators we analysed. The box with three external massive legs should be possible to study, but we do not believe it would be of any particular interest compared to the examples we already gave. For the box with four massive external legs we did not find a parametrisation giving a rational alphabet to all orders in ϵ.

$I_4(s,t;0,0,0,0;m_{12}^2,m_{23}^2,0,0)$: As a last example, we look at the box with massless external legs and two adjacent massive propagators. Explicit expressions for this diagrams can be found in the accompanying `MATHEMATICA` package [38]. We find

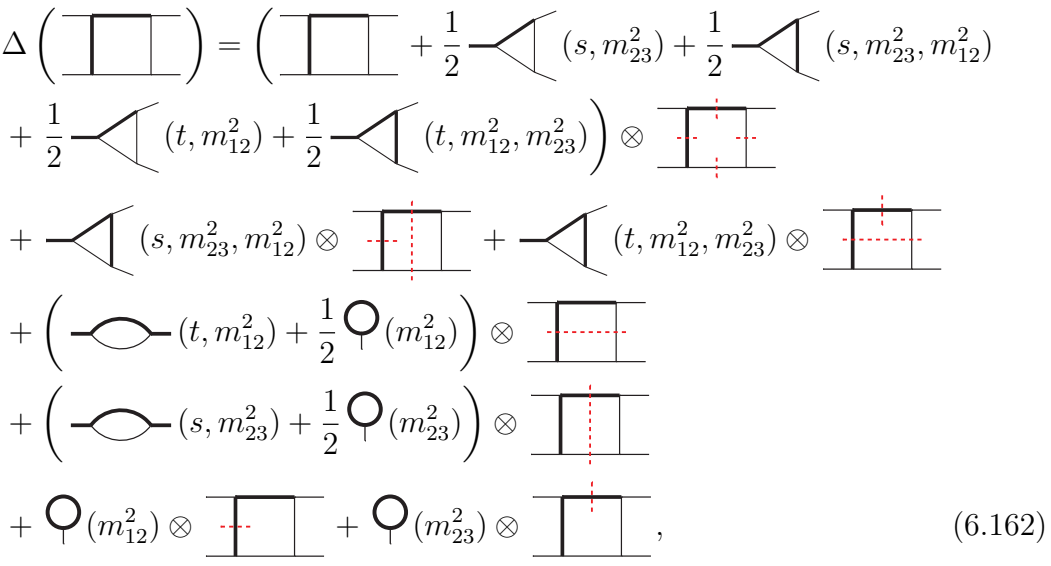

(6.162)

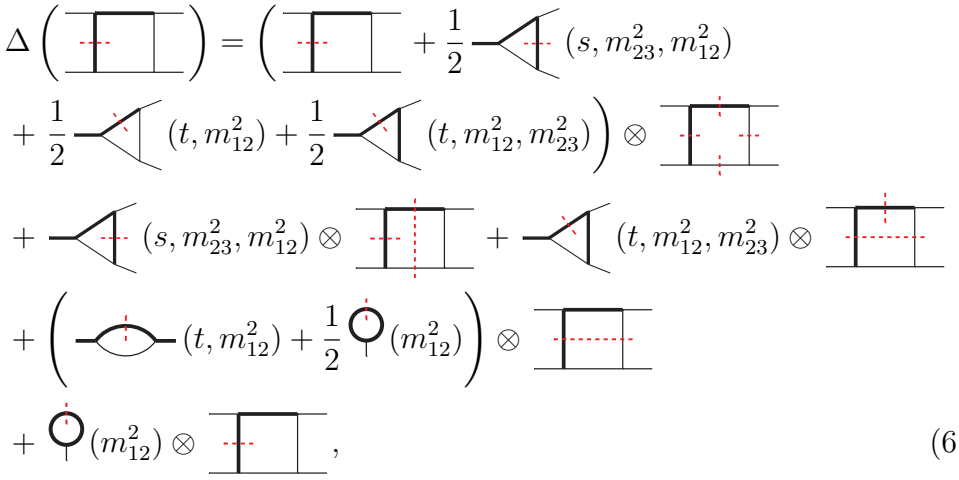

(6.163)

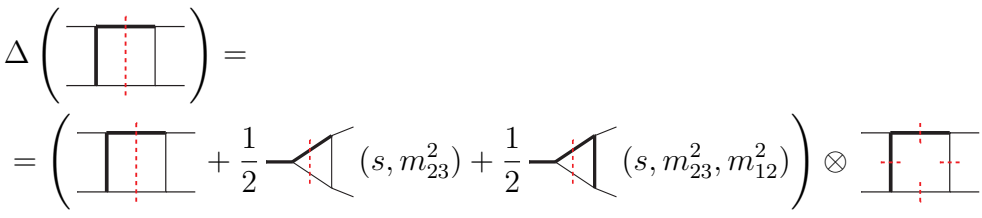

(6.164)

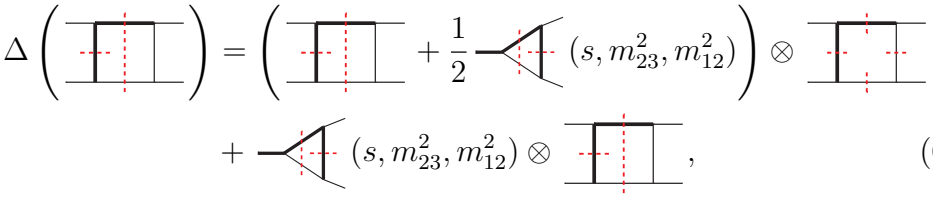

(6.165)

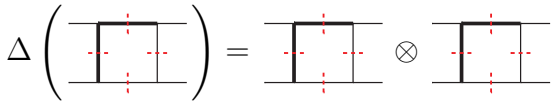

(6.166)

Besides $I_4(s,t;0,0,0,0;m_{12}^2,m_{23}^2,0,0)$, we have also analysed the box with a single internal mass, $I_4(s,t;0,0,0,0;m_{12}^2,0,0,0)$, whose graphical coproduct can be easily obtained by taking $m_{23}^2 \to 0$ in the above expressions. Once again, we explicitly observe all the features we already discussed. The first entry

corresponding to a quadruple cut only contributes at order ϵ^0 because of the cancellation of the poles of the triangles and the box. There are two non-vanishing triple cuts, which only start contributing at order ϵ^1. For this box, we can use (ratios of) invariants as variables to get a rational alphabet, which is consistent with the fact that the triangles appearing with triple cuts do not require more complicated parametrisations.

We believe this example to be important as it checks most of the features of the diagrammatic coproduct we have described up to now. Indeed, it requires dealing with massive and massless propagators, with vanishing and non-vanishing triple cuts and with a non-vanishing quadruple cut, all in the same example. Had we not correctly understood any of these points, or had we made a mistake in computing any of the cut diagrams, we would not have been able to match the coproduct on the two sides of eq. (6.62) for such a complicated case.

Aside from the examples listed here, we explicitly checked the diagrammatic coproduct in the following cases:

- $I_3(p_1^2, 0, 0; m_{12}^2, m_{23}^2, 0)$;
- $I_3(0, p_2^2, p_3^2; m_{12}^2, 0, 0)$;
- $I_3(0, p_2^2, p_3^2; m_{12}^2, 0, m_{13}^2)$;
- $I_4(s, t; p_1^2, 0, 0, 0)$;
- $I_4(s, t; 0, 0, 0, 0; m_{12}^2, 0, 0, 0)$.

As already mentioned, the necessary expressions to perform the checks of all the cases we mentioned can be found in the accompanying `MATHEMATICA` package [38].

6.5 Discontinuities

In the previous sections, we have motivated the existence of a diagrammatic representation of the coproduct of one-loop Feynman diagrams, defined it formally, and given evidence of its validity by explicitly looking at a large selection of examples. We now assume this diagrammatic representation to exist and see what consequences we can draw from it. In particular, in this section we

will review the implications of the diagrammatic coproduct in the study of the discontinuities of Feynman diagrams.

The main tool we will use in this section is the relation between the discontinuity operator and the coproduct, which we recall states that discontinuity operators only act in the first entry of the coproduct, or more formally

$$\Delta \,\mathrm{Disc} = (\mathrm{Disc} \otimes \mathrm{id})\Delta\,. \tag{6.167}$$

We should stress that in this expression Δ is the coproduct acting on functions. However, given our mapping between the graphical coproduct and the coproduct of Feynman integrals, we can easily think of Δ (and Disc) as acting on graphs.

The main conclusion of this section is that the existence of the graphical representation of the coproduct makes the relations between iterated discontinuities, multiple unitarity cuts and the coproduct we developed in chapters 2 and 3 very simple to get.

Before we show this in some examples, let us make a comment on which type of coproduct entries are interesting when studying discontinuities. Because the discontinuity operator acts in the first entry, if we are computing m-iterated discontinuities of a function of weight n, thus getting a weight $n-m$ discontinuity function, the natural type of coproduct entries we are interested in are the ones of weight $(\underbrace{1,\ldots,1}_{m-\text{terms}},n-m)$.

From the perspective of the graphical coproduct, this means that single discontinuities are determined by the diagrams of weight one appearing in the leftmost cofactor, double discontinuities by diagrams of weight two and so on. Furthermore, only diagrams depending on the variables on which we are taking the discontinuity can give a contribution.

This can be illustrated by looking at the three-mass triangle we are very familiar with. We know that the components of weight $(1,n)$ of its coproduct are completely determined by the ϵ^0 coefficient of the bubble contributions in eq. (6.146). In other words,

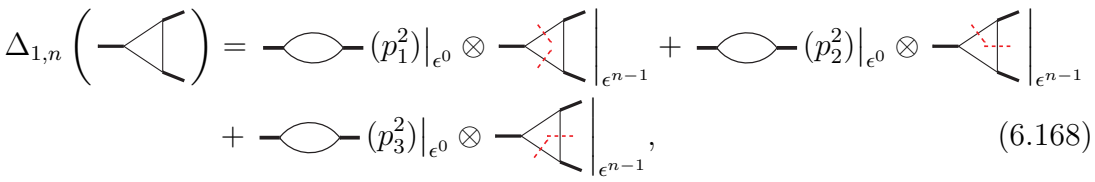

(6.168)

Let's say we are interested in the discontinuity on p_1^2. Of course, we have

$$\text{Disc}_{p_1^2}\left[\quad (p_1^2)\big|_{\epsilon^0}\right] = 2\pi i \tag{6.169}$$

and

$$\text{Disc}_{p_1^2}\left[\quad (p_2^2)\right] = \text{Disc}_{p_1^2}\left[\quad (p_3^2)\right] = 0, \tag{6.170}$$

The right-hand side of eq. (6.169) depends on the normalisation of the diagram, the precise definition of Disc and the $i0$ associated to the invariant. From eq. (6.168) we thus have

$$\text{Disc}_{p_1^2}\left[\quad\right] = 2\pi i \quad , \tag{6.171}$$

which is a function of weight 1. This is exactly the relation we expect between cuts and discontinuities, and we can get the precise relation by following the rules of the chapters 2 and 3.

If we are interested in double discontinuities, we should look at coproduct entries of the form $(1, 1, n)$. Terms of the graphical coproduct with bubbles in the first entry do not contribute because they depend on a single scale, so all double discontinuities are fixed by acting on the ϵ^0 (weight 2) component of the uncut triangle, see eq. (6.146). Using

$$\text{Disc}_{p_1^2,p_2^2}\left[\quad\Big|_{\epsilon^0}\right] = (2\pi i)^2, \tag{6.172}$$

we get

$$\text{Disc}_{p_1^2,p_2^2}\left[\quad\right] = (2\pi i)^2 \quad , \tag{6.173}$$

which is a function of weight 0. This is also the relation we would expect from the discussion of chapter 3.

To finish with this example, we could also have looked at the double discontinuity from another perspective. We know the coproduct of the p_1^2 channel has the diagrammatic representation given in eq. (6.147). Out of the two terms on the right-hand-side, only the first depends on the p_2^2 channel. Instead of acting with the double discontinuity on the uncut triangle, we could thus have computed the discontinuity on p_2^2 of the cut in p_1^2 at order ϵ^0 (which is a weight 1 function)

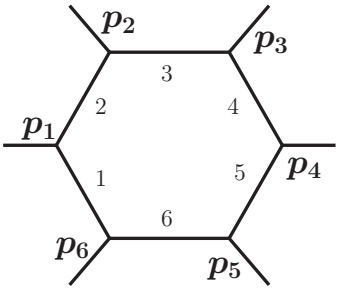

Figure 6.2: Massless hexagon

and got

$$\text{Disc}_{p_2^2}\left[\quad\right]_{\epsilon^0} \sim 2\pi i. \tag{6.174}$$

Combined with the above relation for the p_1^2-discontinuity, this also leads to the expected relation between iterated discontinuities and multiple unitarity cuts.

This same reasoning can be applied to more interesting diagrams such as the boxes. For instance, if we are interested in computing an iterated discontinuity in the s and t-channels in eq. (6.149), it is easy to see that the only contribution would come from the term in the graphical coproduct with the box in the first entry, which is consistent with the (s,t) discontinuity being proportional to the maximal cut.

Instead of going over the same examples we have already studied, we will show how we can use this type of argument to determine the values of cuts we have not computed explicitly. To this end, we consider the fully massless hexagon in $D = 6$ dimensions—see fig. 6.2—which is a weight 3 function. Our goal will be to extract the value of the three and four propagator cuts of this diagram from the knowledge of its symbol. We will then check the results we obtain are consistent with an observation made in [125] on the symbol of this type of Feynman integral, thus giving indirect evidence for the validity of the graphical coproduct in this example.

We start with some notation related to the hexagon. We will use the results and notation introduced in refs. [67, 126]. Instead of the usual momenta p_j, it is convenient to use the so-called dual variables x_j we already used in the

introduction to chapter 5, section 5.1, defined as

$$p_j = x_j - x_{j+1}, \tag{6.175}$$

where indices are defined modulo 6. It is also convenient to define $x_{jk}^2 = (x_j - x_k)^2$. In terms of these variables, we have for instance

$$(p_1 + p_2)^2 = x_{13}^2 \qquad (p_1 + p_2 + p_3)^2 = x_{14}^2 \qquad x_{j,j+1}^2 = p_j^2 = 0. \tag{6.176}$$

Note that we can associate each x_j with an edge of the hexagon and in fig. 6.2 we have numbered the edges consistently with the definition of the x_j. The loop momentum can be defined as $k = x_0 - x_1$, and we then have

$$I_6^{(0)} = \int \frac{d^6 x_0}{i\pi^3} \frac{1}{x_{01}^2 x_{02}^2 x_{03}^2 x_{04}^2 x_{05}^2 x_{06}^2} \tag{6.177}$$

were we have set $\epsilon = 0$ because the integral is finite and we will not study higher orders in ϵ. In the following, we will drop the (0) in superscript.

It is easy to see that $I_6^{(0)}$ is a function of nine variables, which we can choose to be x_{13}^2, x_{14}^2, x_{15}^2, x_{24}^2, x_{25}^2, x_{26}^2, x_{35}^2, x_{36}^2 and x_{46}^2. In exactly six dimensions, this integral is known to be conformally invariant [127], and it can thus only depend on the three-cross ratios

$$u_1 = \frac{x_{15}^2 x_{24}^2}{x_{14}^2 x_{25}^2}, \qquad u_2 = \frac{x_{26}^2 x_{35}^2}{x_{25}^2 x_{36}^2}, \qquad u_3 = \frac{x_{13}^2 x_{46}^2}{x_{14}^2 x_{36}^2}\,. \tag{6.178}$$

This is the reason why setting $\epsilon = 0$ greatly simplifies the discussion of the hexagon (as was the case for the box with four massive legs, see appendix B.4.8).

Following [67], we introduce the quantities

$$f_i = \frac{x^+(1 - x_i^-)}{x^-(1 - x_i^+)}, \quad x_i^\pm = u_i x^\pm, \quad x^\pm = \frac{u_1 + u_2 + u_3 - 1 \pm \sqrt{\Delta_H}}{2u_1 u_2 u_3}\,, \tag{6.179}$$

where

$$\Delta_H = (u_1 + u_2 + u_3 - 1)^2 - 4u_1 u_2 u_3. \tag{6.180}$$

We define H to be the hexagon normalised to its leading singularity:

$$H = x_{14}^2 x_{25}^2 x_{36}^2 \sqrt{\Delta_H} I_6^{(0)}. \tag{6.181}$$

The symbol of H can then be written as

$$\begin{aligned}\mathcal{S}(H) = &- u_1 \otimes u_2 \otimes f_3 - u_1 \otimes u_3 \otimes f_2 + u_1 \otimes (1-u_1) \otimes f_1 f_2 f_3 \\ &- u_2 \otimes u_1 \otimes f_3 - u_2 \otimes u_3 \otimes f_1 + u_2 \otimes (1-u_2) \otimes f_1 f_2 f_3 \\ &- u_3 \otimes u_1 \otimes f_2 - u_3 \otimes u_2 \otimes f_1 + u_3 \otimes (1-u_3) \otimes f_1 f_2 f_3 \,. \end{aligned} \tag{6.182}$$

According to our conjectured diagrammatic coproduct, eq. (6.62), we have

Δ 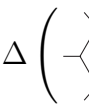 $= \mathfrak{Hex} \otimes \mathcal{C}_6[H] + \sum_{j \in E_H}$ 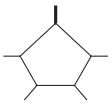 $[\{j\}] \otimes \mathcal{C}_{5,[E_H/\{j\}]}[H]$

$+ \sum_{\substack{j,k \in E_H \\ j<k}} \mathfrak{Box}_{jk} \otimes \mathcal{C}_{4,[E_H/\{j,k\}]}[H]$

$+$  $(x_{13}^2, x_{35}^2, x_{15}^2) \otimes \mathcal{C}_{3,[\{1,3,5\}]}[H] +$  $(x_{24}^2, x_{46}^2, x_{26}^2) \otimes \mathcal{C}_{3,[\{2,4,6\}]}[H]$

$+ \sum_{\substack{j,k \in E_H \\ j<k}}$  $(x_{jk}^2) \otimes \mathcal{C}_{2,[\{j,k\}]}[H]$ (6.183)

where we have introduced some notation to make the expression more compact. $E_H = \{1,2,3,4,5,6\}$ is the set of internal edges of the hexagon. We have defined:

$$\mathfrak{Hex} \equiv$$ 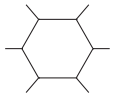 $+ \frac{1}{2} \sum_{j \in E_H}$ 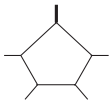 $[\{j\}]$ (6.184)

where

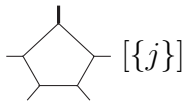 $[\{j\}]$

is the one-mass pentagon obtained by contracting the j-th propagator of the hexagon. Similarly, we defined

$$\mathfrak{Box}_{jk} =$$ 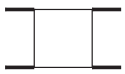 $[\{jk\}] + \frac{1}{2} \sum_{l \in E_H/\{j,k\}}$ 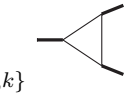 $[\{jkl\}]$ (6.185)

where

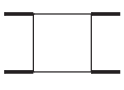 $[\{jk\}]$ and  $[\{jkl\}]$ (6.186)

are the boxes (triangles) obtained by contracting the propagators $\{j,k\}$ ($\{j,k,l\}$)

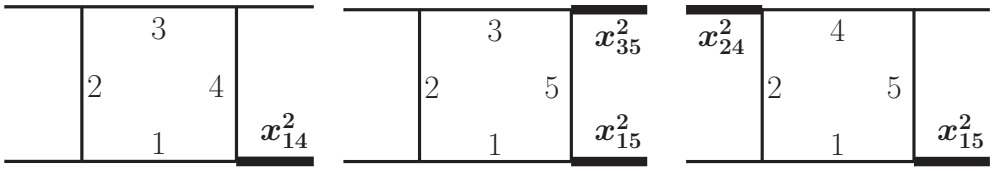

Figure 6.3: Box diagrams corresponding to $\mathfrak{Box}_{56}$, $\mathfrak{Box}_{46}$ and $\mathfrak{Box}_{36}$.

of the hexagon. Several of the external channels of the boxes and triangles will be zero, and we simply used the diagrams above to depict the most general case (see fig. 6.3 for some examples of the boxes that appear).

We note that in eq. (6.183) there are 6 different pentagon contributions, 15 different box contributions (6 one-mass boxes, 6 two-mass-hard boxes and 3 two-mass easy boxes), 2 triangle contributions (from the discussion of section 5.4.1 only two of the three-propagator cuts are non-zero, but there are of course one- and two-mass triangles accompanying the box terms), and 9 non-vanishing bubble contributions (out of the 15 terms appearing in eq. (6.183) six vanish because $x_{j,j+1}^2 = 0$).

Our goal is now to match eqs. (6.182) and (6.183) to extract the values of the three- and four-propagator cuts at leading order in ϵ. These are weight 1 functions, corresponding to a double discontinuity of a weight 3 function, most naturally identified in the $(2,1)$ component of the coproduct of the hexagon. It is easy to see these components correspond to the terms with boxes and triangle contributions in eq. (6.183). Given how discontinuities act on the coproduct, we should be able to determine the values of the cuts by identifying the terms in the first entry that have the correct branch points.

Our plan is the following. From sections 5.5.3, 5.5.4 and 5.5.7 we know that the maximal cuts of boxes with one external massive leg correspond to the coproduct entry $\delta_{s,t}$ of the box, the same is true for two-mass-hard boxes but for two-mass-easy boxes it corresponds to $\delta_{s,st-p_1^2p_3^2}$. For each $\mathfrak{Box}_{jk}$ in eq. (6.183) we should then identify the s and t (or $st - p_1^2p_3^2$) invariants, and then look for the corresponding term in eq. (6.182). We examine one example of each type: $\mathfrak{Box}_{56}$, of the one-mass type, $\mathfrak{Box}_{46}$, of the two-mass-hard type and $\mathfrak{Box}_{36}$, of the two-mass-easy type, see fig. 6.3.

For $\mathfrak{Box}_{56}$, the first diagram in fig. 6.3, we have $s = x_{13}^2$, $t = x_{24}^2$, so we can associate $s \sim u_3$ and $t \sim u_1$. Comparing with eq. (6.182), we then get

$\mathcal{C}_{4,[1234]}[H] = \delta_{u_3,u_1} H = f_2$. Given the $s \leftrightarrow t$ symmetry of the box, we should get the same result when looking at δ_{u_1,u_3}, and that works because $\delta_{u_3,u_1} H = \delta_{u_1,u_3} H$. For all one-mass boxes, this same procedure allows to fix all the corresponding cuts. Note that this case is particularly simple: s and t are always of the form $x_{j,j+2}$ and $x_{k,k+2}$, i.e. they appear only in (the numerator of) one of the u_l, and so can be associated with a single pair (u_j, u_k), $j \neq k$. Finally, given that $x_{j,j+2}$ and $x_{k,k+2}$ appear in the numerator of the cross-ratios, by convention we take the corresponding δ_{u_j,u_k} with positive sign[4]. Going through all the six different one-mass boxes we find

$$\begin{aligned}
&\mathcal{C}_{4,[1234]}[H] = \delta_{u_3,u_1} H = f_2, \quad \mathcal{C}_{4,[1236]}[H] = \delta_{u_2,u_3} H = f_1, \\
&\mathcal{C}_{4,[2345]}[H] = \delta_{u_1,u_2} H = f_3, \quad \mathcal{C}_{4,[3456]}[H] = \delta_{u_2,u_3} H = f_1, \\
&\mathcal{C}_{4,[1456]}[H] = \delta_{u_1,u_3} H = f_2, \quad \mathcal{C}_{4,[1256]}[H] = \delta_{u_1,u_2} H = f_3.
\end{aligned} \tag{6.187}$$

For $\mathfrak{Box}_{46}$—the middle diagram in fig. 6.3—of the two-mass-hard type, $s = x_{13}^2$ and $t = x_{25}^2$. The association with the cross-ratios is slightly more complicated: because t is of the form $x_{j,j+3}^2$ it appears in the denominator of the cross-ratios and thus in two different ones. However, it turns out it never appears in the same cross-ratio as s, which simplifies the analysis a lot. In this particular case, we can have $(s,t) \sim (u_3, u_1)$ or $(s,t) \sim (u_3, u_2)$ because x_{25}^2 appears in both u_1 and u_2, and so, in agreement with the rule of chapters 2 and 3 that one should sum the contributions of symbol letters consistent with a given invariant, we add both contributions. Furthermore, because t appears in the denominator of the cross-ratios we pick up a minus sign. We then get $\mathcal{C}_{4,[1235]}[H] = -f_1 - f_2$. A similar procedure allows to deal with all six two-mass-hard boxes, and we find

$$\begin{aligned}
&\mathcal{C}_{4,[1235]}[H] = -f_1 - f_2, \quad \mathcal{C}_{4,[2346]}[H] = -f_2 - f_3, \\
&\mathcal{C}_{4,[1345]}[H] = -f_1 - f_3, \quad \mathcal{C}_{4,[2456]}[H] = -f_1 - f_2, \\
&\mathcal{C}_{4,[1356]}[H] = -f_2 - f_3, \quad \mathcal{C}_{4,[1246]}[H] = -f_1 - f_3, .
\end{aligned} \tag{6.188}$$

Next, we look at $\mathfrak{Box}_{36}$—the last diagram in fig. 6.3—of the two-mass-easy type. In this case, $s = x_{14}^2$ and $t = x_{25}^2$: they are both of the form $x_{j,j+3}^2$ and so appear in the denominator of the cross-ratios. We would be in trouble if we

[4]This is an arbitrary choice. As long as we are consistent with it, we are only working up to an undetermined overall sign, which is the same for all cuts.

were looking for a δ_{u_j,u_k} as in the two previous cases, because the three cross-ratios depend on either x_{14}^2, x_{25}^2 or both. Luckily, we are looking for terms of the type $\delta_{u_j,1-u_j}$: the condition for the leading singularity of the two-mass-easy box to vanish ($st - p_1^2 p_3^2 = 0$) is equivalent to $u_j = 1$. This makes the analysis quite simple: each of the three two-mass-easy boxes is associated with a single u_j. More specifically, $\mathfrak{Box}_{36}$ is associated with u_1 and so $\mathcal{C}_{4,[1245]}[H] = \delta_{u_1,1-u_1} H = f_1 + f_2 + f_3$. The other two cases give the same result,

$$\mathcal{C}_{4,[1245]}[H] = \text{Cut}_{2356}[H] = \text{Cut}_{1346}[H] = f_1 + f_2 + f_3. \tag{6.189}$$

To complete our analysis, we must look at the three-propagator cuts appearing with the two three-mass triangles in eq. (6.183). Both three-mass triangles only depend on variables of the type $x_{j,j+2}^2$, so the analysis is very simple: they are associated with discontinuities on pairs (u_1, u_2), (u_1, u_3) or (u_2, u_3). We then get

$$\text{Cut}_{135}(H) = \text{Cut}_{246}(H) = f_1 + f_2 + f_3. \tag{6.190}$$

We now claim to have determined all the three and four propagator cuts of the hexagon. However, this assumed the validity of the graphical conjecture, so we would like to have some checks that our results are correct. In ref. [125], it was shown that the $(2,1)$ component of the coproduct of a conformally invariant hexagon was given by the sum of fifteen terms of the form

$$\Delta_{2,1}(H) = \sum_{\substack{j,k \in E_H \\ j<k}} \quad \overset{(jk)}{\square} \otimes \log\left(R_{jk}(H)\right) , \tag{6.191}$$

where the quantities R_{ij} are defined in eq. (7) of [125] (as above, the boxes that appear are not four-mass boxes, but we drew it this way to cover the general case). Unfortunately, the authors only give an explicit expression for the R_{jk} of a hexagon with three non-adjacent massive legs, and present their results in terms of momentum-twistor variables [128–131], which we were not yet able to translate into the variables we are using for the massless hexagon (they should be nothing but a combination of the f_j appearing in eq. (6.182)). Nevertheless, this expression still imposes a constraint on the graphical coproduct of the hexagon: it claims only boxes contribute to the weight $(2,1)$ component of the coproduct

of the hexagon while from eq. (6.183) one would also expect to also have triangle contributions. We can then check if these all cancel in a non-trivial way.

The first thing we can notice is that the contributions of the three-mass triangles cancel. This is easily because these diagrams only appear in four-propagator cuts corresponding to the $\mathfrak{Box}_{jk}$ of the two-mass-hard type and in the first entry of three-propagator cuts. Let us focus on the three-mass triangle with masses x_{13}^2, x_{35}^2 and x_{15}^2. It appears in the first entries of the four-propagator cuts [1235], [1345] and [1356], and in the first entry of the three-propagator cut [135]. From eqs. (6.188) and (6.190), the contribution to eq. (6.183) with this three-mass triangle in the first entry is


$$(x_{13}^2, x_{35}^2, x_{15}^2) \otimes (-(f_1+f_2+f_3)+f_1+f_2+f_3) = 0. \tag{6.192}$$

By the same argument, the contribution of the other three-mass triangle also vanishes. As in the discussion of 5.4.2, we note that the factor of $1/2$ appearing in the diagrammatic coproduct was necessary for this cancellation to occur.

For the other triangle contributions, the situation is not as simple. Indeed, the ϵ-expansions of one- and two-mass triangles give the same type of functions, the square of simple logarithms of the invariants at weight 2. This means contributions from different triangles mix, and we should not check the cancellation of each triangle individually. Instead, we must check the cancellation of terms with a $\log^2(x_{ij}^2)$ in the first entry that come from any of the one- and two-mass triangles appearing in the first entry of eq. (6.183). Going through the algebra, we see that this imposes 10 non-trivial relations between the $R_{jk}(H)$. If we relate them to the quadruple cuts as determined above, all of them are satisfied. This shows the result of [125] is consistent with the diagrammatic coproduct.

We will stop here our discussion about discontinuities and the diagrammatic conjecture. However, we should mention that we have checked that all examples given in chapter 3 to illustrate the relations between Cut, Disc and the coproduct are in agreement with what is dictated by the graphical coproduct of each diagram.

6.6 Differential equations

Throughout this thesis, we discussed many times the relation between discontinuities and the coproduct. However, we never discussed the relation between differential operators and the coproduct, which we had introduced at the same time in eq. (2.21). While discontinuity operators only act in the first entry of the coproduct, differential operators only act in the last entry. More formally,

$$\Delta \frac{\partial}{\partial z} = \left(\mathrm{id} \otimes \frac{\partial}{\partial z}\right) \Delta. \tag{6.193}$$

As a discontinuity operator reduces the weight of a function by one (not counting powers of π), so does a differential operator. For instance, the derivative of a weight one function (a logarithm) is a rational function. We note this is obvious to see from the definition of the MPLs as iterated integrals, eq. (2.2). Computing the derivative of a MPL is thus very simple if its coproduct is known. Let's see how this is done.

The coproduct of a (pure) function F of weight $n+1$ has a component of weight $(n,1)$, which we can generally write as

$$\Delta_{n,1} F = \sum_{a_i \in \mathcal{A}} f_{a_i} \otimes \log(a_i), \tag{6.194}$$

where $\mathcal{A}$ is the symbol alphabet of F, and the cofactors f_{a_i} are weight n functions. Then, the derivative of F is simply given by

$$\frac{\partial}{\partial z} F = \sum_{a_i \in \mathcal{A}} \frac{1}{a_i} \left(\frac{\partial a_i}{\partial z}\right) f_{a_i} \tag{6.195}$$

As a very simple example, we can use eq. (2.13) to compute the derivative of any classical polylogarithm,

$$\frac{\partial}{\partial z} \mathrm{Li}_{n+1} = \frac{1}{z} \mathrm{Li}_n(z), \tag{6.196}$$

which is the well-known differential equation satisfied by classical polylogarithms, which is also obvious from their definition as iterated integrals.

We note the reason why we look at the weight $(n,1)$ component of the coproduct for computing derivatives is the same reason why we looked at the weight $(1,n)$ component of the coproduct for computing discontinuities: once we

act with the differential (discontinuity) operator on the weight 1 cofactor, we obtain a trivial tensor of the form $n \otimes 1$ ($1 \otimes n$ for discontinuities) from which one can read-off the derivative (discontinuity) we are computing. One could of course act on any other non-trivial coproduct entry and coassociativity guarantees we would get the same result. However, reconstructing the function from the non-trivial tensor obtained after acting with the differential (discontinuity) operator would be a complicated task in general.

Since we have a diagrammatic representation of the coproduct of one-loop Feynman integrals, eq. (6.193) should have interesting consequences for the differential equations satisfied by Feynman integrals. This is an interesting subject, given that one of the most powerful modern methods of computing Feynman integrals is by solving differential equations. This method has a long and successful history [59, 77, 78, 80, 132], and has been applied in the calculation of a large variety of physical processes (too large for us to give a complete list of references). Recent reviews can be found in the literature, e.g. [133, 134]. This field has developed a lot in recent years because of the better understanding of the analytic structure of MPLs. For instance, one now knows how to write the differential equation in what is called a canonical basis [59], where they are trivial to solve order by order in the ϵ-expansion in terms of MPLs once the initial condition is known, or in a quasi-finite basis [135] which avoids the introduction of spurious structures that would cancel when combining different contributions.

In this introductory section we will review how the standard method introduced in [80] works through one example, the two-mass bubble. We will then compare it to what we obtain from the graphical coproduct, which will allow us to identify the coefficients of the differential equation as derivatives of cuts. Finally, we will make some comments on the so-called reverse unitarity method [136–138], which allows to use differential equations to compute phase-space integrals.

Differential equations for the two-mass bubble: To get the differential equation satisfied by the two-mass bubble, it is convenient to consider the bubble

topology with general powers of the propagators:

$$I_2(p^2; m_1^2, m_2^2; \nu_1, \nu_2) = \int \frac{d^{2-2\epsilon}k}{i\pi^{1-\epsilon}} \frac{1}{(k^2 - m_1^2)^{\nu_1}} \frac{1}{((k-p)^2 - m_2^2)^{\nu_2}}, \tag{6.197}$$

and we are particularly interested in the case $\nu_1 = \nu_2 = 1$. The reason to keep the exponents general is that taking derivatives is then equivalent to shifting the exponent. Furthermore, by setting one of the ν_i to zero we get a tadpole diagram, and it thus would make sense to consider a system of differential equations including bubbles and tadpoles (we will not do this here as it is not necessary for our discussion). In the following, for simplicity of the expressions we will only keep the ν_i in the arguments of $I_2(p^2; m_1^2, m_2^2; \nu_1, \nu_2) \equiv I_2(\nu_1, \nu_2)$.

We know that the natural variables in terms of which to write the two-mass bubble are the w and $\bar{w}$ variables as defined in eq. (2.33), and are thus looking for the differential equation with respect to those variables. However, when acting on the integrand of eq. (6.197), it is more convenient to take derivatives with respect to p_μ, m_1 and m_2. Let's then relate the differential operators of the two sets of variables

$$\begin{aligned}
p \cdot \partial_p &= 2p^2\, \partial_{p^2} + \frac{2w(1-w)}{w-\bar{w}}\partial_w + \frac{2\bar{w}(\bar{w}-1)}{w-\bar{w}}\partial_{\bar{w}}\,, \\
m_1\, \partial_{m_1} &= 2w\bar{w}\left(\frac{w-1}{w-\bar{w}}\partial_w + \frac{1-\bar{w}}{w-\bar{w}}\partial_{\bar{w}}\right)\,, \\
m_2\, \partial_{m_2} &= 2(1-w)(1-\bar{w})\left(-\frac{w}{w-\bar{w}}\partial_w + \frac{\bar{w}}{w-\bar{w}}\partial_{\bar{w}}\right)\,,
\end{aligned} \tag{6.198}$$

where we use the shorthand $\partial_z \equiv \partial/\partial z$. These relations can be inverted to get

$$\begin{aligned}
p^2\, \partial_{p^2} &= \frac{1}{2}\left(p \cdot \partial_p + m_1\, \partial_{m_1} + m_2\, \partial_{m_2}\right)\,, \\
\partial_w &= \frac{1}{2}\left(\frac{1}{w} m_1\, \partial_{m_1} + \frac{1}{w-1} m_2\, \partial_{m_2}\right)\,, \\
\partial_{\bar{w}} &= \frac{1}{2}\left(\frac{1}{\bar{w}} m_1\, \partial_{m_1} + \frac{1}{\bar{w}-1} m_2\, \partial_{m_2}\right)\,.
\end{aligned} \tag{6.199}$$

The first equation is the so-called dilation operator, which measures the dimensionality of the integral. Aside from being a check on the calculation, it does not lead to any interesting differential equation so we will not consider it further.

We are thus left with two differential operators to study ∂_w and $\partial_{\bar{w}}$. Acting with ∂_w on eq. (6.197) with $\nu_1 = \nu_2 = 1$ and after some algebra, we find

$$\partial_w I_2(1,1) = p^2 \left((\bar{w}-1)I_2(1,2) + \bar{w} I_2(2,1)\right), \tag{6.200}$$

where we only wrote the values of the ν_i in the arguments of I_2. For $\partial_{\bar{w}}$, we find

$$\partial_{\bar{w}} I_2(1,1) = p^2 \left((w-1)I_2(1,2) + w I_2(2,1)\right). \tag{6.201}$$

We must now deal with $I_2(1,2)$ and $I_2(2,1)$. These integrals are related to bubbles by a shift in the exponent. It is well known that there are relations between integrals with different powers of the propagators, known as integration-by-parts identities (IBP), first introduced in [58]. These identities are obtained by noting that in dimensional regularisation

$$\int d^D k \frac{\partial}{\partial k^\mu} i(k_\mu, m_i^2, p_i) = 0, \tag{6.202}$$

where $i(k_\mu, m_i^2, p_i)$ is the integrand of some Feynman integral. Using these relations, which also contain the Lorentz-invariance identities [80], we get a recursion between integrals with different powers of the propagators, which can be solved in terms of a chosen basis [139]. It is a non-trivial result that this can always be done. For the bubble topology the recursion can be solved by hand, but in general one would use one of the available computer implementations of these methods like `FIRE` [140, 141] or `REDUZE` [142]. In our concrete case, we choose the basis to be the tadpole and the bubble with unit powers of the propagators. We then find

$$\begin{aligned} I_2(1,2) =& \frac{2\epsilon}{(p^2)^2(w-\bar{w})^2}\left(\frac{2w\bar{w}-w-\bar{w}}{2(1-w)(1-\bar{w})} I_2(0,1) - I_2(1,0)\right) \\ &+ \frac{(1+2\epsilon)(w+\bar{w})}{p^2(w-\bar{w})^2} I_2(1,1) \end{aligned} \tag{6.203}$$

and

$$\begin{aligned} I_2(2,1) =& \frac{2\epsilon}{(p^2)^2(w-\bar{w})^2}\left(\frac{2w\bar{w}-w-\bar{w}}{2w\bar{w}} I_2(1,0) - I_2(0,1)\right) \\ &- \frac{(1+2\epsilon)(w+\bar{w}-2)}{p^2(w-\bar{w})^2} I_2(1,1). \end{aligned} \tag{6.204}$$

The differential equations can now be written in terms of tadpoles and bubbles. We find

$$\begin{aligned}\partial_w I_2(1,1) &= \frac{\epsilon}{p^2(w-\bar{w})}\left(\frac{I_2(1,0)}{w}+\frac{I_2(0,1)}{1-w}\right)-\frac{1+2\epsilon}{w-\bar{w}}I_2(1,1)\\ \partial_{\bar{w}} I_2(1,1) &= -\frac{\epsilon}{p^2(w-\bar{w})}\left(\frac{I_2(1,0)}{\bar{w}}+\frac{I_2(0,1)}{1-\bar{w}}\right)+\frac{1+2\epsilon}{w-\bar{w}}I_2(1,1),\end{aligned} \tag{6.205}$$

which are symmetric under $w \leftrightarrow \bar{w}$ as they should be given the symmetry of $I_2(1,1)$ under this exchange.

We have thus written the differential equations in terms of simpler diagrams, which we assume have already been computed. Solving the system requires finding an initial condition which is in general not a trivial problem. However, we will not go into that direction as it would take us too far away from the subject of this thesis.

Although valid for a relatively simple example, eq. (6.205) has the general structure of the differential equation of any one-loop diagram. Schematically, it is of the form

$$\partial_z I_n = \sum_i^n \sum_j c_{i,j}\left(\epsilon;\{p_l^2\};\{m_l^2\}\right) I_i^j \tag{6.206}$$

where the sum on i runs over the basis of one-loop Feynman integrals (which we choose to be the integrals I_n with unit power of the propagators as defined in eq. (5.9)[5]) and the sum on j over different types of diagrams with the same number of propagators. For instance, in the differential equations of the two-mass bubble, eq. (6.205), i runs over bubbles and tadpoles, and for 'i =tadpole' j runs over the two different tadpoles. The coefficients $c_{i,j}\left(\epsilon;\{p_i^2\};\{m_i^2\}\right)$ depend trivially on the dimensional regularisation parameter, and are in general algebraic functions of the kinematic invariants. As illustrated by the bubble example above, they are rational in the parametrisation giving a rational symbol alphabet (indeed, they are the derivatives of the logarithm of symbol letters, as we will see shortly).

In the following, we will see how differential equations can be very easily obtained from the diagrammatic coproduct, without needing the intermediate steps of eqs. (6.200), (6.201), (6.203) and (6.204). Not needing to solve IBP identities is particularly interesting, as this is usually a very computer-intensive

[5]We not proven these form a basis for one-loop integrals, but are currently working on this proof.

process. We will also show that the coefficients $c_{i,j}\left(\epsilon;\{p_i^2\};\{m_i^2\}\right)$ are nothing but derivatives of cuts, which we think is a beautiful result.

6.6.1 Cuts and coefficients of differential equations

We now discuss the differential equations of Feynman diagrams from the perspective of the diagrammatic representation of the coproduct. We already know how to get a differential equation once the coproduct of a function is known, so we can apply the same idea to Feynman diagrams. We will illustrate the procedure by deriving the differential equation for the bubble, and then comment on the general case.

We start by rewriting the graphical coproduct of the two-mass bubble, but we arrange the terms according to the first entries and not the second entries as we did in eqs. (6.48) and (6.72),

Δ 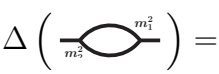 = 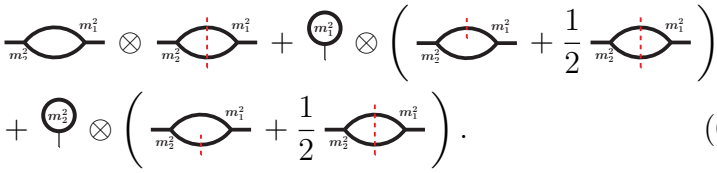

(6.207)

We know the natural coproduct components to consider when computing derivatives are the ones of the form $(n,1)$. This means we should look at the coefficients of weight one in the expansion of the cut diagrams. Because these are weight 0 functions if one counts the weight of ϵ (they are single discontinuities of a weight one function), we should look at the coefficient of the order ϵ^1 of the Laurent expansion of the cuts.

From eq. (6.193), we thus have

∂_w 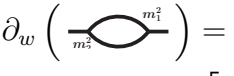 =

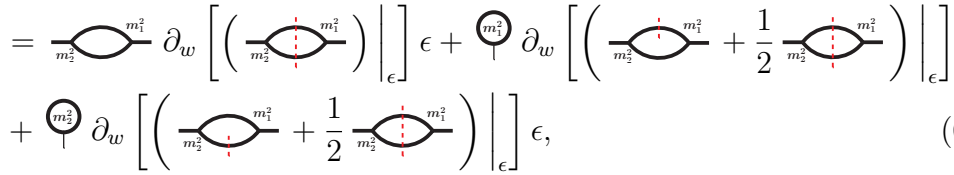

(6.208)

and similarly for $\bar{w}$. We stress this equation is valid *to all orders in* ϵ. This means the differential equation is determined to all orders in ϵ by the first order in the ϵ expansion of the cuts.

We can compute the derivatives of the cuts—see eqs. (6.44), (6.45) and (6.46)—and find

$$\partial_w \left[\left(\; \right) \Big|_\epsilon \right] = -\frac{2}{w-\bar{w}}, \qquad \partial_{\bar{w}} \left[\left(\; \right) \Big|_\epsilon \right] = \frac{2}{w-\bar{w}},$$

$$\partial_w \left[\left(\; + \frac{1}{2} \; \right) \Big|_\epsilon \right] = -\frac{1}{2w},$$

$$\partial_{\bar{w}} \left[\left(\; + \frac{1}{2} \; \right) \Big|_\epsilon \right] = \frac{1}{2\bar{w}},$$

$$\partial_w \left[\left(\; + \frac{1}{2} \; \right) \Big|_\epsilon \right] = -\frac{1}{2(1-w)},$$

$$\partial_{\bar{w}} \left[\left(\; + \frac{1}{2} \; \right) \Big|_\epsilon \right] = \frac{1}{2(1-\bar{w})}. \tag{6.209}$$

These coefficients are antisymmetric under $w \leftrightarrow \bar{w}$ because the diagrams are all normalised to the leading order of the two-propagator cut, which is antisymmetric under this exchange.

The differential equations as obtained from the diagrammatic conjecture are thus

$$\partial_w \left(\; \right) = -\frac{2\epsilon}{w-\bar{w}} \; - \frac{\epsilon}{2w} \; - \frac{\epsilon}{2(1-w)} \; ,$$

$$\partial_{\bar{w}} \left(\; \right) = \frac{2\epsilon}{w-\bar{w}} \; + \frac{\epsilon}{2\bar{w}} \; + \frac{\epsilon}{2(1-\bar{w})} \; . \tag{6.210}$$

To compare these equations with the result obtained through more standard methods—see eq. (6.205)—we must use that

$$I_2(p^2; m_1^2, m_2^2; 1, 1) = \frac{2}{p^2(w-\bar{w})} \; , \tag{6.211}$$

which means

$$\partial_w I_2(p^2; m_1^2, m_2^2; 1, 1) = -\frac{1}{w-\bar{w}} I_2(p^2; m_1^2, m_2^2; 1, 1) + \frac{2}{p^2(w-\bar{w})} \partial_w \; , \tag{6.212}$$

and similarly for $\bar{w}$. We then see the differential equations obtained through the two procedures agree.

This example illustrates how one gets differential equations from the knowl-

edge of the diagrammatic coproduct. This also shows that the coefficients in the differential equations are completely determined by the cuts of the function, as in eq. (6.208).

Of course, what we observe in this example is completely generalisable to other cases. The differential equation is obtained by taking the derivative of the weight one coefficients in the ϵ expansion of their cuts. In the example of the bubble, this meant the coefficients of $\mathcal{O}(\epsilon)$ for all cuts. For triangles and boxes, which are weight two functions, this means we should take the derivatives of the $\mathcal{O}(\epsilon^0)$ coefficient of one- and two-propagator cuts, but the $\mathcal{O}(\epsilon)$ coefficient of three- and four-propagator cuts. For pentagons and hexagons, an interesting thing happens: they are finite functions of weight 3, which means their one- and two-propagator cuts are finite functions of weight 2, with no weight one coefficients in their ϵ-expansion. This means these cuts do not contribute to the weight $(n, 1)$ coproduct components, and hence do not contribute to the differential equations.

By the same argument, we can say that for a general (finite) one-loop diagram with n propagators, n even, all coefficients of the differential equations are determined by the n-, $(n-1)$-, $(n-2)$- and $(n-3)$-propagator cuts, taken at order ϵ for the first two cases, and order ϵ^0 for the last two cases. For n odd, there is one less contribution (the $(n-3)$-propagator no longer has the required weight).

We also conclude that the homogeneous term in the differential equation is determined by the derivative of the order ϵ coefficient of the maximal cut. This is in agreement with the fact that the homogeneous term is proportional to ϵ, which makes it easier to solve the equations order by order in ϵ [59, 134]. The discussion in 5.4.1 then implies that the only one-loop diagrams which might not have an homogeneous term are triangles. Indeed, they are the only non-trivial diagrams that can have a vanishing maximal cut.

This observation allows us to make another consistency check of the validity of the diagrammatic coproduct and of the cut rules presented in chapter 5. In section 5.5.8 we computed the maximal cut of the fully massless pentagon, and showed it was non-zero. According to our discussion above, this should imply that the differential equation of the pentagon has an homogeneous term. We thus went through the exercise of getting the differential equation for the massless pentagon

through standard methods[6], and it does indeed have a homogeneous term.

We finish with two comments. First we note that unlike for discontinuities which were defined only modulo π, one does not lose any information when obtaining the differential equation from the coproduct. Indeed, because the differential operators clip-off the last entry of the coproduct and keep the first entry, the relations one obtains are equalities at the function level, where all ζ-values and powers of π are correctly accounted for[7]. Second, because the symbol alphabet of cut integrals is a subset of the alphabet of the uncut function, the coefficients of differential equations are derivatives of logarithms of symbol letters. If one has found a rational parametrisation of the symbol alphabet, as discussed in section 2.2.3, the coefficients of the differential equations should also be rational functions in those variables.

We have verified for all cases on which we explicitly checked the validity of the graphical coproduct that the differential equations obtained through the method described here give the correct result.

6.6.2 Reverse unitarity

We finish the discussion of differential equations through the perspective of the graphical coproduct by commenting on its implications in the so-called reverse unitarity method [136–138]. We note reverse unitarity was fundamental in the recent calculation of the Higgs production by gluon fusion at three-loops [1].

In an nutshell, this method aims at using tools developed in the calculation of loop integrals (i.e., virtual contributions to a cross-section), in particular the differential equation method, for the calculation of phase-space integrals which appear in the (real) radiative corrections to inclusive cross-sections. The basic idea is that the phase-space integral can be seen as the unitarity cut of a loop amplitude, in the spirit of the optical theorem. For instance, the phase-space integral in a $2\to2$ scattering is closely connected to the integral appearing in the cut on the s-channel of a box.

The argument allowing to use the tools developed for uncut integrals is that cut Feynman integrals (i.e., phase-space integrals) should obey the same

[6] We do not write it explicitly because it is a rather long expression which we will not exploit any further than the comment made here.

[7] Given that it has been a long while since we first mentioned this, we recall factors of π and ζ_n with n even can only appear in the first entry of the coproduct of MPLs, see section 2.2.

differential equations as uncut Feynman integrals, once the contributions of basis integrals that do not have any of the cut propagators have been discarded. One can then use the standard methods of obtaining the differential equations for uncut Feynman integrals, and from this equation read-off the differential equation one needs to compute the cut (phase-space) integral[8].

For instance one could get the differential equation of the box to read the differential equation satisfied by the phase-space integral necessary for $2 \to 2$ scattering. Using the method of the previous section, we get

∂_r 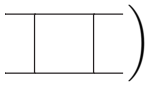 = (6.213)

$= -\frac{1}{r}$ 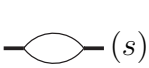 $(s) + \epsilon \left(\frac{1}{1+r} - \frac{1}{r}\right)$ 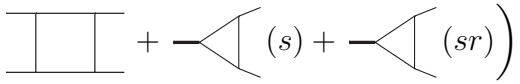

where $r = s/t$, and we would then conclude that

∂_r 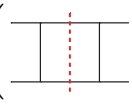 $= -\frac{1}{r}$ 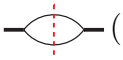 $(s) + \epsilon \left(\frac{1}{1+r} - \frac{1}{r}\right)$ 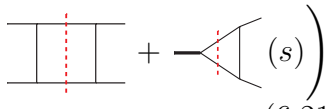 . (6.214)

In the spirit of the optical theorem, the cut going through the propagators could then be thought of as the separation between the amplitude and its complex conjugate, and the cut box would be the matrix element squared of a $2 \to 2$ scattering.

We note eq. (6.213) illustrates the comment we made in the previous section about the homogeneous term of the differential equation of the box being proportional to ϵ but not the bubble contributions, which come from two-propagator cuts.

From the perspective of the graphical coproduct and differential equations, reverse unitarity is a straightforward consequence of the coassociativity of the coproduct which, we recall, fixed the graphical coproduct of cut diagrams based on that of the uncut ones. The fact that the form of the differential equation is the same for cut and uncut diagrams is a simple consequence of the fact that the last entries of the graphical coproduct are the same for cut or uncut diagrams.

[8]We should note that the idea of using cuts or discontinuities to extract the values of complicated phase-space integrals was already used in [102].

For instance, eq. (6.214) is obtained from eq. (6.150) in exactly the same way that eq. (6.213) is obtained from eq. (6.149).

However, from the perspective of the diagrammatic coproduct, 'phase-space-like' cuts are not special in any way: the differential equation of any type of cut has the same property that it is easily obtained from the differential equation of the uncut integral, because its coproduct must be consistent with that of the uncut function. Following the spirit of reverse unitarity, this could provide a differential equation for non-trivial integrals which are hard to evaluate through other methods.

Finally, let us look at the differential equation of maximal cuts. We know the coproduct of a maximal cut has only one term,

$$\Delta\left(\frac{\mathcal{C}_n[I_n]}{\mathrm{LS}[I_n]}\right) = \frac{\mathcal{C}_n[I_n]}{\mathrm{LS}[I_n]} \otimes \frac{\mathcal{C}_n[I_n]}{\mathrm{LS}[I_n]}. \tag{6.215}$$

As explained above, $\mathcal{C}_n[I_n]$ is of weight 0 so one must go to the first order in its ϵ-expansion to get a weight one coefficient. The differential equation satisfied by the maximal cut is then

$$\partial_z\left(\frac{\mathcal{C}_n[I_n]}{\mathrm{LS}[I_n]}\right) = \epsilon\,\partial_z\left(\frac{\mathcal{C}_n[I_n]}{\mathrm{LS}[I_n]}\right)\frac{\mathcal{C}_n[I_n]}{\mathrm{LS}[I_n]}. \tag{6.216}$$

This equation is trivial to solve, and is consistent with the functional form of maximal cuts discussed in 5.4.3.

6.7 Summary and discussion

In this chapter we introduced a completely diagrammatic representation of the coproduct of one-loop scalar Feynman diagrams.

We started by explaining how we arrived at the diagrammatic coproduct in a few simple examples, the bubbles with zero, one or two internal masses. Although simple, the diagrammatic coproduct of these examples—see eqs. (6.8), (6.37) and (6.48)—already have many of the features of the general case.

Having introduced the idea of the diagrammatic coproduct through these simple examples, we then formulated it more generally. In section 6.3 we defined Feynman graphs as purely graphical objects, and in eq. (6.62) defined an algebra morphism on the $\mathbb{Q}$-algebra generated by these objects which we then proved

behaves as a coproduct. We did not show how one can define a full Hopf algebra on Feynman graphs but this will be presented in a separate paper. We finished by explicitly showing how eq. (6.62) looks for diagrams with up to four internal edges, cut or uncut. We observed this reproduced the expected results for bubbles and tadpoles.

We then showed how one could trivially map the coproduct on Feynman graphs to the coproduct of MPLs. Using eq. (6.62), we thus had a diagrammatic representation for the coproduct of Feynman integrals. We made the non-trivial observation that the relations obtained from eq. (6.62) are valid in dimensional regularisation, and explicitly verified that the coproduct of a variety of non-trivial one-loop diagrams with up to four external legs, divergent or finite, was correctly reproduced. We note that this is true despite the fact that some divergences are related to the ultraviolet (for tadpoles), while others are related to the infrared (for bubbles, triangles and boxes). These checks were performed using the results for the cut diagrams computed according to the definition introduced in chapter 5. They thus provide a check of the results presented in both chapters 5 and 6. We also noted that our observations made in section 5.4 about which cuts can vanish, how next-to-maximal cuts and maximal cuts are related in diagrams with an even number of propagators, and about the general functional form of maximal cuts were all consistent with the diagrammatic coproduct, and indeed necessary for it to be valid.

We then studied some consequences of the diagrammatic coproduct of Feynman diagrams. First, we explored the implications for the study of their discontinuities. We saw all the results we obtained in chapters 2 and 3 were trivially contained in the graphical coproduct. Then we showed how the diagrammatic coproduct could be used to determine the value of specific cuts without doing any calculation in a very non-trivial example, the massless hexagon. By interpreting its symbol from the perspective of its graphical coproduct, we identified all its three- and four-propagator cuts. We then checked our results by showing that they confirmed a relation obtained by different arguments in [125].

Finally, we explored the consequences of the graphical coproduct for the differential equations satisfied by Feynman diagrams. We showed that the coefficients of the differential equation of a given diagram, valid to all orders in ϵ, can be obtained by computing the derivative of the weight one coefficient of

the ϵ-expansion of its cuts. In an example, we showed that through this method we obtain the same results as when following the standard procedure to derive differential equations of Feynman integrals, without requiring the use of IBP identities. The validity of the method was also checked for the other diagrams for which the diagrammatic coproduct was explicitly checked [38]. We then noted that the so-called reverse unitarity method was a straightforward consequence of the coassociativity of the coproduct, which completely fixes the diagrammatic coproduct of cut Feynman diagrams, and thus their differential equations. We also noted this procedure can be extended to cuts that do not have an interpretation as phase-space integrals.

It is clear what the next steps should be in the study of the graphical coproduct of Feynman integrals. While we believe we completely understand its structure for one-loop diagrams, many new questions appear at two-loops and beyond. First, it is well known that elliptic integrals appear at two-loops. While this is not a problem in itself for the graphical coproduct, it poses an issue in the mapping between the graphical coproduct and the coproduct on Feynman integrals, because a generalisation of the coproduct of MPLs to elliptic functions is not known, although some interesting progress in that direction has recently been made [35]. Second, even if we restrict ourselves to the case of diagrams that evaluate to MPLs, it is not obvious what a suitable basis would be.

Nevertheless, we are confident that such a construction can be extended beyond one-loop. Indeed, our initial motivations to study this problem, such as the Landau conditions, the first-entry condition or the relation between the coproduct and the discontinuity operator are independent of the loop order. Furthermore, as already mentioned in the introduction, we are aware of some recent work by Francis Brown which seems to be encouraging for this project.

Chapter 7

Conclusions

We now summarise the work presented in this thesis. Given that we have already included a summary and discussion for each chapter, we will be brief.

In chapter 2, we introduced multiple polylogarithms (MPLs), a class of transcendental functions that played a central role in this thesis, as we focused on Feynman integrals that evaluate to this class of functions. We defined some important tools such as the coproduct of the Hopf algebra of MPLs and its maximal iteration, the symbol. Finally, we introduced some important concepts like pure functions, Feynman integrals of uniform weight and the symbol alphabet. All these are very useful tools to describe the analytic structure of Feynman integrals.

We then discussed the discontinuities of Feynman integrals. For that, we defined an operator Disc which evaluates discontinuities across branch cuts of Feynman integrals associated with kinematic invariants, be they internal masses or massive external channels. This operator was trivially generalised to allow the evaluation of iterated discontinuities. We defined a kinematic region where we are away from any discontinuities, the so-called euclidean region. By moving away from this region in a well defined manner, we single out branch cuts associated with specific kinematic invariants.

The coproduct of MPLs is an ideal tool to study the discontinuities of MPLs, and thus the discontinuities of Feynman integrals evaluating to MPLs. We established precise relations between the (k iteration of the) operator Disc and an operator δ which truncates coproduct entries of the form $(\underbrace{1,\ldots,1}_{k},n-k)$. We

made these relations more concrete by explicitly deriving the relations for three-point Feynman diagrams with three-external masses and massless propagators.

In chapter 3, we proceeded with the study of discontinuities of Feynman integrals by giving them a diagrammatic representation. These are the well known unitarity cuts of Feynman diagrams. Rules to define diagrams that reproduce single discontinuities had been established a long time ago, but we generalised them to allow for multiple unitarity cuts. We also introduced a new type of cut, a single propagator cut, that reproduces the discontinuity associated with internal masses. The rules we developed are formulated strictly in real kinematics, and valid in dimensional regularisation. We then obtained a precise relation between unitarity cuts of Feynman diagrams (Cut), discontinuities across branch cuts (Disc), and specific truncations of the coproduct tensor (δ). Through these relations, we obtained a diagrammatic representation of specific coproduct entries.

To evaluate cut diagrams, we had to develop our own computational techniques as the calculation of this type of diagrams is far less developed than that of uncut Feynman integrals. We believe these techniques to be an important part of the work presented here, with possible applications in the calculation of other types of integrals, like e.g. phase-space integrals. Our conjectured relations between Cut, Disc and δ were then verified in a wide variety of examples: one-loop triangles with different configurations of external and internal masses, box diagrams, and a two-loop example, the three-point three-mass two-loop ladder diagram with massless propagators.

We found the exploration of the two-loop diagram to be a particularly interesting example, with features we had not anticipated. For instance, despite the uncut diagram being finite, individual cuts contributing to a given unitarity cut are divergent. Of course, the unitarity cut itself must be finite, as it corresponds to the discontinuity of a finite function. We observed that the cancellation of the singularities occurs in a way very similar to the cancellation of the singularities between real and virtual contributions to a physical cross-section. We believe this type of relation to be new and useful for the general program of the study of infrared singularities.

In this chapter, we also observed that not all coproduct entries could be captured by the unitarity cuts as we had defined them. Perhaps the most striking

example is the two-loop diagram: this is a weight four function, but by our rules we were limited to a series of two unitarity cuts, which means we could not go deeper in the coproduct than the entries of the form $\Delta_{1,1,2}$. This shortcoming of our cutting methods was addressed in chapter 5.

However, before that, we investigated the possibility to fully reconstruct uncut Feynman integrals from the knowledge of their cuts. We reviewed the dispersive representation of Feynman diagrams, the standard procedure to reconstruct a function from its discontinuities. We observed that when written in terms of variables for which the symbol alphabet is rational, the dispersive integral becomes easy to evaluate as it naturally falls in the class of iterated integrals that evaluate to MPLs. We used this observation to find a compact representation for the three-mass triangles with zero, one or two internal masses, as well as the two-loop example mentioned above.

We then explored a variety of methods to reconstruct the symbol or the coproduct of an uncut function from the knowledge of its cuts. In all examples, we observed that the knowledge of a single unitarity cut contained enough information to constrain the symbol of the uncut functions. However, in cases with internal masses we had to postulate rules to determine the symbol alphabet of the functions. It is thus not clear to us how general these methods are, but we believe it would be interesting to study them further as they might lead to purely algebraic ways of computing Feynman integrals.

As already mentioned, in chapter 5 we returned to the study of cut Feynman diagrams. Our goal was to formulate cutting rules that were consistent with the ones developed in chapter 3 but reproduced more of the analytic structure of Feynman integrals by allowing any subset of propagators to be cut. In this chapter, we restricted our discussion to (scalar) one-loop Feynman diagrams. We chose to change the dimensions with the number of propagators in a way that ensures the Feynman integrals evaluate to functions of uniform weight in dimensional regularisation. This choice is equivalent to the choice of a basis of scalar integrals.

Based on ideas coming from the field of generalised unitarity, we constructed a new definition of cut Feynman diagrams, which we denoted $\mathcal{C}$. Instead of

replacing propagators by Dirac δ-functions when they are cut, we now evaluate residues at the poles of cut propagators. The advantage of this method is that it is easily generalisable to situations were the poles do not lie in the integration range of the loop momentum, or even on the real axis. This allowed us to relax the condition of working in real kinematics.

We presented two formulations of our new cutting rules, one in Minkowski space and one in Euclidean space. Although equivalent, the latter is best suited to the evaluation of single propagator cuts, and the former more practical for any other type of cut. In both cases, we were able to find a formal solution to the m-propagator cut of a diagram with n-propagators. This allowed us to draw some general conclusions about cut diagrams. We characterised all cut diagrams that can vanish, found a general relation between maximal and next-to-maximal cuts, and commented on the functional form of maximal cuts.

We then provided results obtained with our new cutting rules for a variety of one-loop Feynman integrals. Through these examples, we showed the consistency between the cutting rules defined in chapters 3 and 5. However, we also showed that one could now compute cuts that were beyond the scope of the rules of chapter 3. For instance, we computed maximal cuts of boxes even in cases where the maximal cut isolates massless three-point vertices, which we would have previously set to zero because of the restriction to use real kinematics. We checked the consistency of our results in several ways. For maximal cuts, we verified they matched the expectation that the leading order should be proportional to the inverse of the square root of the Gram determinant of each diagram. When maximal and non-vanishing next-to-maximal cuts were computed, we checked they agreed with our general relation between these two types of cuts. We were also able to match all the cut integrals in our examples to specific coproduct entries, which provided a check of the higher order in ϵ of our results. Finally, we computed the maximal cut of the fully massless pentagon. As we had foreseen, this cut integral does not vanish.

In our last chapter, we presented what was the motivation for most of the work developed in this thesis. We showed how one can construct a completely diagrammatic representation of the coproduct of one-loop scalar Feynman integrals.

We started by motivating our construction through some simple examples, the zero-, one- and two-mass bubble diagrams. This allowed us to introduce the general form of the diagrammatic coproduct we were after.

We then showed how by using only graphical operations one could construct a graphical coproduct on the algebra generated by one-loop Feynman graphs. In this construction, we restricted ourselves to two types of operations: propagators could be cut or contracted. As we commented in the introduction to chapter 6, these are the same operations that allow to determine the sources of discontinuities of Feynman integrals according to the Landau conditions. We also mentioned that one could in fact construct a complete Hopf algebra on one-loop Feynman graphs, but that this discussion goes beyond the scope of this thesis.

Having defined a purely graphical coproduct acting on Feynman graphs, we then explained how it could be mapped to the coproduct of MPLs, acting on the functions Feynman graphs evaluate to. This mapping allows us to explicitly check its validity by looking at specific Feynman diagrams. Although this is not trivial, we conjectured the graphical coproduct was valid in dimensional regularisation, and should thus be checked order by order in the dimensional regularisation parameter ϵ. This is important because even in the fully massive case there are divergences we must regularise, the ultraviolet singularity of tadpole diagrams.

Because we map the graphical coproduct to the coproduct of MPLs, it must be checked order by order in the ϵ-expansion of the Feynman integrals. We explained how in fact there are two expansions one must do when checking the diagrammatic coproduct: an expansion in the dimensional regularisation parameter, and one expansions in the different coproduct components at a given weight. For each term in this double expansion it is important to understand which diagrams of the graphical coproduct contribute at which order in ϵ.

We then commented on the cancellation of the poles introduced by tadpoles, and how this was important to reproduce the trivial coproduct entries of weight $(0, n)$. Following similar arguments, we can also see that the graphical coproduct is consistent with the first-entry condition.

We checked the validity of the graphical coproduct in a variety of examples. We looked at triangles and boxes with different mass configurations, and explicitly checked the coproduct of the uncut and cut integrals were correctly reproduced

by the graphical representation of their coproduct.

We finished by exploring some consequences of the graphical coproduct. We first examined its implications in the study of discontinuities of Feynman integrals, and argued that the results of chapters 2 and 3 are easily reproduced by the graphical coproduct if one keeps in mind the way discontinuity operators and the coproduct interact. This observation allowed us to determine the values of the three- and four-propagator cuts of the massless hexagon from the knowledge of its symbol, and then use this information to make an indirect check of the graphical coproduct.

Finally, we explored the consequences of the graphical coproduct for differential equations of Feynman integrals. We showed how one could interpret the coefficients of these differential equations as derivatives of cuts, which means we have a way to derive them without needing the usual reduction using IBP relations. We then explained how reverse unitarity was a simple consequence of the coassociativity of the graphical coproduct.

It is quite clear to us how we would like to pursue the work presented in this thesis. The cutting techniques established in chapter 5 are presently restricted to one-loop Feynman integrals. Although we do not foresee any major obstacles in their generalisation beyond one loop, we still have not investigated this issue in detail. In particular, the assumption that we only need to study scalar diagrams will need to be revisited, as it is well known that at two-loops and beyond some numerator factors cannot be reduced.

Once we understand how to generalise our cutting rules, we would like to generalise the diagrammatic coproduct beyond one loop. This generalisation will not be straightforward but we are confident it can be done. Indeed, what motivated us to establish a graphical coproduct at the one-loop order is still valid beyond one loop. However, there are some obstacles: it is not clear how to find a good basis for diagrams at two-loop and above, and we know MPLs are no longer enough to describe all diagrams as elliptic integrals start appearing. Nevertheless, the lessons learned at one loop should help us find a way to overcome these difficulties.

Appendix A

Notation and conventions

Feynman rules. Here we summarise the Feynman rules for cut diagrams in massless scalar theory. For a discussion of their origin, as well as the rules for determining whether a propagator is cut or uncut, see section 3.2.

- Vertex:

$$\bullet = i \tag{A.1}$$

- Complex conjugated vertex:

$$\circ = -i \tag{A.2}$$

- Propagator:

$$\bullet \xrightarrow{p} \bullet = \frac{i}{p^2 + i0} \tag{A.3}$$

  Massive (massless) propagators are drawn with a thick (thin) line.

- Complex conjugated propagator:

$$\circ \xrightarrow{p} \circ = \frac{-i}{p^2 - i0} \tag{A.4}$$

- Cut propagator:

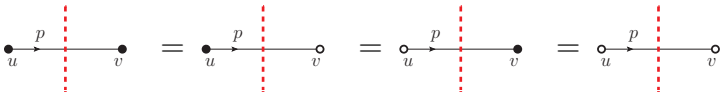

$$= 2\pi\,\delta\left(p^2\right) \quad \text{(A.5)}$$

  There is a theta function restricting the direction of energy flow in a cut propagator. For single cuts, our convention is that energy flows from black to white. For multiple cuts, there are separate color labels for each cut—see section 3.2 for details. There can be multiple thin dotted lines indicating cuts on the same propagator without changing its value. However, each thin dotted line implies complex conjugation of a region of the diagram.

- Cut propagator for cut in an internal mass:

$$= 2\pi\,\delta\left(p^2 - m^2\right). \quad \text{(A.6)}$$

- Loop factor (for loop momentum k, in $D = d - 2\epsilon$ dimensions):

$$\left(\frac{e^{\gamma_E \epsilon}}{\pi^{d/2-\epsilon}}\right) \int d^{d-2\epsilon}k\,. \quad \text{(A.7)}$$

- Different topologies are denoted as follows

  - tadpole of mass m: $\mathrm{Tad}(m^2)$;
  - bubbles of mass m_1 and m_2, and momentum p: $\mathrm{Bub}(p_2^2; m_1^2, m_2^2)$;
  - triangle with external channels p_1^2, p_2^2, p_3^2 and masses m_{12}, m_{23}, m_{13}, where the indices of the masses signal which external legs they connect: $T(p_1^2, p_2^2, p_3^2; m_{12}^2, m_{23}^2, m_{13}^2)$;
  - box with external channels p_1^2, p_2^2, p_3^2, p_4^2 and masses m_{12}, m_{23}, m_{34}, m_{14} (with the same meaning for the indices): $B(s, t; p_1^2, p_2^2, p_3^2, p_4^2; m_{12}^2, m_{23}^2, m_{34}^2, m_{14}^2)$.

  For simplicity, if some of the invariants vanish we might not write them in the argument. For instance, for the box with one external mass, we will write $B(s, t; p_1^2)$. There are two types of boxes with two-external masses, the two-mass-easy, where the massive channels are not adjacent, which we will

denote $B^e(s,t;p_1^2,p_3^2)$, and the two-mass-hard, where the massive channels are adjacent, $B^h(s,t;p_1^2,p_2^2)$.

Kinematic regions. For the three-point three-mass functions with massless propagators at one and two loops, we use the following shorthand for different kinematic regions, with variables $z,\bar{z}$ as defined in eq. (2.29),

$$\begin{aligned} R^*_\triangle: &\quad p_1^2,p_2^2,p_3^2>0, \quad \bar{z}=z^*\,,\\ R^i_\triangle: &\quad p_i^2>0, \text{ and } p_k^2<0 \text{ for all } k\neq i\,,\\ R^{i,j}_\triangle: &\quad p_i^2,p_j^2>0, \text{ and } p_k^2<0 \text{ for all } k\neq i,j. \end{aligned}$$

Feynman rules for chapters 5 and 6. In these two chapters, we use a 'bare' version of the diagrams computed in the previous chapters. For each loop, we include a factor:

$$\left(\frac{e^{\gamma_E\epsilon}}{i\pi^{2-\epsilon}}\right)\int d^{4-2\epsilon}k\,. \tag{A.8}$$

Vertices and propagators come with no factor of i. Diagrams computed with these rules will be denoted I_n, with arguments following the same conventions as for the arguments of the different topologies listed above.

The relation between the two conventions is easy to establish. For instance,

$$I_2(p^2)=i\text{Bub}(p^2),\quad I_3(p^2)=-iT(p^2),\quad \text{and}\quad I_4(s,t)=iB(s,t). \tag{A.9}$$

The relation between cuts computed according to the two sets of rules are also easy to get by compensating for the mismatch in powers of 2π and $\pm i$. For instance, let us relate the results obtained in eqs. (5.85) and (B.55) for the p_1^2 channel cut of the three mass triangle.

The result in eq. (B.55) was computed following the rules of chapter 3, and thus includes a factor i for the vertex where p_1^2 enters the diagrams, and a factor of $(-i)^3$ for the vertices and propagator on the complex conjugated region of the cut diagram. Because the two-propagator cut corresponds to a single discontinuity, there is an explicit factor of (2π). Overall, this gives a factor of (-2π) compared to the definition of $\mathcal{C}_2[I_3]$ given in chapter 5, with which (5.85) was computed.

We should then find that

$$\mathrm{Cut}_{p_1^2} T(p_1^2, p_2^2, p_3^2) = (-2\pi)\mathcal{C}_{2,[(12),(13)]}[I_3(p_1^2, p_2^2, p_3^2)], \tag{A.10}$$

which is indeed true.

As another example, we can compare the maximal cut of the three-mass triangle, seen as a double discontinuity on p_1^2 and p_2^2, computed with our two definitions, eqs. (5.86) and (B.58). According to the rules of chapter 3, we have a factor of i^2 from the vertices where the channels we are cutting in enter the diagram, and a factor of $(-i)$ for the other vertex. Because this corresponds to a double discontinuity, we have an explicit factor of $(2\pi)^2$. Finally, in the definition of the triple cut of chapter 5 there is an explicit factor of (-1) which was included by hand. The two definitions should thus differ by a factor of $(-4\pi^2 i)$. More precisely,

$$\mathrm{Cut}_{p_1^2,p_2^2} T(p_1^2, p_2^2, p_3^2) = (-4\pi^2 i)\mathcal{C}_3[I_3(p_1^2, p_2^2, p_3^2)], \tag{A.11}$$

which is indeed the correct relation.

Definition of c_Γ. In loop calculations, a specific combinations of gamma functions appears very often, which we denote c_Γ,

$$c_\Gamma = \frac{e^{\gamma_E \epsilon}\Gamma^2(1-\epsilon)\Gamma(1+\epsilon)}{\Gamma(1-2\epsilon)}. \tag{A.12}$$

Definition of ${}_2F_1$ and F_1. Results for triangles and their cuts often involve the Gauss hypergeometric function ${}_2F_1$ and one of its generalizations, the F_1 Appell function. They have the Euler-type integral representations

$${}_2F_1\left(\alpha, \beta; \gamma; z\right) = \frac{\Gamma(\gamma)}{\Gamma(\beta)\Gamma(\gamma-\beta)} \int_0^1 dt\, t^{\beta-1}(1-t)^{\gamma-\beta-1}(1-tz)^{-\alpha} \tag{A.13}$$

for $\mathfrak{Re}\,\gamma > \mathfrak{Re}\,\beta > 0$, and

$$F_1\left(\alpha; \beta, \beta'; \gamma; x; y\right) = \frac{\Gamma(\gamma)}{\Gamma(\alpha)\Gamma(\gamma-\alpha)} \int_0^1 dt \frac{t^{\alpha-1}(1-t)^{\gamma-\alpha-1}}{(1-tx)^{\beta}(1-ty)^{\beta'}} \tag{A.14}$$

for $\mathfrak{Re}\,\gamma > \mathfrak{Re}\,\alpha > 0$.

Appendix B

Results

In this appendix, we collect several results of Feynman diagrams that we use in the main text. In the accompanying `MATHEMATICA` package [38] we include more results and expansions of the functions to higher orders than what is presented here.

B.1 One-mass triangles

We give explicit expressions for triangles with one external massive channel. For all the examples considered, we have computed the uncut triangles both through standard Feynman parametrization and through a dispersive integral, and verified agreement of the expressions. Divergent integrals were compared with the results given in ref. [39]. For all triangles with one external massive channel considered in the following subsections, we separate the rational prefactor from the pure transcendental function according to the relation

$$T(p_1^2, 0, 0; m_{12}^2, m_{23}^2, m_{13}^2) = \frac{i}{p_1^2} \mathcal{T}(p_1^2, 0, 0; m_{12}^2, m_{23}^2, m_{13}^2)\,, \tag{B.1}$$

where the internal masses are generic and can be zero. Before expansion in the dimensional regularization parameter ϵ, the results will often involve the functions ${}_2F_1$ and F_1 defined in eqs. (A.13) and (A.14).

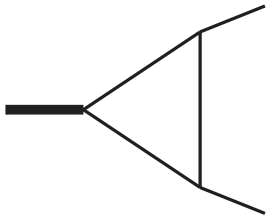

(a) $T(p_1^2, 0, 0; 0, 0, 0)$

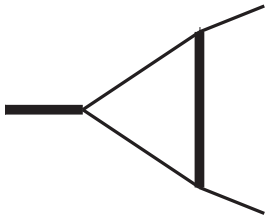

(b) $T(p_1^2, 0, 0; 0, m_{23}^2, 0)$

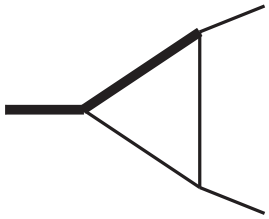

(c) $T(p_1^2, 0, 0; m_{12}^2, 0, 0)$

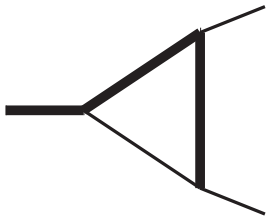

(d) $T(p_1^2, 0, 0; m_{12}^2, m_{23}^2, 0)$

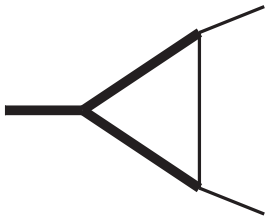

(e) $T(p_1^2, 0, 0; m_{12}^2, 0, m_{13}^2)$

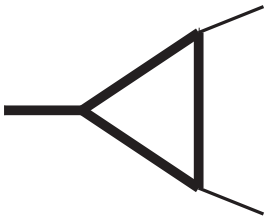

(f) $T(p_1^2, 0, 0; m_{12}^2, m_{23}^2, m_{13}^2)$

Figure B.1: Triangles with one external mass

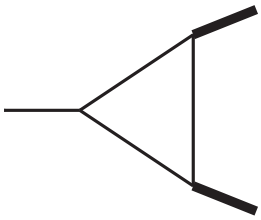

(a) $T(0, p_2^2, p_3^2; 0, 0, 0)$

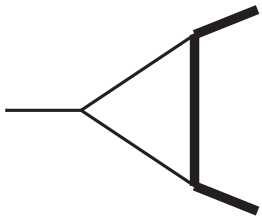

(b) $T(0, p_2^2, p_3^2; 0, m_{23}^2, 0)$

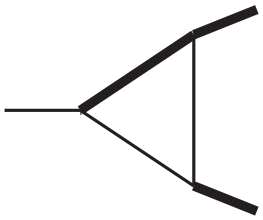

(c) $T(0, p_2^2, p_3^2; m_{12}^2, 0, 0)$

Figure B.2: Triangles with two external mass

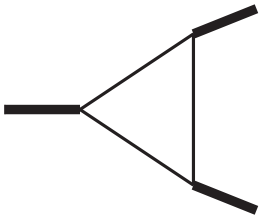

(a) $T(p_1^2, p_2^2, p_3^2; 0, 0, 0)$

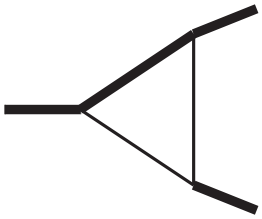

(b) $T(p_1^2, p_2^2, p_3^2; m_{12}^2, 0, 0)$

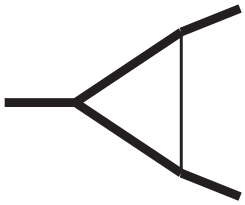

(c) $T(p_1^2, p_2^2, p_3^2; m_{12}^2, 0, m_{13}^2)$

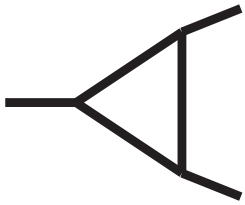

(d) $T(p_1^2, p_2^2, p_3^2; m_{12}^2, m_{23}^2, m_{13}^2)$

Figure B.3: Triangles with three external mass

B.1.1 $T(p_1^2, 0, 0; 0, 0, 0)$

The triangle with one external, eq. (B.1a), massive channel is

$$T(p_1^2, 0, 0; 0, 0, 0) = ic_\Gamma \frac{(-p_1^2)^{-1-\epsilon}}{\epsilon^2}, \tag{B.2}$$

where c_Γ is defined in eq. (A.12). The symbol is

$$\mathcal{S}\left[\mathcal{T}(p_1^2, 0, 0; 0, 0, 0)\right] = -\frac{1}{\epsilon^2} + \frac{p_1^2}{\epsilon} - p_1^2 \otimes p_1^2 + \mathcal{O}(\epsilon)\,. \tag{B.3}$$

Single cuts

$$\mathrm{Cut}_{p_1^2}\left[T(p_1^2, 0, 0; 0, 0, 0)\right] = -2\pi \frac{e^{\gamma_E \epsilon}\Gamma(1-\epsilon)}{\epsilon\Gamma(1-2\epsilon)}(p_1^2)^{-1-\epsilon} \tag{B.4}$$

Double cuts

All double cuts are zero.

B.1.2 $T(p_1^2, 0, 0; 0, m_{23}^2, 0)$

The triangle of fig. B.1b is given by:

$$\begin{aligned}
&T(p_1^2, 0, 0; 0, m_{23}^2, 0) = \\
&= \frac{ie^{\gamma_E\epsilon}}{\epsilon}\left[\frac{(-p_1^2)^{-\epsilon}}{m_{23}^2}\frac{\Gamma(1+\epsilon)\Gamma^2(1-\epsilon)}{\Gamma(2-2\epsilon)}\,{}_2F_1\left(1, 1-\epsilon; 2-2\epsilon; -\frac{p_1^2}{m_{23}^2}\right)\right. \\
&\left. - \left(m_{23}^2\right)^{-1-\epsilon}\frac{\Gamma(1+\epsilon)\Gamma(1-\epsilon)}{\Gamma(2-\epsilon)}\,{}_2F_1\left(1, 1; 2-\epsilon; -\frac{p_1^2}{m_{23}^2}\right)\right] \\
&= \frac{i}{p_1^2}\left(\mathrm{Li}_2\left(\frac{m_{23}^2 + p_1^2}{m_{23}^2}\right) - \frac{\pi^2}{6}\right) + \mathcal{O}(\epsilon)\,.
\end{aligned} \tag{B.5}$$

The symbol is

$$\mathcal{S}\left[\mathcal{T}(p_1^2, 0, 0; 0, m_{23}^2, 0)\right] = m_{23}^2 \otimes \left(\frac{m_{23}^2 + p_1^2}{m_{23}^2}\right) - p_1^2 \otimes \left(\frac{m_{23}^2 + p_1^2}{m_{23}^2}\right) + \mathcal{O}(\epsilon)\,. \tag{B.6}$$

Single cuts

The cut in the external channel p_1^2 is

$$\begin{aligned}
&\mathrm{Cut}_{p_1^2}\left[T(p_1^2,0,0;0,m_{23}^2,0)\right] = \\
&= 2\pi\frac{e^{\gamma_E\epsilon}\Gamma(1-\epsilon)}{\Gamma(2-2\epsilon)}\frac{(p_1^2)^{-\epsilon}}{p_1^2+m_{23}^2}\,{}_2F_1\left(1,1-\epsilon;2-2\epsilon;\frac{p_1^2}{p_1^2+m_{23}^2}\right) \\
&= -\frac{2\pi}{p_1^2}\log\left(\frac{m_{23}^2}{p_1^2+m_{23}^2}\right)+\mathcal{O}(\epsilon)\,. \qquad \text{(B.7)}
\end{aligned}$$

The cut in the internal mass m_{23}^2 is

$$\begin{aligned}
\mathrm{Cut}_{m_{23}^2}\left[T(p_1^2,0,0;0,m_{23}^2,0)\right] &= \frac{2\pi e^{\gamma_E\epsilon}}{\Gamma(2-\epsilon)}\frac{(-m_{23}^2)^{-\epsilon}}{p_1^2+m_{23}^2}\,{}_2F_1\left(1,1-\epsilon;2-\epsilon;\frac{p_1^2}{p_1^2+m_{23}^2}\right) \\
&= \frac{2\pi}{p_1^2}\log\left(\frac{m_{23}^2+p_1^2}{m_{23}^2}\right)+\mathcal{O}(\epsilon)\,. \qquad \text{(B.8)}
\end{aligned}$$

Double cuts

The double cut in the external channel p_1^2 and the internal mass m_{23}^2 is

$$\begin{aligned}
\mathrm{Cut}_{p_1^2,m_{23}^2}\left[T(p_1^2,0,0;0,m_{23}^2,0)\right] &= -4\pi^2 i\frac{e^{\gamma_E\epsilon}}{\Gamma(1-\epsilon)}\frac{(p_1^2)^{-1+\epsilon}(-m_{23}^2)^{-\epsilon}}{(p_1^2+m_{23}^2)^{\epsilon}}\theta(p_1^2+m_{23}^2) \\
&= -\frac{4\pi^2 i}{p_1^2}\theta(p_1^2+m_{23}^2)+\mathcal{O}(\epsilon)\,. \qquad \text{(B.9)}
\end{aligned}$$

B.1.3 $T(p_1^2,0,0;m_{12}^2,0,0)$

The triangle of fig. B.1c is given by:

$$\begin{aligned}
T(p_1^2,0,0;m_{12}^2,0,0) =& -i\frac{e^{\gamma_E\epsilon}\Gamma(1+\epsilon)}{\epsilon(1-\epsilon)}(m_{12}^2)^{-1-\epsilon}\,{}_2F_1\left(1,1+\epsilon;2-\epsilon;\frac{p_1^2}{m_{12}^2}\right) \\
=&\frac{i}{p_1^2}\left[\frac{1}{\epsilon}\log\left(1-\frac{p_1^2}{m_{12}^2}\right)-\mathrm{Li}_2\left(\frac{p_1^2}{m_{12}^2}\right)-\log^2\left(1-\frac{p_1^2}{m_{12}^2}\right)\right. \\
&\left.-\log\left(m_{12}^2\right)\log\left(1-\frac{p_1^2}{m_{12}^2}\right)\right]+\mathcal{O}\left(\epsilon\right)\,. \qquad \text{(B.10)}
\end{aligned}$$

The symbol is

$$\mathcal{S}\left[\mathcal{T}(p_1^2,0,0;m_{12}^2,0,0)\right] = \frac{1}{\epsilon}\frac{m_{12}^2-p_1^2}{m_{12}^2}+m_{12}^2\otimes\frac{m_{12}^2\left(m_{12}^2-p_1^2\right)}{p_1^2}$$

$$+\left(m_{12}^2-p_1^2\right)\otimes\frac{p_1^2}{\left(m_{12}^2-p_1^2\right)^2}+\mathcal{O}\left(\epsilon\right)\,. \tag{B.11}$$

Single cuts

The cut in the external channel p_1^2 is

$$\begin{aligned}\mathrm{Cut}_{p_1^2}\left[T(p_1^2,0,0;m_{12}^2,0,0)\right] &= -2\pi\frac{e^{\gamma_E\epsilon}\Gamma(1-\epsilon)}{\epsilon\Gamma(1-2\epsilon)}\frac{\left(p_1^2-m_{12}^2\right)^{-2\epsilon}}{\left(p_1^2\right)^{1-\epsilon}} \\ &= -\frac{2\pi}{p_1^2\epsilon}-\frac{2\pi}{p_1^2}\left(\log\left(p_1^2\right)-2\log\left(p_1^2-m_{12}^2\right)\right)+\mathcal{O}\left(\epsilon\right)\,.\end{aligned} \tag{B.12}$$

The cut in the internal mass m_{12}^2 is

$$\begin{aligned}&\mathrm{Cut}_{m_{12}^2}\left[T(p_1^2,0,0;m_{12}^2,0,0)\right] = \\ &\quad= -\frac{2\pi e^{\gamma_E\epsilon}}{\epsilon\Gamma(1-\epsilon)}\frac{\left(-m_{12}^2\right)^{-\epsilon}}{p_1^2}\,{}_2F_1\left(1,\epsilon;1-\epsilon;\frac{m_{12}^2}{p_1^2}\right) \\ &\quad= -\frac{2\pi}{p_1^2\epsilon}+\frac{2\pi}{p_1^2}\left(\log\left(m_{12}^2-p_1^2\right)+\log\left(\frac{-m_{12}^2}{-p_1^2}\right)\right)+\mathcal{O}\left(\epsilon\right)\,.\end{aligned}$$

Double cuts

The double cut in the external channel p_1^2 and the internal mass m_{12}^2 is zero.

B.1.4 $T(p_1^2,0,0;m_{12}^2,m_{23}^2,0)$

The triangle of fig. B.1d is given by:

$$\begin{aligned}&T(p_1^2,0,0;m_{12}^2,m_{23}^2,0) = \\ =&\,i\frac{e^{\gamma_E\epsilon}\Gamma(1+\epsilon)}{\epsilon(1-\epsilon)\left(m_{12}^2-m_{23}^2\right)}\left[\left(m_{23}^2\right)^{-\epsilon}\,{}_2F_1\left(1,1;2-\epsilon;\frac{p_1^2}{m_{12}^2-m_{23}^2}\right)\right. \\ &\left.-\left(m_{12}^2\right)^{-\epsilon}\,F_1\left(1;1,\epsilon;2-\epsilon;\frac{p_1^2}{m_{12}^2-m_{23}^2};\frac{p_1^2}{m_{12}^2}\right)\right] \\ =&\frac{i}{p_1^2}\left[\mathrm{Li}_2\left(\frac{m_{12}^2}{m_{23}^2}\right)-\mathrm{Li}_2\left(\frac{m_{12}^2-p_1^2}{m_{23}^2}\right)-\log\left(1-\frac{m_{12}^2-p_1^2}{m_{23}^2}\right)\log\left(1-\frac{p_1^2}{m_{12}^2}\right)\right. \\ &\left.+\log\left(\frac{m_{23}^2}{m_{12}^2}\right)\log\left(1-\frac{p_1^2}{m_{12}^2-m_{23}^2}\right)\right]+\mathcal{O}\left(\epsilon\right)\,.\end{aligned} \tag{B.13}$$

The symbol is

$$\begin{aligned}
&\mathcal{S}\left[\mathcal{T}(p_1^2,0,0;m_{12}^2,m_{23}^2,0)\right] = \\
=&m_{12}^2 \otimes \left(\frac{m_{12}^2-m_{23}^2}{m_{23}^2}\right) + m_{23}^2 \otimes \left(1-\frac{p_1^2}{m_{12}^2-m_{23}^2}\right) \\
&- (m_{12}^2-p_1^2) \otimes \left(1-\frac{m_{12}^2-p_1^2}{m_{23}^2}\right) + \mathcal{O}(\epsilon) \ . \qquad \text{(B.14)}
\end{aligned}$$

Single cuts

The cut in the external channel p_1^2 is

$$\begin{aligned}
&\mathrm{Cut}_{p_1^2}\left[T(p_1^2,0,0;m_{12}^2,m_{23}^2,0)\right] = \\
&=2\pi \frac{e^{\gamma_E \epsilon}\Gamma(1-\epsilon)}{\Gamma(2-2\epsilon)} \frac{(p_1^2-m_{12})^{1-2\epsilon}}{m_{23}^2 (p_1^2)^{1-\epsilon}} \, {}_2F_1\left(1,1-\epsilon;2-2\epsilon;\frac{m_{12}^2-p_1^2}{m_{23}^2}\right) \\
&=\frac{2\pi}{p_1^2}\log\left(1-\frac{m_{12}^2-p_1^2}{m_{23}^2}\right) + \mathcal{O}(\epsilon) \ . \qquad \text{(B.15)}
\end{aligned}$$

The cut in the internal mass m_{12}^2 is

$$\begin{aligned}
&\mathrm{Cut}_{m_{12}^2}\left[T(p_1^2,0,0;m_{12}^2,m_{23}^2,0)\right] = \\
&= -\frac{2\pi}{p_1^2} \frac{e^{\gamma_E \epsilon}}{\Gamma(2-\epsilon)} \frac{(-m_{12}^2)^{1-\epsilon}}{m_{12}^2-m_{23}^2} \, F_1\left(1;1,\epsilon;2-\epsilon;\frac{m_{12}^2}{m_{12}^2-m_{23}^2};\frac{m_{12}^2}{p_1^2}\right) \\
&= -\frac{2\pi}{p_1^2}\log\left(\frac{m_{23}^2}{m_{23}^2-m_{12}^2}\right) + \mathcal{O}(\epsilon) \ . \qquad \text{(B.16)}
\end{aligned}$$

The cut in the internal mass m_{23}^2 is

$$\begin{aligned}
&\mathrm{Cut}_{m_{23}^2}\left[T(p_1^2,0,0;m_{12}^2,m_{23}^2,0)\right] = \\
&= -2\pi \frac{e^{\gamma_E \epsilon}}{\Gamma(2-\epsilon)} \frac{(-m_{23}^2)^{-\epsilon}}{m_{12}^2-m_{23}^2} \, {}_2F_1\left(1,1;2-\epsilon;\frac{p_1^2}{m_{12}^2-m_{23}^2}\right) \\
&=\frac{2\pi}{p_1^2}\log\left(1-\frac{p_1^2}{m_{12}^2-m_{23}^2}\right) + \mathcal{O}(\epsilon) \ . \qquad \text{(B.17)}
\end{aligned}$$

Double cuts

The double cut in the external channel p_1^2 and internal mass m_{23}^2 is

$$\begin{aligned}\mathrm{Cut}_{p_1^2,m_{23}^2}\left[T(p_1^2,0,0;m_{12}^2,m_{23}^2,0)\right] =& \\ =&-4\pi^2 i\frac{e^{\gamma_E\epsilon}}{\Gamma(1-\epsilon)}\frac{(p_1^2)^{-1+\epsilon}(-m_{23}^2)^{-\epsilon}}{(p_1^2-m_{12}^2+m_{23}^2)^{\epsilon}}\theta(p_1^2-m_{12}^2+m_{23}^2)\\ =&-\frac{4\pi^2 i}{p_1^2}\theta(p_1^2-m_{12}^2+m_{23}^2)+\mathcal{O}\left(\epsilon\right)\,. \end{aligned} \tag{B.18}$$

The double cut in the two internal masses is

$$\begin{aligned}\mathrm{Cut}_{m_{12}^2,m_{23}^2}\left[T(p_1^2,0,0;m_{12}^2,m_{23}^2,0)\right] =& \\ =&-4\pi^2 i\frac{e^{\gamma_E\epsilon}}{\Gamma(1-\epsilon)}\frac{(-p_1^2)^{-1+\epsilon}(-m_{23}^2)^{-\epsilon}}{(m_{12}^2-p_1^2-m_{23}^2)^{\epsilon}}\theta(m_{12}^2-p_1^2-m_{23}^2)\theta(m_{23}^2-m_{12}^2)\\ =&\frac{4\pi^2 i}{p_1^2}\theta(m_{12}^2-p_1^2-m_{23}^2)\theta(m_{23}^2-m_{12}^2)+\mathcal{O}\left(\epsilon\right)\,. \end{aligned} \tag{B.19}$$

B.1.5 $T(p_1^2,0,0;m_{12}^2,0,m_{13}^2)$

The triangle of fig. B.1e is given by:

$$\begin{aligned}T(p_1^2,0,0;&m_{12}^2,0,m_{13}^2) =\\ =&i\frac{e^{\gamma_E\epsilon}\Gamma(1+\epsilon)}{\epsilon(1-\epsilon)}(-p_1^2)^{-1-\epsilon}\left[\frac{(w_1-\bar{w}_1)^{-\epsilon}}{(1-\bar{w}_1)}\right.\\ &\left(\frac{(w_1-1)^{1-\epsilon}}{w_1}F_1\left(1-\epsilon;1,\epsilon;2-\epsilon;\frac{w_1-1}{w_1(1-\bar{w}_1)};\frac{w_1-1}{w_1-\bar{w}_1}\right)\right.\\ &\left.-w_1^{-\epsilon}F_1\left(1-\epsilon;1,\epsilon;2-\epsilon;\frac{1}{1-\bar{w}_1};\frac{w_1}{w_1-\bar{w}_1}\right)\right)\\ &\left.-\frac{((w_1-1)(1-\bar{w}_1))^{-\epsilon}}{w_1\bar{w}_1}\,{}_2F_1\left(1,1-\epsilon;2-\epsilon;\frac{1}{w_1\bar{w}_1}\right)\right]\\ =&\frac{i}{p_1^2}\log\left(\frac{w_1}{w_1-1}\right)\log\left(\frac{-\bar{w}_1}{1-\bar{w}_1}\right)+\mathcal{O}\left(\epsilon\right)\,. \end{aligned} \tag{B.20}$$

The symbol is

$$\begin{aligned}&\mathcal{S}\left[\mathcal{T}(p_1^2,0,0;m_{12}^2,0,m_{13}^2)\right]=\\&\quad=\left(\frac{w_1}{1-w_1}\right)\otimes\left(\frac{\bar{w}_1}{1-\bar{w}_1}\right)+\left(\frac{\bar{w}_1}{1-\bar{w}_1}\right)\otimes\left(\frac{w_1}{1-w_1}\right)+\mathcal{O}\left(\epsilon\right)\,.\end{aligned}\tag{B.21}$$

Single cuts

The cut in the external channel p_1^2 is

$$\begin{aligned}&\mathrm{Cut}_{p_1^2}\left[T(p_1^2,0,0;m_{12}^2,0,m_{13}^2)\right]=\\&=-2\pi\frac{e^{\gamma_E\epsilon}\Gamma(1-\epsilon)}{\Gamma(2-2\epsilon)}(p_1^2)^{-1-\epsilon}\frac{(w_1-\bar{w}_1)^{1-2\epsilon}}{\bar{w}_1(w_1-1)}\,{}_2F_1\left(1,1-\epsilon;2-2\epsilon;\frac{w_1-\bar{w}_1}{\bar{w}_1(w_1-1)}\right)\\&=\frac{2\pi}{p_1^2}\left(\log\left(\frac{w_1}{1-w_1}\right)-\log\left(\frac{\bar{w}_1}{1-\bar{w}_1}\right)\right)+\mathcal{O}\left(\epsilon\right)\,.\end{aligned}\tag{B.22}$$

The cut in the internal mass m_{12}^2 is

$$\begin{aligned}&\mathrm{Cut}_{m_{12}^2}\left[T(p_1^2,0,0;m_{12}^2,0,m_{13}^2)\right]=\\&=-2\pi\frac{e^{\gamma_E\epsilon}(-p_1^2)^{-1-\epsilon}}{\Gamma(2-\epsilon)\,(w_1-1)}\bar{w}_1^{-\epsilon}\,(w_1-\bar{w}_1)^{-\epsilon}\;F_1\left(1-\epsilon;1,\epsilon;2-\epsilon;\frac{1}{1-w_1};\frac{-\bar{w}_1}{w_1-\bar{w}_1}\right)\\&=\frac{2\pi}{p_1^2}\log\left(\frac{w_1}{w_1-1}\right)+\mathcal{O}\left(\epsilon\right)\,.\end{aligned}\tag{B.23}$$

The cut in the internal mass m_{13}^2 is

$$\begin{aligned}&\mathrm{Cut}_{m_{13}^2}T(p_1^2,0,0;m_{12}^2,0,m_{13}^2)=\\&=-2\pi\frac{e^{\gamma_E\epsilon}(-p_1^2)^{-1-\epsilon}}{\Gamma(2-\epsilon)}\left[-\frac{((1-w_1)(1-\bar{w}_1))^{-\epsilon}}{w_1\bar{w}_1}\,{}_2F_1\left(1,1-\epsilon;2-\epsilon;\frac{1}{w_1\bar{w}_1}\right)\right.\\&\left.+\frac{(1-w_1)^{1-\epsilon}(w_1-\bar{w}_1)^{-\epsilon}}{w_1(\bar{w}_1-1)}\,F_1\left(1-\epsilon;1,\epsilon;2-\epsilon;\frac{1-w_1}{w_1(\bar{w}_1-1)};\frac{w_1-1}{w_1-\bar{w}_1}\right)\right]\\&=-\frac{2\pi}{p_1^2}\log\left(\frac{-\bar{w}_1}{1-\bar{w}_1}\right)+\mathcal{O}\left(\epsilon\right)\,.\end{aligned}\tag{B.24}$$

Double cuts

All double cuts are zero.

B.1.6 $T(p_1^2, 0, 0; m_{12}^2, m_{23}^2, m_{13}^2)$

The triangle of fig. B.1f is given by[1]:

$$\begin{aligned}
&T(p_1^2,0,0;m_{12}^2,m_{23}^2,m_{13}^2)\\
&\quad=i\frac{e^{\gamma_E\epsilon}\Gamma(1+\epsilon)}{\epsilon}(-p_1^2)^{-1-\epsilon}\left[\frac{(w_1-\bar{w}_1)^{-\epsilon}}{(1-\epsilon)(\mu_{23}+w_1(1-\bar{w}_1))}\right.\\
&\qquad\left(\left(w_1-1\right)^{1-\epsilon}F_1\left(1-\epsilon;1,\epsilon;2-\epsilon;\frac{w_1-1}{\mu_{23}+w_1(1-\bar{w}_1)};\frac{w_1-1}{w_1-\bar{w}_1}\right)\right.\\
&\qquad\left.\left.-\,w_1^{1-\epsilon}F_1\left(1-\epsilon;1,\epsilon;2-\epsilon;\frac{w_1}{\mu_{23}+w_1(1-\bar{w}_1)};\frac{w_1}{w_1-\bar{w}_1}\right)\right)\right.\\
&\qquad\left.-\frac{(-\mu_{23})^{-\epsilon}}{w_1\bar{w}_1-\mu_{23}}F_1\left(1;1,\epsilon;2;\frac{1}{w_1\bar{w}_1-\mu_{23}};\frac{\mu_{23}+(w_1-1)(1-\bar{w}_1)}{\mu_{23}}\right)\right]\\
&\quad=\frac{i}{p_1^2}\left[\log\left(\frac{w_1}{w_1-1}\right)\log\left(\frac{-\bar{w}_1}{1-\bar{w}_1}\right)-G\left(1,0,\frac{\mu_{23}}{(w_1-1)(\bar{w}_1-1)}\right)\right.\\
&\qquad+G\left(1,0,\frac{\mu_{23}}{w_1(\bar{w}_1-1)}\right)+G\left(1,0,\frac{\mu_{23}}{(w_1-1)\bar{w}_1}\right)\\
&\qquad\left.-G\left(1,0,\frac{\mu_{23}}{w_1\bar{w}_1}\right)\right]+\mathcal{O}\left(\epsilon\right)\,.
\end{aligned}\tag{B.25}$$

The symbol is

$$\begin{aligned}
&\mathcal{S}\left[\mathcal{T}(p_1^2,0,0;m_{12}^2,m_{23}^2,m_{13}^2)\right]=\\
&\quad=\mu_{23}\otimes\frac{(\mu_{23}+w_1(1-\bar{w}_1))(\mu_{23}+\bar{w}_1(1-w_1))}{(\mu_{23}-w_1\bar{w}_1)(\mu_{23}-(1-w_1)(1-\bar{w}_1))}+w_1\otimes\frac{\mu_{23}-w_1\bar{w}_1}{\mu_{23}+w_1(1-\bar{w}_1)}\\
&\quad+\bar{w}_1\otimes\frac{\mu_{23}-w_1\bar{w}_1}{\mu_{23}+\bar{w}_1(1-w_1)}+(1-w_1)\otimes\frac{\mu_{23}-(1-w_1)(1-\bar{w}_1)}{\mu_{23}+\bar{w}_1(1-w_1)}\\
&\quad+(1-\bar{w}_1)\otimes\frac{\mu_{23}-(1-w_1)(1-\bar{w}_1)}{\mu_{23}+w_1(1-\bar{w}_1)}+\mathcal{O}\left(\epsilon\right)\,.
\end{aligned}\tag{B.26}$$

[1]We wrote the result in terms of harmonic polylogarithms for simplicity. It has a longer expression in terms of classical polylogarithms which can be easily obtained using

$$G(1,0,x)=\mathrm{Li}_2(x)+\log(1-x)\log(x)\,.$$

Single cuts

The cut in the external channel p_1^2 is

$$\begin{aligned}
&\mathrm{Cut}_{p_1^2}\left[T(p_1^2,0,0;m_{12}^2,m_{23}^2,m_{13}^2)\right] = \\
&\quad = -2\pi\frac{e^{\gamma_E\epsilon}\Gamma(1-\epsilon)}{\Gamma(2-2\epsilon)}(p_1^2)^{-1-\epsilon}\frac{(w_1-\bar{w}_1)^{1-2\epsilon}}{\bar{w}_1(w_1-1)-\mu_{23}} \\
&\qquad {}_2F_1\left(1,1-\epsilon;2-2\epsilon;\frac{w_1-\bar{w}_1}{\bar{w}_1(w_1-1)-\mu_{23}}\right) \\
&\quad = \frac{2\pi}{p_1^2}\log\left(\frac{\mu_{23}+w_1(1-\bar{w}_1)}{\mu_{23}+\bar{w}_1(1-w_1)}\right)+\mathcal{O}(\epsilon)\ .
\end{aligned} \tag{B.27}$$

The cut in the internal mass m_{12}^2 is

$$\begin{aligned}
&\mathrm{Cut}_{m_{12}^2}\left[T(p_1^2,0,0;m_{12}^2,m_{23}^2,m_{13}^2)\right] = \\
&\quad = \frac{2\pi e^{\gamma_E\epsilon}(-p_1^2)^{-1-\epsilon}}{\Gamma(2-\epsilon)}\frac{\bar{w}_1^{1-\epsilon}(w_1-\bar{w}_1)^{-\epsilon}}{\mu_{23}-\bar{w}_1(w_1-1)} \\
&\qquad F_1\left(1-\epsilon;1,\epsilon;2-\epsilon;\frac{\bar{w}_1}{\mu_{23}-\bar{w}_1(w_1-1)};\frac{-\bar{w}_1}{w_1-\bar{w}_1}\right) \\
&\quad = \frac{2\pi}{p_1^2}\log\left(\frac{\mu_{23}-w_1\bar{w}_1}{\mu_{23}+\bar{w}_1(1-w_1)}\right)+\mathcal{O}(\epsilon)\ .
\end{aligned} \tag{B.28}$$

The cut in the internal mass m_{23}^2 is

$$\begin{aligned}
&\mathrm{Cut}_{m_{23}^2}\left[T(p_1^2,0,0;m_{12}^2,m_{23}^2,m_{13}^2)\right] = \\
&\quad = 2\pi\frac{e^{\gamma_E\epsilon}}{\Gamma(1-\epsilon)}\frac{(-p_1^2)^{-1-\epsilon}}{1-\epsilon}\mu_{23}^{1-\epsilon}\frac{{}_2F_1\left(1,1;2-\epsilon;\frac{\mu_{23}}{(\mu_{23}-(1-w_1)(1-\bar{w}_1))(w_1\bar{w}_1-\mu_{23})}\right)}{(\mu_{23}-(1-w_1)(1-\bar{w}_1))(w_1\bar{w}_1-\mu_{23})} \\
&\quad = \frac{2\pi}{p_1^2}\log\left(\frac{(\mu_{23}+w_1(1-\bar{w}_1))(\mu_{23}+\bar{w}_1(1-w_1))}{(\mu_{23}-w_1\bar{w}_1)(\mu_{23}-(1-w_1)(1-\bar{w}_1))}\right) \\
&\qquad +\mathcal{O}(\epsilon)\ .
\end{aligned} \tag{B.29}$$

The cut in the internal mass m_{13}^2 is

$$\begin{aligned}
&\mathrm{Cut}_{m_{13}^2}\left[T(p_1^2,0,0;m_{12}^2,m_{23}^2,m_{13}^2)\right] = \\
&\quad = -2\pi\frac{e^{\gamma_E\epsilon}}{\Gamma(2-\epsilon)}(-p_1^2)^{-1-\epsilon}\left[\frac{(1-w_1)^{1-\epsilon}(w_1-\bar{w}_1)^{-\epsilon}}{w_1(\bar{w}_1-1)-\mu_{23}}\right. \\
&\qquad \left. F_1\left(1-\epsilon;1,\epsilon;2-\epsilon;\frac{1-w_1}{w_1(\bar{w}_1-1)-\mu_{23}};\frac{w_1-1}{w_1-\bar{w}_1}\right)\right.
\end{aligned} \tag{B.30}$$

$$-\frac{((1-w_1)(1-\bar{w}_1))^{1-\epsilon}\,{}_2F_1\left(1,1-\epsilon;2-\epsilon;\frac{(1-w_1)(1-\bar{w}_1)}{(w_1(\bar{w}_1-1)-\mu_{23})(\bar{w}_1(w_1-1)-\mu_{23})}\right)}{(w_1(\bar{w}_1-1)-\mu_{23})(\bar{w}_1(w_1-1)-\mu_{23})}\Bigg]$$
$$=\frac{2\pi}{p_1^2}\log\left(\frac{\mu_{23}-(1-w_1)(1-\bar{w}_1)}{\mu_{23}+\bar{w}_1(1-w_1)}\right)+\mathcal{O}(\epsilon)\ . \tag{B.31}$$

Double cuts

The double cut in the external channel p_1^2 and internal mass m_{23}^2 is

$$\begin{aligned}&\mathrm{Cut}_{p_1^2,m_{23}^2}\left[T(p_1^2,0,0;m_{12}^2,m_{23}^2,m_{13}^2)\right]=\\ =&-4\pi^2 i\frac{e^{\gamma_E\epsilon}}{\Gamma(1-\epsilon)}(p_1^2)^{-1-\epsilon}\left(\bar{w}_1(w_1-1)-\mu_{23}\right)^{-\epsilon}\left(-w_1(\bar{w}_1-1)+\mu_{23}\right)^{-\epsilon}\\ &\theta(\bar{w}_1(w_1-1)-\mu_{23})\theta(-w_1(\bar{w}_1-1)+\mu_{23})\\ =&-\frac{4\pi^2 i}{p_1^2}\theta(\bar{w}_1(w_1-1)-\mu_{23})\theta(-w_1(\bar{w}_1-1)+\mu_{23})+\mathcal{O}(\epsilon)\ .\end{aligned} \tag{B.32}$$

The double cut in the internal masses m_{12}^2 and m_{23}^2 is

$$\begin{aligned}&\mathrm{Cut}_{m_{12}^2,m_{23}^2}\left[T(p_1^2,0,0;m_{12}^2,m_{23}^2,m_{13}^2)\right]=\\ =&-4\pi^2 i\frac{e^{\gamma_E\epsilon}}{\Gamma(1-\epsilon)}(-p_1^2)^{-1-\epsilon}\left(\mu_{23}-(w_1\bar{w}_1-\mu_{23})(\mu_{23}-(1-w_1)(1-\bar{w}_1))\right)^{-\epsilon}\\ &\theta(w_1\bar{w}_1-\mu_{23})\theta\left(\mu_{23}-(w_1\bar{w}_1-\mu_{23})(\mu_{23}-(1-w_1)(1-\bar{w}_1))\right)\\ =&\frac{4\pi^2 i}{p_1^2}\theta(w_1\bar{w}_1-\mu_{23})\theta\left(\mu_{23}-(w_1\bar{w}_1-\mu_{23})(\mu_{23}-(1-w_1)(1-\bar{w}_1))\right)+\mathcal{O}(\epsilon)\ .\end{aligned} \tag{B.33}$$

The double cut in the internal masses m_{13}^2 and m_{23}^2 is

$$\begin{aligned}&\mathrm{Cut}_{m_{13}^2,m_{23}^2}\left[T(p_1^2,0,0;m_{12}^2,m_{23}^2,m_{13}^2)\right]=\\ &\quad=-4\pi^2 i\frac{e^{\gamma_E\epsilon}}{\Gamma(1-\epsilon)}(-p_1^2)^{-1-\epsilon}\theta((1-w_1)(1-\bar{w}_1)-\mu_{23})\\ &\qquad\left(\mu_{23}-(w_1\bar{w}_1-\mu_{23})(\mu_{23}-(1-w_1)(1-\bar{w}_1))\right)^{-\epsilon}\\ &\qquad\theta\left(\mu_{23}-(w_1\bar{w}_1-\mu_{23})(\mu_{23}-(1-w_1)(1-\bar{w}_1))\right)\\ &\quad=\frac{4\pi^2 i}{p_1^2}\theta\left(\mu_{23}-(w_1\bar{w}_1-\mu_{23})(\mu_{23}-(1-w_1)(1-\bar{w}_1))\right)\\ &\qquad\theta((1-w_1)(1-\bar{w}_1)-\mu_{23})+\mathcal{O}(\epsilon)\ .\end{aligned} \tag{B.34}$$

All other double cuts are zero.

B.2 Two-mass triangles

We give explicit expressions for triangles with two external massive channels. For all the examples given, we have computed the uncut triangles both through standard Feynman parametrization and through a dispersive integral, and verified agreement of the expressions. Divergent integrals were compared with the results given in ref. [39]. For all triangles with two external massive channels considered in the following subsections, we separate the rational prefactor from the pure transcendental function according to the relation

$$T(0,p_2^2,p_3^2;m_{12}^2,m_{23}^2,m_{13}^2) = \frac{i}{p_2^2-p_3^2}\mathcal{T}(0,p_2^2,p_3^2;m_{12}^2,m_{23}^2,m_{13}^2)\,, \tag{B.35}$$

where the internal masses are generic and can be zero. Before expansion in the dimensional regularization parameter ϵ, the results will often involve the functions ${}_2F_1$ and F_1 defined in eqs. (A.13) and (A.14).

B.2.1 $T(0,p_2^2,p_3^2;0,0,0)$

The triangle with two external massive channels, eq. (B.2a), is

$$T(0,p_2^2,p_3^2;0,0,0) = -i\frac{c_\Gamma}{\epsilon^2}\frac{(-p_2^2)^{-\epsilon}-(-p_3^2)^{-\epsilon}}{p_2^2-p_3^2}, \tag{B.36}$$

where c_Γ is defined in eq. (A.12). The symbol is

$$\mathcal{S}\left[\mathcal{T}(0,p_2^2,p_3^2;0,0,0)\right] = -\frac{p_2^2}{\epsilon}+\frac{p_3^2}{\epsilon}+p_2^2\otimes p_2^2-p_3^2\otimes p_3^2+\mathcal{O}(\epsilon)\,. \tag{B.37}$$

Single cuts

The cut in the p_2^2 is

$$\mathrm{Cut}_{p_2^2}\left[T(0,p_2^2,p_3^2;0,0,0)\right] = -2\pi\frac{e^{\gamma_E\epsilon}\Gamma(1-\epsilon)}{\epsilon\Gamma(1-2\epsilon)}\frac{(p_2^2)^{-\epsilon}}{p_2^2-p_3^2}, \tag{B.38}$$

and the cut in p_3^2 is obtained by symmetry.

Double cuts

All double cuts are zero.

B.2.2 $T(0, p_2^2, p_3^2; 0, m_{23}^2, 0)$

The triangle of fig. B.2b is given by:

$$\begin{aligned}
T(0,p_2^2,p_3^2;0,m_{23}^2,0) =& \\
=& i\frac{e^{\gamma_E\epsilon}\Gamma(1+\epsilon)}{\epsilon(1-\epsilon)}\frac{(m_{23}^2)^{-\epsilon}}{p_2^2-p_3^2}\left[\frac{p_2^2}{p_2^2-m_{23}^2}\,{}_2F_1\left(1,1-2\epsilon;2-\epsilon;\frac{p_2^2}{p_2^2-m_{23}^2}\right)\right. \\
&\left.-\frac{p_3^2}{p_3^2-m_{23}^2}\,{}_2F_1\left(1,1-2\epsilon;2-\epsilon;\frac{p_3^2}{p_3^2-m_{23}^2}\right)\right] \\
=& \frac{i}{p_2^2-p_3^2}\left[\frac{1}{\epsilon}\log\left(\frac{m_{23}^2-p_2^2}{m_{23}^2-p_3^2}\right)+\mathrm{Li}_2\left(\frac{p_2^2}{p_2^2-m_{23}^2}\right)-\mathrm{Li}_2\left(\frac{p_3^2}{p_3^2-m_{23}^2}\right)\right. \\
&\left.-\frac{1}{2}\log^2\left(m_{23}^2-p_2^2\right)+\frac{1}{2}\log^2\left(m_{23}^2-p_3^2\right)\right]+\mathcal{O}(\epsilon)\,. \qquad \text{(B.39)}
\end{aligned}$$

The symbol is

$$\begin{aligned}
\mathcal{S}\left[\mathcal{T}(0,p_2^2,p_3^2;0,m_{23}^2,0)\right] =& \frac{1}{\epsilon}\frac{m_{23}^2-p_2^2}{m_{23}^2-p_3^2}+m_{23}^2\otimes\frac{p_3^2(m_{23}^2-p_2^2)}{p_2^2(m_{23}^2-p_3^2)} \\
&+\left(m_{23}^2-p_2^2\right)\otimes\frac{p_2^2}{\left(m_{23}^2-p_2^2\right)^2}-\left(m_{23}^2-p_3^2\right)\otimes\frac{p_3^2}{\left(m_{23}^2-p_3^2\right)^2}+\mathcal{O}(\epsilon)\,. \qquad \text{(B.40)}
\end{aligned}$$

Single cuts

The cut in the external channel p_2^2 is

$$\begin{aligned}
\mathrm{Cut}_{p_2^2}\left[T(0,p_2^2,p_3^2;0,m_{23}^2,0)\right] =& -2\pi\frac{e^{\gamma_E\epsilon}\Gamma(1-\epsilon)}{\epsilon\Gamma(1-2\epsilon)}\frac{(p_2^2)^\epsilon(p_2^2-m_{23}^2)^{-2\epsilon}}{p_2^2-p_3^2} \\
=& -\frac{2\pi}{\epsilon(p_2^2-p_3^2)}-\frac{2\pi}{p_2^2-p_3^2}\left[\log\left(p_2^2\right)-2\log\left(p_2^2-m_{23}^2\right)\right]+\mathcal{O}(\epsilon)\,. \qquad \text{(B.41)}
\end{aligned}$$

The cut in the external channel p_3^2 is trivial to obtain from the symmetry of the function. The cut in the internal mass m_{23}^2 is

$$\begin{aligned}
\mathrm{Cut}_{m_{23}^2}\left[T(0,p_2^2,p_3^2;0,m_{23}^2,0)\right] =& \\
=& -\frac{\pi e^{\gamma_E\epsilon}}{\epsilon\Gamma(1-\epsilon)}\frac{\Gamma(1+2\epsilon)}{p_2^2-p_3^2}\left\{\frac{\Gamma(1-\epsilon)}{\Gamma(1+\epsilon)}(-p_2^2)^{-\epsilon}\left(1-\frac{m_{23}^2}{p_2^2}\right)^{-2\epsilon}\right.
\end{aligned}$$

$$
\begin{aligned}
&-\frac{(-p_2^2)^{-\epsilon}}{\Gamma(1+2\epsilon)}\,{}_2F_1\left(\epsilon,2\epsilon;1+2\epsilon;1-\frac{m_{23}^2}{p_2^2}\right)-\left(p_2^2\leftrightarrow p_3^2\right)\Big\}\\
=&\frac{2\pi}{p_2^2-p_3^2}\left[\log\left(\frac{-p_3^2}{m_{23}^2-p_3^2}\right)-\log\left(\frac{-p_2^2}{m_{23}^2-p_2^2}\right)\right]+\mathcal{O}(\epsilon)\,.
\end{aligned}
\tag{B.42}
$$

Double cuts

All double cuts are zero.

B.2.3 $T(0,p_2^2,p_3^2;m_{12}^2,0,0)$

The triangle of fig. B.2c is given by:

$$
\begin{aligned}
&T(0,p_2^2,p_3^2;m_{12}^2,0,0)=\\
&\quad=i\frac{e^{\gamma_E\epsilon}\Gamma(1+\epsilon)}{\epsilon}\left[\frac{(-p_3^2)^{-\epsilon}}{m_{12}^2}\frac{\Gamma^2(1-\epsilon)}{\Gamma(2-2\epsilon)}\,{}_2F_1\left(1,1-\epsilon;2-2\epsilon;\frac{p_2^2-p_3^2}{m_{12}^2}\right)\right.\\
&\qquad\left.-\frac{(m_{12}^2)^{-1-\epsilon}}{1-\epsilon}\,F_1\left(1;1,\epsilon;2-\epsilon;\frac{p_2^2-p_3^2}{m_{12}^2};\frac{p_2^2}{m_{12}^2}\right)\right]\\
&\quad=\frac{i}{(p_2^2-p_3^2)}\left[\mathrm{Li}_2\left(\frac{p_2^2}{m_{12}^2}\right)-\mathrm{Li}_2\left(\frac{p_2^2-m_{12}^2}{p_3^2}\right)+\frac{1}{2}\log^2\left(-\frac{p_3^2}{m_{12}^2}\right)\right.\\
&\qquad\left.-\log\left(\frac{p_2^2-m_{12}^2}{p_3^2}\right)\log\left(\frac{m_{12}^2-p_2^2+p_3^2}{p_3^2}\right)+\frac{\pi^2}{3}\right]+\mathcal{O}(\epsilon)\,.
\end{aligned}
\tag{B.43}
$$

The symbol is

$$
\begin{aligned}
\mathcal{S}\big[\mathcal{T}(0,p_2^2,p_3^2;m_{12}^2,0,0)\big]&=m_{12}^2\otimes\left(\frac{p_2^2}{p_3^2}\right)+p_3^2\otimes\left(\frac{m_{12}^2-p_2^2+p_3^2}{m_{12}^2}\right)\\
&+\left(m_{12}^2-p_2^2\right)\otimes\left(\frac{-p_3^2m_{12}^2}{p_2^2(p_2^2-m_{12}^2-p_3^2)}\right)+\mathcal{O}(\epsilon)\,.
\end{aligned}
\tag{B.44}
$$

Single cuts

The cut in the external channel p_2^2 is

$$
\begin{aligned}
&\mathrm{Cut}_{p_2^2}\left[T(0,p_2^2,p_3^2;m_{12}^2,0,0)\right]=\\
&\quad=-2\pi\frac{e^{\gamma_E\epsilon}\Gamma(1-\epsilon)}{\Gamma(2-2\epsilon)}\frac{(p_2^2-m_{12}^2)^{1-2\epsilon}}{(p_2^2)^{-\epsilon}m_{12}^2p_3^2}\,{}_2F_1\left(1,1-\epsilon;2-2\epsilon;\frac{(p_2^2-p_3^2)(p_2^2-m_{12}^2)}{m_{12}^2p_3^2}\right)\\
&\quad=\frac{2\pi}{p_2^2-p_3^2}\left(\log\left(\frac{p_2^2}{m_{12}^2}\right)+\log\left(\frac{p_2^2-m_{12}^2-p_3^2}{-p_3^2}\right)\right)+\mathcal{O}(\epsilon)\,.
\end{aligned}
\tag{B.45}
$$

The cut in the external channel p_3^2 is

$$\begin{aligned}
&\mathrm{Cut}_{p_3^2}\left[T(0,p_2^2,p_3^2;m_{12}^2,0,0)\right] = \\
&\quad = -2\pi\frac{e^{\gamma_E\epsilon}\Gamma(1-\epsilon)}{\Gamma(2-2\epsilon)}\frac{(p_3^2)^{-\epsilon}}{p_2^2-p_3^2-m_{12}^2}\,{}_2F_1\left(1,1-\epsilon;2-2\epsilon;\frac{p_2^2-p_3^2}{p_2^2-p_3^2-m_{12}^2}\right) \\
&\quad = \frac{2\pi}{p_2^2-p_3^2}\left(\log\left(m_{12}^2\right)-\log\left(m_{12}^2-p_2^2+p_3^2\right)\right)+\mathcal{O}(\epsilon)\,. \qquad \text{(B.46)}
\end{aligned}$$

The cut in the internal mass m_{12}^2 is

$$\begin{aligned}
&\mathrm{Cut}_{m_{12}^2}\left[T(0,p_2^2,p_3^2;m_{12}^2,0,0)\right] = \\
&\quad = \frac{2\pi e^{\gamma_E\epsilon}}{\Gamma(2-\epsilon)}\frac{(m_{12}^2-p_2^2)^{-\epsilon}}{p_3^2}\left(\frac{m_{12}^2}{p_2^2}\right)^{-\epsilon}F_1\left(1-\epsilon;1,\epsilon;2-\epsilon;\frac{p_3^2-p_2^2}{p_3^2};\frac{m_{12}^2}{m_{12}^2-p_2^2}\right) \\
&\quad = \frac{2\pi}{p_2^2-p_3^2}\left(\log\left(-p_2^2\right)-\log\left(-p_3^2\right)\right)+\mathcal{O}(\epsilon)\,. \qquad \text{(B.47)}
\end{aligned}$$

Double cuts

The double cut in the external channels p_2^2 and p_3^2 is

$$\begin{aligned}
&\mathrm{Cut}_{p_2^2,p_3^2}\left[T(0,p_2^2,p_3^2;m_{12}^2,0,0)\right] = \\
&\qquad = \frac{4\pi^2 i e^{\gamma_E\epsilon}}{\Gamma(1-\epsilon)}\frac{(p_3^2)^{-\epsilon}(p_2^2-p_3^2-m_{12}^2)^{-\epsilon}}{(m_{12}^2)^{\epsilon}(p_2^2-p_3^2)^{1-2\epsilon}}\theta(p_2^2-p_3^2-m_{12}^2) \\
&\qquad = \frac{4\pi^2 i}{p_2^2-p_3^2}\theta(p_2^2-p_3^2-m_{12}^2)+\mathcal{O}(\epsilon)\,. \qquad \text{(B.48)}
\end{aligned}$$

The double cut in the external channel p_3^2 and the internal mass m_{12}^2 is

$$\begin{aligned}
&\mathrm{Cut}_{p_3^2,m_{12}^2}\left[T(0,p_2^2,p_3^2;m_{12}^2,0,0)\right] = \\
&\qquad = -4\pi^2 i\frac{e^{\gamma_E\epsilon}}{\Gamma(1-\epsilon)}\frac{(p_3^2)^{-\epsilon}(-m_{12}^2)^{-\epsilon}}{(p_3^2-p_2^2)^{1-\epsilon}}(p_3^2+m_{12}^2-p_2^2)^{-\epsilon}\theta(p_3^2+m_{12}^2-p_2^2) \\
&\qquad = \frac{4\pi^2 i}{p_2^2-p_3^2}\theta(p_3^2+m_{12}^2-p_2^2)\,. \qquad \text{(B.49)}
\end{aligned}$$

The double cut in the external channel p_2^2 and the internal mass m_{12}^2 is zero.

B.3 Three-mass triangles

We now present expressions for triangles with three external massive legs. We start by discussing the diagram with massless propagators. We then describe how we computed the triangles with one or two massive propagators, for which we give a very simple expression that allows us to evaluate the diagrams very easily to arbitrary order in ϵ. This follows what was done for the triangle with massless propagators in section 4.2. Our method does not work for the case with three massive propagators, where we were not able to find a rational parametrization, and we thus rely on the result in ref. [143]. We will comment further on the choice of variables for this example in section B.3.5 below. For the cases treated in this section we will not compute mass discontinuities, as they do not add anything to what we have already illustrated in the context of previous examples. We separate the rational prefactor from the pure transcendental function according to the relation

$$T(p_1^2,p_2^2,p_3^2;m_{12}^2,m_{23}^2,m_{13}^2)=\frac{i}{p_1^2(z-\bar{z})}\mathcal{T}(p_1^2,p_2^2,p_3^2;m_{12}^2,m_{23}^2,m_{13}^2)\,, \tag{B.50}$$

where the internal masses are generic and can be zero.

B.3.1 $T(p_1^2,p_2^2,p_3^3;0,0,0)$

Many different expressions are known for the three-mass triangle integral, fig. B.3a, both in arbitrary dimensions [98, 144] as well as an expansion around four space-time dimensions in dimensional regularization [65, 99, 145, 146]. We showed in section 4.2 a way to compute it through a dispersive integral [36].

Here we follow [65] in writing the result of the integral in the form

$$T(p_1^2,p_2^2,p_3^2;0,0,0)=-\frac{i}{p_1^2}\frac{2}{z-\bar{z}}\mathcal{P}_2(z)+\mathcal{O}(\epsilon), \tag{B.51}$$

where

$$\mathcal{P}_2(z) \;=\; \mathrm{Li}_2(z)-\mathrm{Li}_2(\bar{z})+\frac{1}{2}\log(z\bar{z})\log\left(\frac{1-z}{1-\bar{z}}\right)\,, \tag{B.52}$$

We thus have

$$\begin{aligned}\mathcal{T}(p_1^2,p_2^2,p_3^2;0,0,0) &= \mathcal{T}(z,\bar{z})\\ &= -2\mathrm{Li}_2(z)+2\mathrm{Li}_2(\bar{z})-\log(z\bar{z})\log\left(\frac{1-z}{1-\bar{z}}\right). \end{aligned} \tag{B.53}$$

The symbol of the one-loop three mass triangle is

$$\mathcal{S}\left[\mathcal{T}(z,\bar{z})\right] = (z\bar{z})\otimes\frac{1-\bar{z}}{1-z}+((1-z)(1-\bar{z}))\otimes\frac{z}{\bar{z}}+\mathcal{O}(\epsilon) \tag{B.54}$$

We note that in this expression the first entry condition is explicit despite the use of the variables z and $\bar{z}$.

Single cuts

The cut in the external channel p_1^2 is

$$\begin{aligned}&\mathrm{Cut}_{p_1^2}\left[T(p_1^2,p_2^2,p_3^2;0,0,0)\right] =\\ &\quad= -\frac{2\pi e^{\gamma_E\epsilon}\Gamma(1-\epsilon)}{\Gamma(2-2\epsilon)}\frac{(p_1^2)^{-1-\epsilon}}{(z-1)\bar{z}}\,{}_2F_1\left(1,1-\epsilon;2-2\epsilon;\frac{z-\bar{z}}{(z-1)\bar{z}}\right)\\ &\quad=\frac{2\pi}{p_1^2(z-\bar{z})}\log\left(\frac{z(1-\bar{z})}{\bar{z}(1-z)}\right)+\mathcal{O}(\epsilon)\,. \end{aligned} \tag{B.55}$$

The cut in the external channel p_2^2 is

$$\begin{aligned}&\mathrm{Cut}_{p_2^2}\left[T(p_1^2,p_2^2,p_3^2;0,0,0)\right] =\\ &\quad=\frac{2\pi e^{\gamma_E\epsilon}\Gamma(1-\epsilon)}{\Gamma(2-2\epsilon)}\frac{(-p_1^2)^{-1-\epsilon}}{(1-z)(-z\bar{z})^{\epsilon}}\,{}_2F_1\left(1,1-\epsilon;2-2\epsilon;\frac{z-\bar{z}}{z-1}\right)\\ &\quad=\frac{2\pi}{p_1^2(z-\bar{z})}\log\left(\frac{1-z}{1-\bar{z}}\right)+\mathcal{O}(\epsilon)\,. \end{aligned} \tag{B.56}$$

The cut in the external channel p_3^2 is

$$\begin{aligned}&\mathrm{Cut}_{p_3^2}\left[T(p_1^2,p_2^2,p_3^2;0,0,0)\right] =\\ &\quad=\frac{2\pi e^{\gamma_E\epsilon}\Gamma(1-\epsilon)}{\Gamma(2-2\epsilon)}\frac{(-p_1^2)^{-1-\epsilon}}{\bar{z}(-(1-z)(1-\bar{z}))^{\epsilon}}\,{}_2F_1\left(1,1-\epsilon;2-2\epsilon;-\frac{z-\bar{z}}{\bar{z}}\right)\\ &\quad=\frac{2\pi}{p_1^2(z-\bar{z})}\log\left(\frac{\bar{z}}{z}\right)+\mathcal{O}(\epsilon)\,. \end{aligned} \tag{B.57}$$

Double cuts

The double cuts in p_1^2 and p_2^2 and in p_1^2 and p_3^2, although computed in different kinematic regions, are equal:

$$\begin{aligned}\mathrm{Cut}_{p_1^2,p_2^2}\left[T(p_1^2,p_2^2,p_3^2;0,0,0)\right] &= \mathrm{Cut}_{p_1^2,p_3^2}\left[T(p_1^2,p_2^2,p_3^2;0,0,0)\right] \qquad \text{(B.58)}\\ &= 4\pi^2 i\frac{e^{\gamma_E\epsilon}}{\Gamma(1-\epsilon)}\frac{(p_1^2)^{-1-\epsilon}}{(z-\bar{z})^{1-2\epsilon}}(-z\bar{z}(1-z)(1-\bar{z}))^{-\epsilon}\\ &= \frac{4\pi^2 i}{p_1^2(z-\bar{z})}+\mathcal{O}(\epsilon)\,. \qquad \text{(B.59)}\end{aligned}$$

The double cut in p_2^2 and p_3^2 is

$$\begin{aligned}&\mathrm{Cut}_{p_2^2,p_3^2}\left[T(p_1^2,p_2^2,p_3^2;0,0,0)\right] =\\ &\quad= 4\pi^2 i\frac{e^{\gamma_E\epsilon}}{\Gamma(1-\epsilon)}\frac{(-p_1^2)^{-1-\epsilon}}{(z-\bar{z})^{1-2\epsilon}}(z\bar{z}(1-z)(1-\bar{z}))^{-\epsilon}\\ &\quad= -\frac{4\pi^2 i}{p_1^2(z-\bar{z})}+\mathcal{O}(\epsilon)\,. \qquad \text{(B.60)}\end{aligned}$$

B.3.2 Computation of triangles with three external and one or two internal masses

Triangles with two external masses are easily computed with standard techniques to arbitrary order in ϵ. However, that is no longer the case for triangles with three external masses [65]. In section 4.2, see also ref. [36], it was shown that the triangle with three external masses and massless internal propagators was easily computable to arbitrary order in ϵ through a double dispersion integral over its double cut. We now show this is also possible when there are one or two massive propagators. In the following, we will use the variables

$$\alpha\bar{\alpha} = x = \frac{s_2}{p_1^2}\,, \qquad\qquad (1-\alpha)(1-\bar{\alpha}) = y = \frac{s_3}{p_1^2}\,,$$

where s_2 and s_3 are integration variables in dispersion relations.

We will use the shorthand $T(p_i^2;m_{jk}^2)$ for any of the three-mass triangles. We now proceed as in section 4.2:

$$T(p_i^2;m_{jk}^2) = -\frac{1}{(2\pi i)^2}\int_{c_2}\frac{ds_2}{s_2-p_2^2}\int_{c_3}\frac{ds_3}{s_3-p_3^2}\left(\mathrm{Cut}_{p_2^2,p_3^2}T(p_i^2;m_{jk}^2)\right)\Big|_{p_2^2=s_2,p_3^2=s_3}$$

$$= \frac{i}{4\pi^2 p_1^2} \int_{c_\alpha} d\alpha \int_{c_{\bar{\alpha}}} d\bar{\alpha} \frac{\left(\mathrm{Cut}_{p_2^2,p_3^2} \mathcal{T}(p_i^2; m_{jk}^2)\right)\Big|_{z=\alpha,\bar{z}=\bar{\alpha}}}{(\alpha\bar{\alpha} - z\bar{z})((1-\alpha)(1-\bar{\alpha}) - (1-z)(1-\bar{z}))} \,. \tag{B.61}$$

The only difference between the triangles with one and two massive propagators are the integration contours c_2 and c_3, and c_α and $c_{\bar{\alpha}}$. For the case with one internal mass,

$$c_2 = [m_{12}^2, \infty) \,, \quad c_3 = [0, \infty) \quad \text{and} \quad c_\alpha = [1, \infty) \,, \quad c_{\bar{\alpha}} = (-\infty, \mu_{12}] \,,$$

and for the case with two internal masses,

$$c_2 = [m_{12}^2, \infty) \,, \quad c_3 = [m_{13}^2, \infty) \quad \text{and} \quad c_\alpha = [w_1, \infty) \,, \quad c_{\bar{\alpha}} = (-\infty, \bar{w}_1] \,.$$

For either case, the functions $\left(\mathrm{Cut}_{p_2^2,p_3^2} \mathcal{T}(p_i^2; m_{jk}^2)\right)\Big|_{z=\alpha,\bar{z}=\bar{\alpha}}$ are given by powers of logarithms whose arguments are linear in both α and $\bar{\alpha}$. The integral in eq. (B.61) is thus trivial to solve in terms of polylogarithms to the desired order in ϵ. The change of variables

$$\beta = \frac{a_\beta}{\alpha} \qquad\qquad \gamma = \frac{1 - a_\gamma}{1 - \bar{\alpha}} \,,$$

where $a_\beta = 1$ or w_1 and $a_\gamma = \mu_{12}$ or $\bar{w}_1$ respectively for the cases with one and two internal massive propagators, makes the integration particularly simple to perform. The results for the finite terms of these two triangles, given below in eqs. (B.63) and (B.70), were computed with this method, and checked to agree with the result in ref. [143]. In our method, as mentioned above, higher orders in ϵ become trivial to compute.

B.3.3 $T(p_1^2, p_2^2, p_3^3; m_{12}^2, 0, 0)$

The triangle of fig. B.3b is given by

$$T(p_1^2, p_2^2, p_3^3; m_{12}^2, 0, 0) = \frac{i}{p_1^2(z - \bar{z})} \mathcal{T}\left(p_1^2, z, \bar{z}, \mu_{12}\right) \,, \tag{B.62}$$

where $\mathcal{T}\left(p_1^2, z, \bar{z}, \mu_{12}\right)$ is a pure function given by

$$\begin{aligned}\mathcal{T}\left(p_1^2, z, \bar{z}, \mu_{12}\right) =& G\left(1, z, \mu_{12}\right) + G\left(1, \frac{\mu_{12}}{z}, \bar{z}\right) - G\left(1, \frac{\mu_{12}}{\bar{z}}, z\right) - G\left(1, \bar{z}, \mu_{12}\right) \\ & - \mathrm{Li}_2(z) + \mathrm{Li}_2(\bar{z}) + \log(1-z)\log\left(1 - \frac{\mu_{12}}{z}\right) \\ & + \log\left(1 - \frac{1}{\mu_{12}}\right)\log\left(\frac{1-z}{1-\bar{z}}\right) - \log(1-\bar{z})\log\left(1 - \frac{\mu_{12}}{\bar{z}}\right) \\ & + \log\left(1-\mu_{12}\right)\log\left(\frac{z(1-\bar{z})\left(\bar{z}-\mu_{12}\right)}{\bar{z}(1-z)\left(z-\mu_{12}\right)}\right) + \mathcal{O}(\epsilon)\,. \end{aligned} \tag{B.63}$$

The symbol of its finite part is

$$\begin{aligned}\mathcal{S}\left[\mathcal{T}\left(p_1^2, z, \bar{z}, \mu_{12}\right)\right] =& \mu_{12} \otimes \frac{\bar{z}(z-\mu_{12})}{z(\bar{z}-\mu_{12})} + (1-z)(1-\bar{z}) \otimes \frac{(z-\mu_{12})}{(\bar{z}-\mu_{12})} \\ & + (z\bar{z}-\mu_{12}) \otimes \frac{z(1-\bar{z})(\bar{z}-\mu_{12})}{\bar{z}(1-z)(z-\mu_{12})} + (1-\mu_{12}) \otimes \frac{(1-z)(\bar{z}-\mu_{12})}{(1-\bar{z})(z-\mu_{12})}\,. \end{aligned} \tag{B.64}$$

Single cuts

The cut in the p_1^2 channel is

$$\begin{aligned}\mathrm{Cut}_{p_1^2}\left[T(p_1^2, p_2^2, p_3^3; m_{12}^2, 0, 0)\right] =& -2\pi \frac{e^{\gamma_E \epsilon}\Gamma(1-\epsilon)}{\Gamma(2-2\epsilon)}\left(p_1^2\right)^{-1-\epsilon} \\ & \frac{(1-\mu_{12})^{1-2\epsilon}}{(1-z)(\mu_{12}-\bar{z})}\,{}_2F_1\left(1, 1-\epsilon, 2-2\epsilon, \frac{(1-\mu_{12})(z-\bar{z})}{(1-z)(\mu_{12}-\bar{z})}\right) \\ =& \frac{2\pi}{p_1^2(z-\bar{z})}\log\left(\frac{(1-\bar{z})(z-\mu_{12})}{(z-1)(\mu_{12}-\bar{z})}\right) + \mathcal{O}\left(\epsilon\right)\,. \end{aligned} \tag{B.65}$$

The cut in the p_2^2 channel is

$$\begin{aligned}\mathrm{Cut}_{p_2^2}\left[T(p_1^2, p_2^2, p_3^3; m_{12}^2, 0, 0)\right] =& -2\pi \frac{e^{\gamma_E \epsilon}\Gamma(1-\epsilon)}{\Gamma(2-2\epsilon)}\left(-p_1^2\right)^{-1-\epsilon} \\ & \frac{(\mu_{12}-z\bar{z})^{1-2\epsilon}(-z\bar{z})^{\epsilon}}{\bar{z}(1-z)(z-\mu_{12})}\,{}_2F_1\left(1, 1-\epsilon; 2-2\epsilon; \frac{(z-\bar{z})(\mu_{12}-z\bar{z})}{\bar{z}(1-z)(z-\mu_{12})}\right) \\ =& \frac{2\pi}{p_1^2(z-\bar{z})}\log\left(\frac{-\bar{z}(1-z)(z-\mu_{12})}{z(1-\bar{z})(\mu_{12}-\bar{z})}\right) + \mathcal{O}\left(\epsilon\right)\,. \end{aligned} \tag{B.66}$$

The cut in the p_3^2 channel is

$$\begin{aligned}
&\mathrm{Cut}_{p_3^2}\left[T(p_1^2,p_2^2,p_3^3;m_{12}^2,0,0)\right] = \\
&= -2\pi\frac{e^{\gamma_E\epsilon}\Gamma(1-\epsilon)}{\Gamma(2-2\epsilon)}\left(-p_1^2\right)^{-1-\epsilon}\frac{((z-1)(1-\bar{z}))^{-\epsilon}}{\mu_{12}-\bar{z}}\,{}_2F_1\left(1,1-\epsilon;2-2\epsilon;\frac{z-\bar{z}}{\mu_{12}-\bar{z}}\right) \\
&= \frac{2\pi}{p_1^2(z-\bar{z})}\log\left(\frac{\mu_{12}-\bar{z}}{\mu_{12}-z}\right)+\mathcal{O}\left(\epsilon\right)\,. \qquad \text{(B.67)}
\end{aligned}$$

Double cuts

The double cut in the p_i^2 and p_j^2 channels is

$$\begin{aligned}
&\mathrm{Cut}_{p_i^2,p_j^2}\left[T(p_1^2,p_2^2,p_3^3;m_{12}^2,0,0)\right] = \\
&= \Theta_{ij}\frac{4\pi^2 i e^{\gamma_E\epsilon}}{\Gamma(1-\epsilon)}\left((-1)^a p_1^2\right)^{-1-\epsilon}(z-\bar{z})^{-1+2\epsilon}\left((z-1)(1-\bar{z})(\bar{z}-\mu_{12})(z-\mu_{12})\right)^{-\epsilon} \\
&= \frac{4\pi^2 i}{p_1^2(z-\bar{z})}(-1)^a\Theta_{ij}+\mathcal{O}(\epsilon)\,, \qquad \text{(B.68)}
\end{aligned}$$

where $a=0$ for $(i,j)=(1,2)$ or $(1,3)$, and $a=1$ for $(i,j)=(2,3)$. The theta functions are

$$\begin{aligned}
\Theta_{12} &= \theta(z-1)\theta(1-\bar{z})\theta(z-\mu_{12})\theta(\bar{z}-\mu_{12}) \\
\Theta_{13} &= \theta(1-z)\theta(1-\bar{z})\theta(z-\mu_{12})\theta(\mu_{12}-\bar{z}) \\
\Theta_{23} &= \theta(z-1)\theta(1-\bar{z})\theta(z-\mu_{12})\theta(\mu_{12}-\bar{z})\,.
\end{aligned}$$

B.3.4 $T(p_1^2,p_2^2,p_3^3;m_{12}^2,0,m_{13}^2)$

The triangle of fig. B.3c is given by

$$T(p_1^2,p_2^2,p_3^3;m_{12}^2,0,m_{13}^2) = \frac{i}{p_1^2(z-\bar{z})}\mathcal{T}\left(p_1^2,z,\bar{z},w_1,\bar{w}_1\right), \qquad \text{(B.69)}$$

where $\mathcal{T}\left(p_1^2,z,\bar{z},w_1,\bar{w}_1\right)$ is a pure function given by

$$\begin{aligned}
&\mathcal{T}\left(p_1^2,z,\bar{z},w_1,\bar{w}_1\right) = \\
&\quad G\left(\frac{w_1}{z},\frac{w_1(\bar{w}_1-1)}{\bar{w}_1+(1-z)(1-\bar{z})-1},1\right)+G\left(\frac{w_1}{\bar{z}},w_1,1\right)-G\left(\frac{w_1}{z},w_1,1\right) \\
&\quad -G\left(\frac{w_1}{\bar{z}},\frac{w_1(\bar{w}_1-1)}{\bar{w}_1+(1-z)(1-\bar{z})-1},1\right)-\mathrm{Li}_2\left(\frac{z\bar{z}}{w_1\bar{w}_1}\right)-G\left(\frac{w_1}{z},\frac{w_1\bar{w}_1}{z\bar{z}},1\right) \\
&\quad -G\left(\bar{w}_1,\frac{w_1\bar{w}_1}{\bar{z}},z\right)+\log\left(1-\frac{1}{\bar{w}_1}\right)\log\left(\frac{w_1-z}{w_1-\bar{z}}\right)
\end{aligned}$$

$$+\log\left(1-\frac{\bar{z}}{w_1}\right)\log\left(1-\frac{z}{\bar{w}_1}\right)+\mathcal{O}(\epsilon)\,. \tag{B.70}$$

The symbol of its finite part is

$$\begin{aligned}\mathcal{S}\left[\mathcal{T}\left(p_1^2,z,\bar{z},w_1,\bar{w}_1\right)\right]&=(z\bar{z}-w_1\bar{w}_1)\otimes\frac{z(w_1-\bar{z})(\bar{w}_1-\bar{z})}{\bar{z}(w_1-z)(\bar{w}_1-z)}\\&+((1-z)(1-\bar{z})-(1-w_1)(1-\bar{w}_1))\otimes\frac{(1-\bar{z})(w_1-z)(\bar{w}_1-z)}{(1-z)(w_1-\bar{z})(\bar{w}_1-\bar{z})}\\&+(1-w_1)\otimes\frac{(1-z)(w_1-\bar{z})}{(1-\bar{z})(w_1-z)}+w_1\otimes\frac{\bar{z}(w_1-z)}{z(w_1-\bar{z})}\\&+(1-\bar{w}_1)\otimes\frac{(1-z)(\bar{w}_1-\bar{z})}{(1-\bar{z})(\bar{w}_1-z)}+\bar{w}_1\otimes\frac{\bar{z}(\bar{w}_1-z)}{z(\bar{w}_1-\bar{z})}\,.\end{aligned} \tag{B.71}$$

Single cuts

The cut in the p_1^2 channel is

$$\begin{aligned}\mathrm{Cut}_{p_1^2}\left[T(p_1^2,p_2^2,p_3^3;m_{12}^2,0,m_{13}^2)\right]=&-2\pi\frac{e^{\gamma_E\epsilon}\Gamma(1-\epsilon)}{\Gamma(2-2\epsilon)}\left(p_1^2\right)^{-1-\epsilon}\\&\frac{(w_1-\bar{w}_1)^{1-2\epsilon}}{(z-w_1)(\bar{z}-\bar{w}_1)}\,{}_2F_1\left(1,1-\epsilon,2-2\epsilon,\frac{(z-\bar{z})(w_1-\bar{w}_1)}{(z-w_1)(\bar{z}-\bar{w}_1)}\right)\\=&\frac{2\pi}{p_1^2(z-\bar{z})}\log\left(\frac{(z-\bar{w}_1)(w_1-\bar{z})}{(\bar{w}_1-\bar{z})(z-w_1)}\right)+\mathcal{O}\left(\epsilon\right).\end{aligned} \tag{B.72}$$

The cut in the p_2^2 channel is

$$\begin{aligned}\mathrm{Cut}_{p_2^2}\left[T(p_1^2,p_2^2,p_3^3;m_{12}^2,0,m_{13}^2)\right]=&2\pi\frac{e^{\gamma_E\epsilon}\Gamma(1-\epsilon)}{\Gamma(2-2\epsilon)}\left(-p_1^2\right)^{-1-\epsilon}\\&\frac{(-z\bar{z})^{\epsilon}(w_1\bar{w}_1-z\bar{z})^{1-2\epsilon}}{\bar{z}(w_1-z)(z-\bar{w}_1)}\,{}_2F_1\left(1,1-\epsilon,2-2\epsilon,\frac{(z-\bar{z})(w_1\bar{w}_1-z\bar{z})}{\bar{z}(w_1-z)(z-\bar{w}_1)}\right)\\=&\frac{2\pi}{p_1^2(z-\bar{z})}\log\left(\frac{-\bar{z}(z-\bar{w}_1)(w_1-z)}{z(w_1-\bar{z})(\bar{w}_1-\bar{z})}\right)+\mathcal{O}\left(\epsilon\right).\end{aligned} \tag{B.73}$$

The cut in the p_3^2 channel is

$$\begin{aligned}\mathrm{Cut}_{p_3^2}\left[T(p_1^2,p_2^2,p_3^3;m_{12}^2,0,m_{13}^2)\right]=&-2\pi\frac{e^{\gamma_E\epsilon}\Gamma(1-\epsilon)}{\Gamma(2-2\epsilon)}\left(p_1^2\right)^{-1-\epsilon}\\&\frac{u_3^{\epsilon}(u_3-\mu_{13})^{1-2\epsilon}}{(\bar{z}-1)(z-\bar{w}_1)(z-w_1)}\,{}_2F_1\left(1,1-\epsilon,2-2\epsilon,\frac{(z-\bar{z})(u_3-\mu_{13})}{(\bar{z}-1)(z-\bar{w}_1)(z-w_1)}\right)\end{aligned}$$

$$=\frac{2\pi}{p_1^2(z-\bar{z})}\log\left(\frac{(z-1)(\bar{z}-\bar{w}_1)(w_1-\bar{z})}{(1-\bar{z})(z-\bar{w}_1)(z-w_1)}\right)+\mathcal{O}(\epsilon). \tag{B.74}$$

Double cuts

The double cut in the p_i^2 and p_j^2 channels is

$$\begin{aligned}
&\mathrm{Cut}_{p_i^2,p_j^2}\left[T(p_1^2,p_2^2,p_3^3;m_{12}^2,0,m_{13}^2)\right]=\\
&=\Theta_{ij}\frac{4\pi^2 i e^{\gamma_E\epsilon}}{\Gamma(1-\epsilon)}\left((-1)^a p_1^2\right)^{-1-\epsilon}(z-\bar{z})^{-1+2\epsilon}\left((z-w_1)(\bar{z}-\bar{w}_1)(z-\bar{w}_1)(\bar{z}-\bar{w}_1)\right)^{-\epsilon}\\
&=\frac{4\pi^2 i}{p_1^2(z-\bar{z})}(-1)^a\Theta_{ij}+\mathcal{O}(\epsilon)\,,
\end{aligned} \tag{B.75}$$

where $a=0$ for $(i,j)=(1,2)$ or $(1,3)$, and $a=1$ for $(i,j)=(2,3)$. The theta functions are

$$\begin{aligned}
\Theta_{12}&=\theta(z-w_1)\theta(w_1-\bar{z})\theta(z-\bar{w}_1)\theta(\bar{z}-\bar{w}_1)\\
\Theta_{13}&=\theta(w_1-z)\theta(w_1-\bar{z})\theta(z-\bar{w}_1)\theta(\bar{w}_1-\bar{z})\\
\Theta_{23}&=\theta(z-w_1)\theta(w_1-\bar{z})\theta(z-\bar{w}_1)\theta(\bar{w}_1-\bar{z})\,.
\end{aligned}$$

B.3.5 $T(p_1^2,p_2^2,p_3^3;m_{12}^2,m_{23}^2,m_{13}^2)$

For the triangle of fig. B.3d we take the expression from ref. [143], adjusted to match our conventions:

$$T(p_1^2,p_2^2,p_3^3;m_{12}^2,m_{23}^2,m_{13}^2)=\frac{i}{p_1^2(z-\bar{z})}\mathcal{T}(p_1^2,p_2^2,p_3^2;m_{12}^2,m_{23}^2,m_{13}^2)\,, \tag{B.76}$$

where

$$\mathcal{T}(p_1^2,p_2^2,p_3^2;m_{12}^2,m_{23}^2,m_{13}^2)=\sum_{i=1}^{3}\sum_{\sigma=\pm}\left[\mathrm{Li}_2\left(\frac{y_{0i}-1}{y_{i\sigma}}\right)-\mathrm{Li}_2\left(\frac{y_{0i}}{y_{i\sigma}}\right)\right]\,. \tag{B.77}$$

The y_{0i} and $y_{i\pm}$ are given by

$$\begin{aligned} y_{0i} = \frac{-1}{2u_i\sqrt{\lambda_z}}\big[&u_i(u_i - u_{i+1} - u_{i-1} + 2\mu_{i-1,i+1} - \mu_{i,i+1} - \mu_{i-1,i}) \\ &- (u_{i+1} - u_{i-1})(\mu_{i-1,i} - \mu_{i,i+1}) - \sqrt{\lambda_z}(u_i - \mu_{i-1,i} + \mu_{i,i+1})\big], \\ y_{i\pm} = y_{0i} - \frac{1}{2u_i}&\left[u_i - \mu_{i-1,i} + \mu_{i,i+1} \pm \sqrt{\lambda_i}\right]. \end{aligned} \tag{B.78}$$

Here, the indices $i \pm 1$ are defined cyclically. The variables u_i, μ_{ij} are defined in eqs. (2.27) and (2.31), and the λ_i for $i = z, 1, 2, 3$ are defined as

$$\begin{aligned} &\lambda_z = \lambda(1, u_1, u_2), \quad \lambda_1 = \lambda(1, mu_{12}, \mu_{13}), \\ &\lambda_2 = \lambda(u_2, mu_{12}, \mu_{23}), \quad \lambda_3 = \lambda(u_3, mu_{13}, \mu_{23}). \end{aligned} \tag{B.79}$$

To get as close as possible to a rational symbol alphabet, we use the variables z, $\bar{z}$, w_1, $\bar{w}_1$ and μ_{23}, which are adapted to the p_1^2 channel. Since this triangle is fully symmetric, it is easy to choose variables adapted to any of the other two channels. However, given our choice, square roots of $\lambda_2 \equiv \lambda(u_2, \mu_{12}, \mu_{23})$ and $\lambda_3 \equiv \lambda(u_3, \mu_{13}, \mu_{23})$ make an unavoidable appearance. Written in a form where the first entries may be readily identified with the three channel thresholds and the three internal masses, the symbol of the triangle is

$$\begin{aligned} &\mathcal{S}\left[\mathcal{T}\left(p_1^2, z, \bar{z}, w_1, \bar{w}_1, \mu_{23}\right)\right] = \\ &w_1\,(1-\bar{w}_1) \otimes \frac{T_{1-}}{T_{1+}} + \frac{1}{2}\left(-z\bar{z} + w_1\bar{w}_1 - \sqrt{\lambda_2} + \mu_{23}\right) \otimes \frac{T_{2-}}{T_{2+}} \\ &+ \frac{1}{2}\left(\bar{z}z - z - \bar{z} - w_1\bar{w}_1 + w_1 + \bar{w}_1 + \sqrt{\lambda_3} - \mu_{23}\right) \otimes \frac{T_{3-}}{T_{3+}} + w_1\bar{w}_1 \otimes \frac{T_{2+}}{(-z)T_{1-}} \\ &+ (1-w_1)\,(1-\bar{w}_1) \otimes \frac{(z-1)T_{1+}}{T_{3-}} + 4\mu_{23} \otimes \frac{zT_{3+}}{(1-z)T_{2-}}. \end{aligned} \tag{B.80}$$

The $T_{i\pm}$ are given by the general formula

$$\begin{aligned} T_{i\pm} = &- u_i(-u_i + u_{i+1} + u_{i-1} + \mu_{i,i+1} + \mu_{i,i-1} - 2\mu_{i+1,i-1}) \\ &+ (u_{i+1} - u_{i-1})(\mu_{i,i+1} - \mu_{i,i-1}) \pm \sqrt{\lambda_z\lambda_i}\,. \end{aligned} \tag{B.81}$$

In particular, we have

$$\begin{aligned}
T_{1\pm} &= -2(z\bar{z} + w_1\bar{w}_1 - \mu_{23}) + (w_1 + \bar{w}_1)(z + \bar{z}) \pm (w_1 - \bar{w}_1)(z - \bar{z}) \\
T_{2\pm} &= (z\bar{z} + w_1\bar{w}_1 - \mu_{23})(z + \bar{z}) - 2z\bar{z}(w_1 + \bar{w}_1) \pm (z - \bar{z})\sqrt{\lambda_2} \\
T_{3\pm} &= z^2(1 - \bar{z}) + \bar{z}^2(1 - z) + (w_1 + \bar{w}_1)(2z\bar{z} - z - \bar{z}) \\
&\quad + (\mu_{23} - w_1\bar{w}_1)(z + \bar{z} - 2) \pm (z - \bar{z})\sqrt{\lambda_3}\,.
\end{aligned}$$

We note that $T_{1\pm}$ can be written in a simpler form, but where the $\pm$ notation is less clear:

$$\begin{aligned}
T_{1+} &= 2\left(\mu_{23} - (w_1 - \bar{z})(\bar{w}_1 - z)\right) \\
T_{1-} &= 2\left(\mu_{23} - (w_1 - z)(\bar{w}_1 - \bar{z})\right)\,.
\end{aligned} \tag{B.82}$$

Since the triangle depends on the external momenta through the invariants, it depends on z and $\bar{z}$ only through the symmetric combinations $u_2 = z\bar{z}$, $u_3 = (1-z)(1-\bar{z})$. Therefore, once we have removed the rational prefactor, the symbol above is antisymmetric under the exchange $z \leftrightarrow \bar{z}$. However, we note that this antisymmetry is not superficially apparent in the last three terms.

Single cuts

We now show how it is possible to choose variables such that each of the single cuts has a rational alphabet. However, unlike what happens for all other configurations of masses, for each cut we must choose different variables. For instance, in eq. (B.80) we chose variables that rationalize the symbol of the p_1^2 cut (indeed, the $T_{1\pm}$ are rational, as seen in eq. (B.82)). In this section, we give the cut results in terms of two slightly different sets of variables: either we normalize invariants by the same invariant associated with the channel being cut, or by a different invariant. Our notation is that p_i^2 is the channel used for normalization, and p_j^2 is the cut channel in the case where it is different.

We start with variables where we cut in the same channel we normalize by, namely p_i^2. To be more precise, the variables we choose are

$$w_i = \frac{1 + \mu_{ij} - \mu_{jk} + \sqrt{\lambda(u_j, \mu_{ij}, \mu_{jk})}}{2}\,, \quad \bar{w}_i = \frac{1 + \mu_{ij} - \mu_{jk} - \sqrt{\lambda(u_j, \mu_{ij}, \mu_{jk})}}{2}\,,$$

$$z = \frac{1 + u_j - u_k + \sqrt{\lambda(1, u_j, u_k)}}{2}\,, \quad \bar{z} = \frac{1 + u_j - u_k - \sqrt{\lambda(1, u_j, u_k)}}{2}\,, \tag{B.83}$$

related to the invariants through

$$\begin{aligned} z\bar{z} = u_j = \frac{p_j^2}{p_i^2}\,, \quad (1-z)(1-\bar{z}) = u_k = \frac{p_k^2}{p_i^2}\,, \quad \mu_{jk} = \frac{m_{jk}^2}{p_i^2}\,, \\ w_i\bar{w}_i = \mu_{ij} = \frac{m_{ij}^2}{p_i^2}\,, \quad (1-w_i)(1-\bar{w}_i) = \mu_{ik} = \frac{m_{ik}^2}{p_i^2}\,. \end{aligned} \tag{B.84}$$

This is a slight abuse of notation, as strictly speaking the z and $\bar{z}$ variables are different for each i. For $i = 1$, these are the variables defined in eq. (2.29) and eq. (2.33) and the ones used for eq. (B.80).

In terms of these variables, the single cut in the p_i^2 channel is

$$\begin{aligned} \mathrm{Cut}_{p_i^2}\left[T(p_1^2, p_2^2, p_3^3; m_{12}^2, m_{23}^2, m_{13}^2)\right] = -2\pi \frac{e^{\gamma_E}\Gamma(1-\epsilon)}{\Gamma(2-2\epsilon)}(p_i^2)^{-1-\epsilon} \\ \frac{(w_i - \bar{w}_i)^{1-2\epsilon}}{(z-w_i)(\bar{z}-\bar{w}_i) - \mu_{jk}}\, {}_2F_1\left(1, 1-\epsilon; 2-2\epsilon; \frac{(z-\bar{z})(w_i-\bar{w}_i)}{(z-w_i)(\bar{z}-\bar{w}_i)-\mu_{jk}}\right) \\ = \frac{2\pi}{p_i^2(z-\bar{z})} \log\left(\frac{(w_i-\bar{z})(\bar{w}_i - z) - \mu_{jk}}{(w_i - z)(\bar{w}_i - \bar{z}) - \mu_{jk}}\right) + \mathcal{O}(\epsilon)\,. \end{aligned} \tag{B.85}$$

Setting $(i, j, k) = (1, 2, 3)$ and comparing with eq. (B.80), we see that the expected relation between cuts and coproduct entries holds.

Requiring that we normalize invariants by the channel being cut might be too restrictive. We now show how to define variables that do not have this requirement, but in terms of which the symbol alphabet is still rational. We define

$$\begin{aligned} w_j = \frac{u_j + \mu_{ij} - \mu_{jk} + \sqrt{\lambda(u_j, \mu_{ij}, \mu_{jk})}}{2}\,, \quad \bar{w}_j = \frac{u_j + \mu_{ij} - \mu_{jk} - \sqrt{\lambda(u_j, \mu_{ij}, \mu_{jk})}}{2}\,, \\ z = \frac{1 + u_j - u_k + \sqrt{\lambda(1, u_j, u_k)}}{2}, \quad \bar{z} = \frac{1 + u_j - u_k - \sqrt{\lambda(1, u_j, u_k)}}{2}\,, \end{aligned} \tag{B.86}$$

related to the invariants through slightly more complicated relations,

$$z\bar{z} = u_j = \frac{p_j^2}{p_i^2}\,, \quad (1-z)(1-\bar{z}) = u_k = \frac{p_k^2}{p_i^2}\,, \quad \mu_{ik} = \frac{m_{ik}^2}{p_i^2}\,,$$

$$w_j\bar{w}_j = u_j\mu_{ij} = u_j\frac{m_{ij}^2}{p_i^2}\,, \quad (u_j - w_j)(u_j - \bar{w}_j) = u_j\mu_{jk} = u_j\frac{m_{jk}^2}{p_i^2}\,. \tag{B.87}$$

As above, there is a slight abuse of notation in the definition of the z and $\bar{z}$ variables.

In terms of these variables, the single cut in the p_j^2 channel is

$$\begin{aligned}\mathrm{Cut}_{p_j^2}\left[T(p_1^2,p_2^2,p_3^3;m_{12}^2,m_{23}^2,m_{13}^2)\right] =& -2\pi\frac{e^{\gamma_E}\Gamma(1-\epsilon)}{\Gamma(2-2\epsilon)}(-p_i^2)^{-1-\epsilon}\\ &\frac{(-z\bar{z})^{\epsilon}(w_j-\bar{w}_j)^{1-2\epsilon}}{(z-w_j)(\bar{z}-\bar{w}_j)-z\bar{z}\mu_{ik}}\,{}_2F_1\left(1,1-\epsilon;2-2\epsilon;\frac{(z-\bar{z})(w_j-\bar{w}_j)}{(z-w_j)(\bar{z}-\bar{w}_j)-z\bar{z}\mu_{ik}}\right)\\ =&\frac{2\pi}{p_i^2(z-\bar{z})}\log\left(\frac{z\bar{z}\mu_{ik}-(z-w_j)(\bar{z}-\bar{w}_j)}{z\bar{z}\mu_{ik}-(z-\bar{w}_j)(\bar{z}-w_j)}\right)+\mathcal{O}(\epsilon)\,.\end{aligned} \tag{B.88}$$

As promised, the symbol letters are rational.

Double cuts

We now give the results for the double cuts in terms of the two sets of variables. For the variables in eq. (B.83), we compute the double cut in channels p_i^2 and p_j^2. It is given by

$$\begin{aligned}&\mathrm{Cut}_{p_i^2,p_j^2}\left[T(p_1^2,p_2^2,p_3^3;m_{12}^2,m_{23}^2,m_{13}^2)\right] = \\ &=\frac{4\pi^2 i e^{\gamma_E}}{\Gamma(1-\epsilon)}\frac{(p_i^2)^{-1-\epsilon}}{(z-\bar{z})^{1-2\epsilon}}\left(\mu_{jk}-(z-w_i)(\bar{z}-\bar{w}_i)\right)^{-\epsilon}\left((z-\bar{w}_i)(\bar{z}-w_i)-\mu_{jk}\right)^{-\epsilon}\Theta_{ij},\end{aligned} \tag{B.89}$$

where

$$\Theta_{ij} = \theta\left(\mu_{jk}-(z-w_i)(\bar{z}-\bar{w}_i)\right)\theta\left((z-\bar{w}_i)(\bar{z}-w_i)-\mu_{jk}\right)\,.$$

For the variables of eq. (B.86), we compute the double cut in channels p_j^2 and p_k^2. It is given by

$$\begin{aligned}&\mathrm{Cut}_{p_j^2,p_k^2}T(p_1^2,p_2^2,p_3^3;m_{12}^2,m_{23}^2,m_{13}^2) = \\ &=\frac{4\pi^2 i e^{\gamma_E}}{\Gamma(1-\epsilon)}\frac{(-p_i^2)^{-1-\epsilon}}{(-z\bar{z})^{-\epsilon}(z-\bar{z})^{1-2\epsilon}}\Theta_{jk}\frac{\left(z\bar{z}\mu_{ik}-(z-w_j)(\bar{z}-\bar{w}_j)\right)^{-\epsilon}}{\left((z-\bar{w}_j)(\bar{z}-w_j)-z\bar{z}\mu_{ik}\right)^{\epsilon}},\end{aligned} \tag{B.90}$$

where

$$\Theta_{jk} = \theta\left((z-\bar{w}_j)(\bar{z}-w_j)-z\bar{z}\mu_{ik}\right)\theta\left(z\bar{z}\mu_{ik}-(z-w_j)(\bar{z}-\bar{w}_j)\right)\,.$$

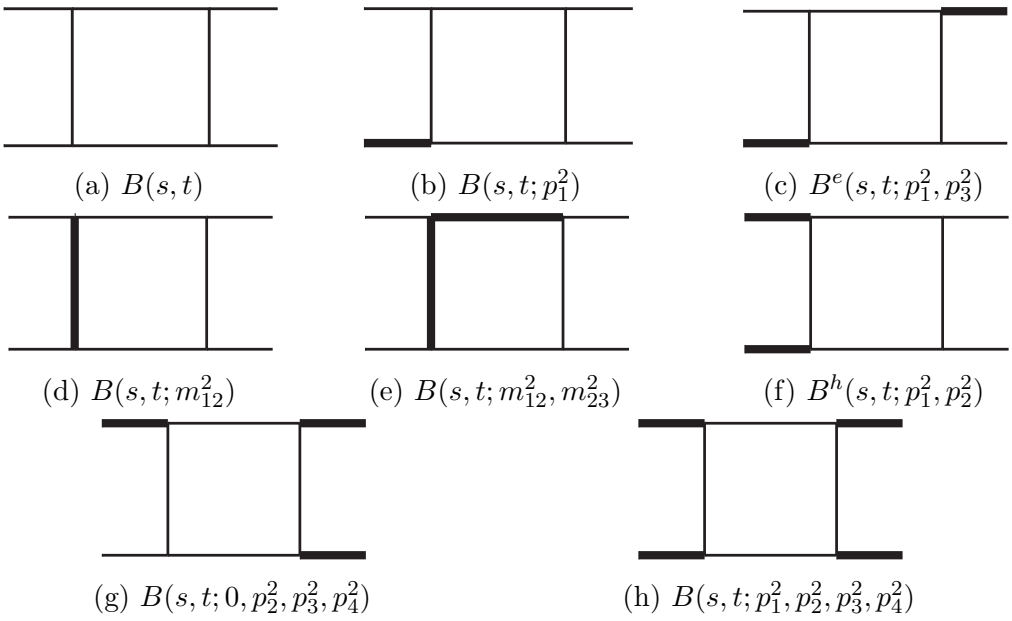

(a) $B(s,t)$ (b) $B(s,t;p_1^2)$ (c) $B^e(s,t;p_1^2,p_3^2)$

(d) $B(s,t;m_{12}^2)$ (e) $B(s,t;m_{12}^2,m_{23}^2)$ (f) $B^h(s,t;p_1^2,p_2^2)$

(g) $B(s,t;0,p_2^2,p_3^2,p_4^2)$ (h) $B(s,t;p_1^2,p_2^2,p_3^2,p_4^2)$

Figure B.4: Box diagrams

B.4 Boxes

B.4.1 Zero-mass box

The zero-mass box, fig. B.4a, evaluates to a well known result, see e.g. [98,102],

$$I_4(s,t) = 2\frac{c_\Gamma}{\epsilon}\left\{\frac{\Gamma^2(1-\epsilon)\Gamma^2(1+\epsilon)}{\epsilon\Gamma(1+2\epsilon)\Gamma(1-2\epsilon)}\frac{2}{st}\left(-\frac{s+t}{st}\right)^{\epsilon}\right. \tag{B.91}$$
$$\left. -\frac{(-s)^{-2-\epsilon}}{1+\epsilon}\,{}_2F_1\left(1,1;2+\epsilon;-\frac{t}{s}\right) - \frac{(-t)^{-2-\epsilon}}{1+\epsilon}\,{}_2F_1\left(1,1;2+\epsilon;-\frac{s}{t}\right)\right\},$$

where c_Γ is defined in eq. (A.12).

B.4.2 One-mass box

For the one-mass box, fig. B.4b, we take the result from [80],

$$I_4(s,t;p_4^2) = \frac{2c_\Gamma}{\epsilon^2 s\,t}\left\{\left(\frac{s\,t}{s-p_4^2}\right)^{-\epsilon}\,{}_2F_1\left(-\epsilon,-\epsilon;1-\epsilon;\frac{p_4^2-s-t}{p_4^2-s}\right)\right.$$
$$\left. + \left(\frac{s\,t}{t-p_4^2}\right)^{-\epsilon}\,{}_2F_1\left(-\epsilon,-\epsilon;1-\epsilon;\frac{p_4^2-s-t}{p_4^2-t}\right)\right.$$

$$-\left(-\frac{s\,t\,p_4^2}{(s-p_4^2)(t-p_4^2)}\right)^{-\epsilon}\,{}_2F_1\left(-\epsilon,-\epsilon;1-\epsilon;\frac{p_4^2(p_4^2-s-t)}{(s-p_4^2)(t-p_4^2)}\right)\Bigg\}. \tag{B.92}$$

B.4.3 Two-mass-easy box

For the two-mass-easy box, fig. B.4c, we take the result from [147],

$$\begin{aligned} I_4^e(s,t;p_2^2,p_4^2) = 2\frac{c_\Gamma}{\epsilon^2(st-p_2^2p_4^2)}\Bigg\{&(-s)^{-\epsilon}+(-t)^{-\epsilon}-(-p_2^2)^{-\epsilon}-(-p_4^2)^{-\epsilon} \\ &+\sum_{j=0}^{3}(-1)^j\left(\frac{s+t-p_2^2-p_4^2}{\alpha_j}\right)^{\epsilon}\,{}_2F_1\left(\epsilon,\epsilon;1+\epsilon;\frac{st-p_2^2p_4^2}{\alpha_j}\right)\Bigg\}, \end{aligned} \tag{B.93}$$

with

$$\begin{aligned} \alpha_0 &= \left(p_2^2-s\right)\left(p_2^2-t\right) & \alpha_1 &= \left(p_2^2-s\right)\left(s-p_4^2\right) \\ \alpha_2 &= \left(p_4^2-s\right)\left(p_4^2-t\right) & \alpha_3 &= \left(p_2^2-t\right)\left(t-p_4^2\right). \end{aligned} \tag{B.94}$$

B.4.4 Zero-mass box with one internal mass

The zero-mass box with one internal mass, fig. B.4d was computed by direct integration of Mellin-Barnes representation,

$$I_4(s,t;m_{12}^2) = \frac{(-s)^{-2-\epsilon}}{(r-\mu_{12})}\sum_{j=-2}^{\infty} i_4^{(j)}\left(r;\mu_{12}\right)\,\epsilon^j \tag{B.95}$$

where $r = s/t$ and $\mu_{12} = m_{12}^2/s$, with

$$i_4^{(-2)}\left(r;\mu_{12}\right) = 1 \tag{B.96}$$

$$i_4^{(-1)}\left(r;\mu_{12}\right) = 2\log\left(-\mu_{12}\right) - 2G\left(-r,-\mu_{12}\right) - 2\log(r) \tag{B.97}$$

$$\begin{aligned} i_4^{(0)}\left(r;\mu_{12}\right) = &-\frac{1}{2}\log\left(-\mu_{12}\right) + G\left(1,0,-\mu_{12}\right) + 4\log(r)G\left(-r,-\mu_{12}\right) \\ &- 4G\left(-r,0,-\mu_{12}\right) + 4G\left(-r,-r,-\mu_{12}\right) - \frac{13\pi^2}{12}. \end{aligned} \tag{B.98}$$

The coefficients $i_4^{(j)}(r;\mu_{12})$ for $j = 1,2,3$ can be found in the accompanying MATHEMATICA package, [38].

B.4.5 Zero-mass box with two adjacent internal masses

The zero-mass box with two adjacent internal masses, fig. B.4e was computed by direct integration of Mellin-Barnes representation,

$$I_4(s,t;m_{12}^2,m_{23}^2) = \frac{(-s)^{-2-\epsilon}}{(r-\mu_{12}-r\mu_{23})}\sum_{j=-2}^{\infty} i_4^{(j)}(r;\mu_{12},\mu_{23})\,\epsilon^j \tag{B.99}$$

where $r = s/t$, $\mu_{12} = m_{12}^2/s$ and $\mu_{23} = m_{23}^2/s$, with

$$i_4^{(-2)}(r;\mu_{12},\mu_{23}) = 0 \tag{B.100}$$

$$\begin{aligned} i_4^{(-1)}(r;\mu_{12},\mu_{23}) = &- G(-1,-\mu_{23}) - G(-r,-\mu_{12}) + \log(-\mu_{12}) \\ &+ \log(-\mu_{23}) - \log(r) \end{aligned} \tag{B.101}$$

$$\begin{aligned} i_4^{(0)}(r;\mu_{12},\mu_{23}) = &-G(-1,-\mu_{23})\,G(1-\mu_{23},-\mu_{12}) + 3G(-1,-1,-\mu_{23}) \\ &+ G(1-\mu_{23},0,-\mu_{12}) - \log(-\mu_{12})\,G(-1,-\mu_{23}) - \log(-\mu_{23})\log(r) \\ &+ 2G(-1,-\mu_{23})\,G((\mu_{23}-1)\,r,-\mu_{12}) - G(-r,0,-\mu_{12}) \\ &+ G(r,0,-\mu_{23}) - G(-\mu_{23}-r,-r,-\mu_{12}) - \frac{1}{2}\log^2(-\mu_{23}) \\ &+ 2G((\mu_{23}-1)\,r,-r,-\mu_{12}) + 2\log(r)G(-1,-\mu_{23}) \\ &- 3G(-1,0,-\mu_{23}) + 2G(-r,-r,-\mu_{12}) - \frac{1}{2}\log^2(-\mu_{12}) \\ &+ 2\log(r)G((\mu_{23}-1)\,r,-\mu_{12}) + \log(-\mu_{23})\,G(-\mu_{23}-r,-\mu_{12}) \\ &- 2\log(-\mu_{23})\,G((\mu_{23}-1)\,r,-\mu_{12}) + 2\log(r)G(-r,-\mu_{12}) \\ &- 2G((\mu_{23}-1)\,r,0,-\mu_{12}) - \log(r)G(-\mu_{23}-r,-\mu_{12}) \\ &- \log(r)G(r,-\mu_{23}) + \log(-\mu_{23})\log(-\mu_{12}) - \pi^2. \end{aligned} \tag{B.102}$$

The coefficients $i_4^{(j)}(r;\mu_{12},\mu_{23})$ for $j = 1,2$ can be found in the accompanying MATHEMATICA package, [38].

B.4.6 Two-mass-hard box

The two-mass-hard box, fig. B.4f, is an interesting example. Up to order ϵ^0, the result can be written in terms of Mandelstam invariants without the appearance of any square roots. However, from order ϵ^1 on, square roots appear. These are connected to the three-mass triangle one obtains by pinching one of the propagators. We can thus find the appropriate variables by introducing variables that rationalise the square root appearing in that three-mass triangles. For $I_4^h(s,t;p_1^2,p_2^2)$, we thus define

$$z\bar{z} = \frac{p_1^2}{s} \qquad (1-z)(1-\bar{z}) = \frac{p_2^2}{s} \qquad r = \frac{t}{s}. \tag{B.103}$$

Then,

$$I_4^h(s,t;p_1^2,p_2^2) = \frac{(-s)^{-2-\epsilon}}{r} \sum_{j=-2}^{\infty} i_4^{(j)}(r,z,\bar{z})\ \epsilon^j. \tag{B.104}$$

Up to order ϵ^0, the expression for the two-mass-hard box can be found e.g. in [98] and is remarkably simple,

$$\begin{aligned} I_4^h(s,t;p_1^2,p_2^2) = (-s)^{-2-\epsilon} c_\Gamma \frac{(z\bar{z})^\epsilon r^{-1-2\epsilon}}{((1-z)(1-\bar{z}))^{-\epsilon}} \left(\frac{1}{\epsilon^2} + 2\mathrm{Li}_2\left(1-\frac{r}{z\bar{z}}\right) \right. \\ \left. +2\mathrm{Li}_2\left(1-\frac{r}{(1-z)(1-\bar{z})}\right) - \frac{\pi^2}{12} \right) + \mathcal{O}(\epsilon). \end{aligned} \tag{B.105}$$

We then get

$$i_4^{(-2)}(r,z,\bar{z}) = 1 \tag{B.106}$$

$$i_4^{(-1)}(r,z,\bar{z}) = \log(z\bar{z}) + \log((1-z)(1-\bar{z})) - 2\log(r) \tag{B.107}$$

$$\begin{aligned} i_4^{(0)}(r,z,\bar{z}) &= 2\mathrm{Li}_2\left(1-\frac{r}{(1-z)(1-\bar{z})}\right) + 2\mathrm{Li}_2\left(1-\frac{r}{z\bar{z}}\right) \\ &\quad - 2\log(r)\log(z\bar{z}) + 2\log^2(r) + \frac{1}{2}\log^2((1-z)(1-\bar{z})) + \frac{1}{2}\log^2(z\bar{z}) \\ &\quad - 2\log(r)\log((1-z)(1-\bar{z})) + \log((1-z)(1-\bar{z}))\log(z\bar{z}) - \frac{\pi^2}{12}. \end{aligned} \tag{B.108}$$

The coefficients up to order ϵ^2 were computed by direct Mellin-Barnes integration and can be found in the accompanying MATHEMATICA package, [38].

B.4.7 Three masses

We give the result for the box, fig. B.4g , with three external massive legs, as computed in [98], because it appears as a subdiagram in the single unitarity cuts of the two-loop ladder.

$$\begin{aligned}
&B(s,t;p_2^2,p_3^2,p_4^2) = \\
&= i\frac{c_\Gamma}{st-p_2^2p_4^2}\left\{\frac{2}{\epsilon^2}\left[(-s)^{-\epsilon}+(-t)^{-\epsilon}-(-p_2^2)^{-\epsilon}-(-p_3^2)^{-\epsilon}-(-p_4^2)^{-\epsilon}\right]\right. \\
&+\frac{1}{\epsilon^2}\frac{(-p_2^2)^{-\epsilon}(-p_3^2)^{-\epsilon}}{(-t)^{-\epsilon}}+\frac{1}{\epsilon^2}\frac{(-p_3^2)^{-\epsilon}(-p_4^2)^{-\epsilon}}{(-s)^{-\epsilon}}-2\mathrm{Li}_2\left(1-\frac{p_2^2}{s}\right) \\
&\left.-2\mathrm{Li}_2\left(1-\frac{p_4^2}{t}\right)+2\mathrm{Li}_2\left(1-\frac{p_2^2p_4^2}{st}\right)-\log^2\frac{s}{t}\right\}+\mathcal{O}(\epsilon)\,.
\end{aligned} \tag{B.109}$$

The t-channel cut, which appears as a subdiagram in the double unitarity cuts of the two-loop ladder is computed using the relation $\mathrm{Disc}_t = -\mathrm{Cut}_t$.

$$\begin{aligned}
&\mathrm{Cut}_t B^{3m}(s,t;p_2^2,p_3^2,p_4^2) = (2\pi)^2\frac{e^{\gamma_E\epsilon}}{\pi^{2-\epsilon}}\int d^{4-2\epsilon}k\frac{\delta\left((k+p_1)^2\right)\delta((k-p_4)^2)}{(k^2+i0)((k+p_1+p_2)^2-i0)} \\
&=\frac{e^{\gamma_E\epsilon}\Gamma(1-\epsilon)}{\Gamma(1-2\epsilon)}\frac{2\pi}{st-p_2^2p_4^2}\left[\frac{2}{\epsilon}t^{-\epsilon}-\frac{1}{\epsilon}t^{\epsilon}(-p_2^2)^{-\epsilon}(-p_3^2)^{-\epsilon}+2\log\left(1-\frac{p_4^2}{t}\right)\right. \\
&\left.-2\log\left(1-\frac{p_2^2p_4^2}{st}\right)-2\log(-s)+2\log t\right]\theta(t)+\mathcal{O}(\epsilon)\,.
\end{aligned} \tag{B.110}$$

B.4.8 Four mass box

The four-mass box, fig. B.4h, is finite in four dimensions, and, as was shown in [99], it may in fact be expressed by the same function as the three-mass triangle. In [99], this is shown by deriving a Mellin-Barnes representation of each diagram, and showing that they are equivalent if one makes the following identification

$$u_2 \to U = \frac{p_2^2p_4^2}{st}, \qquad u_3 \to V = \frac{p_1^2p_3^2}{st} \tag{B.111}$$

where the u_i are the dimensionless variables of the triangle we are familiar with, see 2.27. U and V are variables invariant under conformal symmetry, which is

one of the symmetries of the four mass box.

We will now show another derivation of this result, but instead of finding an equivalence of Mellin-Barnes representations we will find an equivalence of the parametric representation of both integrals. More precisely, we will find that the four-mass boxes has the same parametric representation as the one derived for the three-mass triangle in [65].

According to our conventions, for $D = 4$ we have

$$B(s,t;p_1^2,p_2^2,p_3^2,p_4^2) = \frac{1}{\pi^2}\int d^4k \frac{1}{k^2(k+p_1+p_2)^2(k+p_2)^2(k-p_3)^2}, \tag{B.112}$$

and for later use we define

$$\begin{aligned} Z &= \frac{1}{2}\left(1+U-V+\sqrt{\lambda(1,U,V)}\right), \\ \bar{Z} &= \frac{1}{2}\left(1+U-V-\sqrt{\lambda(1,U,V)}\right). \end{aligned} \tag{B.113}$$

We show in section 3.5.8 how these variables arise naturally in the calculation of cuts.

Introducing Feynman parameters and carrying out the loop momentum integral in the usual way, we get:

$$\begin{aligned} &B(s,t;p_1^2,p_2^2,p_3^2,p_4^2) = \\ &= i\prod_{i=1}^{4}\left(\int_0^\infty dx_i\right)\frac{\delta\left(1-\sum_{i\in S}x_i\right)}{\left(-x_1x_3s_{12}-x_2x_4s_{23}-x_1x_4p_3^2-x_1x_2p_2^2-x_2x_3p_1^2-x_3x_4p_4^2\right)^2}. \end{aligned} \tag{B.114}$$

We choose $S = \{x_1, x_2, x_3, x_4\}$.

Following [99], we change variables for the x_1, x_2 and x_3 integrations:

$$x_i = (1-x_4)\beta_i\,, \qquad i = 1,2,3 \tag{B.115}$$

and get:

$$\begin{aligned} &B(s,t;p_1^2,p_2^2,p_3^2,p_4^2) = i\prod_{i=1}^{3}\left(\int_0^1 d\beta_i\right) \\ &\int_0^1 dx_4 \frac{\delta\left(1-\sum_{i=1}^{3}\beta_i\right)}{\left[(1-x_4)\left(\beta_1\beta_2p_2^2+\beta_1\beta_3s+\beta_2\beta_3p_1^2\right)+x_4\left(\beta_1p_3^2+\beta_2t+\beta_3p_4^2\right)\right]^2}. \end{aligned} \tag{B.116}$$

The x_4 integration can be easily performed to get:

$$B(s,t;p_1^2,p_2^2,p_3^2,p_4^2) = \tag{B.117}$$
$$= i\int_0^1 d\beta_1 \int_0^1 d\beta_2 \int_0^1 d\beta_3 \frac{\delta\left(1-\sum_{i=1}^3 \beta_i\right)}{(\beta_1\beta_2 p_2^2 + \beta_1\beta_3 s + \beta_2\beta_3 p_1^2)\,(\beta_1 p_3^2 + \beta_2 t + \beta_3 p_4^2)},$$

which matches the result of [99].

However, we now proceed in a different direction. According to the result we prove below, eq. (B.125), we have:

$$B(s,t;p_1^2,p_2^2,p_3^2,p_4^2) = \tag{B.118}$$
$$= i\int_0^\infty d\beta_1 \int_0^\infty d\beta_2 \int_0^\infty d\beta_3 \frac{\delta\left(1-\sum_{i\in S'} \beta_i\right)}{(\beta_1\beta_2 p_2^2 + \beta_1\beta_3 s + \beta_2\beta_3 p_1^2)\,(\beta_1 p_3^2 + \beta_2 t + \beta_3 p_4^2)}$$

where S' is any non-empty set of $\{\beta_1,\beta_2,\beta_3\}$.

For simplicity of notation, we define:

$$a_i = \frac{p_i^2}{s} \qquad\qquad b_i = \frac{p_i^2}{t} \tag{B.119}$$

Picking the set S' to be $S' = \{\beta_2\}$, we get:

$$B(s,t;p_1^2,p_2^2,p_3^2,p_4^2) = \tag{B.120}$$
$$= i\frac{1}{st}\int_0^\infty d\beta_1 \int_0^\infty d\beta_3 \frac{1}{(\beta_1 a_2 + \beta_1\beta_3 + \beta_3 a_1)\,(1+\beta_1 b_3 + \beta_3 b_4)},$$

which is similar to the parametric representation of the three-mass triangle of [65].

The calculation can now be finished in the same as was done for the three-mass triangle. Integrating over β_1:

$$B(s,t;p_1^2,p_2^2,p_3^2,p_4^2) = \tag{B.121}$$
$$= \frac{ib_4}{st}\int_0^\infty d\beta_3 \frac{\log(\beta_3+a_2) - \log b_3 + \log(1+\beta_3 b_4) - \log(\beta_3 a_1)}{(\beta_3 b_4 + Z)(\beta_3 b_4 + \bar{Z})}.$$

Changing variables to $\alpha_3 = b_4\beta_3$, we get:

$$B(s,t;p_1^2,p_2^2,p_3^2,p_4^2) = \tag{B.122}$$
$$= \frac{i}{st}\int_0^\infty \frac{1}{(\alpha_3+Z)(\alpha_3+\bar{Z})}\Big(\log(\alpha_3+U) - \log V + \log(1+\alpha_3) - \log\alpha_3\Big).$$

We have now brought the calculation of the four-mass box to exactly the same form as the three-mass triangle, with the identification $z \to Z$ and $\bar{z} \to \bar{Z}$. We can thus write

$$B(s,t;p_1^2,p_2^2,p_3^2,p_4^2;0) = \frac{i}{st}\frac{2}{Z-\bar{Z}}\mathcal{P}_2\left(Z\right), \tag{B.123}$$

where $\mathcal{P}_2$ is defined in eq. (B.52). This result agrees with [99].

The symbol is

$$\begin{aligned}&\mathcal{S}\left[B(s,t;p_1^2,p_2^2,p_3^2,p_4^2)\right] = \\ &= \frac{i}{st}\frac{1}{Z-\bar{Z}}\left[\left(Z\bar{Z}\right)\otimes\frac{1-Z}{1-\bar{Z}} + \left((1-Z)(1-\bar{Z})\right)\otimes\frac{\bar{Z}}{Z}\right].\end{aligned} \tag{B.124}$$

As for the three-mass triangle, the first entry condition is manifest.

Proof of the result used in eq. (B.118):

We show that for a function $F(\{x_i\})$ of homogeneity m the following result holds:

$$\begin{aligned}I = \prod_{i=1}^{n}\left(\int_0^\infty dx_i\right)\delta\left(1-\sum_{i=1}^{n}x_i\right)F(\{x_i\}) = \\ = \prod_{i=1}^{n}\left(\int_0^\infty dx_i\right)\delta\left(1-\sum_{i\in S}x_i\right)\left(1+\sum_{i\in X/S}x_i\right)^{n+m}F(\{x_i\}),\end{aligned} \tag{B.125}$$

where S is any non-empty set of $X = \{x_1,\ldots,x_n\}$.

When $m = -n$, this becomes:

$$\prod_{i=1}^{n}\left(\int_0^\infty dx_i\right)\delta\left(1-\sum_{i=1}^{n}x_i\right)F(\{x_i\}) = \prod_{i=1}^{n}\left(\int_0^\infty dx_i\right)\delta\left(1-\sum_{i\in S}x_i\right)F(\{x_i\}). \tag{B.126}$$

The Cheng-Wu theorem is a particular case of this result (at least in the way it is presented in the book [148] ; unfortunately, we couldn't find Cheng and Wu's original formulation to see how it is presented there).

To prove this result, we define η as the sum of the elements of S. Without

loss of generality, we have

$$\eta = \sum_{i=1}^{j} x_i \,, \qquad\qquad j < n, \tag{B.127}$$

We define $n-1$ new variables to rescale all the integration variables except one (we pick x_j) such that

$$x_i = \eta x_i' \,, \qquad\qquad i \neq j. \tag{B.128}$$

Then

$$x_j = \eta - \sum_{i=1}^{j-1} x_i = \eta \left(1 - \sum_{i=1}^{j-1} x_i'\right) \equiv \eta x_j', \tag{B.129}$$

where in the last equality we introduced a new variable x_j' as

$$x_j' = 1 - \sum_{i=1}^{j-1} x_i'. \tag{B.130}$$

Using these definitions,

$$\begin{aligned} I &= \left(\prod_{i=1}^{n} \int_0^\infty dx_i\right) \delta\left(1 - \sum_{i=1}^{n} x_i\right) F(\{x_i\}) \qquad\qquad (B.131)\\ &= \left(\prod_{i=1}^{n} \int_0^\infty dx_i'\right) \int_0^\infty \frac{d\eta}{\eta^{1-n}} \delta\left(1 - \eta\left(1 + \sum_{i=j+1}^{n} x_i'\right)\right) \delta\left(1 - \sum_{i=1}^{j} x_i'\right) F(\{\eta x_i'\}), \end{aligned}$$

where the first delta function comes from

$$\delta\left(1 - \sum_{i=1}^{n} x_i\right) = \delta\left(1 - \eta\left(1 + \sum_{i=j+1}^{n} x_i'\right)\right) \,, \tag{B.132}$$

and the second delta function (along with the integral over x_j') implements the definition of x_j',

$$\int_0^\infty dx_j' \, \delta\left(x_j' - \left(1 - \sum_{i=1}^{j-1} x_i'\right)\right) = \int_0^\infty dx_j' \, \delta\left(1 - \sum_{i=1}^{j} x_i'\right) = 1 \,. \tag{B.133}$$

If $F(\{x_i\})$ is homogeneous of degree m, then

$$F(\{x_i\}) = F(\{\eta x_i'\}) = \eta^m F(\{x_i'\}), \tag{B.134}$$

and we have

$$I = \left(\prod_{i=1}^{n} \int_0^\infty dx_i'\right) \int_0^\infty \frac{d\eta}{\eta^{1-n-m}} \delta\left(1 - \eta\left(1 + \sum_{i=j+1}^{n} x_i'\right)\right) \delta\left(1 - \sum_{i=1}^{j} x_i'\right) F(\{x_i'\}). \tag{B.135}$$

It is now straightforward to do the η integral and get:

$$I = \left(\prod_{i=1}^{n} \int_0^\infty dx_i'\right) \left(1 + \sum_{i=j+1}^{n} x_i'\right)^{n+m} \delta\left(1 - \sum_{i=1}^{j} x_i'\right) F(\{x_i'\}), \tag{B.136}$$

which proves our result.

Appendix C

Cuts of the three-mass three-point ladder

C.1 Explicit results for the single unitarity cuts

We present the results we obtained for the single unitarity cuts. These results were computed and numerically checked in the region where $\bar{z} = z^*$. For cut [45] the hypergeometric function was expanded using `HypExp` [100]. We write everything in terms of multiple polylogarithms as defined in Section 2.2 to simplify the comparison between different terms.

C.1.1 Unitarity cuts in the p_3^2 channel

$$\begin{aligned}&\mathrm{Cut}_{p_3^2,[12],R_\triangle^*} T_L(p_1^2,p_2^2,p_3^2) = \\ &= \frac{i\, c_\Gamma^2\, (p_1^2)^{-2-2\epsilon}}{(1-z)(1-\bar{z})(z-\bar{z})} \sum_{k=-2}^{\infty} \epsilon^k \left[(-2\pi i)\, f_{[12]}^{(k,1)}(z,\bar{z}) + (-2\pi i)^2\, f_{[12]}^{(k,2)}(z,\bar{z})\right],\end{aligned} \tag{C.1}$$

$$\begin{aligned}f_{[12]}^{(-2,1)}(z,\bar{z}) &= \log\frac{z}{\bar{z}}\,,\\ f_{[12]}^{(-2,2)}(z,\bar{z}) &= 0\,,\\ f_{[12]}^{(-1,1)}(z,\bar{z}) &= -G\left(0,\frac{1}{z};\frac{1}{\bar{z}}\right) + G\left(0,\frac{1}{\bar{z}};\frac{1}{z}\right) + \log\frac{z}{\bar{z}}\left[G\left(\frac{1}{z};\frac{1}{\bar{z}}\right) + G\left(\frac{1}{\bar{z}};\frac{1}{z}\right)\right]\end{aligned}$$

$$
\begin{aligned}
&- 2\log[(1-z)(1-\bar{z})]\log\frac{z}{\bar{z}}\,,\\
f^{(-1,2)}_{[12]}(z,\bar{z}) &= \frac{1}{2}\log\frac{z}{\bar{z}}\,,\\
f^{(0,1)}_{[12]}(z,\bar{z}) &= -2\left[G\left(0,\frac{1}{z},\frac{1}{\bar{z}};\frac{1}{\bar{z}}\right)-G\left(0,\frac{1}{\bar{z}},\frac{1}{z};\frac{1}{z}\right)\right]-\frac{1}{12}\log^3\frac{z}{\bar{z}}\\
&\quad - 2\log[(1-z)(1-\bar{z})]\log\frac{z}{\bar{z}}\left[G\left(\frac{1}{z};\frac{1}{\bar{z}}\right)+G\left(\frac{1}{\bar{z}};\frac{1}{z}\right)\right]\\
&\quad + 2\log[(1-z)(1-\bar{z})]\left[G\left(0,\frac{1}{z};\frac{1}{\bar{z}}\right)-G\left(0,\frac{1}{\bar{z}};\frac{1}{z}\right)\right]\\
&\quad + \frac{1}{2}\log\frac{z}{\bar{z}}\left[G\left(\frac{1}{z};\frac{1}{\bar{z}}\right)+G\left(\frac{1}{\bar{z}};\frac{1}{z}\right)\right]^2+\frac{\pi^2}{6}\log\frac{z}{\bar{z}}\\
&\quad + 2\log^2[(1-z)(1-\bar{z})]\log\frac{z}{\bar{z}}-\frac{1}{4}\log^2(z\bar{z})\log\frac{z}{\bar{z}}\,,\\
f^{(0,2)}_{[12]}(z,\bar{z}) &= \frac{1}{2}\log\frac{z}{\bar{z}}\left[G\left(\frac{1}{z};\frac{1}{\bar{z}}\right)+G\left(\frac{1}{\bar{z}};\frac{1}{z}\right)\right]-\log[(1-z)(1-\bar{z})]\log\frac{z}{\bar{z}}\\
&\quad - \frac{1}{2}\left[G\left(0,\frac{1}{z};\frac{1}{\bar{z}}\right)-G\left(0,\frac{1}{\bar{z}};\frac{1}{z}\right)\right]-\frac{1}{2}\log^2\frac{z}{\bar{z}}\,.
\end{aligned}
\tag{C.2}
$$

$$
\begin{aligned}
&\mathrm{Cut}_{p_3^2,[45],R^*_\triangle}T_L(p_1^2,p_2^2,p_3^2) = \\
&= \frac{i\,c_\Gamma^2\,(p_1^2)^{-2-2\epsilon}}{(1-z)(1-\bar{z})(z-\bar{z})}\sum_{k=-2}^{\infty}\epsilon^k\,\left[(-2\pi i)\,f^{(k,1)}_{[45]}(z,\bar{z})+(-2\pi i)^2\,f^{(k,2)}_{[45]}(z,\bar{z})\right]\,,
\end{aligned}
\tag{C.3}
$$

$$
\begin{aligned}
f^{(-2,1)}_{[45]}(z,\bar{z}) &= \log\frac{z}{\bar{z}}\,,\\
f^{(-2,2)}_{[45]}(z,\bar{z}) &= 0\,,\\
f^{(-1,1)}_{[45]}(z,\bar{z}) &= -G\left(0,\frac{1}{z};\frac{1}{\bar{z}}\right)+G\left(0,\frac{1}{\bar{z}};\frac{1}{z}\right)+\log\frac{z}{\bar{z}}\left[G\left(\frac{1}{z};\frac{1}{\bar{z}}\right)+G\left(\frac{1}{\bar{z}};\frac{1}{z}\right)\right]\\
&\quad - 2\log[(1-z)(1-\bar{z})]\log\frac{z}{\bar{z}}\,,\\
f^{(-1,2)}_{[45]}(z,\bar{z}) &= -\frac{1}{2}\log\frac{z}{\bar{z}}\,,\\
f^{(0,1)}_{[45]}(z,\bar{z}) &= -2\left[G\left(0,\frac{1}{z},\frac{1}{\bar{z}};\frac{1}{\bar{z}}\right)-G\left(0,\frac{1}{\bar{z}},\frac{1}{z};\frac{1}{z}\right)\right]+\frac{\pi^2}{6}\log\frac{z}{\bar{z}}\\
&\quad - 2\log[(1-z)(1-\bar{z})]\log\frac{z}{\bar{z}}\left[G\left(\frac{1}{z};\frac{1}{\bar{z}}\right)+G\left(\frac{1}{\bar{z}};\frac{1}{z}\right)\right]
\end{aligned}
$$

$$
\begin{aligned}
&+ 2\log[(1-z)(1-\bar{z})]\left[G\left(0,\frac{1}{z};\frac{1}{\bar{z}}\right) - G\left(0,\frac{1}{\bar{z}};\frac{1}{z}\right)\right] - \frac{1}{3}\log^3\frac{z}{\bar{z}} \\
&+ \frac{1}{2}\log\frac{z}{\bar{z}}\left[G\left(\frac{1}{z};\frac{1}{\bar{z}}\right) + G\left(\frac{1}{\bar{z}};\frac{1}{z}\right)\right]^2 + 2\log^2[(1-z)(1-\bar{z})]\log\frac{z}{\bar{z}}\,, \\
f^{(0,2)}_{[45]}(z,\bar{z}) = &-\frac{1}{2}\left[G\left(0,\frac{1}{\bar{z}};\frac{1}{z}\right) - G\left(0,\frac{1}{z};\frac{1}{\bar{z}}\right)\right] + \log[(1-z)(1-\bar{z})]\log\frac{z}{\bar{z}} \\
&- \frac{1}{2}\log\frac{z}{\bar{z}}\left[G\left(\frac{1}{z};\frac{1}{\bar{z}}\right) + G\left(\frac{1}{\bar{z}};\frac{1}{z}\right)\right] - \frac{1}{2}\log^2\frac{z}{\bar{z}}\,. \qquad \text{(C.4)}
\end{aligned}
$$

$$
\begin{aligned}
&\mathrm{Cut}_{p_3^2,[135],R^*_\triangle} T_L(p_1^2,p_2^2,p_3^2) = \qquad \text{(C.5)} \\
&= \frac{i\,c_\Gamma^2\,(p_1^2)^{-2-2\epsilon}}{(1-z)(1-\bar{z})(z-\bar{z})}\sum_{k=-1}^{\infty}\epsilon^k\left[(-2\pi i)\,f^{(k,1)}_{[135]}(z,\bar{z}) + (-2\pi i)^2\,f^{(k,2)}_{[135]}(z,\bar{z})\right],
\end{aligned}
$$

$$
\begin{aligned}
f^{(-2,1)}_{[135]}(z,\bar{z}) &= -\log\frac{z}{\bar{z}}\,, \\
f^{(-2,2)}_{[135]}(z,\bar{z}) &= 0\,, \\
f^{(-1,1)}_{[135]}(z,\bar{z}) &= G\left(0,\frac{1}{z};\frac{1}{\bar{z}}\right) - G\left(0,\frac{1}{\bar{z}};\frac{1}{z}\right) - \log\frac{z}{\bar{z}}\left[G\left(\frac{1}{z};\frac{1}{\bar{z}}\right) + G\left(\frac{1}{\bar{z}};\frac{1}{z}\right)\right] \\
&\quad + 2\log[(1-z)(1-\bar{z})]\log\frac{z}{\bar{z}} + \frac{1}{2}\log\frac{z}{\bar{z}}\log(z\bar{z})\,, \\
f^{(-1,2)}_{[135]}(z,\bar{z}) &= 0\,, \\
f^{(0,1)}_{[135]}(z,\bar{z}) &= 2\left[G\left(0,\frac{1}{z},\frac{1}{\bar{z}};\frac{1}{\bar{z}}\right) - G\left(0,\frac{1}{\bar{z}},\frac{1}{z};\frac{1}{z}\right)\right] + 6[\mathrm{Li}_3(z) - \mathrm{Li}_3(\bar{z})] \\
&\quad + 2\log[(1-z)(1-\bar{z})]\log\frac{z}{\bar{z}}\left[G\left(\frac{1}{z};\frac{1}{\bar{z}}\right) + G\left(\frac{1}{\bar{z}};\frac{1}{z}\right)\right] \\
&\quad - \frac{1}{2}\log\frac{z}{\bar{z}}\left[G\left(\frac{1}{z};\frac{1}{\bar{z}}\right) + G\left(\frac{1}{\bar{z}};\frac{1}{z}\right)\right]^2 - \frac{3}{2}[\mathrm{Li}_2(z) - \mathrm{Li}_2(\bar{z})]\log(z\bar{z}) \\
&\quad + \frac{1}{2}\log(z\bar{z})\log\frac{z}{\bar{z}}\left[G\left(\frac{1}{z};\frac{1}{\bar{z}}\right) + G\left(\frac{1}{\bar{z}};\frac{1}{z}\right)\right] - \frac{2}{3}\pi^2\log\frac{z}{\bar{z}} \\
&\quad - 2\log[(1-z)(1-\bar{z})]\left[G\left(0,\frac{1}{z};\frac{1}{\bar{z}}\right) - G\left(0,\frac{1}{\bar{z}};\frac{1}{z}\right)\right] \\
&\quad - \frac{1}{2}\log(z\bar{z})\left[G\left(0,\frac{1}{z};\frac{1}{\bar{z}}\right) - G\left(0,\frac{1}{\bar{z}};\frac{1}{z}\right)\right] + \frac{5}{24}\log^3\frac{z}{\bar{z}} \\
&\quad - 2\log^2[(1-z)(1-\bar{z})]\log\frac{z}{\bar{z}} - \log[(1-z)(1-\bar{z})]\log(z\bar{z})\log\frac{z}{\bar{z}}
\end{aligned}
$$

$$
\begin{aligned}
&- \frac{3}{2}[\mathrm{Li}_2(z) + \mathrm{Li}_2(\bar{z})] \log \frac{z}{\bar{z}} - \frac{1}{8} \log^2(z\bar{z}) \log \frac{z}{\bar{z}} \,, \\
f^{(0,2)}_{[135]}(z,\bar{z}) &= \frac{1}{2} \log^2 \frac{z}{\bar{z}} \,.
\end{aligned} \tag{C.6}
$$

$$
\begin{aligned}
&\mathrm{Cut}_{p_3^2,[234],R^*_\triangle} T_L(p_1^2, p_2^2, p_3^2) = \\
&= \frac{i\, c_\Gamma^2\, (p_1^2)^{-2-2\epsilon}}{(1-z)(1-\bar{z})(z-\bar{z})} \sum_{k=-1}^{\infty} \epsilon^k \left[(-2\pi i)\, f^{(k,1)}_{[234]}(z,\bar{z}) + (-2\pi i)^2\, f^{(k,2)}_{[234]}(z,\bar{z}) \right] ,
\end{aligned} \tag{C.7}
$$

$$
\begin{aligned}
f^{(-2,1)}_{[234]}(z,\bar{z}) &= -\log \frac{z}{\bar{z}} \,, \\
f^{(-2,2)}_{[234]}(z,\bar{z}) &= 0 \,, \\
f^{(-1,1)}_{[234]}(z,\bar{z}) &= G\left(0, \frac{1}{z}; \frac{1}{\bar{z}}\right) - G\left(0, \frac{1}{\bar{z}}; \frac{1}{z}\right) - \log \frac{z}{\bar{z}} \left[G\left(\frac{1}{z}; \frac{1}{\bar{z}}\right) + G\left(\frac{1}{\bar{z}}; \frac{1}{z}\right) \right] \\
&\quad + 2 \log[(1-z)(1-\bar{z})] \log \frac{z}{\bar{z}} - \frac{1}{2} \log \frac{z}{\bar{z}} \log(z\bar{z}) \,, \\
f^{(-1,2)}_{[234]}(z,\bar{z}) &= 0 \,, \\
f^{(0,1)}_{[234]}(z,\bar{z}) &= 2 \left[G\left(0, \frac{1}{z}, \frac{1}{\bar{z}}; \frac{1}{\bar{z}}\right) - G\left(0, \frac{1}{\bar{z}}, \frac{1}{z}; \frac{1}{z}\right) \right] - 6[\mathrm{Li}_3(z) - \mathrm{Li}_3(\bar{z})] \\
&\quad - \frac{1}{2} \log \frac{z}{\bar{z}} \left[G\left(\frac{1}{z}; \frac{1}{\bar{z}}\right) + G\left(\frac{1}{\bar{z}}; \frac{1}{z}\right) \right]^2 + \frac{3}{2}[\mathrm{Li}_2(z) + \mathrm{Li}_2(\bar{z})] \log \frac{z}{\bar{z}} \\
&\quad + 2 \log[(1-z)(1-\bar{z})] \log \frac{z}{\bar{z}} \left[G\left(\frac{1}{z}; \frac{1}{\bar{z}}\right) + G\left(\frac{1}{\bar{z}}; \frac{1}{z}\right) \right] \\
&\quad - \frac{1}{2} \log(z\bar{z}) \log \frac{z}{\bar{z}} \left[G\left(\frac{1}{z}; \frac{1}{\bar{z}}\right) + G\left(\frac{1}{\bar{z}}; \frac{1}{z}\right) \right] \\
&\quad - 2 \log[(1-z)(1-\bar{z})] \left[G\left(0, \frac{1}{z}; \frac{1}{\bar{z}}\right) - G\left(0, \frac{1}{\bar{z}}; \frac{1}{z}\right) \right] \\
&\quad + \frac{1}{2} \log(z\bar{z}) \left[G\left(0, \frac{1}{z}; \frac{1}{\bar{z}}\right) - G\left(0, \frac{1}{\bar{z}}; \frac{1}{z}\right) \right] + \frac{1}{3} \log^3 \frac{z}{\bar{z}} \\
&\quad + \frac{3}{2}[\mathrm{Li}_2(z) - \mathrm{Li}_2(\bar{z})] \log(z\bar{z}) - 2 \log^2[(1-z)(1-\bar{z})] \log \frac{z}{\bar{z}} \\
&\quad + \frac{1}{4} \log^2(z\bar{z}) \log \frac{z}{\bar{z}} + \log[(1-z)(1-\bar{z})] \log(z\bar{z}) \log \frac{z}{\bar{z}} + \frac{\pi^2}{3} \log \frac{z}{\bar{z}} \,, \\
f^{(0,2)}_{[234]}(z,\bar{z}) &= \frac{1}{2} \log^2 \frac{z}{\bar{z}} \,.
\end{aligned} \tag{C.8}
$$

C.1.2 Unitarity cuts in the p_2^2 channel

$$\begin{aligned}
&\mathrm{Cut}_{p_2^2,[46],R_\triangle^*} T_L(p_1^2,p_2^2,p_3^2) \qquad\qquad (C.9)\\
&= \frac{i\, c_\Gamma^2\, (p_1^2)^{-2-2\epsilon}}{(1-z)(1-\bar z)(z-\bar z)} \sum_{k=-1}^{\infty} \epsilon^k \left[(-2\pi i)\, f_{[46]}^{(k,1)}(z,\bar z) + (-2\pi i)^2\, f_{[46]}^{(k,2)}(z,\bar z)\right],
\end{aligned}$$

$$\begin{aligned}
f_{[46]}^{(-1,1)}(z,\bar z) &= -\mathrm{Li}_2(z) + \mathrm{Li}_2(\bar z)\,,\\
f_{[46]}^{(-1,2)}(z,\bar z) &= 0\,,\\
f_{[46]}^{(0,1)}(z,\bar z) &= G\left(0,\frac{1}{z},\frac{1}{\bar z};1\right) - G\left(0,\frac{1}{\bar z},\frac{1}{z};1\right) - 4[\mathrm{Li}_3(1-z) - \mathrm{Li}_3(1-\bar z)]\\
&\quad - 2[\mathrm{Li}_3(z) - \mathrm{Li}_3(\bar z)] - 2[\mathrm{Li}_2(z) + \mathrm{Li}_2(\bar z)]\log\frac{1-z}{1-\bar z}\\
&\quad - \frac{1}{2}\log\frac{z}{\bar z}\log^2\frac{1-z}{1-\bar z} - \frac{1}{2}\log^2[(1-z)(1-\bar z)]\log\frac{z}{\bar z}\\
&\quad - \log[(1-z)(1-\bar z)]\log(z\bar z)\log\frac{1-z}{1-\bar z} + \frac{2\pi^2}{3}\log\frac{1-z}{1-\bar z}\,,\\
&\quad + [\mathrm{Li}_2(z) - \mathrm{Li}_2(\bar z)]\log(z\bar z)\\
f_{[46]}^{(0,2)}(z,\bar z) &= \frac{1}{2}[\mathrm{Li}_2(z) - \mathrm{Li}_2(\bar z)]\,. \qquad\qquad (C.10)
\end{aligned}$$

$$\begin{aligned}
&\mathrm{Cut}_{p_2^2,[136],R_\triangle^*} T_L(p_1^2,p_2^2,p_3^2) \qquad\qquad (C.11)\\
&= \frac{i\, c_\Gamma^2\, (p_1^2)^{-2-2\epsilon}}{(1-z)(1-\bar z)(z-\bar z)} \sum_{k=-1}^{\infty} \epsilon^k \left[(-2\pi i)\, f_{[136]}^{(k,1)}(z,\bar z) + (-2\pi i)^2\, f_{[136]}^{(k,2)}(z,\bar z)\right],
\end{aligned}$$

$$\begin{aligned}
f_{[136]}^{(-1,1)}(z,\bar z) &= \mathrm{Li}_2(z) - \mathrm{Li}_2(\bar z)\,,\\
f_{[136]}^{(-1,2)}(z,\bar z) &= 0\,,\\
f_{[136]}^{(0,1)}(z,\bar z) &= -G\left(0,\frac{1}{z},\frac{1}{\bar z};1\right) + G\left(0,\frac{1}{\bar z},\frac{1}{z};1\right) + 4[\mathrm{Li}_3(1-z) - \mathrm{Li}_3(1-\bar z)]\\
&\quad + 5[\mathrm{Li}_3(z) - \mathrm{Li}_3(\bar z)] + 2[\mathrm{Li}_2(z) + \mathrm{Li}_2(\bar z)]\log\frac{1-z}{1-\bar z}
\end{aligned}$$

$$
\begin{aligned}
&+\frac{1}{2}\log\frac{z}{\bar{z}}\log^2\frac{1-z}{1-\bar{z}}+\frac{1}{2}\log^2[(1-z)(1-\bar{z})]\log\frac{z}{\bar{z}}\\
&+\log[(1-z)(1-\bar{z})]\log(z\bar{z})\log\frac{1-z}{1-\bar{z}}-\frac{2}{3}\pi^2\log\frac{1-z}{1-\bar{z}}\,,\\
&-2[\mathrm{Li}_2(z)-\mathrm{Li}_2(\bar{z})]\log(z\bar{z})\\
f^{(0,2)}_{[136]}(z,\bar{z})\;&=0\,.
\end{aligned}
\tag{C.12}
$$

C.2 Computation and explicit results for double unitarity cuts

We briefly outline our approach to the calculation of the double unitarity cuts of fig. 3.12 and fig. 3.13. We then give explicit results for these integrals, written in terms of multiple polylogarithms to simplify the comparison between different terms.

C.2.1 Calculation of double unitarity cuts

Cut [456], $R^{1,3}_{\triangle}$, fig. 3.12a:

Because cut [45] factorizes the two loop integrations, this cut is just the product of an uncut one-loop triangle with one mass (p_3^2) and the double cut of a three-mass triangle, with masses p_1^2, p_2^2 and p_3^2, in the channels p_1^2 and p_3^2.

$$
\begin{aligned}
&\mathrm{Cut}_{[456],R^{1,3}_{\triangle}}T_L(p_1^2,p_2^2,p_3^2)=\\
&=-i\frac{e^{\gamma_E\epsilon}}{\pi^{2-\epsilon}}(2\pi)^3\int \mathrm{d}^{4-2\epsilon}k_1\,\delta\left(k_1^2\right)\delta\left((p_3-k_1)^2\right)\delta\left((p_1+k_1)^2\right)T(p_3^2)\\
&=-4\pi^2 i\frac{c_\Gamma e^{\gamma_E\epsilon}}{\epsilon^2\Gamma(1-\epsilon)}(p_1^2)^{-2-2\epsilon}u_3^{-1-2\epsilon}e^{i\pi\epsilon}\frac{z^{-\epsilon}(-\bar{z})^{-\epsilon}}{(z-\bar{z})^{1-2\epsilon}}\,.
\end{aligned}
\tag{C.13}
$$

Cut [1256], $R^{1,3}_{\triangle}$, fig. 3.12b:

The integrand has a simple pole inside the integration region. We can still make sense of the integral by keeping track of the $i0$ prescription associated to the propagators and the invariants, and we obtain

$$
\begin{aligned}
&\mathrm{Cut}_{[1256],R^{1,3}_{\triangle}}T_L(p_1^2,p_2^2,p_3^2)=\\
&=-i\frac{e^{\gamma_E\epsilon}}{\pi^{2-\epsilon}}(2\pi)^2\int \mathrm{d}^{4-2\epsilon}k_1\frac{\delta\left(k_1^2\right)\delta\left((p_1-k_1)^2\right)}{(p_3+k_1)^2-i0}\mathrm{Cut}_{p_3^2}T\left(p_3^2,(p_3+k)^2\right)
\end{aligned}
$$

$$
\begin{aligned}
=& i\frac{e^{2\gamma_E\epsilon}}{\pi^{2-\epsilon}}\frac{\Gamma(1-\epsilon)}{\epsilon\Gamma(1-2\epsilon)}(2\pi)^3\int \mathrm{d}^{4-2\epsilon}k\frac{\delta\left(k^2\right)\delta\left((p_1-k)^2\right)}{(p_3+k)^2-i0}\frac{(p_3^2+i0)^{-\epsilon}}{(p_3^2+i0)-((p_3+k)^2-i0)}\\
=& -4\pi^2 i\frac{e^{2\gamma_E\epsilon}}{\epsilon\Gamma(1-2\epsilon)}(p_1^2)^{-2-2\epsilon}u_3^{-\epsilon}\\
&\int_0^1 \mathrm{d}x\frac{x^{-\epsilon}(1-x)^{-\epsilon}}{(u_3+z-1-x(z-\bar{z})-i0)(z-1-x(z-\bar{z})-i0)}\,,
\end{aligned}
\tag{C.14}
$$

where in each line we were careful to keep the $\pm i0$ prescription associated with propagators and invariants. The integrand in the last line has poles at

$$
0<x_p\equiv\frac{(1-z)(-\bar{z})}{z-\bar{z}}<1 \qquad \text{and} \qquad x=\frac{z-1}{z-\bar{z}}<0\,.
$$

While the location of the second pole lies outside the integration region, the first singularity lies inside, and we must hence split the integral into its principle value and imaginary part,

$$
\lim_{0\to 0}\frac{1}{a\pm i0}=\mathrm{PV}\left(\frac{1}{a}\right)\mp i\pi\delta(a)\,.
$$

which is valid in a distribution sense. We then obtain

$$
\begin{aligned}
&\int_0^1 \mathrm{d}x\frac{x^{-\epsilon}(1-x)^{-\epsilon}}{(u_3+z-1-x(z-\bar{z})-i0)(z-1-x(z-\bar{z}))}\\
&\quad=\mathrm{PV}\int_0^1 \mathrm{d}x\frac{x^{-\epsilon}(1-x)^{-\epsilon}}{(u_3+z-1-x(z-\bar{z}))(z-1-x(z-\bar{z}))}\\
&\quad+i\pi\int_0^1 \mathrm{d}x\frac{x^{-\epsilon}(1-x)^{-\epsilon}}{(z-1-x(z-\bar{z}))}\delta(u_3+z-1-x(z-\bar{z}))\,.
\end{aligned}
\tag{C.15}
$$

Both integrals are finite and can easily be performed order by order in ϵ in terms of polylogarithms.

Cut [1236], $R^{1,3}_{\triangle}$, fig. 3.12c:

Using the strategy outlined in Section 3.6.4, we immediately obtain

$$
\begin{aligned}
&\mathrm{Cut}_{[1236],R^{1,3}_{\triangle}}T_L(p_1^2,p_2^2,p_3^2)= \qquad\qquad (C.16)\\
&=i\frac{e^{\gamma_E\epsilon}}{\pi^{2-\epsilon}}(2\pi)^2\int \mathrm{d}^{4-2\epsilon}k\delta\left(k^2\right)\delta\left((p_3-k)^2\right)\mathrm{Cut}_{(p_1-k)^2}B^h(p_3^2,(p_1-k)^2;p_1^2,p_2^2)\,.
\end{aligned}
$$

Inserting the analytic expression for the cut box (see appendix B.4) and parametrizing the remaining cut integration, we obtain an integral with an endpoint singularity. After subtraction of the singularity, all the integrals are finite and can be expanded under the integration sign. We obtain

$$\begin{aligned}
&\mathrm{Cut}_{[1236],R_{\triangle}^{1,3}} T_L(p_1^2,p_2^2,p_3^2) = \\
&\quad = 8\pi^2 i \frac{e^{\gamma_E \epsilon} c_\Gamma}{\Gamma(1-\epsilon)} (p_1^2)^{-2-2\epsilon} u_3^{-1-2\epsilon} z^\epsilon (-\bar{z})^\epsilon \int_0^{\frac{z}{z-\bar{z}}} \mathrm{d}x \frac{x^{-\epsilon}(1-x)^{-\epsilon}}{(z-x(z-\bar{z}))^{1+2\epsilon}} \\
&\quad \times \left[\frac{1}{\epsilon} + \log\left(1 - \frac{z-x(z-\bar{z})}{z\bar{z}}\right) + \log\left(1-z+x(z-\bar{z})\right) \right] . \qquad \text{(C.17)}
\end{aligned}$$

The remaining integral is easy to perform.

Cut [2346], $R_{\triangle}^{1,3}$, fig. 3.12d:

Using the routing of the loop momenta shown in fig. 3.12d, we compute this cut by integrating over the cut of a two-mass triangle. However, when using the result for the cut triangle, we need to correct for the fact that the vertex attached to propagators 2, 3 and 5 has a different color, compared to the usual cut triangle. Note also that it is convenient to introduce the variable y defined in eq. (3.104). We obtain

$$\begin{aligned}
&\mathrm{Cut}_{[2346],R_{\triangle}^{1,3}} T_L(p_1^2,p_2^2,p_3^2) = \\
&= -i \left(\frac{e^{\gamma_E\epsilon}}{\pi^{2-\epsilon}}\right) (2\pi)^2 \int \mathrm{d}^{4-2\epsilon}k_1 \frac{\delta(k_1^2)\,\delta((p_2+k_1)^2)}{(p_3-k_1)^2} \mathrm{Cut}_{(p_3-k_1)^2} T\left(p_3^2,(p_3-k_1)^2\right) \\
&= -4\pi^2 i \frac{e^{2\gamma_E\epsilon}}{\epsilon\Gamma(1-2\epsilon)} (p_1^2)^{-2-2\epsilon} u_3^{-1-2\epsilon} \int_0^1 \mathrm{d}x\, x^{-\epsilon}(1-x)^{-\epsilon} \\
&\quad \int_0^1 \mathrm{d}y\, y^{-2\epsilon}(1-y)^{-1-\epsilon} \delta\left(u_2 + y(z(1-\bar{z}) - x(z-\bar{z}))\right) \\
&= -4\pi^2 i \frac{e^{2\gamma_E\epsilon}}{\epsilon\Gamma(1-2\epsilon)} (p_1^2)^{-2-2\epsilon} u_3^{-1-2\epsilon} z^{-2\epsilon} (-\bar{z})^{-2\epsilon} \\
&\quad \int_0^{\frac{z}{z-\bar{z}}} \mathrm{d}x \frac{x^{-\epsilon}(1-x)^{-\epsilon}}{(z-x(z-\bar{z}))^{1+\epsilon}} \frac{1}{(z-z\bar{z}-x(z-\bar{z}))^{-3\epsilon}} . \qquad \text{(C.18)}
\end{aligned}$$

The integral has an endpoint singularity that needs to be subtracted before expansion in ϵ under the integration sign. The y variable is restricted to the interval $[0,1]$ because of the θ-function of the cut triangle subdiagram. We find

it simpler to use the δ-function associated with the cut on $(p_2+k_1)^2$ to perform the y integration, which in turn imposes some limits on the range of integration of x.

Cut [1356], $R^{1,3}_{\triangle}$, fig. 3.12f:

The integral is

$$\begin{aligned}
&\mathrm{Cut}_{[1356],R^{1,3}_{\triangle}} T_L(p_1^2,p_2^2,p_3^2) = \qquad\qquad (C.19)\\
&= -i\frac{e^{\gamma_E\epsilon}}{\pi^{2-\epsilon}}(2\pi)^2\int \mathrm{d}^{4-2\epsilon}k_1 \frac{\delta\left(k_1^2\right)\delta\left((p_1-k_1)^2\right)}{(p_2+k_1)^2}\mathrm{Cut}_{(p_2+k_1)^2}T\left(p_3^2,(p_2+k_1)^2\right)\\
&= \frac{-4\pi^2 i e^{2\gamma_E\epsilon}}{\epsilon\Gamma(1-2\epsilon)}(p_1^2)^{-2-2\epsilon}\int_0^{\frac{-\bar{z}(1-z)}{z-\bar{z}}}\mathrm{d}x\frac{x^{-\epsilon}(1-x)^{-\epsilon}(-\bar{z}(1-z)-x(z-\bar{z}))^{-1-\epsilon}}{(1-z+x(z-\bar{z}))}\,.
\end{aligned}$$

The restriction on the integration range of x is imposed by the θ-function of the cut triangle subdiagram. After subtracting the singularity, the integral can be performed oder by order in ϵ.

Cut [456], $R^{1,2}_{\triangle}$, fig. 3.13a:

The calculation of this cut in region $R^{1,2}_{\triangle}$ is done in exactly the same way as in region $R^{1,3}_{\triangle}$. However, we write the result differently so that we are away from the branch cuts in this region:

$$\begin{aligned}
&\mathrm{Cut}_{[456],R^{1,2}_{\triangle}} T_L(p_1^2,p_2^2,p_3^2) =\\
&= -i\frac{e^{\gamma_E\epsilon}}{\pi^{2-\epsilon}}(2\pi)^3\int \mathrm{d}^{4-2\epsilon}k_1\delta\left(k_1^2\right)\delta\left((p_3-k_1)^2\right)\delta\left((p_1+k_1)^2\right)T(p_3^2)\\
&= -4\pi^2 i\frac{c_\Gamma e^{\gamma_E\epsilon}}{\epsilon^2\Gamma(1-\epsilon)}(p_1^2)^{-2-2\epsilon}e^{i\pi\epsilon}((z-1)(1-\bar{z}))^{-1-2\epsilon}\frac{(z\bar{z})^{-\epsilon}}{(z-\bar{z})^{1-2\epsilon}}\,. \qquad (C.20)
\end{aligned}$$

Cut [2346], $R^{1,2}_{\triangle}$, fig. 3.13b:

The calculation of this cut in $R^{1,2}_{\triangle}$ is simpler than in region $R^{1,3}_{\triangle}$. We get

$$\begin{aligned}
&\mathrm{Cut}_{[2346],R^{1,2}_{\triangle}} T_L(p_1^2,p_2^2,p_3^2) = \qquad\qquad (C.21)\\
&= -i\left(\frac{e^{\gamma_E\epsilon}}{\pi^{2-\epsilon}}\right)(2\pi)^2\int \mathrm{d}^{4-2\epsilon}k_1 \frac{\delta\left(k_1^2\right)\delta\left((p_2-k_1)^2\right)}{(p_1+k_1)^2}\mathrm{Cut}_{(p_1+k_1)^2}T\left(p_3^2,(p_1+k_1)^2\right)\\
&= 4\pi^2 i\frac{e^{2\gamma_E\epsilon}}{\epsilon\Gamma(1-2\epsilon)}(p_1^2)^{-2-2\epsilon}u_2^{-\epsilon}\int_0^{\frac{1-\bar{z}}{z-\bar{z}}}\mathrm{d}x\, x^{-\epsilon}(1-x)^{-\epsilon}\frac{(1-\bar{z}-x(z-\bar{z}))^{-1-\epsilon}}{z(1-\bar{z})-x(z-\bar{z})}\,.
\end{aligned}$$

After subtraction of the singularity, the integral is easy to perform.

Cut [1356], $R_{\triangle}^{1,2}$, fig. 3.13c:

The computation of this cut is very similar to the previous one. We have

$$\begin{aligned}
&\mathrm{Cut}_{[1356],R_{\triangle}^{1,2}} T_L(p_1^2,p_2^2,p_3^2) = \qquad\qquad (C.22)\\
&= -i\left(\frac{e^{\gamma_E\epsilon}}{\pi^{2-\epsilon}}\right)(2\pi)^2\int \mathrm{d}^{4-2\epsilon}k_1 \frac{\delta\left(k_1^2\right)\delta\left((p_1-k_1)^2\right)}{(p_2+k_1)^2}\mathrm{Cut}_{(p_2+k_1)^2}T\left(p_3^2,(p_2+k_1)^2\right)\\
&= 4\pi^2 i\frac{e^{2\gamma_E\epsilon}}{\epsilon\Gamma(1-2\epsilon)}(p_1^2)^{-2-2\epsilon}\int_0^{\frac{\bar z(z-1)}{z-\bar z}}\mathrm{d}x\, x^{-\epsilon}(1-x)^{-\epsilon}\frac{(\bar z(z-1)-x(z-\bar z))^{-1-\epsilon}}{z-1-x(z-\bar z)}\,.
\end{aligned}$$

The restriction on the integration range of x is imposed by the θ-function of the cut triangle subdiagram. The endpoint singularity is dealt with as before.

Cut [1236], $R_{\triangle}^{1,2}$, fig. 3.13d:

This cut is slightly harder to compute in region $R_{\triangle}^{1,2}$ than in region $R_{\triangle}^{1,3}$. We follow the same technique of integrating over the cut of a two-mass hard box, although we have to be careful to correct for the different factors of $\pm i$ between the subdiagram entering in fig. 3.13d and a standard cut box that would have black vertices on one side of the cut and white vertices on the other side. It is also useful to introduce the y variable defined in eq. (3.104), and to integrate over it with the δ-function on propagator (p_3+k). The y variable is restricted to the interval $[0,1]$ because of the θ-function on $(p_1-k)^2$:

$$\begin{aligned}
&\mathrm{Cut}_{[1236],R_{\triangle}^{1,2}} T_L(p_1^2,p_2^2,p_3^2) =\\
&= i\frac{e^{\gamma_E\epsilon}}{\pi^{2-\epsilon}}(2\pi)^2\int \mathrm{d}^{4-2\epsilon}k\,\delta\left(k^2\right)\delta\left((p_3+k)^2\right)\mathrm{Cut}_{(p_1-k)^2}B^{2mh}(p_1^2,p_2^2;p_3^2,(p_1-k)^2)\\
&= -8\pi^2 i\frac{e^{\gamma_E\epsilon}c_\Gamma}{\Gamma(1-\epsilon)}(p_1^2)^{-2-2\epsilon}\frac{u_2^\epsilon}{((z-1)(1-\bar z))^{1+\epsilon}}\int_0^1\mathrm{d}x\, x^{-\epsilon}(1-x)^{-\epsilon}\\
&\quad\int_0^1\mathrm{d}y\, y^{1-2\epsilon}(1-y)^{-1-2\epsilon}\delta\big(u_3+y(z-1-x(z-\bar z))\big)\\
&\quad\left[\frac{1}{\epsilon}+\log y+\log\left(u_2-(1-y)\right)-\log u_2\right]\\
&= -8\pi^2 i\frac{e^{\gamma_E\epsilon}c_\Gamma}{\Gamma(1-\epsilon)}(p_1^2)^{-2-2\epsilon}\frac{u_2^\epsilon}{((z-1)(1-\bar z))^{3\epsilon}}\int_0^{\frac{\bar z(z-1)}{z-\bar z}}\mathrm{d}x\frac{x^{-\epsilon}(1-x)^{-\epsilon}}{(z-1-x(z-\bar z))^{1-4\epsilon}}
\end{aligned}$$

$$\big(\bar{z}(z-1)-x(z-\bar{z})\big)^{-1-2\epsilon}\left[\frac{1}{\epsilon}+\log\big((z-1)(1-\bar{z})\big)-\log\big(z-1-x(z-\bar{z})\big)\right.$$
$$\left.-\log(z\bar{z})+\log\left(z\bar{z}-\frac{\bar{z}(z-1)-x(z-\bar{z})}{z-1-x(z-\bar{z})}\right)\right] \tag{C.23}$$

The restriction on the integration range of x is imposed when integrating over y. The endpoint singularity is dealt with as before.

C.2.2 Double unitarity cuts in the p_1^2 and p_3^2 channels in region $R_{\triangle}^{1,3}$

In this section we present the analytic results for all the nonvanishing cuts in the p_1^2 and p_3^2 channels in region $R_{\triangle}^{1,3}$, where $\bar{z}<0<z<1$.

$$\begin{aligned}&\mathrm{Cut}_{[456],R_{\triangle}^{1,3}}T_L(p_1^2,p_2^2,p_3^2)= \\ &=\frac{i\,c_\Gamma^2\,(p_1^2)^{-2-2\epsilon}(-2\pi i)^2}{(1-z)(1-\bar{z})(z-\bar{z})}\sum_{k=-2}^{\infty}\epsilon^k\left[f^{(k,2)}_{[456],R_{\triangle}^{1,3}}(z,\bar{z})+(-2\pi i)\,f^{(k,3)}_{[456],R_{\triangle}^{1,3}}(z,\bar{z})\right],\end{aligned} \tag{C.24}$$

$$\begin{aligned}f^{(-2,2)}_{[456],R_{\triangle}^{1,3}}&=1\,,\\ f^{(-2,3)}_{[456],R_{\triangle}^{1,3}}&=0\,,\\ f^{(-1,2)}_{[456],R_{\triangle}^{1,3}}&=2\log(z-\bar{z})-2\log[(1-z)(1-\bar{z})]-\log(-z\bar{z})\,,\\ f^{(-1,3)}_{[456],R_{\triangle}^{1,3}}&=-\frac{1}{2}\,,\\ f^{(0,2)}_{[456],R_{\triangle}^{1,3}}&=\frac{1}{2}\left[-2\log(z-\bar{z})+2\log[(1-z)(1-\bar{z})]+\log(-z\bar{z})\right]^2-\frac{\pi^2}{2}\,,\\ f^{(0,3)}_{[456],R_{\triangle}^{1,3}}&=\log[(1-z)(1-\bar{z})]-\log(z-\bar{z})+\frac{1}{2}\log(-z\bar{z})\,.\end{aligned} \tag{C.25}$$

$$\begin{aligned}&\mathrm{Cut}_{[1236],R_{\triangle}^{1,3}}T_L(p_1^2,p_2^2,p_3^2)= \\ &=\frac{i\,c_\Gamma^2\,(p_1^2)^{-2-2\epsilon}(-2\pi i)^2}{(1-z)(1-\bar{z})(z-\bar{z})}\sum_{k=-2}^{\infty}\epsilon^k\left[f^{(k,2)}_{[1236],R_{\triangle}^{1,3}}(z,\bar{z})+(-2\pi i)\,f^{(k,3)}_{[1236],R_{\triangle}^{1,3}}(z,\bar{z})\right],\end{aligned} \tag{C.26}$$

$$
\begin{aligned}
f^{(-2,2)}_{[1236],R^{1,3}_{\triangle}} &= 1\,,\\
f^{(-2,3)}_{[1236],R^{1,3}_{\triangle}} &= 0\,,\\
f^{(-1,2)}_{[1236],R^{1,3}_{\triangle}} &= 2\log\left(z-\bar{z}\right) - 2\log\left[(1-z)(1-\bar{z})\right] - 2\log z\,,\\
f^{(-1,3)}_{[1236],R^{1,3}_{\triangle}} &= 0\,,\\
f^{(0,2)}_{[1236],R^{1,3}_{\triangle}} &= 2\mathrm{Li}_2(z) - 2\mathrm{Li}_2\left(\frac{z}{\bar{z}}\right) - 2\mathrm{Li}_2\left(\bar{z}\right) + 2\log^2\left(1-\bar{z}\right) + 2\log^2\left(z-\bar{z}\right)\\
&\quad + 4\log(1-z)\log\left(1-\bar{z}\right) - 4\log(1-z)\log\left(z-\bar{z}\right) + 4\log z\log\left(1-\bar{z}\right)\\
&\quad - 4\log z\log\left(z-\bar{z}\right) - 4\log\left(1-\bar{z}\right)\log\left(z-\bar{z}\right) + 2\log^2(1-z) + 2\log^2 z\\
&\quad - \log^2\left(-\bar{z}\right) + 4\log z\log(1-z) - \frac{2\pi^2}{3}\,,\\
f^{(0,3)}_{[1236],R^{1,3}_{\triangle}} &= 0\,.
\end{aligned}
\tag{C.27}
$$

$$
\begin{aligned}
&\mathrm{Cut}_{[1256],R^{1,3}_{\triangle}} T_L(p_1^2,p_2^2,p_3^2) = \\
&= \frac{i\,c_\Gamma^2\,(p_1^2)^{-2-2\epsilon}(-2\pi i)^2}{(1-z)(1-\bar{z})(z-\bar{z})}\sum_{k=-1}^{\infty}\epsilon^k\left[f^{(k,2)}_{[1256],R^{1,3}_{\triangle}}(z,\bar{z}) + (-2\pi i)\,f^{(k,3)}_{[1256],R^{1,3}_{\triangle}}(z,\bar{z})\right],
\end{aligned}
\tag{C.28}
$$

$$
\begin{aligned}
f^{(-1,2)}_{[1256],R^{1,3}_{\triangle}} &= \log z - \log\left(-\bar{z}\right)\,,\\
f^{(-1,3)}_{[1256],R^{1,3}_{\triangle}} &= \frac{1}{2}\,,\\
f^{(0,2)}_{[1256],R^{1,3}_{\triangle}} &= 2\mathrm{Li}_2\left(\frac{z}{\bar{z}}\right) + 2\mathrm{Li}_2\left(\bar{z}\right) - 2\mathrm{Li}_2(z) + \frac{3}{2}\log^2\left(-\bar{z}\right) - 2\log z\log\left(1-\bar{z}\right)\\
&\quad + 2\log z\log\left(z-\bar{z}\right) - \log z\log\left(-\bar{z}\right) + 2\log(1-z)\log\left(-\bar{z}\right)\\
&\quad + 2\log\left(1-\bar{z}\right)\log\left(-\bar{z}\right) - 2\log\left(z-\bar{z}\right)\log\left(-\bar{z}\right) - \frac{1}{2}\log^2 z\\
&\quad - 2\log(1-z)\log z + \frac{\pi^2}{6}\,,\\
f^{(0,3)}_{[1256],R^{1,3}_{\triangle}} &= \log\left(z-\bar{z}\right) - \log\left[(1-z)\left(1-\bar{z}\right)\right] - \frac{1}{2}\log\left(-z\bar{z}\right)\,.
\end{aligned}
\tag{C.29}
$$

$$\mathrm{Cut}_{[1356],R^{1,3}_{\triangle}} T_L(p_1^2,p_2^2,p_3^2) = \tag{C.30}$$
$$= \frac{i\, c_\Gamma^2\, (p_1^2)^{-2-2\epsilon}(-2\pi i)^2}{(1-z)(1-\bar{z})(z-\bar{z})} \sum_{k=-2}^{\infty} \epsilon^k \left[f^{(k,2)}_{[1356],R^{1,3}_{\triangle}}(z,\bar{z}) + (-2\pi i)\, f^{(k,3)}_{[1356],R^{1,3}_{\triangle}}(z,\bar{z}) \right],$$

$$\begin{aligned}
f^{(-2,2)}_{[1356],R^{1,3}_{\triangle}} &= -1\,, \\
f^{(-2,3)}_{[1356],R^{1,3}_{\triangle}} &= 0\,, \\
f^{(-1,2)}_{[1356],R^{1,3}_{\triangle}} &= 2\log\left[(1-z)(1-\bar{z})\right] - 2\log\left(z-\bar{z}\right) + 2\log\left(-\bar{z}\right) + \log(z)\,, \\
f^{(-1,3)}_{[1356],R^{1,3}_{\triangle}} &= 0\,, \\
f^{(0,2)}_{[1356],R^{1,3}_{\triangle}} &= -\mathrm{Li}_2\left(\frac{z}{\bar{z}}\right) - 3\mathrm{Li}_2\left(\bar{z}\right) - 2\log^2\left(1-\bar{z}\right) - 2\log^2\left(z-\bar{z}\right) \\
&\quad - 4\log(1-z)\log\left(1-\bar{z}\right) + 4\log(1-z)\log\left(z-\bar{z}\right) \\
&\quad - 2\log z\log\left(1-\bar{z}\right) + 2\log z\log\left(z-\bar{z}\right) + 4\log\left(1-\bar{z}\right)\log\left(z-\bar{z}\right) \\
&\quad - \log z\log\left(-\bar{z}\right) - 4\log\left(1-\bar{z}\right)\log\left(-\bar{z}\right) + 4\log\left(z-\bar{z}\right)\log\left(-\bar{z}\right) \\
&\quad - \frac{5}{2}\log^2\left(-\bar{z}\right) - 4\log(1-z)\log\left(-\bar{z}\right) - 2\log^2(1-z) \\
&\quad - \log^2 z - 2\log z\log(1-z) + \frac{\pi^2}{6}\,, \\
f^{(0,3)}_{[1356],R^{1,3}_{\triangle}} &= 0\,.
\end{aligned} \tag{C.31}$$

$$\mathrm{Cut}_{[2346],R^{1,3}_{\triangle}} T_L(p_1^2,p_2^2,p_3^2) = \tag{C.32}$$
$$= \frac{i\, c_\Gamma^2\, (p_1^2)^{-2-2\epsilon}(-2\pi i)^2}{(1-z)(1-\bar{z})(z-\bar{z})} \sum_{k=-2}^{\infty} \epsilon^k \left[f^{(k,2)}_{[2346],R^{1,3}_{\triangle}}(z,\bar{z}) + (-2\pi i)\, f^{(k,3)}_{[2346],R^{1,3}_{\triangle}}(z,\bar{z}) \right],$$

$$\begin{aligned}
f^{(-2,2)}_{[2346],R^{1,3}_{\triangle}} &= -1\,, \\
f^{(-2,3)}_{[2346],R^{1,3}_{\triangle}} &= 0\,, \\
f^{(-1,2)}_{[2346],R^{1,3}_{\triangle}} &= 2\log\left[(1-z)(1-\bar{z})\right] - 2\log\left(z-\bar{z}\right) + \log z\,,
\end{aligned}$$

$$
\begin{aligned}
f^{(-1,3)}_{[2346],R^{1,3}_{\triangle}} &= 0\,,\\
f^{(0,2)}_{[2346],R^{1,3}_{\triangle}} &= \mathrm{Li}_2\left(\frac{z}{\bar{z}}\right) + 3\mathrm{Li}_2\left(\bar{z}\right) - 2\log^2\left(1-\bar{z}\right) - 2\log^2\left(z-\bar{z}\right) + \frac{3}{2}\log^2\left(-\bar{z}\right)\\
&\quad - 4\log(1-z)\log\left(1-\bar{z}\right) + 4\log(1-z)\log\left(z-\bar{z}\right) - \frac{1}{2}\log^2 z\\
&\quad + 2\log z\log\left(z-\bar{z}\right) + 4\log\left(1-\bar{z}\right)\log\left(z-\bar{z}\right) - 2\log^2(1-z)\\
&\quad - 2\log z\log\left(1-\bar{z}\right) - 2\log z\log(1-z) + \frac{5\pi^2}{6}\,,\\
f^{(0,3)}_{[2346],R^{1,3}_{\triangle}} &= 0\,.
\end{aligned}
\tag{C.33}
$$

C.2.3 Double unitarity cuts in the p_1^2 and p_2^2 channels in region $R^{1,2}_{\triangle}$

In this section we present the analytic results for all the nonvanishing cuts in the p_1^2 and p_2^2 channels in region $R^{1,2}_{\triangle}$, where $0 < \bar{z} < 1 < z$.

$$
\begin{aligned}
&\mathrm{Cut}_{[456],R^{1,2}_{\triangle}} T_L(p_1^2,p_2^2,p_3^2)\\
&= \frac{i\,c_\Gamma^2\,(p_1^2)^{-2-2\epsilon}(-2\pi i)^2}{(1-z)(1-\bar{z})(z-\bar{z})}\sum_{k=-2}^{\infty}\epsilon^k\left[f^{(k,2)}_{[456],R^{1,2}_{\triangle}}(z,\bar{z}) + (-2\pi i)\,f^{(k,3)}_{[456],R^{1,2}_{\triangle}}(z,\bar{z})\right],
\end{aligned}
\tag{C.34}
$$

$$
\begin{aligned}
f^{(-2,2)}_{[456],R^{1,2}_{\triangle}} &= 1\,,\\
f^{(-2,3)}_{[456],R^{1,2}_{\triangle}} &= 0\,,\\
f^{(-1,2)}_{[456],R^{1,2}_{\triangle}} &= 2\log\left(z-\bar{z}\right) - 2\log\left[(z-1)\left(1-\bar{z}\right)\right] - \log\left(z\bar{z}\right)\,,\\
f^{(-1,3)}_{[456],R^{1,2}_{\triangle}} &= 0\,,\\
f^{(0,2)}_{[456],R^{1,2}_{\triangle}} &= 2\log^2\left(1-\bar{z}\right) + 2\log^2\left(z-\bar{z}\right) + \frac{1}{2}\log^2\bar{z} + 4\log(z-1)\log\left(1-\bar{z}\right)\\
&\quad - 4\log(z-1)\log\left(z-\bar{z}\right) + 2\log(z-1)\log\bar{z} + 2\log z\log\left(1-\bar{z}\right)\\
&\quad - 2\log z\log\left(z-\bar{z}\right) - 4\log\left(1-\bar{z}\right)\log\left(z-\bar{z}\right) + \log z\log\bar{z}\\
&\quad - 2\log\left(z-\bar{z}\right)\log\bar{z} + 2\log^2(z-1) + \frac{1}{2}\log^2 z + 2\log z\log(z-1)\\
&\quad + 2\log\left(1-\bar{z}\right)\log\bar{z}\,,
\end{aligned}
$$

$$f^{(0,3)}_{[456],R^{1,2}_{\triangle}} = 0\,. \tag{C.35}$$

$$\begin{aligned}
&\mathrm{Cut}_{[1236],R^{1,2}_{\triangle}} T_L(p_1^2,p_2^2,p_3^2) = \\
&= \frac{i\,c_\Gamma^2\,(p_1^2)^{-2-2\epsilon}(-2\pi i)^2}{(1-z)(1-\bar z)(z-\bar z)} \sum_{k=-2}^{\infty} \epsilon^k \left[f^{(k,2)}_{[1236],R^{1,2}_{\triangle}}(z,\bar z) + (-2\pi i)\, f^{(k,3)}_{[1236],R^{1,2}_{\triangle}}(z,\bar z)\right],
\end{aligned} \tag{C.36}$$

$$\begin{aligned}
f^{(-2,2)}_{[1236],R^{1,2}_{\triangle}} &= 1\,,\\
f^{(-2,3)}_{[1236],R^{1,2}_{\triangle}} &= 0\,,\\
f^{(-1,2)}_{[1236],R^{1,2}_{\triangle}} &= 2\log(z-\bar z) - 2\log\left[(z-1)(1-\bar z)\right] - 2\log\bar z\,,\\
f^{(-1,3)}_{[1236],R^{1,2}_{\triangle}} &= 0\,,\\
f^{(0,2)}_{[1236],R^{1,2}_{\triangle}} &= 2\mathrm{Li}_2(1-z) - 2\mathrm{Li}_2(\bar z) - 2\mathrm{Li}_2\left(\frac{\bar z}{z}\right) + 2\log^2(1-\bar z) + 2\log^2(z-\bar z)\\
&\quad + 4\log(z-1)\log(1-\bar z) - 4\log(z-1)\log(z-\bar z) + 4\log(z-1)\log\bar z\\
&\quad - 4\log(1-\bar z)\log(z-\bar z) + 4\log(1-\bar z)\log\bar z - 4\log(z-\bar z)\log\bar z\\
&\quad - \log^2 z + 2\log z\log(z-1) + 2\log^2\bar z + 2\log^2(z-1)\,,\\
f^{(0,3)}_{[1236],R^{1,2}_{\triangle}} &= 0\,.
\end{aligned} \tag{C.37}$$

$$\begin{aligned}
&\mathrm{Cut}_{[1356],R^{1,2}_{\triangle}} T_L(p_1^2,p_2^2,p_3^2) = \\
&= \frac{i\,c_\Gamma^2\,(p_1^2)^{-2-2\epsilon}(-2\pi i)^2}{(1-z)(1-\bar z)(z-\bar z)} \sum_{k=-2}^{\infty} \epsilon^k \left[f^{(k,2)}_{[1356],R^{1,2}_{\triangle}}(z,\bar z) + (-2\pi i)\, f^{(k,3)}_{[1356],R^{1,2}_{\triangle}}(z,\bar z)\right],
\end{aligned} \tag{C.38}$$

$$\begin{aligned}
f^{(-2,2)}_{[1356],R^{1,2}_{\triangle}} &= -1\,,\\
f^{(-2,3)}_{[1356],R^{1,2}_{\triangle}} &= 0\,,\\
f^{(-1,2)}_{[1356],R^{1,2}_{\triangle}} &= 2\log\left[(z-1)(1-\bar z)\right] - 2\log(z-\bar z) + 2\log\bar z + \log z\,,\\
f^{(-1,3)}_{[1356],R^{1,2}_{\triangle}} &= 0\,,
\end{aligned}$$

$$
\begin{aligned}
f^{(0,2)}_{[1356],R^{1,2}_{\triangle}} &= -3\mathrm{Li}_2\left(\bar{z}\right) + \mathrm{Li}_2\left(\frac{\bar{z}}{z}\right) - 2\log^2\left(1-\bar{z}\right) - 2\log^2\left(z-\bar{z}\right) - 2\log^2\bar{z} \\
&\quad - 4\log(z-1)\log\left(1-\bar{z}\right) + 4\log(z-1)\log\left(z-\bar{z}\right) - 4\log(z-1)\log\bar{z} \\
&\quad - 2\log z\log\left(1-\bar{z}\right) + 2\log z\log\left(z-\bar{z}\right) + 4\log\left(1-\bar{z}\right)\log\left(z-\bar{z}\right) \\
&\quad - 4\log\left(1-\bar{z}\right)\log\bar{z} + 4\log\left(z-\bar{z}\right)\log\bar{z} - 2\log^2(z-1) - \frac{\log^2(z)}{2} \\
&\quad - 2\log z\log\bar{z} - 2\log z\log(z-1) + \frac{\pi^2}{3}\,, \\
f^{(0,3)}_{[1356],R^{1,2}_{\triangle}} &= 0\,.
\end{aligned}
\tag{C.39}
$$

$$
\begin{aligned}
&\mathrm{Cut}_{[1356],R^{1,2}_{\triangle}} T_L(p_1^2,p_2^2,p_3^2) = \\
&= \frac{i\,c_\Gamma^2\,(p_1^2)^{-2-2\epsilon}(-2\pi i)^2}{(1-z)(1-\bar{z})(z-\bar{z})}\sum_{k=-2}^{\infty}\epsilon^k\left[f^{(k,2)}_{[1356],R^{1,2}_{\triangle}}(z,\bar{z}) + (-2\pi i)\,f^{(k,3)}_{[1356],R^{1,2}_{\triangle}}(z,\bar{z})\right],
\end{aligned}
\tag{C.40}
$$

$$
\begin{aligned}
f^{(-2,2)}_{[1356],R^{1,2}_{\triangle}} &= -1\,, \\
f^{(-2,3)}_{[1356],R^{1,2}_{\triangle}} &= 0\,, \\
f^{(-1,2)}_{[1356],R^{1,2}_{\triangle}} &= 2\log\left[(z-1)\left(1-\bar{z}\right)\right] - 2\log\left(z-\bar{z}\right) + \log\bar{z}\,, \\
f^{(-1,3)}_{[1356],R^{1,2}_{\triangle}} &= 0\,, \\
f^{(0,2)}_{[1356],R^{1,2}_{\triangle}} &= \mathrm{Li}_2\left(\frac{\bar{z}}{z}\right) - 3\mathrm{Li}_2(1-z) - 2\log^2\left(1-\bar{z}\right) - 2\log^2\left(z-\bar{z}\right) - \frac{1}{2}\log^2\bar{z} \\
&\quad - 4\log(z-1)\log\left(1-\bar{z}\right) + 4\log(z-1)\log\left(z-\bar{z}\right) - 2\log(z-1)\log\bar{z} \\
&\quad + 4\log\left(1-\bar{z}\right)\log\left(z-\bar{z}\right) - 2\log\left(1-\bar{z}\right)\log\bar{z} + 2\log\left(z-\bar{z}\right)\log\bar{z} \\
&\quad - 2\log^2(z-1) + \frac{3}{2}\log^2 z - 3\log z\log(z-1) - \frac{\pi^2}{6}\,, \\
f^{(0,3)}_{[1356],R^{1,2}_{\triangle}} &= 0\,.
\end{aligned}
\tag{C.41}
$$

Appendix D

A brief comment on non-generic internal masses

Throughout this thesis, we have assumed all internal masses to be distinct. However, diagrams with equal internal masses are particularly interesting in phenomenological applications, so we now show how to obtain relations for these cases from the ones we established in the generic case. If two propagators have the same mass m, then it is no longer correct that the cut on one of the propagator of mass m will reproduce the full discontinuity of the function on the m^2 variable, so that relations such as eq. (3.11) and eq. (3.17) must be modified.

If a Feynman diagram has more than one propagator with mass m^2, it is the *sum* of all the single cuts of propagators of mass m^2 that is related to the m^2-discontinuity of the integral. It is thus sufficient to consider the case where all internal masses are distinct: to get the discontinuity in the degenerate case we sum the discontinuities (or cuts, which are well defined for generic masses) associated with each of the masses that we want to make equal, and then take the equal mass limit.

Let us give an example. Consider the diagram of section B.1.5 in the limit $m_{12}^2 = m_{13}^2$, $T(p_1^2, 0, 0; m^2, 0, m^2)$. This diagram is finite in four dimensions, and it is given by

$$T(p_1^2, 0, 0; m^2, 0, m^2) = -\frac{i}{p_1^2} \log^2\left(\frac{1+\gamma}{\gamma-1}\right) + \mathcal{O}(\epsilon), \tag{D.1}$$

where we defined the usual quantity

$$\gamma = \sqrt{1 - 4\frac{m^2}{p_1^2}}. \tag{D.2}$$

For concreteness we work in the region where $p_1^2 < 0$ and $m^2 > 0$, in which case $\gamma > 1$.

The result of the cut in p_1^2 is computed in the region $p_1^2 > 4m^2 > 0$ where $\gamma < 1$ and we get

$$\mathrm{Cut}_{p_1^2}\left[T(p_1^2, 0, 0; m^2, 0, m^2)\right] = \frac{4\pi}{p_1^2} \log\left(\frac{1+\gamma}{1-\gamma}\right). \tag{D.3}$$

The discontinuity in m^2 can be computed directly from eq. (D.1). The result is

$$\mathrm{Disc}_{m^2}\left[T(p_1^2, 0, 0; m^2, 0, m^2)\right] = \frac{4\pi}{p_1^2} \log\left(\frac{1+\gamma}{1-\gamma}\right). \tag{D.4}$$

Let us now see how these results are related to the case with generic masses, i.e. $m_{12}^2 \neq m_{13}^2$. In the equal mass limit,

$$w_1 \longrightarrow \frac{1+\gamma}{2} \qquad \text{and} \qquad \bar{w}_1 \longrightarrow \frac{1-\gamma}{2}. \tag{D.5}$$

It is easy to see that eq. (D.1) and eq. (D.3) are obtained from eq. (B.20) and eq. (B.22) under this limit. More interestingly, we can verify from eq. (D.4) above and the cuts of massive propagators given in eq. (B.23) and eq. (B.24) that

$$\begin{aligned} &\mathrm{Disc}_{m^2}\left[T(p_1^2, 0, 0; m^2, 0, m^2)\right] = \\ &= \left[\mathrm{Cut}_{m_{12}^2} T(p_1^2, 0, 0; m_{12}^2, 0, m_{13}^2) + \mathrm{Cut}_{m_{13}^2} T(p_1^2, 0, 0; m_{12}^2, 0, m_{13}^2)\right]\Big|_{\substack{m_{12}^2=m^2 \\ m_{13}^2=m^2}} \end{aligned} \tag{D.6}$$

which illustrates the point we made above.

We close with a comment on divergences. When combining single cuts to take the degenerate mass limit, one should first add all relevant single-propagator cuts and then take the limit. Indeed, individual terms in the sum might become divergent in this limit, but these divergences are of course not meaningful and cancel in the sum. As an example, consider the diagram of section B.1.4 in the

limit $m_{12}^2 = m_{23}^2$, $T(p_1^2, 0, 0; m^2, m^2, 0)$. The two cuts in internal masses are given in eqs. (B.16) and (B.17) and they are divergent for $m_{12}^2 = m_{23}^2$. However, their sum, which corresponds to the m^2-discontinuity of $T(p_1^2, 0, 0; m^2, m^2, 0)$, is finite, as it should be.

Bibliography

[1] C. Anastasiou, C. Duhr, F. Dulat, F. Herzog, and B. Mistlberger, *Higgs Boson Gluon-Fusion Production in QCD at Three Loops*, *Phys. Rev. Lett.* **114** (2015) 212001, [1503.06056].

[2] G. Passarino and M. J. G. Veltman, *One Loop Corrections for e+ e- Annihilation Into mu+ mu- in the Weinberg Model*, *Nucl. Phys.* **B160** (1979) 151.

[3] Z. Bern, L. J. Dixon, D. C. Dunbar, and D. A. Kosower, *One loop n point gauge theory amplitudes, unitarity and collinear limits*, *Nucl.Phys.* **B425** (1994) 217–260, [hep-ph/9403226].

[4] Z. Bern, L. J. Dixon, D. C. Dunbar, and D. A. Kosower, *Fusing gauge theory tree amplitudes into loop amplitudes*, *Nucl. Phys.* **B435** (1995) 59–101, [hep-ph/9409265].

[5] R. Britto, F. Cachazo, and B. Feng, *Generalized unitarity and one-loop amplitudes in N=4 super-Yang-Mills*, *Nucl. Phys.* **B725** (2005) 275–305, [hep-th/0412103].

[6] R. Britto, E. Buchbinder, F. Cachazo, and B. Feng, *One-loop amplitudes of gluons in SQCD*, *Phys.Rev.* **D72** (2005) 065012, [hep-ph/0503132].

[7] E. I. Buchbinder and F. Cachazo, *Two-loop amplitudes of gluons and octa-cuts in N=4 super Yang-Mills*, *JHEP* **0511** (2005) 036, [hep-th/0506126].

[8] P. Mastrolia, *On Triple-cut of scattering amplitudes*, *Phys.Lett.* **B644** (2007) 272–283, [hep-th/0611091].

[9] C. Anastasiou, R. Britto, B. Feng, Z. Kunszt, and P. Mastrolia, *D-dimensional unitarity cut method*, *Phys. Lett.* **B645** (2007) 213–216, [hep-ph/0609191].

[10] D. Forde, *Direct extraction of one-loop integral coefficients*, *Phys. Rev.* **D75** (2007) 125019, [0704.1835].

[11] E. Nigel Glover and C. Williams, *One-Loop Gluonic Amplitudes from Single Unitarity Cuts*, *JHEP* **0812** (2008) 067, [0810.2964].

[12] P. Mastrolia, *Double-Cut of Scattering Amplitudes and Stokes' Theorem*, *Phys.Lett.* **B678** (2009) 246–249, [0905.2909].

[13] S. Caron-Huot, *Loops and trees*, *JHEP* **1105** (2011) 080, [1007.3224].

[14] D. A. Kosower and K. J. Larsen, *Maximal Unitarity at Two Loops*, *Phys. Rev.* **D85** (2012) 045017, [1108.1180].

[15] H. Johansson, D. A. Kosower, and K. J. Larsen, *Two-Loop Maximal Unitarity with External Masses*, *Phys. Rev.* **D87** (2013), no. 2 025030, [1208.1754].

[16] M. Søgaard, *Global Residues and Two-Loop Hepta-Cuts*, *JHEP* **09** (2013) 116, [1306.1496].

[17] M. Søgaard and Y. Zhang, *Unitarity Cuts of Integrals with Doubled Propagators*, *JHEP* **07** (2014) 112, [1403.2463].

[18] L. Landau, *On analytic properties of vertex parts in quantum field theory*, *Nucl.Phys.* **13** (1959) 181–192.

[19] R. Cutkosky, *Singularities and discontinuities of Feynman amplitudes*, *J.Math.Phys.* **1** (1960) 429–433.

[20] R. Eden, P. Landshoff, D. Olive, and J. Polkinghorne, *The Analytic S-Matrix*. Cambridge at the University Press, 1966.

[21] G. 't Hooft and M. Veltman, *DIAGRAMMAR*, *NATO Adv.Study Inst.Ser.B Phys.* **4** (1974) 177–322.

[22] E. Remiddi, *Dispersion Relations for Feynman Graphs*, *Helv.Phys.Acta* **54** (1982) 364.

[23] M. Veltman, *Diagrammatica: The Path to Feynman rules*, *Cambridge Lect.Notes Phys.* **4** (1994) 1–284.

[24] A. Goncharov, *Galois symmetries of fundamental groupoids and noncommutative geometry*, *Duke Math.J.* **128** (2005) 209, [math/0208144].

[25] A. B. Goncharov, *Multiple polylogarithms and mixed Tate motives*, math/0103059.

[26] M. Caffo, H. Czyz, S. Laporta, and E. Remiddi, *The Master differential equations for the two loop sunrise selfmass amplitudes*, *Nuovo Cim.* **A111** (1998) 365–389, [hep-th/9805118].

[27] S. Müller-Stach, S. Weinzierl, and R. Zayadeh, *A Second-Order Differential Equation for the Two-Loop Sunrise Graph with Arbitrary Masses*, *Commun.Num.Theor.Phys.* **6** (2012) 203–222, [1112.4360].

[28] S. Caron-Huot and K. J. Larsen, *Uniqueness of two-loop master contours*, *JHEP* **10** (2012) 026, [1205.0801].

[29] L. Adams, C. Bogner, and S. Weinzierl, *The two-loop sunrise graph with arbitrary masses*, 1302.7004.

[30] S. Bloch and P. Vanhove, *The elliptic dilogarithm for the sunset graph*, 1309.5865.

[31] E. Remiddi and L. Tancredi, *Schouten identities for Feynman graph amplitudes; The Master Integrals for the two-loop massive sunrise graph*, *Nucl. Phys.* **B880** (2014) 343–377, [1311.3342].

[32] E. Remiddi and L. Tancredi, *Schouten identities and the two-loop sunrise graph*, *PoS* **LL2014** (2014) 053.

[33] L. Adams, C. Bogner, and S. Weinzierl, *The two-loop sunrise graph in two space-time dimensions with arbitrary masses in terms of elliptic dilogarithms*, *J. Math. Phys.* **55** (2014), no. 10 102301, [1405.5640].

[34] L. Adams, C. Bogner, and S. Weinzierl, *The two-loop sunrise integral around four space-time dimensions and generalisations of the Clausen and Glaisher functions towards the elliptic case*, 1504.03255.

[35] J. Broedel, N. Matthes, and O. Schlotterer, *Relations between elliptic multiple zeta values and a special derivation algebra*, 1507.02254.

[36] S. Abreu, R. Britto, C. Duhr, and E. Gardi, *From multiple unitarity cuts to the coproduct of Feynman integrals*, *JHEP* **1410** (2014) 125, [1401.3546].

[37] S. Abreu, R. Britto, and H. Grönqvist, *Cuts and coproducts of massive triangle diagrams*, *JHEP* **07** (2015) 111, [1504.00206].

[38] S. Abreu, MATHEMATICA *package with results for diagrams and their cuts used in the check of the diagrammatic coproduct*, 2015. http://www2.ph.ed.ac.uk/~s1039321/resultsOfDiagramsDiagCoprod.zip.

[39] R. K. Ellis and G. Zanderighi, *Scalar one-loop integrals for QCD*, *JHEP* **0802** (2008) 002, [0712.1851].

[40] E. Remiddi and J. Vermaseren, *Harmonic polylogarithms*, *Int.J.Mod.Phys.* **A15** (2000) 725–754, [hep-ph/9905237].

[41] T. Gehrmann and E. Remiddi, *Two loop master integrals for $\gamma^* \to 3$ jets: The Planar topologies*, *Nucl.Phys.* **B601** (2001) 248–286, [hep-ph/0008287].

[42] M. Y. Kalmykov and O. Veretin, *Single scale diagrams and multiple binomial sums*, *Phys.Lett.* **B483** (2000) 315–323, [hep-th/0004010].

[43] M. Y. Kalmykov, B. Ward, and S. Yost, *Multiple (inverse) binomial sums of arbitrary weight and depth and the all-order epsilon-expansion of generalized hypergeometric functions with one half-integer value of parameter*, *JHEP* **0710** (2007) 048, [0707.3654].

[44] R. Bonciani, G. Degrassi, and A. Vicini, *On the Generalized Harmonic Polylogarithms of One Complex Variable*, *Comput.Phys.Commun.* **182** (2011) 1253–1264, [1007.1891].

[45] J. Ablinger, J. Blumlein, and C. Schneider, *Harmonic Sums and Polylogarithms Generated by Cyclotomic Polynomials*, *J.Math.Phys.* **52** (2011) 102301, [1105.6063].

[46] J. Ablinger, J. Blümlein, and C. Schneider, *Analytic and Algorithmic Aspects of Generalized Harmonic Sums and Polylogarithms*, *J.Math.Phys.* **54** (2013) 082301, [1302.0378].

[47] A. B. Goncharov, *Multiple polylogarithms, cyclotomy and modular complexes*, *Math.Res.Lett.* **5** (1998) 497–516, [1105.2076].

[48] C. Duhr, *Hopf algebras, coproducts and symbols: an application to Higgs boson amplitudes*, *JHEP* **1208** (2012) 043, [1203.0454].

[49] K. T. Chen, *Iterated path integrals*, *Bull. Amer. Math. Soc.* **83** (1977) 831.

[50] A. B. Goncharov, M. Spradlin, C. Vergu, and A. Volovich, *Classical Polylogarithms for Amplitudes and Wilson Loops*, *Phys.Rev.Lett.* **105** (2010) 151605, [1006.5703].

[51] A. Goncharov, *A simple construction of Grassmannian polylogarithms*, 0908.2238.

[52] F. C. Brown, *Multiple zeta values and periods of moduli spaces $\mathfrak{M}_{0,n}$*, *Annales Sci.Ecole Norm.Sup.* **42** (2009) 371, [math/0606419].

[53] C. Duhr, H. Gangl, and J. R. Rhodes, *From polygons and symbols to polylogarithmic functions*, *JHEP* **1210** (2012) 075, [1110.0458].

[54] F. Brown, *On the decomposition of motivic multiple zeta values*, 1102.1310.

[55] S. Weinzierl, *Hopf algebras and Dyson-Schwinger equations*, 2015. 1506.09119.

[56] N. Arkani-Hamed, J. L. Bourjaily, F. Cachazo, and J. Trnka, *Local Integrals for Planar Scattering Amplitudes*, *JHEP* **06** (2012) 125, [1012.6032].

[57] F. Cachazo, *Sharpening The Leading Singularity*, 0803.1988.

[58] K. G. Chetyrkin and F. V. Tkachov, *Integration by Parts: The Algorithm to Calculate beta Functions in 4 Loops*, *Nucl. Phys.* **B192** (1981) 159–204.

[59] J. M. Henn, *Multiloop integrals in dimensional regularization made simple*, *Phys.Rev.Lett.* **110** (2013) 251601, [1304.1806].

[60] J. M. Henn, A. V. Smirnov, and V. A. Smirnov, *Analytic results for planar three-loop four-point integrals from a Knizhnik-Zamolodchikov equation*, *JHEP* **1307** (2013) 128, [1306.2799].

[61] J. M. Henn and V. A. Smirnov, *Analytic results for two-loop master integrals for Bhabha scattering I*, *JHEP* **1311** (2013) 041, [1307.4083].

[62] J. M. Henn, A. V. Smirnov, and V. A. Smirnov, *Evaluating single-scale and/or non-planar diagrams by differential equations*, *JHEP* **03** (2014) 088, [1312.2588].

[63] M. Argeri, S. Di Vita, P. Mastrolia, E. Mirabella, J. Schlenk, U. Schubert, and L. Tancredi, *Magnus and Dyson Series for Master Integrals*, *JHEP* **03** (2014) 082, [1401.2979].

[64] C. Bogner and S. Weinzierl, *Periods and Feynman integrals*, *J.Math.Phys.* **50** (2009) 042302, [0711.4863].

[65] F. Chavez and C. Duhr, *Three-mass triangle integrals and single-valued polylogarithms*, *JHEP* **1211** (2012) 114, [1209.2722].

[66] V. Del Duca, C. Duhr, and V. A. Smirnov, *The One-Loop One-Mass Hexagon Integral in D=6 Dimensions*, *JHEP* **07** (2011) 064, [1105.1333].

[67] L. J. Dixon, J. M. Drummond, and J. M. Henn, *The one-loop six-dimensional hexagon integral and its relation to MHV amplitudes in N=4 SYM*, *JHEP* **06** (2011) 100, [1104.2787].

[68] V. Del Duca, L. J. Dixon, J. M. Drummond, C. Duhr, J. M. Henn, and V. A. Smirnov, *The one-loop six-dimensional hexagon integral with three massive corners*, *Phys. Rev.* **D84** (2011) 045017, [1105.2011].

[69] S. Weinzierl, *On the solutions of the scattering equations*, *JHEP* **04** (2014) 092, [1402.2516].

[70] L. J. Dixon, J. M. Drummond, and J. M. Henn, *Bootstrapping the three-loop hexagon*, *JHEP* **1111** (2011) 023, [1108.4461].

[71] L. J. Dixon, J. M. Drummond, and J. M. Henn, *Analytic result for the two-loop six-point NMHV amplitude in N=4 super Yang-Mills theory*, *JHEP* **1201** (2012) 024, [1111.1704].

[72] J. Drummond, *Generalised ladders and single-valued polylogarithms*, *JHEP* **1302** (2013) 092, [1207.3824].

[73] L. J. Dixon, C. Duhr, and J. Pennington, *Single-valued harmonic polylogarithms and the multi-Regge limit*, *JHEP* **1210** (2012) 074, [1207.0186].

[74] J. Drummond, C. Duhr, B. Eden, P. Heslop, J. Pennington, and V. A. Smirnov, *Leading singularities and off-shell conformal integrals*, *JHEP* **08** (2013) 133, [1303.6909].

[75] L. J. Dixon, J. M. Drummond, M. von Hippel, and J. Pennington, *Hexagon functions and the three-loop remainder function*, *JHEP* **1312** (2013) 049, [1308.2276].

[76] L. J. Dixon, J. M. Drummond, C. Duhr, and J. Pennington, *The four-loop remainder function and multi-Regge behavior at NNLLA in planar N = 4 super-Yang-Mills theory*, *JHEP* **06** (2014) 116, [1402.3300].

[77] A. V. Kotikov, *Differential equations method: New technique for massive Feynman diagrams calculation*, *Phys. Lett.* **B254** (1991) 158–164.

[78] A. V. Kotikov, *Differential equations method: The Calculation of vertex type Feynman diagrams*, *Phys. Lett.* **B259** (1991) 314–322.

[79] A. V. Kotikov, *Differential equation method: The Calculation of N point Feynman diagrams*, *Phys. Lett.* **B267** (1991) 123–127.

[80] T. Gehrmann and E. Remiddi, *Differential equations for two loop four point functions*, *Nucl.Phys.* **B580** (2000) 485–518, [hep-ph/9912329].

[81] C. Duhr, *Mathematical aspects of scattering amplitudes*, in *Theoretical Advanced Study Institute in Elementary Particle Physics: Journeys Through the Precision Frontier: Amplitudes for Colliders (TASI 2014) Boulder, Colorado, June 2-27, 2014*, 2014. 1411.7538.

[82] E. Panzer, *Feynman integrals and hyperlogarithms*, 1506.07243.

[83] D. Gaiotto, J. Maldacena, A. Sever, and P. Vieira, *Pulling the straps of polygons*, *JHEP* **1112** (2011) 011, [1102.0062].

[84] N. Usyukina and A. I. Davydychev, *Exact results for three and four point ladder diagrams with an arbitrary number of rungs*, *Phys.Lett.* **B305** (1993) 136–143.

[85] R. Britto, F. Cachazo, and B. Feng, *New recursion relations for tree amplitudes of gluons*, *Nucl. Phys.* **B715** (2005) 499–522, [hep-th/0412308].

[86] R. Britto, F. Cachazo, B. Feng, and E. Witten, *Direct proof of tree-level recursion relation in Yang-Mills theory*, *Phys. Rev. Lett.* **94** (2005) 181602, [hep-th/0501052].

[87] R. Britto, *Loop Amplitudes in Gauge Theories: Modern Analytic Approaches*, *J. Phys.* **A44** (2011) 454006, [1012.4493].

[88] Z. Bern and Y.-t. Huang, *Basics of Generalized Unitarity*, *J. Phys.* **A44** (2011) 454003, [1103.1869].

[89] H. Ita, *Susy Theories and QCD: Numerical Approaches*, *J. Phys.* **A44** (2011) 454005, [1109.6527].

[90] R. K. Ellis, Z. Kunszt, K. Melnikov, and G. Zanderighi, *One-loop calculations in quantum field theory: from Feynman diagrams to unitarity cuts*, *Phys. Rept.* **518** (2012) 141–250, [1105.4319].

[91] O. Steinmann, *Über den Zusammenhang zwischen den Wightmanfunktionen und der retardierten Kommutatoren*, *Helv.Phys.Acta.* **33** (1960) 257.

[92] O. Steinmann, *Wightman-funktionen und retardierten kommutatoren*, *Helv.Phys.Acta.* **33** (1960) 347.

[93] H. Stapp, *Inclusive cross-sections are discontinuities*, *Phys.Rev.* **D3** (1971) 3177.

[94] P. Ball, V. M. Braun, and H. G. Dosch, *Form-factors of semileptonic D decays from QCD sum rules*, *Phys.Rev.* **D44** (1991) 3567–3581.

[95] R. Feynman, *Quantum theory of gravitation*, *Acta Phys.Polon.* **24** (1963) 697–722.

[96] R. Feynman, *Problems in quantizing the gravitational field, and the massless yang-mills field*, in *Magic without magic* (J. Klauder, ed.), pp. 355–375. San Francisco, 1972.

[97] R. Feynman, *Closed loop and tree diagrams*, in *Magic without magic* (J. Klauder, ed.), pp. 377–408. San Francisco, 1972.

[98] Z. Bern, L. J. Dixon, and D. A. Kosower, *Dimensionally regulated pentagon integrals*, *Nucl.Phys.* **B412** (1994) 751–816, [hep-ph/9306240].

[99] N. Usyukina and A. I. Davydychev, *An Approach to the evaluation of three and four point ladder diagrams*, *Phys.Lett.* **B298** (1993) 363–370.

[100] T. Huber and D. Maitre, *HypExp 2, Expanding Hypergeometric Functions about Half-Integer Parameters*, *Comput.Phys.Commun.* **178** (2008) 755–776, [0708.2443].

[101] C. Anastasiou, R. Britto, B. Feng, Z. Kunszt, and P. Mastrolia, *Unitarity cuts and Reduction to master integrals in d dimensions for one-loop amplitudes*, *JHEP* **03** (2007) 111, [hep-ph/0612277].

[102] W. van Neerven, *Dimensional Regularization Of Mass And Infrared Singularities In Two Loop On-Shell Vertex Functions*, *Nucl.Phys.* **B268** (1986) 453.

[103] F. C. Brown, *Single-valued multiple polylogarithms in one variable*, *C. R. Acad. Sci. Paris, Ser. I* **338** (2004) 527.

[104] R. Britto and B. Feng, *Unitarity cuts with massive propagators and algebraic expressions for coefficients*, *Phys. Rev.* **D75** (2007) 105006, [hep-ph/0612089].

[105] R. K. Ellis, W. T. Giele, and Z. Kunszt, *A Numerical Unitarity Formalism for Evaluating One-Loop Amplitudes*, *JHEP* **03** (2008) 003, [0708.2398].

[106] W. T. Giele, Z. Kunszt, and K. Melnikov, *Full one-loop amplitudes from tree amplitudes*, *JHEP* **04** (2008) 049, [0801.2237].

[107] R. Britto and E. Mirabella, *Single Cut Integration*, *JHEP* **01** (2011) 135, [1011.2344].

[108] N. Arkani-Hamed, F. Cachazo, and J. Kaplan, *What is the Simplest Quantum Field Theory?*, *JHEP* **1009** (2010) 016, [0808.1446].

[109] S. Badger, H. Frellesvig, and Y. Zhang, *Hepta-Cuts of Two-Loop Scattering Amplitudes*, *JHEP* **04** (2012) 055, [1202.2019].

[110] K. J. Larsen, *Global Poles of the Two-Loop Six-Point N=4 SYM integrand*, *Phys. Rev.* **D86** (2012) 085032, [1205.0297].

[111] H. Johansson, D. A. Kosower, and K. J. Larsen, *Maximal Unitarity for the Four-Mass Double Box*, *Phys. Rev.* **D89** (2014), no. 12 125010, [1308.4632].

[112] M. Søgaard and Y. Zhang, *Multivariate Residues and Maximal Unitarity*, *JHEP* **12** (2013) 008, [1310.6006].

[113] M. Søgaard and Y. Zhang, *Massive Nonplanar Two-Loop Maximal Unitarity*, *JHEP* **12** (2014) 006, [1406.5044].

[114] A. Brandhuber, S. McNamara, B. J. Spence, and G. Travaglini, *Loop amplitudes in pure Yang-Mills from generalised unitarity*, *JHEP* **10** (2005) 011, [hep-th/0506068].

[115] G. Ossola, C. G. Papadopoulos, and R. Pittau, *Reducing full one-loop amplitudes to scalar integrals at the integrand level*, *Nucl. Phys.* **B763** (2007) 147–169, [hep-ph/0609007].

[116] M. E. Peskin, *Simplifying Multi-Jet QCD Computation*, in *13th Mexican School of Particles and Fields (MSPF 2008) San Carlos, Sonora, Mexico, October 2-11, 2008*, 2011. 1101.2414.

[117] O. V. Tarasov, *Connection between Feynman integrals having different values of the space-time dimension*, *Phys. Rev.* **D54** (1996) 6479–6490, [hep-th/9606018].

[118] S. Abreu, R. Britto, C. Duhr, and E. Gardi, *Graphical coproduct of one-loop Feynman graphs*, *—to appear—* (2015).

[119] D. Kreimer, *On the Hopf algebra structure of perturbative quantum field theories*, *Adv. Theor. Math. Phys.* **2** (1998) 303–334, [q-alg/9707029].

[120] A. Connes and D. Kreimer, *Hopf algebras, renormalization and noncommutative geometry*, *Commun. Math. Phys.* **199** (1998) 203–242, [hep-th/9808042].

[121] C. Bergbauer and D. Kreimer, *Hopf algebras in renormalization theory: Locality and Dyson-Schwinger equations from Hochschild cohomology*, *IRMA Lect. Math. Theor. Phys.* **10** (2006) 133–164, [hep-th/0506190].

[122] D. Kreimer and E. Panzer, *Renormalization and Mellin transforms*, 1207.6321.

[123] E. Panzer, *Renormalization, Hopf algebras and Mellin transforms*, 2014. 1407.4943.

[124] G. Sterman, *An Introduction to Quantum Field Theory*. Cambridge University Press.

[125] M. Spradlin and A. Volovich, *Symbols of One-Loop Integrals From Mixed Tate Motives*, *JHEP* **11** (2011) 084, [1105.2024].

[126] V. Del Duca, C. Duhr, and V. A. Smirnov, *The massless hexagon integral in D = 6 dimensions*, *Phys. Lett.* **B703** (2011) 363–365, [1104.2781].

[127] J. M. Drummond, J. Henn, V. A. Smirnov, and E. Sokatchev, *Magic identities for conformal four-point integrals*, *JHEP* **01** (2007) 064, [hep-th/0607160].

[128] A. Hodges, *Eliminating spurious poles from gauge-theoretic amplitudes*, *JHEP* **05** (2013) 135, [0905.1473].

[129] A. Hodges, *The Box Integrals in Momentum-Twistor Geometry*, *JHEP* **08** (2013) 051, [1004.3323].

[130] C. Vergu, *Twistors, strings and supersymmetric gauge theories*. PhD thesis, Paris U., VI-VII, 2008. 0809.1807.

[131] N. Arkani-Hamed, J. L. Bourjaily, F. Cachazo, S. Caron-Huot, and J. Trnka, *The All-Loop Integrand For Scattering Amplitudes in Planar N=4 SYM*, *JHEP* **01** (2011) 041, [1008.2958].

[132] E. Remiddi, *Differential equations for Feynman graph amplitudes*, *Nuovo Cim.* **A110** (1997) 1435–1452, [hep-th/9711188].

[133] M. Argeri and P. Mastrolia, *Feynman Diagrams and Differential Equations*, *Int. J. Mod. Phys.* **A22** (2007) 4375–4436, [0707.4037].

[134] J. M. Henn, *Lectures on differential equations for Feynman integrals*, *J. Phys.* **A48** (2015) 153001, [1412.2296].

[135] E. Panzer, *On hyperlogarithms and Feynman integrals with divergences and many scales*, *JHEP* **03** (2014) 071, [1401.4361].

[136] C. Anastasiou, L. J. Dixon, and K. Melnikov, *NLO Higgs boson rapidity distributions at hadron colliders*, *Nucl. Phys. Proc. Suppl.* **116** (2003) 193–197, [hep-ph/0211141].

[137] C. Anastasiou, L. J. Dixon, K. Melnikov, and F. Petriello, *Dilepton rapidity distribution in the Drell-Yan process at NNLO in QCD*, *Phys. Rev. Lett.* **91** (2003) 182002, [hep-ph/0306192].

[138] C. Anastasiou, L. J. Dixon, K. Melnikov, and F. Petriello, *High precision QCD at hadron colliders: Electroweak gauge boson rapidity distributions at NNLO*, *Phys. Rev.* **D69** (2004) 094008, [hep-ph/0312266].

[139] S. Laporta, *High precision calculation of multiloop Feynman integrals by difference equations*, *Int. J. Mod. Phys.* **A15** (2000) 5087–5159, [hep-ph/0102033].

[140] A. V. Smirnov and V. A. Smirnov, *FIRE4, LiteRed and accompanying tools to solve integration by parts relations*, *Comput. Phys. Commun.* **184** (2013) 2820–2827, [1302.5885].

[141] A. V. Smirnov, *FIRE5: a C++ implementation of Feynman Integral REduction*, *Comput. Phys. Commun.* **189** (2014) 182–191, [1408.2372].

[142] A. von Manteuffel and C. Studerus, *Reduze 2 - Distributed Feynman Integral Reduction*, 1201.4330.

[143] A. Denner, *Techniques for calculation of electroweak radiative corrections at the one loop level and results for W physics at LEP-200*, *Fortsch.Phys.* **41** (1993) 307–420, [0709.1075].

[144] C. Anastasiou, E. N. Glover, and C. Oleari, *Scalar one loop integrals using the negative dimension approach*, *Nucl.Phys.* **B572** (2000) 307–360, [hep-ph/9907494].

[145] A. I. Davydychev and M. Y. Kalmykov, *New results for the epsilon expansion of certain one, two and three loop Feynman diagrams*, *Nucl.Phys.* **B605** (2001) 266–318, [hep-th/0012189].

[146] T. Birthwright, E. N. Glover, and P. Marquard, *Master integrals for massless two-loop vertex diagrams with three offshell legs*, *JHEP* **0409** (2004) 042, [hep-ph/0407343].

[147] A. Brandhuber, B. Spence, and G. Travaglini, *From trees to loops and back*, *JHEP* **01** (2006) 142, [hep-th/0510253].

[148] V. A. Smirnov, *Analytic tools for Feynman integrals*, *Springer Tracts Mod.Phys.* **250** (2012) 1–296.

Publications

Samuel Abreu, Ruth Britto, Claude Duhr and Einan Gardi. *From multiple unitarity cuts to the coproduct of Feynman integrals*, JHEP, 2014.

Samuel Abreu, Ruth Britto, and Hanna Grönqvist. *Cuts and coproducts of massive triangle diagrams*, JHEP, 2015.